Promoter CpG island hypermethylation in the development of cutaneous melanoma

Promoter CpG island hypermethylation in the development of cutaneous melanoma

Financial support for the publication of this thesis was kindly provided by Galderma Benelux B.V.

ISBN: 978-90-5335-987-7

Printed by Ridderprint B.V.

Promoter CpG island hypermethylation in the development of cutaneous melanoma

Proefschrift

ter verkrijging van
de graad van Doctor aan de Universiteit Leiden,
op gezag van Rector Magnificus prof.mr. C.J.J.M. Stolker,
volgens besluit van het College voor Promoties
te verdedigen op woensdag 4 februari 2015
klokke 16.15 uur

door

Linda Gao
geboren te Beijing
in 1984

Promotiecommissie

Promotor	Prof.dr. R. Willemze
Co-promotor	Dr. R. van Doorn
Overige leden	Prof.dr. J.J. van den Oord *Catholic University Leuven (KU Leuven), Leuven, Belgium*
	Prof.dr. W.J. Mooi *VU University Medical Center (VUmc), Amsterdam*
	Prof.dr.ir. S.M. van der Maarel

Table of contents

Abbreviations

AJCC	American Joint Committee on Cancer
BMCA	bisulphite melting curve analysis
BRAF	B-Raf proto-oncogene, serine/threonine kinase
BrdU	5-bromo-2´-deoxyuridine
BSA	bisulphite sequencing analysis
C10rf106	chromosome 1 open reading frame 106
CDH1	cadherin 1, type 1, E-cadherin (epithelial)
CDH11	cadherin 11, type 2, OB-cadherin (osteoblast)
CDKN2A	cyclin-dependent kinase inhibitor 2A
CLDN11	claudin 11
CpG	cytosine-phosphate-guanine dinucleotide in linear sequence
CPSF6	cleavage and polyadenylation specific factor 6,68kDa
D176A	aspartic acid at amino acid 176 replaced by alanine, MAPK13 mutant
DNMT	DNA (cytosine-5-)-methyltransferase
EFCAB1	EF-hand calcium binding domain 1
EZH2	enhancer of zeste 2 polycomb repressive complex 2 subunit
F324S	phenylalanine at amino acid 324 replaced by serine, MAPK13 mutant
FAMMM	familial atypical multiple mole melanoma
HDAC	histone deacetylase
HIST1H3E	histone cluster 1, H3e
HOXA9	homeobox A9
LEP	leptin
MAGEA	melanoma antigen family A
MAGEB	melanoma antigen family B
MAPK13	mitogen-activated protein kinase 13
MBD	methyl-CpG-binding domain proteins
MCHR1	melanin-concentrating hormone receptor 1
MeCP2	methyl CpG binding protein 2
MeDIP	methylated DNA immune precipitation
MITF	microphthalmia-associated transcription factor
NRAS	neuroblastoma RAS viral (v-ras) oncogene homolog
OIS	oncogene-induced senescence
p38δ	p38 MAP kinase protein, isoform δ
PLEKHG6	pleckstrin homology domain containing, family G (with RhoGef domain) member 6
PPP1R3C	protein phosphatase 1, regulatory subunit 3C
RASEF	RAS and EF-hand domain containing
Rb	retinoblastoma protein
ROS	reactive oxygen species
SYNPO2	synaptopodin 2 (myopodin)
TBP	TATA box binding protein
TIMP3	TIMP metallopeptidase inhibitor 3
TNM	tumor depth (T), lymph node status (N), and distant metastasis (M) classification
V600E	valine at amino acid 600 replaced by glutamic acid, BRAF mutant

Chapter 1

General introduction

Clinical aspects of melanoma

Cutaneous melanoma is a type of cancer that originates from melanocytes residing in the skin. It is characterized by a propensity to metastasize and resistance to chemotherapy. The majority of cutaneous melanoma can be divided into four subtypes: superficial spreading, nodular, lentigo maligna, and acral lentiginous melanoma[1]. A prediction of the course of disease and the survival rate depends largely on the extent of the cancer at the time of diagnosis in the patient. The American Joint Committee on Cancer (AJCC) staging system is generally applied in the clinic to categorize melanoma into defined stages based on TNM classification[2]. Melanoma is divided into four stage categories, where stage I is a thin localized tumor, stage II a thick localized tumor, stage III the presence of regional lymph node metastases and stage IV the presence of distant metastases. The 5-year overall survival rate for stage I is approximately 90%, for stage II 70%, stage III 60% and stage IV 20%[2]. In a proportion of patients the sentinel node procedure is performed to examine the presence of nodal micrometastases. In addition to the presence of nodal micrometastases, the prognosis of melanoma patients without apparent metastatic disease is determined by tumor thickness, microscopic ulceration, mitotic rate, tumor site, sex and age of the patient[1]. For a localized tumor, surgical resection is the principle therapy. For melanoma that has metastasized to distant sites, the two main treatment modalities are molecular targeted therapy, developed and tested in clinical trials for *BRAF*, *MEK* and *KIT* mutant melanoma, and immune-based therapy that have lead to a better prognosis for patients with stage IV melanoma[3].

Epidemiology of melanoma

The incidence of cutaneous melanoma in the Netherlands for men and women was 9.0 and 12.2 per 100.000 person-years respectively over a five-year period of 1989-1993. For the period of 2004-2008, the incidence for males and females was 17.9 and 21.5 per 100.000 person-years respectively. The ten-year relative survival rate of cutaneous melanoma for men and women in the Netherlands was 77% and 88% respectively over 2004-2008. The mortality rate, standardized for age, was 2.2 per 100.000 person-years in 1989 and has since increased to 3.9 per 100.000 person-years in 2009. The mortality rate for individuals between 0-44 years however has remained stable; a significant increase has been observed for individuals older than 45 years, with the largest increase in mortality rate for individuals older than 65 years[4].

Risk factors for melanoma

Environmental melanoma risk factors include intermittent exposure to sunlight, sunburn and the use of tanning beds. Protection from sunlight exposure can reduce the risk of developing melanoma[5,6]. Aside from these environmental factors, several phenotypic markers of an individual are considered to be indicative of a risk for melanoma. These

markers include the presence of more than 100 naevi or more than five dysplastic naevi on the body, a fair skin type, red or blond hair color, blue eye color, freckles, the presence of actinic keratosis or lentigines and a history of basal cell carcinoma or squamous cell carcinoma[7-9]. In addition to phenotypic characteristics, genetic variants that predispose to the development of melanoma have been identified using genome-wide association studies. The variations often occur in genes that are implicated in the pigmentation response and in naevus development[10,11]. In approximately 10% of cases there is familial clustering of melanoma. This autosomal dominantly inherited genetic condition is termed familial melanoma, hereditary melanoma or familial atypical multiple mole melanoma (FAMMM) syndrome; generally defined as melanoma occurring in 3 or more members of a family, with a first-degree relationship between at least two affected members. An estimated 40% of patients with familial melanoma carry a mutation in *CDKN2A*, a gene that encodes the $p16^{INK4A}$ and $p14^{ARF}$ tumor suppressor proteins. A founder mutation in *CDKN2A* has also been identified in familial melanoma kindreds known as the p16-Leiden deletion[12]. Individuals with melanoma predisposition by *CDKN2A* mutation who live at lower latitudes have a higher melanoma incidence, suggesting a correlation with sunlight exposure[13]. The life-time risk to develop melanoma of individuals that carry a *CDKN2A* mutation is approximately 70%, together with a risk of 17% for pancreatic cancer[14].

Melanoma development

Melanoma develops from melanocytes, the melanin-producing cells localized in the basal layer of the epidermis and in the hair follicles. A melanoma can develop *de novo*, or from an existing common naevus or dysplastic naevus. Melanocytic naevi, both common and dysplastic, are important in relation to melanoma because they can be regarded as simulants of melanoma and as markers for individuals at increased risk for melanoma development[15].

Common naevus and dysplastic naevus

A common naevus, or mole, is a benign melanocytic neoplasm that consists of clusters of melanocytes that underwent limited rounds of proliferation. A common naevus is often smaller than 5 millimeters in diameter and round or oval in shape, with a distinct edge. A dysplastic naevus is generally larger than 5 millimeters in diameter and may differ in color, surface, symmetry and border from a common naevus[16,17]. A dysplastic naevus can be distinguished from a common naevus based on the presence of architectural disorder and cytologic atypia which can be mild to severe[15,18]. Dysplastic naevus cells have been observed to produce more reactive oxygen species (ROS) than normal melanocytes in the skin[19]. Compared to common naevus cells, dysplastic naevus cells showed abnormalities in pathway components involved in the processes of cell proliferation and apoptosis[20-23]. Dysplastic naevi are suspected to harbor additional somatic alterations compared to

common naevi. A dysplastic naevus can arise *de novo*, or from an existing common naevus[24].

There are clinical and histopathological criteria to distinguish a common naevus and dysplastic naevus from melanoma. However, substantial inter-observer variability in separating melanocytic naevi from melanoma remains[25]. Especially the differentiation between melanoma in its early stages and a dysplastic naevus remains challenging since the histological features used as criteria for dysplastic naevus overlap to some extent with those for early-stage melanoma[16].

The majority of common naevi demonstrate maturation, a histological feature indicative of a benign lesion, with a decrease in the pigmentary activity and size of the naevus cells at the periphery of the lesion in the dermis. In line with this are findings that melanocytic naevi very rarely develop into melanoma in the general population, the estimated annual transformation rate of a common naevus into melanoma is 1 in 200.000 for men and women younger than 40 years, and 1 in 33.000 for men older than 60 years[26]. Despite the low transformation frequency of naevi into melanoma, both common and dysplastic naevi are associated with an increased melanoma risk. Additionally, individuals who have dysplastic naevi often have an elevated amount of common naevi[15].

A model of melanoma progression

Melanocytic naevi are also important in relation to melanoma because they are potential precursors of melanoma. Cutaneous melanoma develops in over half of the cases *de novo*, but in an estimated 20%-50% of cases from a common or dysplastic naevus. Observations have been made of individuals with pre-existing naevi that underwent malignant change, next to patients that had histological dysplasia in contiguity to their melanoma[15]. Common naevi harbor frequent mutation of *BRAF* and mutations in *NRAS* or *KRAS* at lower frequencies, while dysplastic naevi were found to harbor *BRAF* mutation and allelic deletion at chromosome 9p21[27-29]. These genetic alterations have also been frequently found in melanoma, sometimes in cases where a melanoma and adjacent naevus in the same patient were examined[30-32]. Melanocytes in the skin are assumed to undergo initial rounds of proliferation as a result of the aberrant activity of a mutated oncogene such as *BRAF*. This initial growth is followed by a stable cell cycle arrest that is part of the oncogene-induced senescence (OIS) response, an important mechanism that acts to prevent further malignant activity of the melanocytes and gives rise to a benign melanocytic lesion, a common naevus[33].

The model of melanoma development and progression as proposed by Clark describes the histologic changes that accompany the development of a common naevus, dysplastic naevus and the different stages of melanoma (Figure 1)[34]. In this process, benign melanocytes acquire a variety of increasingly malignant phenotypic features that result in melanoma. Formation of a common naevus is regarded as the first step in the

phenotypic change of normal melanocytes in the skin, placing the common naevus at the start of the melanoma development and progression model. The development of a dysplastic naevus is generally regarded as an intermediate step between common naevus and melanoma. In the stage of melanoma, the melanoma cells of a localized tumor display an increasing loss of cellular differentiation and have the ability of unlimited proliferation. In the radial-growth phase, the tumor expands mainly in a horizontal direction in the epidermis of the skin. In the vertical-growth phase, melanoma cells cross the basement membrane and grow further into the dermis of the skin. The capacity of melanoma cells to invade the dermis is significantly correlated with their capacity to metastasize. In the stage of metastatic melanoma, cells dissociate from the primary tumor and migrate through surrounding stroma to invade lymph or blood vessels. From there, melanoma cells can spread via lymph or blood to distant body sites and form secondary tumors (Figure 1).

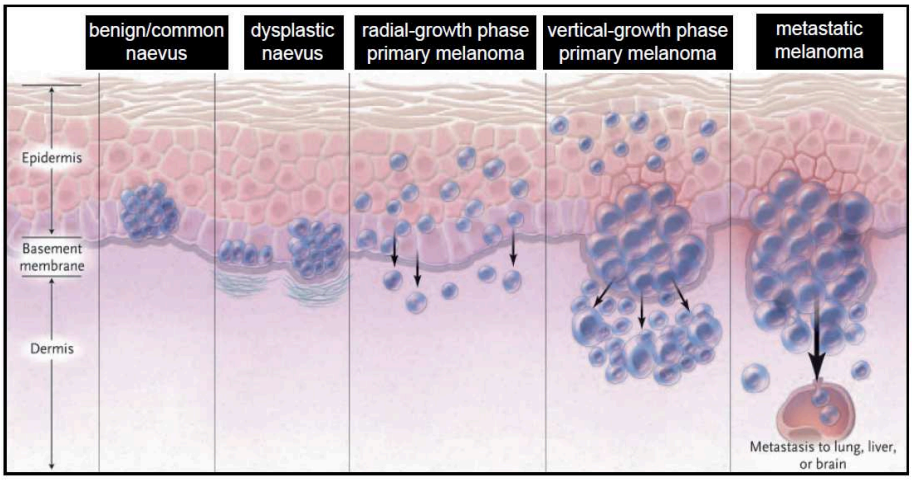

Figure 1. Schematic representation of different stages in the development of melanoma. (Adapted from reference 34 with permission of Massachusetts Medical Society, copyright 2006.)

Genetic alterations in melanoma

Research through the years has identified a multitude of genes that are affected in melanoma by genetic alterations, leading to aberrant signaling of cellular pathways that contribute to the malignant phenotype of melanoma cells. Table 1 lists the melanoma oncogenes and tumor suppressor genes that have been extensively studied, some of which will be described here.

Activating mutations in *BRAF* occur in approximately 50% of all melanomas, they are most commonly found in cutaneous melanoma of intermittently sun-exposed skin and rare in mucosal and acral melanoma. Most frequently, valine at amino acid 600 is replaced by glutamic acid (V600E) by mutation of a single nucleotide (GTG to GAG) in the kinase-encoding exon 15, leading to a consecutive active conformation of the protein. Another

mutation at the same site substitutes lysine for valine (V600K) by mutation of two nucleotides (GTG to AAG)[35,36].

NRAS mutations are also found in cutaneous melanoma, including those that arise in intermittently sun-exposed skin and other types of melanoma, at a frequency of approximately 20%. *NRAS* mutations occur most frequently in codon 61 and have also been identified in codon 12, 13 and 18[37]. *NRAS* and *BRAF* mutations are almost never found simultaneously in melanoma. Similar to *BRAF* mutation, *NRAS* mutation leads to hyperactivation of the MEK/ERK signaling pathway[38,39].

CDKN2A is located on chromosome 9p21 and encodes two distinct proteins, $p16^{INK4A}$ and $p14^{ARF}$, from two transcript variants that differ in their first exons. *CDKN2A* mutations and deletions have been found at a frequency of 19% and 38% respectively in melanomas[40]. $p16^{INK4A}$ binds to and inhibits G1 cyclin-dependent kinase (Cdk) 4 and 6. Cdk4/6 phosphorylate and inactivate the retinoblastoma protein (Rb) to allow progression of the cell cycle into the S-phase. Loss of $p16^{INK4A}$ therefore promotes Rb inactivation, leading to uncontrolled cell proliferation. It has been proposed that disruption of the $p16^{INK4A}$-Rb pathway, mainly by *CDKN2A* inactivation, may be an important next step in the melanoma progression model. Together with the activation of *hTERT* to maintain minimal telomere length and other additional molecular alterations, disruption of the $p16^{INK4A}$-Rb pathway allows neval melanocytes to overcome senescence and acquire the ability for unrestrained proliferation[35]. Often melanomas that harbor *BRAF* mutation also have deletion or mutation of *CDKN2A* [38,39]. $p14^{ARF}$ is known to stabilize p53, a tumor suppressor protein that responds to a variety of cellular stresses and regulates the expression of target genes to induce a tumor restrictive response such as cell cycle arrest, apoptosis or DNA repair. Mutations in the encoding gene, *TP53*, were found in 19% of melanoma cases[40]. Germline *CDKN2A* mutation occurs in an estimated 40% of patients with familial melanoma.

The *PTEN* (phosphatase and tensin homolog) tumor suppressor is inactivated by deletion or mutation in 25% and 12% of melanoma cases respectively[40]. *PTEN* mutations are often found together with *BRAF* mutation[41,42]. The loss of *PTEN* in some melanomas, especially in melanomas that also harbor *BRAF* mutation, leads to consecutive activation of the *PI3K* pathway. Experiments conducted in mice showed that deletion of *PTEN* or *CDKN2A* alone in mouse melanocytes did not lead to development of melanoma[43,44]. However, the combination of either *PTEN* or *CDKN2A* deletion with a mutation such as $BRAF^{V600E}$ can give rise to melanoma[45]. This underscores the understanding that loss of *CDKN2A* or *PTEN* alone is only one event in the process and that additional molecular alterations are needed for full melanoma development.

As the melanocyte master regulator, *MITF* (microphthalmia-associated transcription factor) is important in the differentiation and survival of melanocytes and

maintains melanocyte progenitor cells in adults. Amplification of *MITF* has been found in 4% of melanomas. In addition a rare inherited *MITF* gene variant is known to predispose to familial melanoma[46]. Many melanomas are dependent on *MITF* as a survival factor and loss of *MITF* activity renders melanoma cells sensitive to chemotherapeutic agents[38,39].

Melanomas that arise on chronically sun-exposed skin, on mucous membrane (mucosal melanoma) and on palms, soles and nail bed (acral melanoma) show relatively low frequency of *BRAF* mutation but harbor alterations in other genes. Activating mutations and amplifications of the tyrosine kinase *KIT* have been found in these melanomas. Activation of *KIT* results in proliferation and survival advantages via induction of the *MAPK* and *PI3K* pathways. Alterations in components of the $p16^{INK4A}$-Rb pathway that impact cell cycle regulation have also been identified, such as amplification of cyclin D1 (*CCND1*) and cyclin-dependent kinase 4 (*CDK4*) mutation[39,47].

Table 1. Genes affected by mutation, amplification or deletion in melanoma as adapted from references 38 and 39. M, mutation; A, amplification; D, deletion.

Gene	Alteration	Frequency	Affected pathways/processes
Kinases or signaling factors			
BRAF	M	50%	MAPK
NRAS	M	20%	MAPK, PI3K and RALGDS
KIT	M or A	3% M; 6% A	MAPK and PI3K
CDK4	A	3%	Cell cycle
CCND1	A	10%	Cell cycle
PPP6C	M	9%	Cell cycle
RAC1	M	5%	PAK
STK19	M	4%	unknown
MAP3K5, MAP3K9	M	24%	JNK, p38 MAPK
Transcription factors			
MITF	A	4%	Melanocyte lineage, cell cycle
Tumor suppressors			
CDKN2A	M or D	19% M; 38% D	Cell cycle
TP53	M	19%	Cell cycle
ARF	M	12%	Cell cycle
PTEN	M or D	12% M; 25% D	PI3K
Epigenetic regulators			
ARID2	M	9%	Chromatin remodeling
EZH2	M	3%	Chromatin remodeling

Recently new genes with somatic mutations have been identified through exome sequencing in melanoma, these include *PPP6C* and *RAC1*, encoding a phosphatase involved in cell cycle regulation and a GTPase involved in regulating cell adhesion and migration respectively, and the kinase-encoding *STK19*[40] (Table 1). Somatic mutations have also been identified in *MAP3K5* and *MAP3K9*, activators of the JNK and p38 MAPK signaling pathways[48].

Epigenetics

Human DNA is organized into 23 chromosome pairs that together contain over 25.000 protein-coding genes. DNA is stored in a condensed form in the nucleus of the cell. In order to achieve such condensed packaging, the DNA molecule is wrapped around histones, highly conserved proteins that are present in the nucleus of all eukaryotic cells. Histones are grouped into five classes (H1, H2A, H2B, H3 and H4). Two sets of histone classes H2A, H2B, H3 and H4 bind to 147 DNA base pairs as an octamere to form a repeating unit known as the nucleosome (Figure 2). The fifth histone class H1 serves as a linker histone and binds to the nucleosome to enable the organization of the nucleosomes into a higher-order structure, the 30-nm filament[49] (Figure 2). Together the DNA molecule and histone proteins form a DNA-protein polymer known as chromatin.

Epigenetic regulation of gene expression

Chromatin is a dynamic macromolecular structure that can exist in different configurations. The structure of chromatin can differ in packaging density that ranges from a relatively loose form known as euchromatin where active gene transcription can take place, to a highly condensed form known as heterochromatin where transcriptional activity is silenced, such as at the centromeres and telomeres of chromosomes. Euchromatin consists in large part of coding sequences and makes up less than 4% of the genome in mammals. Some heterochromatic structures remain permanently silent (constitutive heterochromatin) and genes that are located in such regions will rarely be expressed in any cell type, while other heterochromatic structures (facultative heterochromatin) can be found at the coding regions of the genome and function to silence only in certain cells during a specific cell cycle or stage in development[50-52].The range of variation that exists in chromatin structure can be introduced via different mechanisms, including chromatin remodeling, histone modifications and DNA methylation which will be briefly introduced here.

Chromatin remodeling

Chromatin remodeling is one of the mechanisms by which changes in chromatin structure can be introduced. In chromatin remodeling, protein complexes hydrolyze ATP in order to bring about non-covalent modifications in the chromatin structure. This ATP-dependent remodeling includes the replacement of a regular histone protein with another histone variant, the moving of a histone octamere along the DNA strand (nucleosome sliding), the removal of a histone octamere (nucleosome eviction) and the creation of a DNA loop on the surface of the histone octamere (DNA looping). Through these chromatin remodeling processes, DNA regions that were previously occluded or ‘tucked away’ in the chromatin structure become accessible for binding by protein complexes[53].

Histone modifications

The second mechanism by which changes in chromatin structure are introduced is the addition of posttranslational modifications to histone proteins within the nucleosome. Several different types of posttranslational histone modifications have been identified so far, including histone acetylation, methylation and phosphorylation. The presence of such a modification results in an altered electrostatic charge or structure of a histone protein. This in turn induces changes in the contact between nucleosome units, leading to a change in chromatin organization. Histone modifications can also serve as a target site for chromatin remodeling complexes[54,55].

DNA methylation

Another well-known epigenetic mechanism of inducing alterations in the chromatin structure is DNA methylation. With this modification, a methyl group is added to a cytosine nucleotide of the DNA to yield 5'-methylcytosine (Figure 3). In mammals, DNA methylation takes place at CpG dinucleotides in the linear DNA sequence. CpG dinucleotides are non-randomly distributed in the human genome in focused, CpG-rich regions known as CpG islands. CpG islands can be found at the 5'end region of over half of all human genes consisting of the promoter, untranslated region and the first exon. DNA methylation is known to have an important role in developmental processes such as X-chromosome inactivation and genomic imprinting. DNA methylation patterns in mammals are established during embryonic development and they are maintained in each cell division. Specialized enzymes, DNA methyltransferases (DNMTs), catalyze the *de novo* addition of methyl groups or function to maintain existent DNA methylation. In the genome of higher eukaryotes, an enrichment of methylated DNA is found in regions that consist of noncoding DNA or repetitive DNA sequences such as at the heterochromatic structure of centromeres[56].

DNA methylation also functions to silence gene transcription. One way is through the interaction of methylcytosine with methyl-CpG-binding domain proteins (MBDs). In humans, the methyl-CpG-binding protein MeCP2 binds to methylcytosine in order to recruit histone deacetylases (HDACs), specialized enzymes that deacetylate the lysine residues of histone proteins. This histone deacetylation subsequently induces alterations of the nucleosome to mediate repression of transcriptional activity. The presence of methylcytosine can also prevent binding of transcription factors which only bind to CpG sequences in the DNA that are not methylated, leading to the inhibiton of gene transcription[57]. Other forms of modifications to cytosine within the CpG dinucleotide have also been found that are believed to be involved in regulation of gene expression, including the addition of a hydroxyl group to the 5'-methyl group of a methylcytosine to yield 5'-hydroxymethylcytosine[58].

Together the before mentioned mechanisms make chromatin a dynamic DNA-organizing entity that determines when and which genes are expressed. Epigenetics is therefore defined as changes in gene transcription caused by modulation of chromatin, which are not caused by changes in the DNA sequence. Epigenetics is important for establishing and maintaining a healthy state of an organism as aberrant alterations in the epigenetic machinery cause a variety of diseases in humans, including developmental and neurological disorders[59-61]. Moreover, it has become increasingly clear from the substantial number of studies performed in the past two decades that cancer is a disease that is caused by not only genetic alterations, but also epigenetic alterations that involve DNA cytosine methylation and histone modifications[62].

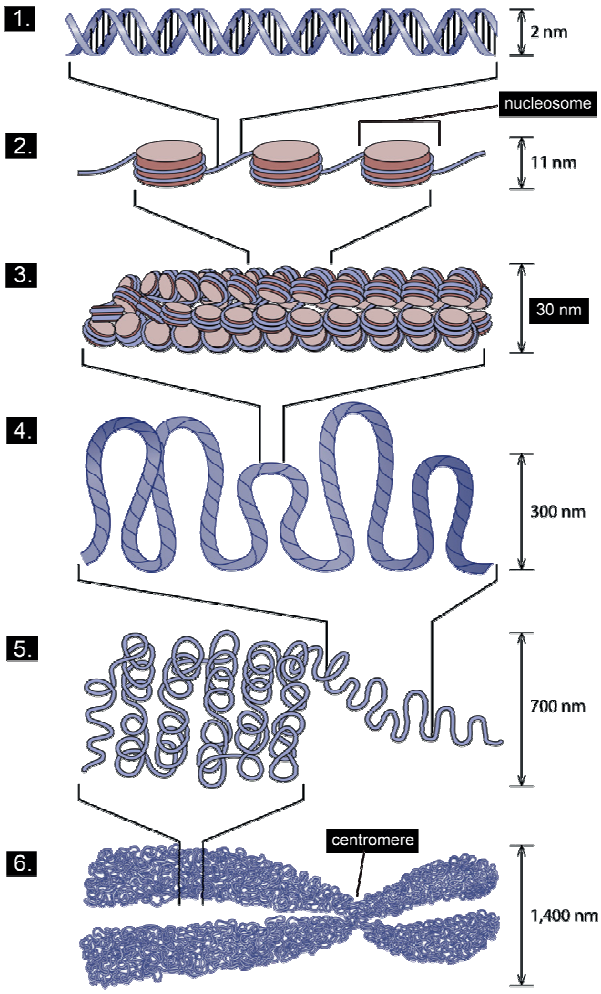

Figure 2. Organization of chromatin[63]: **1.** A short region of the DNA double helix **2.** A DNA strand wrapped around a histone octamere to comprise a nucleosome **3.** 30-nm chromatin fibre of stacked nucleosomes **4.** A section of the chromosome in an extended form **5.** A condensed section of the chromosome **6.** An entire mitotic chromosome. (Adapted from reference 63 with permission of American Society for Microbiology, copyright 2011.)

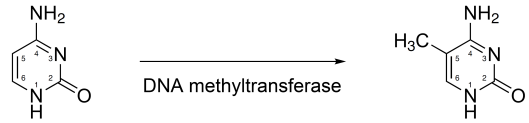

Figure 3. DNA methyltransferase catalyzes the addition of a methyl group to the fifth carbon atom within the pyrimidine ring of the cytosine base to yield 5'-methylcytosine.

DNA methylation in cancer

Since the discovery of 5'-methylcytosine in DNA, studies have observed differences in the DNA methylation pattern between normal cells and cancer cells. Cancer cells were found to have a global loss of the 5'-methyl modification (hypomethylation) across the genome[64,65]. Global genomic hypomethylation has been observed in a number of human cancer types such as B-cell chronic lymphocytic leukemia, cervical cancer, prostate cancer and metastatic hepatocellular cancer[66-69]. Since stable DNA methylation in the genome functions to maintain chromosomal integrity, a loss of this modification contributes to genomic instability, a hallmark of cancer[70,71]. Additionally, the loss of repressive methylation marks may lead to aberrant transcriptional activity of oncogenes that contribute to the malignant transformation of normal cells to cancer cells[72]. In contrast to most of the genome, CpG islands located in the promoter region in normal human cells are largely unmethylated, with methylation of only a very small percentage of the cytosines[73,74]. In cancer cells, often an aberrant increase of methylation (hypermethylation) at these promoter CpG island regions has been observed that correlates with transcriptional silencing of the genes involved[75] (Figure 4). Aberrant promoter hypermethylation has also been found in cutaneous melanoma. Some of the genes that have been identified as promoter hypermethylated are known to be involved in a variety of cellular processes (Table 2). Known tumor suppressor genes that are inactivated by mutation have also been observed to be inactivated by hypermethylation in cutaneous melanoma such as *CDKN2A*, *CDH1*, *PTEN* and *ARF*[76-79]. Promoter CpG island hypermethylation can therefore contribute to melanoma development through the inactivation of tumor suppressor genes.

DNA methylation alterations in cutaneous melanoma

Several studies have investigated DNA methylation alterations in cutaneous melanoma so far. Initial studies of methylation in cutaneous melanoma have focused on the investigation of promoter methylation of one candidate gene at a time. Promoter hypermethylation of *P27Kip1*, *RASSF1A*, *Maspin* and *APC* has been found in this way[80-83]. Other studies have analyzed a selected group of candidate genes and observed the presence of methylation[84-88]. The global demethylating agent 5'-aza-2'-deoxycytidine (Decitabine) has often been used in methylation studies. When added to cells, 5'-aza-2'-deoxycytidine incorporates in the DNA and interacts with DNA methyltransferases to

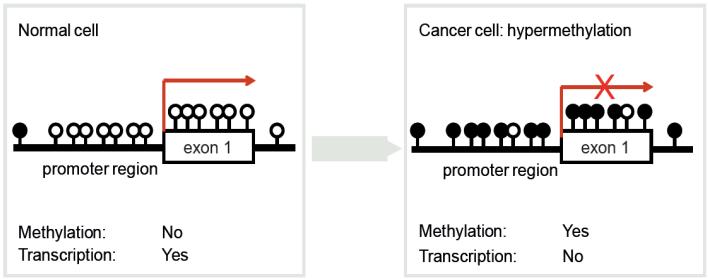

Figure 4. Schematic representation of a gene promoter region in a normal cell (left) versus a cancer cell (right). Hypermethylation in the cancer cell leads to transcriptional silencing of the gene.

inhibit cytosine methylation in subsequent rounds of DNA synthesis during cell replication[89,90]. 5'-aza-2'-deoxycytidine is therefore applied to investigate associations between promoter hypermethylation and transcriptional repression, with the assumption that erasing methylation will lead to re-activation of gene expression. A number of studies have applied the gene re-activation principle of 5'-aza-2'-deoxycytidine treatment to screen for methylation alterations in cutaneous melanoma. These studies subjected 5'-aza-2'-deoxycytidine-treated melanoma cell lines to microarray analysis, subsequently analyzing the methylation status of those genes that showed significant upregulated expression in the treated cell lines[91,92]. Other screening approaches have aimed to directly analyze methylation, such as methylated DNA immune precipitation (MeDIP). MeDIP uses methyl-binding proteins to precipitate methylated sequences in the genome. The obtained sequences are subsequently hybridized to CpG island arrays in order to identify the genes involved[93,94]. Hypermethylation of *COL1A2*, *NPM2*, *HSPB6*, *DDIT4L* and *MT1G* has been found in this way[95]. DNA methylation screening based on direct hybridization of sample DNA eliminated the need for methyl-binding antibodies and circumvented the issues associated with MeDIP. The HumanMethylation27K Beadchip array, consisting of oligonucleotide-coated beads for hybridization of bisulphite-treated DNA, has been used for the analysis of cultured melanoma cell lines and resulted in the identification of *WNT10B*, *TUB*, *ALOX12B* and *SLC6A11*[96,97]. Using the GoldenGate methylation array, 1505 CpG loci across 807 cancer-related genes have been analyzed in biopsy tissue from benign

Table 2. Genes that have previously been found to be hypermethylated in cutaneous melanoma.

Hypermethylated genes in cutaneous melanoma
Apoptosis: *RASSF1A, TNFRSF10C, TP53*
Cell Cycle: *CDKN1B, CDKN1C, CDKN2A*
Cell fate determination: *APC, WIF1*
Differentiation: *HOXB13*
Extracellular matrix: *COL1A2*
Immune response: *HLA class I, MAGE1, MAGEA2, A3, A4*
Invasion / Metastasis: *CDH1, CDH8, CDH13, SERPINB5, TFPI-2, TIMP3, SYK*
Signaling: *PTEN*

naevi and invasive melanomas, where hypermethylation of *FRZB* was found, together with hypomethylation of *EMR3* and *RUNX3* in melanoma[98]. Table 3 gives a summary of the methylation studies that have been performed prior to the genome-wide methylation study described in this thesis; they are categorized according to applied analysis method and type of studied material.

Table 3. Overview of methylation studies performed prior to the genome-wide methylation study described in Chapter 2 of this thesis with reference numbers to respective papers.

		Reference																		
		76	**77**	**78**	**79**	**80**	**81**	**82**	**83**	**84**	**85**	**86**	**87**	**88**	**91**	**92**	**95**	**96**	**97**	**98**
method[1]	CG	x	x	x	x	x	x	x	x	x	x	x	x	x						
	DM														x	x				
	IP																x			
	MA																	x	x	x
material[2]	CL	x	x		x	x	x	x	x	x	x	x		x	x	x	x	x	x	
	BT	x	x	x		x	x	x	x		x	x		x						x
	S			x									x							

[1] **method applied:**
CG: candidate gene(s), methylation status analysis of a single gene or a group of genes
DM: demethylation, expression profiling after 5'-aza treatment
IP: immuno-precipitation, precipitation of methylated sequences with methyl-binding proteins
MA: methylation array, direct hybridization of bisulphite-treated DNA to array

[2] **material used**:
CL: melanoma cell lines
BT: biopsy tissue
S: serum

Aims

Studies of DNA methylation alterations in melanoma that have been performed thus far provide a scattered view on the methylation alterations that are present in cutaneous melanoma. In most studies a selection of candidate genes has been analyzed. Those studies aimed at a more broad analysis of DNA methylation in the genome, have been performed on cultured melanoma cell lines or metastatic melanoma biopsies. In one study DNA methylation was analyzed in primary biopsy samples on only 807 selected cancer-related genes, but a study of promoter CpG island methylation alterations at a genome-wide level was still lacking. The analyses performed in this study have been permitted by the introduction of reliable beadchip technology (Illumina's Infinium platform) capable of analyzing methylation at high resolution with high reproducibility on a genome-wide scale, and the availability for these studies of fresh-frozen primary melanoma tumor samples.

Our aims were to perform genome-wide promoter CpG island methylation profiling of primary cutaneous melanoma biopsy specimens using Illumina's HumanMethylation27K Beadchip technology, in order to identify novel genes that are affected by aberrant promoter methylation in primary melanoma in comparison to common naevus (described in Chapter 2). In addition we asked whether genes that are affected by DNA hypermethylation in primary melanoma may have a tumor suppressive role in the development of melanoma. This question is addressed in Chapter 2 and Chapter 3. Still relatively little is known about methylation alterations in dysplastic naevi and it remains challenging to distinguish dysplastic naevus from early-stage primary melanoma. In Chapter 4 we aimed to examine promoter CpG island hypermethylation in dysplastic naevi and to investigate the diagnostic value of the methylation status of a five-gene panel in distinguishing primary melanoma from dysplastic naevus. In Chapter 5, gene expression differences between melanocytes from dysplastic naevus and melanocytes from normal skin are examined. Up to now only few (epi)genetic alterations have been identified that confer the capacity to melanoma cells for invasion and dissemination. Much of the genetic and epigenetic basis of the metastatic capacity of melanoma remains unknown. Our aim in Chapter 6 was to investigate differential methylation events in primary melanoma with and without metastatic capacity and whether these events have prognostic value in predicting metastatic disease. Finally in Chapter 7, the results described in Chapters 2 to 6 are summarized and put into perspective with existent literature. It is also discussed to which extent the set aims at the start of this thesis have been met and what additional experiments are needed to answer remaining questions.

References

1. Saldanha, G. *et al.* Cutaneous melanoma subtypes show different BRAF and NRAS mutation frequencies. *Clin. Cancer Res.* **12**(15), 4499-4505 (2006).
2. Balch, C.M. *et al.* Final version of 2009 AJCC melanoma staging and classification. *J. Clin. Oncol.* **27**(36), 6199-6206 (2009).
3. Johnson, D.B. and Sosman, J.A. Update on the targeted therapy of melanoma. *Curr. Treat. Options. Oncol.* **14**(2), 280-292 (2013).
4. Hollestein, L.M. *et al.* Trends of cutaneous melanoma in The Netherlands: increasing incidence rates among all Breslow thickness categories and rising mortality rates since 1989. *Ann. Oncol.* **23**(2), 524-530 (2012).
5. Armstrong, B.K. and Kricker, A. The epidemiology of UV induced skin cancer. *J. Photochem. Photobiol. B* **63**(1-3), 8-18 (2001).
6. Tucker, M.A. and Goldstein, A.M. Melanoma etiology: where are we? *Oncogene* **22**(20), 3042-3052 (2003).
7. Gandini, S. *et al.* Meta-analysis of risk factors for cutaneous melanoma: III. Family history, actinic damage and phenotypic factors. *Eur. J. Cancer* **41**(14), 2040-2059 (2005).
8. Gandini, S. *et al.* Meta-analysis of risk factors for cutaneous melanoma: II. Sun exposure. *Eur. J. Cancer* **41**(1), 45-60 (2005).
9. Gandini, S. *et al.* Meta-analysis of risk factors for cutaneous melanoma: I. Common and atypical naevi. *Eur. J. Cancer* **41**(1), 28-44 (2005).
10. Falchi, M. *et al.* Genome-wide association study identifies variants at 9p21 and 22q13 associated with development of cutaneous nevi. *Nat. Genet.* **41**(8), 915-919 (2009).
11. Gudbjartsson, D.F. *et al.* ASIP and TYR pigmentation variants associate with cutaneous melanoma and basal cell carcinoma. *Nat. Genet.* **40**(7), 886-891 (2008).
12. Gruis, N.A. *et al.* Homozygotes for CDKN2 (p16) germline mutation in Dutch familial melanoma kindreds. *Nat. Genet.* **10**(3), 351-353 (1995).
13. Bishop, D.T. *et al.* Geographical variation in the penetrance of CDKN2A mutations for melanoma. *J. Natl. Cancer Inst.* **94**(12), 894-903 (2002).
14. Vasen, H.F. *et al.* Risk of developing pancreatic cancer in families with familial atypical multiple mole melanoma associated with a specific 19 deletion of p16 (p16-Leiden). *Int. J. Cancer* **87**(6), 809-811 (2000).
15. Elder, D.E. Dysplastic naevi: an update. *Histopathology* **56**(1), 112-120 (2010).
16. Friedman, R.J. *et al*. The "dysplastic" nevus. *Clin. Dermatol.* **27**(1), 103-115 (2009).
17. Tucker, M.A. Melanoma epidemiology. *Hematol. Oncol. Clin. North Am.* **23**(3), 383-95, vii (2009).
18. Hussein, M.R. Melanocytic dysplastic naevi occupy the middle ground between benign melanocytic naevi and cutaneous malignant melanomas: emerging clues. *J. Clin. Pathol.* **58**(5), 453-456 (2005).
19. Pavel, S. *et al.* Disturbed melanin synthesis and chronic oxidative stress in dysplastic naevi. *Eur. J. Cancer* **40**(9), 1423-1430 (2004).
20. Alekseenko, A. *et al.* Cyclin D1 and D3 expression in melanocytic skin lesions. *Arch. Dermatol. Res.* **302**(7), 545-550 (2010).
21. Levin, D.B. *et al.* Detection of p53 mutations in benign and dysplastic nevi. *Cancer Res.* **55**(19), 4278-4282 (1995).
22. Prieto, V.G. *et al.* Galectin-3 expression is associated with tumor progression and pattern of sun exposure in melanoma. *Clin. Cancer Res.* **12**(22), 6709-6715 (2006).
23. Sharma, B.K. *et al.* Aberrant DNA methylation silences the novel heat shock protein H11 in melanoma but not benign melanocytic lesions. *Dermatology* **213**(3), 192-199 (2006).
24. Clark, W.H., Jr. *et al.* A study of tumor progression: the precursor lesions of superficial spreading and nodular melanoma. *Hum. Pathol.* **15**(12), 1147-1165 (1984).
25. Naeyaert, J.M. and Brochez, L. Clinical practice. Dysplastic nevi. *N. Engl. J. Med.* **349**(23), 2233-2240 (2003).
26. Tsao, H. *et al.* The transformation rate of moles (melanocytic nevi) into cutaneous melanoma: a population-based estimate. *Arch. Dermatol.* **139**(3), 282-288 (2003).
27. Park, W.S. *et al.* Allelic deletion at chromosome 9p21(p16) and 17p13(p53) in microdissected sporadic dysplastic nevus. *Hum. Pathol.* **29**(2), 127-130 (1998).
28. Pollock, P.M. *et al.* High frequency of BRAF mutations in nevi. *Nat. Genet.* **33**(1), 19-20 (2003).
29. Sini, M.C. *et al.* Molecular alterations at chromosome 9p21 in melanocytic naevi and melanoma. *Br. J. Dermatol.* **158**(2), 243-250 (2008).

30. Bogdan, I. *et al.* Melanoma ex naevo: a study of the associated naevus. *Melanoma Res.* **13**(2), 213-217 (2003).
31. Dadzie, O.E. *et al.* RAS and RAF mutations in banal melanocytic aggregates contiguous with primary cutaneous melanoma: clues to melanomagenesis. *Br. J. Dermatol.* **160**(2), 368-375 (2009).
32. Eskandarpour, M. *et al.* Frequency of UV-inducible NRAS mutations in melanomas of patients with germline CDKN2A mutations. *J. Natl. Cancer Inst.* **95**(11), 790-798 (2003).
33. Mooi, W.J. and Peeper, D.S. Oncogene-induced cell senescence--halting on the road to cancer. *N. Engl. J. Med.* **355**(10), 1037-1046 (2006).
34. Miller, A.J. and Mihm, M.C., Jr. Melanoma. *N. Engl. J. Med.* **355**(1), 51-65 (2006).
35. Michaloglou, C. *et al.* BRAF(E600) in benign and malignant human tumours. *Oncogene* **27**(7), 877-895 (2008).
36. Rubinstein, J.C. *et al.* Incidence of the V600K mutation among melanoma patients with BRAF mutations, and potential therapeutic response to the specific BRAF inhibitor PLX4032. *J. Transl. Med.* **8**, 67 (2010).
37. Demunter, A. *et al.* A novel N-ras mutation in malignant melanoma is associated with excellent prognosis. *Cancer Res.* **61**(12), 4916-4922 (2001).
38. Chin, L., Garraway, L.A., and Fisher, D.E. Malignant melanoma: genetics and therapeutics in the genomic era. *Genes Dev.* **20**(16), 2149-2182 (2006).
39. Flaherty, K.T., Hodi, F.S., and Fisher, D.E. From genes to drugs: targeted strategies for melanoma. *Nat. Rev. Cancer* **12**(5), 349-361 (2012).
40. Hodis, E. *et al.* A landscape of driver mutations in melanoma. *Cell* **150**(2), 251-263 (2012).
41. Daniotti, M. *et al.* BRAF alterations are associated with complex mutational profiles in malignant melanoma. *Oncogene* **23**(35), 5968-5977 (2004).
42. Tsao, H. *et al.* Genetic interaction between NRAS and BRAF mutations and PTEN/MMAC1 inactivation in melanoma. *J. Invest Dermatol.* **122**(2), 337-341 (2004).
43. Inoue-Narita, T. *et al.* Pten deficiency in melanocytes results in resistance to hair graying and susceptibility to carcinogen-induced melanomagenesis. *Cancer Res.* **68**(14), 5760-5768 (2008).
44. Serrano, M. *et al.* Role of the INK4a locus in tumor suppression and cell mortality. *Cell* **85**(1), 27-37 (1996).
45. Vredeveld, L.C. *et al.* Abrogation of BRAFV600E-induced senescence by PI3K pathway activation contributes to melanomagenesis. *Genes Dev.* **26**(10), 1055-1069 (2012).
46. Yokoyama, S. *et al.* A novel recurrent mutation in MITF predisposes to familial and sporadic melanoma. *Nature* **480**(7375), 99-103 (2011).
47. Takata, M., Murata, H., and Saida, T. Molecular pathogenesis of malignant melanoma: a different perspective from the studies of melanocytic nevus and acral melanoma. *Pigment Cell Melanoma Res.* **23**(1), 64-71 (2010).
48. Stark, M.S. *et al.* Frequent somatic mutations in MAP3K5 and MAP3K9 in metastatic melanoma identified by exome sequencing. *Nat. Genet.* **44**(2), 165-169 (2012).
49. Ramakrishnan, V. Histone structure and the organization of the nucleosome. *Annu. Rev. Biophys. Biomol. Struct.* **26**, 83-112 (1997).
50. Back, F. The variable condition of euchromatin and heterochromatin. *Int. Rev. Cytol.* **45**, 25-64 (1976).
51. Craig, J.M. Heterochromatin--many flavours, common themes. *Bioessays* **27**(1), 17-28 (2005).
52. Wolffe, A.P. New insights into chromatin function in transcriptional control. *FASEB J.* **6**(15), 3354-3361 (1992).
53. Mueller-Planitz, F., Klinker, H., and Becker, P.B. Nucleosome sliding mechanisms: new twists in a looped history. *Nat. Struct. Mol. Biol.* **20**(9), 1026-1032 (2013).
54. Jenuwein, T. and Allis, C.D. Translating the histone code. *Science* **293**(5532), 1074-1080 (2001).
55. Musselman, C.A. *et al.* Perceiving the epigenetic landscape through histone readers. *Nat. Struct. Mol. Biol.* **19**(12), 1218-1227 (2012).
56. Herman, J.G. and Baylin, S.B. Gene silencing in cancer in association with promoter hypermethylation. *N. Engl. J. Med.* **349**(21), 2042-2054 (2003).
57. Wade, P.A. Methyl CpG binding proteins: coupling chromatin architecture to gene regulation. *Oncogene* **20**(24), 3166-3173 (2001).
58. Dahl, C., Gronbaek, K., and Guldberg, P. Advances in DNA methylation: 5-hydroxymethylcytosine revisited. *Clin. Chim. Acta* **412**(11-12), 831-836 (2011).
59. Berry, A.C. Rubinstein-Taybi syndrome. *J. Med. Genet.* **24**(9), 562-566 (1987).
60. Lim, D.H. and Maher, E.R. Human imprinting syndromes. *Epigenomics.* **1**(2), 347-369 (2009).

61. Van den Veyver, I.B. and Zoghbi, H.Y. Methyl-CpG-binding protein 2 mutations in Rett syndrome. *Curr. Opin. Genet. Dev.* **10**(3), 275-279 (2000).
62. Jones, P.A. and Baylin, S.B. The epigenomics of cancer. *Cell* **128**(4), 683-692 (2007).
63. Jansen, A. and Verstrepen, K.J. Nucleosome positioning in Saccharomyces cerevisiae. *Microbiol. Mol. Biol. Rev.* **75**(2), 301-320 (2011).
64. Feinberg, A.P. and Vogelstein, B. Hypomethylation distinguishes genes of some human cancers from their normal counterparts. *Nature* **301**(5895), 89-92 (1983).
65. Gama-Sosa, M.A. *et al.* The 5-methylcytosine content of DNA from human tumors. *Nucleic Acids Res.* **11**(19), 6883-6894 (1983).
66. Bedford, M.T. and van Helden, P.D. Hypomethylation of DNA in pathological conditions of the human prostate. *Cancer Res.* **47**(20), 5274-5276 (1987).
67. Kim, Y.I. *et al.* Global DNA hypomethylation increases progressively in cervical dysplasia and carcinoma. *Cancer* **74**(3), 893-899 (1994).
68. Lin, C.H. *et al.* Genome-wide hypomethylation in hepatocellular carcinogenesis. *Cancer Res.* **61**(10), 4238-4243 (2001).
69. Wahlfors, J. *et al.* Genomic hypomethylation in human chronic lymphocytic leukemia. *Blood* **80**(8), 2074-2080 (1992).
70. Hanahan, D. and Weinberg, R.A. The hallmarks of cancer. *Cell* **100**(1), 57-70 (2000).
71. Tuck-Muller, C.M. *et al.* DNA hypomethylation and unusual chromosome instability in cell lines from ICF syndrome patients. *Cytogenet. Cell Genet.* **89**(1-2), 121-128 (2000).
72. Feinberg, A.P. and Vogelstein, B. Hypomethylation of ras oncogenes in primary human cancers. *Biochem. Biophys. Res. Commun.* **111**(1), 47-54 (1983).
73. Cooper, D.N. Eukaryotic DNA methylation. *Hum. Genet.* **64**(4), 315-333 (1983).
74. Ehrlich, M. DNA methylation in cancer: too much, but also too little. *Oncogene* **21**(35), 5400-5413 (2002).
75. Jones, P.A. and Baylin, S.B. The fundamental role of epigenetic events in cancer. *Nat. Rev. Genet.* **3**(6), 415-428 (2002).
76. Freedberg, D.E. *et al.* Frequent p16-independent inactivation of p14ARF in human melanoma. *J. Natl. Cancer Inst.* **100**(11), 784-795 (2008).
77. Gonzalgo, M.L. *et al.* Low frequency of p16/CDKN2A methylation in sporadic melanoma: comparative approaches for methylation analysis of primary tumors. *Cancer Res.* **57**(23), 5336-5347 (1997).
78. Mirmohammadsadegh, A. *et al.* Epigenetic silencing of the PTEN gene in melanoma. *Cancer Res.* **66**(13), 6546-6552 (2006).
79. Tsutsumida, A. *et al.* Epigenetic silencing of E- and P-cadherin gene expression in human melanoma cell lines. *Int. J. Oncol.* **25**(5), 1415-1421 (2004).
80. Spugnardi, M. *et al.* Epigenetic inactivation of RAS association domain family protein 1 (RASSF1A) in malignant cutaneous melanoma. *Cancer Res.* **63**(7), 1639-1643 (2003).
81. Wada, K. *et al.* Aberrant expression of the maspin gene associated with epigenetic modification in melanoma cells. *J. Invest Dermatol.* **122**(3), 805-811 (2004).
82. Worm, J. *et al.* Aberrant p27Kip1 promoter methylation in malignant melanoma. *Oncogene* **19**(44), 5111-5115 (2000).
83. Worm, J. *et al.* Genetic and epigenetic alterations of the APC gene in malignant melanoma. *Oncogene* **23**(30), 5215-5226 (2004).
84. Furuta, J. *et al.* Silencing of Peroxiredoxin 2 and aberrant methylation of 33 CpG islands in putative promoter regions in human malignant melanomas. *Cancer Res.* **66**(12), 6080-6086 (2006).
85. Hoon, D.S. *et al.* Profiling epigenetic inactivation of tumor suppressor genes in tumors and plasma from cutaneous melanoma patients. *Oncogene* **23**(22), 4014-4022 (2004).
86. Liu, S. *et al.* Identification of novel epigenetically modified genes in human melanoma via promoter methylation gene profiling. *Pigment Cell Melanoma Res.* **21**(5), 545-558 (2008).
87. Marini, A. *et al.* Epigenetic inactivation of tumor suppressor genes in serum of patients with cutaneous melanoma. *J. Invest Dermatol.* **126**(2), 422-431 (2006).
88. Tanemura, A. *et al.* CpG island methylator phenotype predicts progression of malignant melanoma. *Clin. Cancer Res.* **15**(5), 1801-1807 (2009).
89. Friedman, S. The effect of 5-azacytidine on E. coli DNA methylase. *Biochem. Biophys. Res. Commun.* **89**(4), 1328-1333 (1979).
90. Jones, P.A. and Taylor, S.M. Cellular differentiation, cytidine analogs and DNA methylation. *Cell* **20**(1), 85-93 (1980).

91. Muthusamy, V. *et al.* Epigenetic silencing of novel tumor suppressors in malignant melanoma. *Cancer Res.* **66**(23), 11187-11193 (2006).
92. Nobeyama, Y. *et al.* Silencing of tissue factor pathway inhibitor-2 gene in malignant melanomas. *Int. J. Cancer* **121**(2), 301-307 (2007).
93. Ballestar, E. *et al.* Methyl-CpG binding proteins identify novel sites of epigenetic inactivation in human cancer. *EMBO J.* **22**(23), 6335-6345 (2003).
94. Weber, M. *et al.* Chromosome-wide and promoter-specific analyses identify sites of differential DNA methylation in normal and transformed human cells. *Nat. Genet.* **37**(8), 853-862 (2005).
95. Koga, Y. *et al.* Genome-wide screen of promoter methylation identifies novel markers in melanoma. *Genome Res.* **19**(8), 1462-1470 (2009).
96. Bonazzi, V.F. *et al.* Cross-platform array screening identifies COL1A2, THBS1, TNFRSF10D and UCHL1 as genes frequently silenced by methylation in melanoma. *PLoS. One.* **6**(10), e26121 (2011).
97. Sigalotti, L. *et al.* Whole genome methylation profiles as independent markers of survival in stage IIIC melanoma patients. *J. Transl. Med.* **10**, 185 (2012).
98. Conway, K. *et al.* DNA-methylation profiling distinguishes malignant melanomas from benign nevi. *Pigment Cell Melanoma Res.* **24**(2), 352-360 (2011).

Chapter 2

Genome-wide promoter methylation analysis identifies epigenetic silencing of *MAPK13* in primary cutaneous melanoma

Linda Gao[1], Marjon A. Smit[2], Joost J. van den Oord[3], Jelle J. Goeman[4], Els M. E. Verdegaal[5], Sjoerd H. van der Burg[5], Marguerite Stas[6], Samuel Beck[7], Nelleke A. Gruis[1], Cornelis P. Tensen[1], Rein Willemze[1], Daniel S. Peeper[2,*] and Remco van Doorn[1,*]

[1]Department of Dermatology, Leiden University Medical Center, Leiden, The Netherlands
[2]Division of Molecular Oncology, The Netherlands Cancer Institute, Amsterdam, The Netherlands
[3]Department of Pathology, KU Leuven, Leuven, Belgium
[4]Department of Medical Statistics, Leiden University Medical Center, Leiden, The Netherlands
[5]Department of Clinical Oncology, Leiden University Medical Center, Leiden, The Netherlands
[6]Department of Surgical Oncology, KU Leuven, Leuven, Belgium
[7]Leiden Cytology and Pathology Laboratory, Leiden, The Netherlands
*These authors contributed equally to this work.

Pigment Cell & Melanoma Research 2013; 26(4):542-54

Abstract

The involvement of epigenetic alterations in the pathogenesis of melanoma is increasingly recognized. Here, we performed genome-wide DNA methylation analysis of primary cutaneous melanoma and benign melanocytic naevus interrogating 14,495 genes using BeadChip technology. This genome-wide view of promoter methylation in primary cutaneous melanoma revealed an array of recurrent DNA methylation alterations with potential diagnostic applications. Among 106 frequently hypermethylated genes, there were many novel methylation targets and tumor suppressor genes. Highly recurrent methylation of the *HOXA9*, *MAPK13*, *CDH11*, *PLEKHG6*, *PPP1R3C*, and *CLDN11* genes was established. Promoter methylation of *MAPK13*, encoding p38δ, was present in 67% of primary and 85% of metastatic melanomas. Restoration of MAPK13 expression in melanoma cells exhibiting epigenetic silencing of this gene reduced proliferation, indicative of tumor suppressive functions. This study demonstrates that DNA methylation alterations are widespread in melanoma and suggests that epigenetic silencing of *MAPK13* contributes to melanoma progression.

Introduction

Cutaneous melanoma is a malignancy arising from melanocytes residing in the skin. The mortality rate of melanoma is high due to its propensity to metastasize and resistance to chemotherapy. The pathological diagnosis, especially distinction of early stage melanoma from benign melanocytic naevus, can be difficult. Also determination of the prognosis and prediction whether metastatic disease will develop is often troublesome. In spite of the recent advent of kinase inhibitors and immunomodulatory treatments, the prognosis of patients with disseminated disease remains poor. Recent years have seen major advances in our understanding of the genetics of melanoma with the identification of recurrent somatic mutations in multiple oncogenes and tumor suppressor genes[1,2]. Mutations in the *BRAF* and *NRAS* oncogenes are the most important drivers of melanoma development, activating the mitogen-activated protein kinase (MAPK) pathway that mediates proliferative signals. This signaling pathway is additionally disrupted in melanoma by recurrent mutations in *MAP2K1*, *MAP2K2*, *MAP3K5*, and *MAP3K9*[3,4].

Cancer genomes are not only characterized by the presence of mutations and chromosomal aberrations, but also by epigenetic alterations. Aberrant methylation of CpG islands located in gene promoters is an epigenetic mechanism with an essential role in tumorigenesis. Promoter hypermethylation is associated with transcriptional downregulation affecting a multitude of genes in cancer cells. DNA methylation often manifests in tumor type-specific patterns and in melanoma several established tumor suppressor genes are affected by promoter hypermethylation. Conversely, tumor

genomes exhibit DNA hypomethylation, which may promote genomic instability and inappropriate gene expression[5,6].

Melanoma cells acquire the capacity for unrestrained proliferation, escape from cellular senescence, evasion of apoptosis, and metastatic dissemination during disease progression. There is increasing appreciation for the impact of DNA methylation alterations in conferring these malignant characteristics to incipient tumor cells[7]. Hence, the delineation of epigenetic alterations in melanoma could be applied in the molecular diagnosis and prognosis of melanoma. In addition, there are possible therapeutic implications as epigenetic alterations, as opposed to genetic abnormalities, can be pharmacologically reversed. Furthermore, recent findings showing the significant loss of DNA hydroxymethylation in melanoma as well as occurrence of mutations in *IDH1*, *EZH2*, *ARID2*, and other *SWI/SNF* complex members underscore the role of epigenetic deregulation in melanoma tumorigenesis[2,8].

Studies on DNA methylation in melanoma published thus far have mostly employed candidate gene approaches on melanoma metastatic lesions or cell lines[6]. In this study, we characterized promoter methylation on a genome-wide scale by generating epigenomic maps with BeadChip technology that quantifies the methylation levels of 14,495 human genes in primary cutaneous melanomas and benign melanocytic naevi. This approach enabled the identification of many novel and highly recurrent hypermethylated genes in primary melanoma. Our results show that melanoma is characterized by widespread epigenetic alterations, with multiple genes selectively affected by methylation at high frequency. Several hypermethylated genes have tumor suppressive properties, further supporting the contribution of epigenetic deregulation to the pathogenesis of melanoma.

Methods

Patient samples

Fresh-frozen biopsy specimens were obtained from primary cutaneous melanoma tumors of 24 patients. Detailed clinicopathological characteristics of these primary cutaneous melanoma biopsies can be found in Table S1A. As controls, fresh-frozen biopsy specimens from benign nevoid lesions of five individuals were obtained. Handling and review of melanoma and naevus samples were performed as previously described[9]. Briefly, frozen naevus and primary melanoma excision samples were sectioned, and the percentage of naevus or melanoma cells were assessed on an H&E-stained section. Only cases in which at least 70% of the cells were naevus or melanoma cells were included. Subsequently, four 10 µm thick sections were cut, and finally, another H&E section was made and analyzed to confirm the percentage of naevus or melanoma cells. All 29 samples were subjected to genome-wide promoter methylation analysis. *BRAF* and *NRAS* mutation status of the

biopsy specimens was determined using allele-specific PCRs for detection of $BRAF^{V600E}$, $BRAF^{V600K}$, $NRAS^{G12D}$, $NRAS^{Q61K}$, $NRAS^{Q61L}$, $NRAS^{Q61R}$, and $NRAS^{Q61H}$ mutations on a CFX384 Real-Time Detection System (Bio-Rad, Hercules, CA, USA) as previously described[10]. For validation of identified methylation targets, an independent sample set of BFPE (fixed in Boonfix and embedded in paraffin) biopsy specimens from primary cutaneous melanoma tumors of 15 patients and fresh-frozen biopsy samples from benign nevoid lesions of 10 individuals was used. All skin biopsy specimens were required to contain at least 70% melanocytic cells. For additional validation analyses of methylation status, an extra sample set of fresh-frozen biopsy specimens from melanoma cutaneous metastases of seven patients and cultured melanoma cell lines was used. To obtain the cell lines, melanoma cells were isolated from melanoma metastases of 13 patients and cultured briefly in DMEM+ GlutaMax-I (Gibo, Carlsbad, CA, USA) supplemented with 10% fetal bovine serum (Thermo Scientific, Waltham, MA, USA), 100 units/ml penicillin, and 0.1 mg/ml streptomycin (Gibco). Clinical information on the patients of which the cell lines were derived can be found in Table S1B. DNA from all samples was extracted using either the Genomic Tip kit (Qiagen, Hilden, Germany) or RecoverAll Nucleic Acid kit (Ambion, Carlsbad, CA, USA), followed by bisulfite conversion with the EZ DNA methylation kit (Zymo Research, Orange, CA, USA). Completeness of conversion was tested for each sample by direct bisulfite sequencing analysis of three gene promoters with known methylation status.

Illumina Infinium methylation assay and statistical analysis

The Infinium methylation assay was performed at a certified Illumina service provider (Service XS, Leiden, The Netherlands). Bisulfite-converted DNA was hybridized onto Infinium HumanMethylation27 BeadChips (Illumina, San Diego, CA, USA) following manufacturer's protocol. Resulting β-values from the Infinium methylation assay, ranging from 0 to 1, were quantile normalized to correct for unequal distributions within and between samples due to technical variation. Average β-values were calculated for the primary melanoma and naevus sample groups. To find differential methylation distributions, we applied a statistical test that was able to detect both consistent as sporadically occurring differential methylation alterations across the melanoma and naevus sample groups[11]. *P* values for this test were robustly calculated by permutations. Multiple testing correction was performed with Benjamini and Hochberg's False Discovery Rate method[12]. To generate Heatmap colors, relative β-values were calculated by scaling β-values per sample to the existing range of β-values over all samples for each individual probe plotted.

Bisulphite melting curve analysis (BMCA) and bisulphite sequencing analysis (BSA)

Bisulfite primer sequences were designed to amplify CpG islands located in the promoter region of the genes of interest, encompassing or in close proximity of the corresponding 50-mer probe sequence on the BeadChip (Table S2A, Figure S1). Sensitivity of each bisulfite primer set was validated using mixtures, 1:1, 1:3, 1:9, and 1:9.5, of completely methylated CpGenome universal methylated DNA (Chemicon, Hampshire, UK) and unmethylated semen DNA, respectively. This showed that methylation could accurately be detected whether at least 10% of total analyzed DNA was methylated. In BMCA, melting curves were generated for CpG island amplicons of candidate gene promoters. A promoter was considered methylated if the melting temperature peak corresponding to methylated DNA had a height of 0.5 or more relative to the melting curve peak corresponding to unmethylated DNA for this sample. For BSA, promoter methylation was defined as a density of methylated CpG dinucleotides in the CpG island amplicon of 15% or more, a threshold value used in previous studies[13,14].

5-aza-2'-deoxycytidine treatment

Melanoma cell lines 06.24 and 94.13 were used for demethylation experiments where cells seeded at 15% confluency were treated with 2 µM 5-aza-2'-deoxycytidine (Decitabine; Sigma, St. Louis, MO, USA) for 96 hrs. Culture medium was replaced with medium containing freshly prepared 5-aza-2'-deoxycytidine every 24h. Cells were harvested for RNA extraction with the RNeasy Mini kit (Qiagen). RNA was DNase treated with RQ1 RNase-free DNase (Promega, Madison, WI, USA) before cDNA was generated using the iScript cDNA synthesis kit (Bio-Rad). qRT-PCR was performed with iQ SYBR Green Supermix on a MyiQ Real-Time PCR Detection System (Bio-Rad). qRT-PCR primers were designed to span exon-exon barriers (Table S2B). Expression of the reference genes *TBP* and *CPSF6* was validated using geNorm analysis[15].

Viral transduction of human melanoma cells, fibroblasts, and melanocytes

The pcDNA3.1-HA, pcDNA3.1-HA-MAPK13-WT, pcDNA3.1-HAMAPK13-D176A, and pcDNA3.1-HA-MAPK13-F324S constructs were kindly provided by Dr. D. Engelberg and subcloned into the Moloney murine leukemia virus (MoMuLV)-based pBABE retroviral vector with a puromycin expression cassette (pBABE-puro)[16]. The melanoma cell lines 634, 453A0, 93.08, 9304C, and 04.07 (Table S1B), the human fibroblast cell line TIG-3 (expressing the ecotropic receptor, *hTERT*, and shRNA targeting $p16^{INK4A}$), Phoenix, and HEK293T cells were cultured in DMEM (Gibco) supplemented with 9% fetal bovine serum (PAA Laboratories GmbH, Pasching, Austria), 2 mM glutamine, 100 U/ml penicillin, and 0.1 mg/ml streptomycin (Gibco). Human melanocytes were isolated from the epidermis of neonatal foreskins[17], and cultured in Medium 254 (Cascade Biologics) supplemented with melanocyte growth supplement (HMGS, Cascade Biologics), 100 U/ml penicillin, and 0.1

mg/ml streptomycin (Gibco). For retroviral transduction, Phoenix cells were used as producers of retrovirus. Production of retrovirus was performed as described (http://www.stanford.edu/group/nolan/retroviral_systems/phx.html). For proliferation assays of the melanoma cell lines, cells were transduced with retrovirus encoding either of the pBABE-puro-p38δ expression constructs, selected for successful proviral integration by puromycin, and seeded at equal numbers for either incubation with BrdU for 1.5h 9–12 days post-infection, fixed and stained with crystal violet 15–19 days post-infection or counted every 3–4 days starting at 3 days post-infection for at least 3 weeks. Samples were harvested for Western blot analysis 9 days post-infection. For proliferation assays of the fibroblast cell line TIG-3, cells were transduced with shRNA-encoding retrovirus, selected with puromycin, and plated at equal densities for transduction with $BRAF^{V600E}$-encoding retrovirus, followed by blasticidin selection. Cells were subsequently seeded at equal numbers and either incubated for 1.5h with BrdU 3 days post-infection or fixed and stained with crystal violet 3-7 days post-infection. Samples were harvested for Western blot analysis 2 days post-infection. For lentiviral transduction, HEK293T cells were used as producers of lentivirus; production of lentivirus was performed as previously described[18]. Human melanocytes were transduced with shRNA-encoding lentivirus, cultured for one week, and transduced with $BRAF^{V600E}$-encoding lentivirus followed by selection with blasticidin. Cells were seeded at equal numbers, analyzed for BrdU incorporation, fixed and stained with crystal violet, and harvested for Western blot analysis 15 days post-infection. For Western blot, antibodies against BRAF (sc-5284; Santa Cruz Biotechnology, Dallas, TX, USA), MAPK13 (AF1519; R&D Systems, Abingdon, UK), *β*-actin (AC-74; Sigma), and α-tubulin (T5168; Sigma) were used.

Database Accession numbers

The data discussed in this publication have been deposited in NCBI's Gene Expression Omnibus[19], and are accessible through GEO Series accession number GSE45266 (http://www.ncbi.nlm.nih.gov/geo/query/acc.cgi?acc=GSE45266).

Results

Genome-wide DNA methylation profiling of primary cutaneous melanomas and naevi

DNA methylation profiles of 24 primary cutaneous melanomas and five benign naevi were generated with Infinium BeadChip technology that interrogates 27,578 CpG loci in the promoter regions of 14,495 genes at single-nucleotide resolution. Normalized *β*-values were used as a measure of methylation and showed a bimodal distribution indicating the presence of a distinct subset of methylated CpG loci in the investigated samples among a large number of unmethylated CpG loci (Figure 1A). Detailed information on each melanoma and naevus sample can be found in Table S1A. The DNA methylation profiles of

the primary melanomas and benign naevi showed an almost complete separation with the exception of one naevus sample (N3) that segregated with a primary melanoma sample (PM6) (Figure 1B). We suspect that aberrant clustering of this naevus sample is due to non-biological sources of variation in methylation BeadChip results, as the methylation pattern of this benign naevus for the most differentially methylated genes is distinct from those of primary melanomas and similar to those of other naevus samples (Figure 2A). We calculated and used the average *β*-value difference to represent methylation differences occurring between the primary melanomas and naevi. Figure 1C visualizes the average *β*-values of all interrogated probes and shows the presence of statistically significant probes with average *β*-value difference exceeding 0.2 or less than 0.2 between the primary melanomas and naevi, indicating the presence of hyper- and hypomethylated CpG loci, respectively, between the two sample groups.

We sought to identify genes aberrantly methylated in primary melanoma when compared with naevus; CpG probes that showed a significant methylation difference by comparative statistical analysis ($P < 0.05$) and had an absolute average *β*-value difference between the primary melanomas and naevi exceeding 0.2 were considered differentially methylated. Using these criteria, 120 probes corresponding to 106 unique genes were found to be hypermethylated in primary melanoma (Figure 2A); 46 probes corresponding to 44 unique genes were hypomethylated (Figure 2B). The Heatmaps in Figure 2A, B illustrate that despite heterogeneity of methylation among the primary melanoma samples, multiple gene promoters demonstrate highly recurrent and selective methylation alterations in primary melanoma. We found *HOXA9*, *C1orf106*, *HIST1H3E*, *MAPK13*, and *LEP* as the most frequently hypermethylated in primary melanoma. Among the 106 differentially hypermethylated genes, five were imprinted; *CYP1B1*, *GPT*, *KCNQ1*, *MEST*, and *NNAT*. In addition, we identified *HLA-DRA*, *SLC1A2*, *MGC35206*, *PRSS2*, and *SIRPB1* as the most frequently differentially hypomethylated genes. Several identified genes have previously been reported to be aberrantly methylated in melanoma or in other cancer types as indicated in the columns on the right (Figure 2A, B). All significantly hyper- and hypomethylated genes prioritized by average *β*-value difference can be found in Table S3A, B.

Further analysis of genes aberrantly methylated in primary melanoma

To categorize methylation events aggregating in genes of particular classes or in the same signaling pathway, we performed gene ontology analysis using the DAVID bioinformatics resource[20]. Functional classification of the 106 hypermethylated genes showed enrichment for homeobox genes (*HOXA9*, *HOXD12*, *OTP*, *VSX1*, *FOXD2*, *MSX1*), G-protein-coupled receptor genes, and genes with sulfotransferase and kinase activity. Homeobox and other genes are silenced by polycomb proteins through histone modifications that can

be co-regulated with DNA methylation. Genes hypermethylated in cancer are more frequently targets of polycomb complexes[21,22]. Correspondingly, we observed that 22 of 106 (21%) genes within our set of hypermethylated genes were validated polycomb targets[23], corresponding to a 1.8-fold enrichment for polycomb target genes. In colorectal cancer, mutant *BRAF* and *NRAS* have been found to associate with a CpG island methylator phenotype. However, the subset of *BRAF* and *NRAS* mutant melanomas did not exhibit a higher degree of CpG island methylation (average β-value for all interrogated CpG loci) and did not cluster separately, consistent with previous findings on candidate genes in melanoma cell lines[24]. We assessed whether the mitotic rate may correlate with methylation patterns, but found no significant association when analyzing hierarchical clustering data and the set of frequently hypermethylated genes in melanoma samples with high and with low mitotic rates.

Recently, exome and whole genome sequence analyses have characterized the mutational landscape of melanoma. As genetic and epigenetic mechanisms often commonly affect cancer genes, we sought to integrate our epigenetic findings with results from these studies. Among the 50 most frequently mutated genes identified in an exome sequencing study of 147 melanomas, the *COL14A1* and *SLC15A2* genes also emerged from our study as frequently hypermethylated[25]. Among the 100 genes with the most significant functional mutation burden determined by exome sequencing of 121 melanoma samples, the *PDE4DIP* gene overlapped with our set of frequently hypermethylated genes[2]. There were several genes found to be affected by genomic rearrangements in a whole genome sequencing study of 25 melanomas, including the *ANKDD1A*, *CRB1*, *EFCAB1*, *HLA-G*, *NDST4*, *PDE4DIP*, and *SERPINB5* genes that we found to be frequently hypermethylated in melanoma[1]. In particular, the *PDE4DIP* gene appears to be inactivated by genetic mechanisms as well as through promoter hypermethylation in melanoma.

Among the identified aberrantly methylated genes, we sought to delineate genes whose epigenetic deregulation might contribute to the malignant phenotype of melanoma cells. Several genes we found to be hypermethylated in melanoma are annotated by the CancerGenes resource[26] as tumor suppressor genes, including *CDH11*, *CHFR*, *GNMT*, *NR4A1*, *RARB*, and *SERPINB5*. Among the 44 hypomethylated genes, *RUNX1* and *RUNX3* have been established as oncogenes, albeit in different tumor types.

Validation of identified hypermethylated genes in primary melanoma by bisulphite melting curve analysis and bisulphite sequencing analysis

Among the 106 genes identified as differentially hypermethylated in primary melanoma, we selected *HOXA9*, *MAPK13*, *CDH11*, *PLEKHG6*, *PPP1R3C*, and *CLDN11* for validation by analysis of promoter methylation status. *HOXA9*, *MAPK13*, and *CDH11* were selected

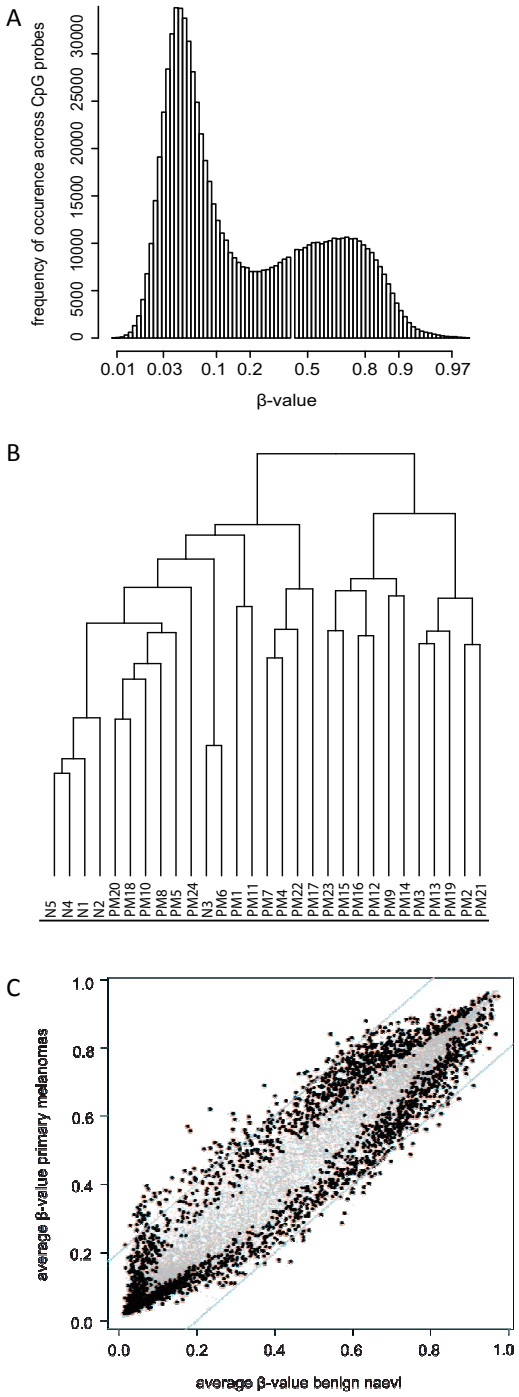

Figure 1. Distribution of genome-wide DNA methylation data in primary melanoma and naevus samples. (**A**) The frequency (vertical axis) of normalized, logit-transformed *β*-values at a range from 0 to 1 (horizontal axis) across all CpG probes on the BeadChip in all samples. Normalized *β*-values were used as a measure of methylation with a *β*-value of 0 corresponding to complete absence of methylation and a *β*-value of 1 corresponding to the presence of full methylation. (**B**) Hierarchical clustering of the 24 primary melanoma and five benign naevus samples. Clustering analysis was based on correlation distance and average linkage of the normalized *β*-values of all interrogated CpG probes. PM, primary melanoma; N, naevus. (**C**) The average *β*-values of all interrogated CpG probes in the primary melanoma sample group (vertical axis) and naevus sample group (horizontal axis) plotted as individual gray dots. CpG probes showing statistically significant differential methylation between the primary melanomas and benign naevi are depicted as black dots (P <0.05). CpG probes with average *β*-value difference between the melanoma and naevus sample groups exceeding 0.2 or less than 0.2 are located outside the diagonal lines in the scatter plot.

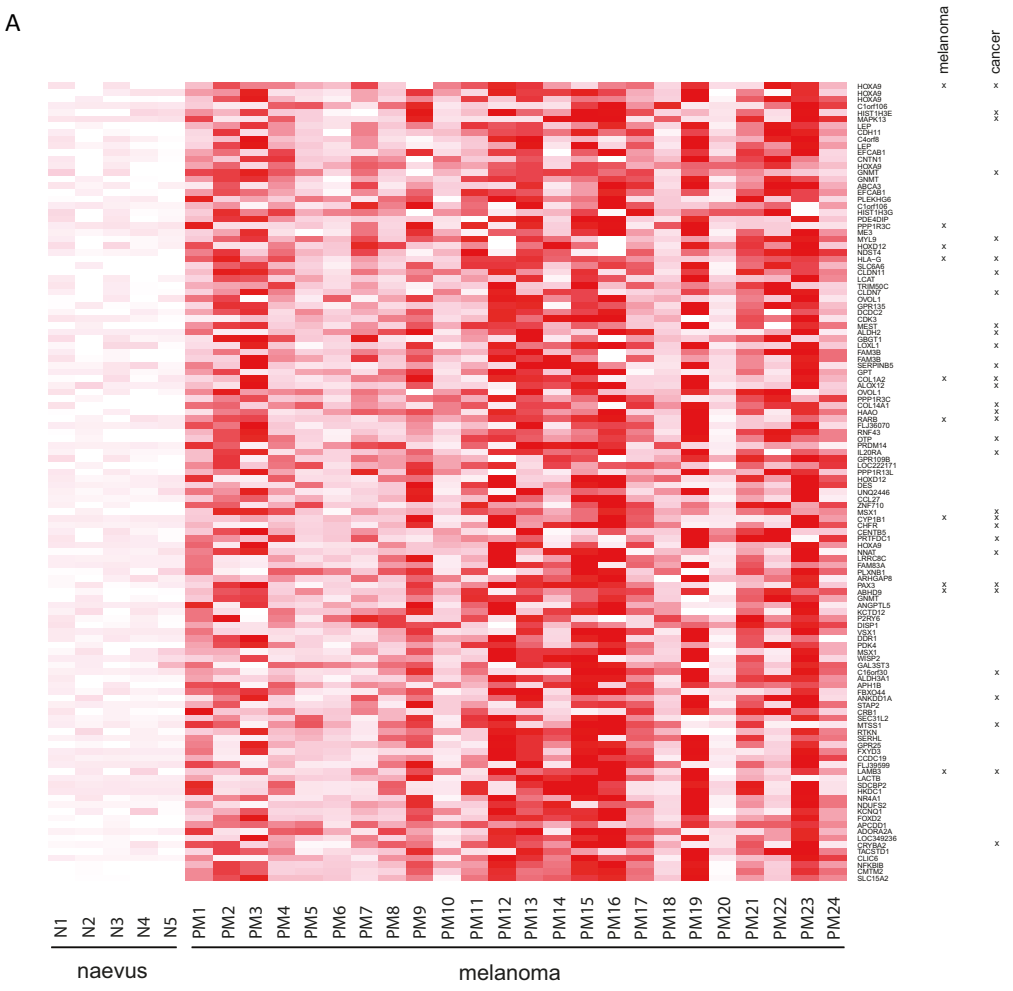

Figure 2. **Comparative analysis of the genome-wide DNA methylation data**. (**A**) Heatmap highlighting the 120 CpG probes corresponding to 106 unique genes that were identified as hypermethylated in the primary melanomas (P <0.05 and average β-value difference >0.2) when compared to naevi. Genes previously reported as hypermethylated in melanoma or other cancer types are marked with 'x' in columns on the right side. PM, primary melanoma; N, naevus.

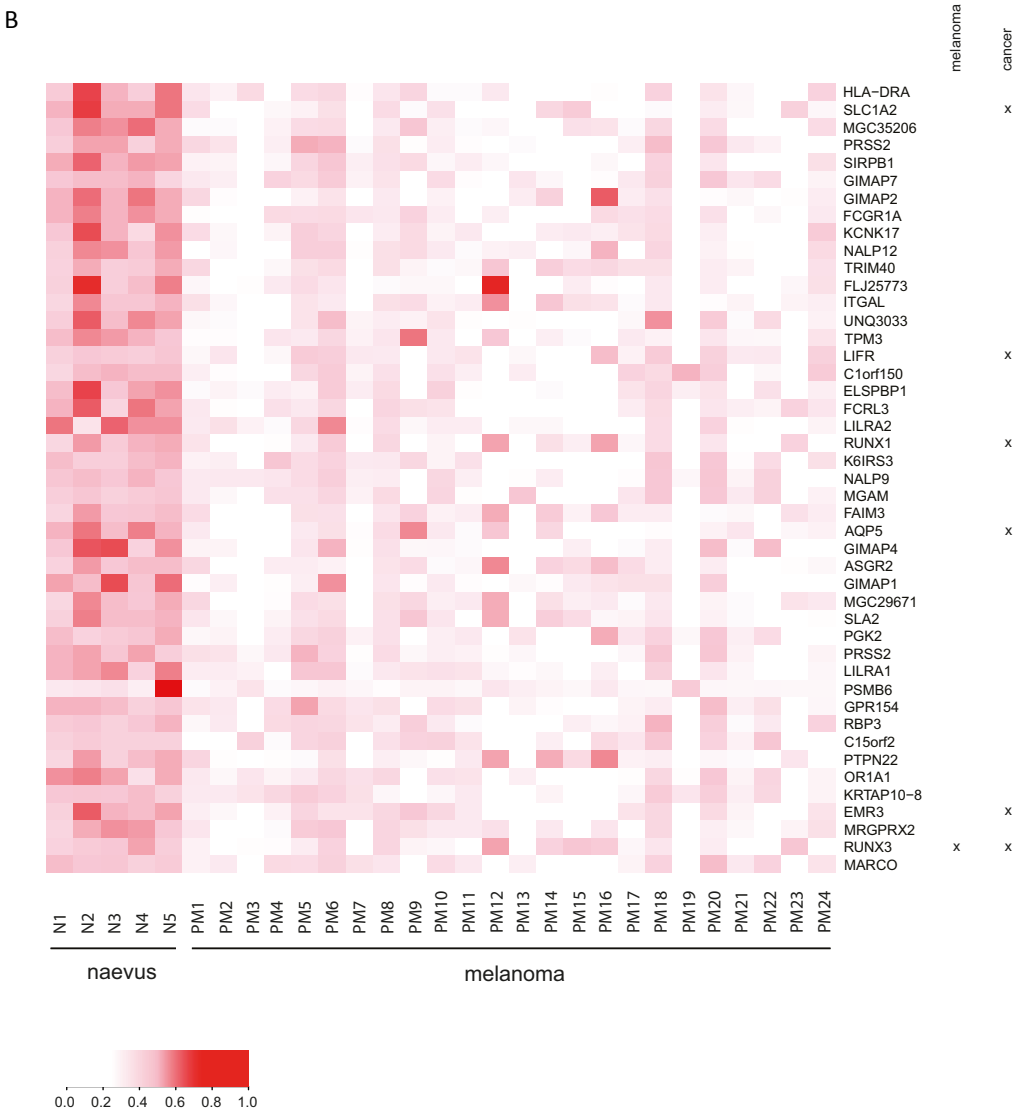

Figure 2. **Comparative analysis of the genome-wide DNA methylation data**. (**B**) Heatmap highlighting the 46 CpG probes corresponding to 44 unique genes that were found hypomethylated in primary melanomas (P <0.05 and average β-value difference <0.2) as compared to naevi. Genes previously reported as hypomethylated in melanoma or other cancer types are marked with 'x' in columns on the right side. Heatmap colors were created by scaling the β-values per sample to the existing range of β-values over all 29 investigated samples for each individual probe plotted. PM, primary melanoma; N, naevus.

based on their position in the top 10 of the most frequently hypermethylated genes; *PLEKHG6*, *PPP1R3C*, and *CLDN11* were selected based on their potential functional relevance in melanoma. Bisulfite melting curve analysis (BMCA) was used for validation on two sample sets; the first consisted of the 24 primary melanomas and five benign naevi originally subjected to genome-wide methylation analysis, the second was an independent set of 15 primary melanoma and 10 naevus biopsy specimens. Melting temperatures corresponding to the unmethylated and methylated amplicons of the six genes can be found in Table S2A. For each gene at least one primary melanoma biopsy, one melanoma cell line and one naevus biopsy were additionally analyzed with bisulfite sequencing analysis (BSA) in order to assess methylation density of the interrogated CpG island amplicons.

BMCA showed that the analyzed CpG regions of the *HOXA9*, *MAPK13*, *CDH11*, *PLEKHG6*, *PPP1R3C*, and *CLDN11* promoters were frequently methylated in the primary melanomas (Figure 3A, top graphs). In contrast, promoter methylation of *CDH11*, *PLEKHG6*, *PPP1R3C*, and *CLDN11* was absent in the naevi (Figure 3A, bottom graphs). For *MAPK13*, four naevi showed small melting curve elevations at an intermediary melting temperature, corresponding to methylation of a few single CpG dinucleotides within a further unmethylated promoter as demonstrated by BSA (Figure 3B). The *HOXA9* gene showed promoter methylation in a subset of naevus samples. Bisulfite sequencing results confirmed that the analyzed promoter regions of *HOXA9*, *MAPK13*, *CDH11*, *PLEKHG6*, *PPP1R3C*, and *CLDN11* contained a high density of methylated CpG dinucleotides in primary melanomas (Figure 3B). In summary, we found that *HOXA9*, *MAPK13*, *CDH11*, *PLEKHG6*, *PPP1R3C*, and *CLDN11* were methylated in 85, 67, 44, 67, 51, and 28% of primary melanomas, respectively, whereas significant promoter methylation of *MAPK13*, *CDH11*, *PLEKHG6*, *PPP1R3C*, and *CLDN11* could not be detected in the naevi (Table 1).

Methylation of *HOXA9*, *MAPK13*, *CDH11*, *PLEKHG6*, *PPP1R3C*, and *CLDN11* was additionally analyzed in cutaneous melanoma metastases biopsy specimens and early passage melanoma cell lines using BMCA and BSA (Figure S2), showing that an even higher percentage of these samples was hypermethylated for the analyzed genes (Table 1). In one of the early passage melanoma cell lines, methylation of *MAPK13* was mono-allelic, whereas methylation was bi-allelic in 12 of 13 melanoma cell lines. For tumor biopsies, which contain admixed skin-resident cells, mono-allelic cannot be reliably distinguished from bi-allelic methylation using BMCA.

MAPK13 is epigenetically silenced in melanoma cells

Next, we analyzed whether promoter methylation of *MAPK13*, *CDH11*, and *PLEKHG6* was associated with gene silencing. Melanoma cell lines 06.24 and 94.13 were included in our panel of 13 melanoma cell lines used for validation experiments and demonstrated

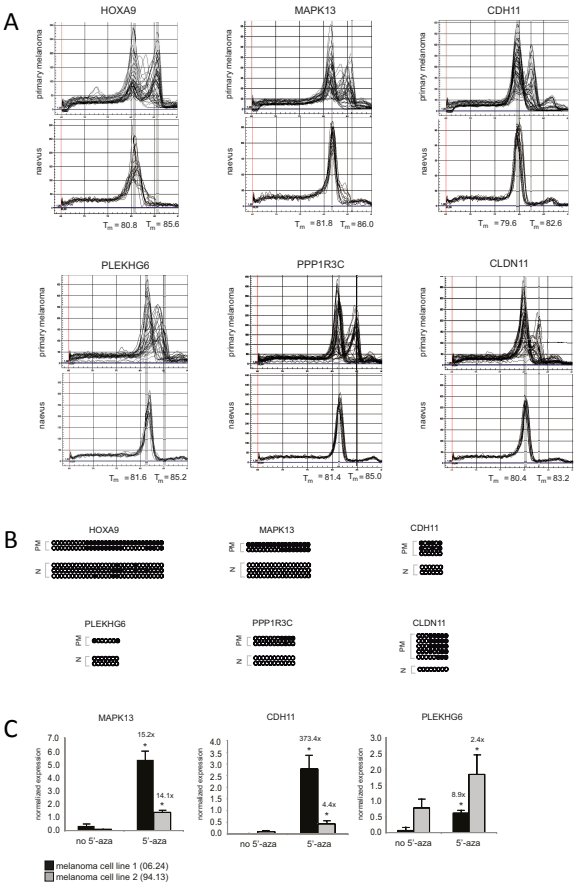

Figure 3. Bisulfite melting curve analysis and direct bisulfite sequencing analysis of *HOXA9*, *MAPK13*, *CDH11*, *PLEKHG6*, *PPP1R3C*, and *CLDN11*. (**A**) Bisulfite melting curve profiles of 39 primary melanomas plotted together in one graph (top) and of 15 naevi plotted overlapping in one graph (bottom) for each gene. The primary melanomas show a peak in their melting curve patterns at the melting temperatures (Tms) for methylated DNA (85.6, 86.0, 82.6, 85.2, 85.0, and 83.2°C for *HOXA9*, *MAPK13*, *CDH11*, *PLEKHG6*, *PPP1R3C*, and *CLDN11*, respectively), an additional peak at the Tm for unmethylated DNA (80.8, 81.8, 79.6, 81.6, 81.4, and 80.4°C for *HOXA9*, *MAPK13*, *CDH11*, *PLEKHG6*, *PPP1R3C*, and *CLDN11*, respectively) and peaks at intermediate Tms. In contrast, the naevi show only a peak at the Tm for unmethylated DNA while a peak at the Tm for methylated DNA is absent. Methylated DNA peaks in the melting curve pattern with a height of 0.5 or more relative to the unmethylated DNA peaks were considered indicative of methylation for the investigated CpG island amplicon. (**B**) Bisulfite sequencing analysis of CpG dinucleotides in the *HOXA9*, *MAPK13*, *CDH11*, *PLEKHG6*, *PPP1R3C*, and *CLDN11* promoter regions in a selected number of primary melanomas (PM) and naevi (N). An unmethylated cytosine of an interrogated CpG dinucleotide is depicted as a white circle, a methylated cytosine as a black circle, a partially methylated cytosine as a gray circle. An investigated CpG island amplicon was considered methylated if the density of methylated CpG dinucleotides was 15% or more. (**C**) The effect of demethylation on *MAPK13*, *CDH11*, and *PLEKHG6* expression in the 06.24 and 94.13 melanoma cell lines cultured in the presence or absence of 2µM 5-aza-2'-deoxycytidine for 96h. Data are representative of duplicate treatment experiments, error bars indicate standard deviation from triplicate qRT-PCR experiments. The fold induction in expression upon treatment with 5-aza-2'-deoxycytidine is indicated above the bars. A two-sided t-test was applied for statistical analysis. **P* <0.05.

Table 1. Overview of the validation results performed in naevi, primary melanoma, and metastatic melanoma for six genes identified as hypermethylated with genome-wide DNA methylation profiling. Numbers indicate the percentage of samples scored as methylated within the sample group.

Gene	% naevus (n=15)	% primary melanoma Infinium sample set (n=24)	% primary melanoma Independent sample set (n=15)	total % primary melanoma (n=39)	% melanoma metastasis (n=7)	% melanoma cells metastatic (n=13)	total % metastatic melanoma (n=20)
HOXA9	47	88	80	85	100	92	95
MAPK13	0	67	67	67	86	85	85
CDH11	0	46	40	44	43	85	70
PLEKHG6	0	71	60	67	86	85	85
PPP1R3C	0	54	47	51	57	54	55
CLDN11	0	29	27	28	43	46	45

promoter methylation for *MAPK13*, *CDH11*, and *PLEKHG6*. Both cell lines were treated with 5-aza-2'-deoxycytidine, and effect on gene expression was analyzed by qRT-PCR. Expression of all three genes, which was nearly undetectable to low in untreated melanoma cells, was increased significantly upon treatment with 5-aza-2'- deoxycytidine (Figure 3C). These results suggest that expression of *MAPK13*, *CDH11*, and *PLEKHG6* is epigenetically regulated and that the observed promoter methylation in melanoma is associated with transcriptional downregulation. We proceeded to examine whether MAPK13 protein expression correlated with promoter methylation status in human melanocytes, fibroblasts, and our panel of melanoma cell lines. Western blot analysis showed that melanoma cells with *MAPK13* promoter methylation (94.13, 607B, 93.08, Mz7.4, 634, 05.06, 06.24, 453A0, and 94.07) did not express significant levels of MAPK13 (Figure 4A). In contrast, expression was observed in fibroblasts, in melanocytes, and in melanoma cell lines with unmethylated *MAPK13* promoters (9304C and 04.07) or with mono-allelic methylation (518A2). MAPK13 protein levels were higher in the unmethylated melanoma cells compared with melanocytes. This can be explained by the $BRAF^{V600E}$-mutation that melanoma cell lines 9304C and 04.07 harbor, as we observed in fibroblasts that ectopic expression of $BRAF^{V600E}$ increased MAPK13 protein expression (Figure S4A).

MAPK13 acts cytostatically in melanoma cells

We found that *MAPK13* was among the most frequently methylated genes in primary cutaneous melanoma and that promoter hypermethylation was associated with gene silencing. In addition, *MAPK13* promoter methylation was present in primary melanomas and melanoma cell lines carrying either *BRAF* mutations, *NRAS* mutations, as well as in primary melanomas lacking mutations in these oncogenes (Table S1A, B). Furthermore, we found that this gene was expressed in human melanocytes and fibroblasts, but silenced in

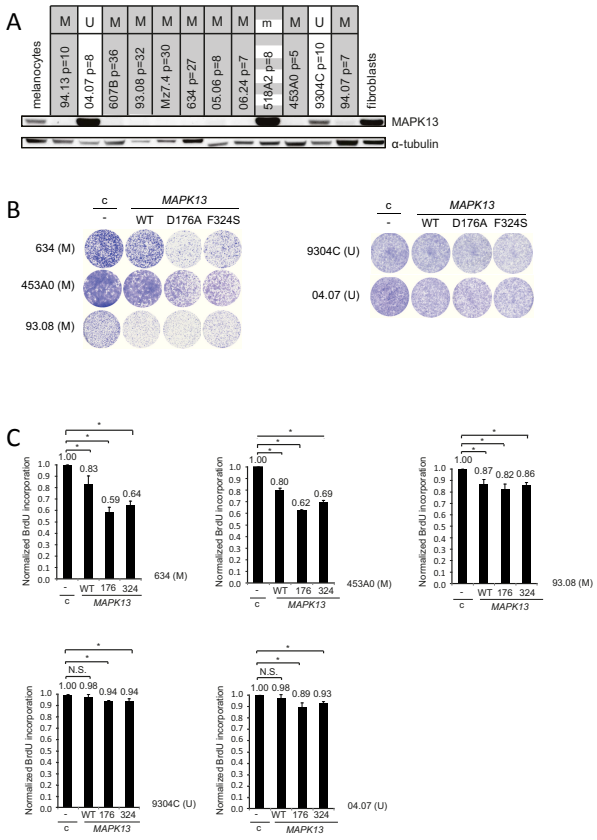

Figure 4. Restoration of MAPK13 expression in melanoma cells with *MAPK13* promoter methylation attenuates proliferation. (**A**) Thirteen melanoma cell lines, human melanocytes, and fibroblasts (TIG-3) were analyzed for MAPK13 protein expression with α-tubulin serving as loading control. The *MAPK13* promoter methylation status of each cell line is depicted; M, methylated (gray); U, unmethylated (white); m, mono-allelic methylation (striped). (**B**) Melanoma cell lines 634, 453A0, 93.08, 9304C, and 04.07 were transduced using retroviral vectors (pBABE-puro-HA-MAPK13) expressing $MAPK13^{WT}$ or either of the active kinase mutants $MAPK13^{D176A}$ and $MAPK13^{F324S}$ and selected for integration of the construct. Empty vectors were used as controls (c). Samples were seeded at equal densities and stained with crystal violet 15-19 days post-infection. *MAPK13* promoter methylation status is indicated for each cell line; M, methylated (left); U, unmethylated (right). (**C**) Samples of transduced melanoma cell lines 634, 453A0, 93.08, 9304C, and 04.07 were seeded at equal numbers and analyzed for BrdU incorporation 9-12 days post-infection. The percentage of BrdU-positive cells was normalized to empty vector controls (c). Error bars indicate standard deviation from triplicate measurements; two-tailed t-test was applied for statistical analysis. *MAPK13* promoter methylation status is indicated for each cell line; M, methylated (top row); U, unmethylated (bottom row). **P* <0.05; N.S., not significant.

melanoma cells with *MAPK13* promoter hypermethylation. Previous reports suggested a tumor suppressive role of MAPK13 [27]. Therefore, we asked whether MAPK13 could have a tumor suppressive role in melanoma. *MAPK13* encodes p38δ, one of four p38 isoforms of the p38 MAPK family of proteins. The p38 MAPK signaling pathway is activated upon environmental and genotoxic stress, and its activation affects cellular proliferation, differentiation, survival, and migration[28]. The observed methylation and transcriptional shutdown of *MAPK13* in melanoma would predict that re-establishment of its expression affects an essential tumor property. To investigate whether restoration of MAPK13 expression changed melanoma cell behavior, five melanoma cell lines, three of which (634, 453A0, and 93.08) with *MAPK13* methylation and two (9304C and 04.07) without, were retrovirally transduced with vectors expressing either wild-type MAPK13 ($MAPK13^{WT}$) or variants mutated at either Asp176 ($MAPK13^{D176A}$) or Phe324 ($MAPK13^{F324S}$); these kinase mutants were previously shown to have constitutive activity and to phosphorylate ATF2[29]. Retroviral transduction led to comparable expression levels of the three different MAPK13 constructs across the five cell lines (Figure S3A).

Interestingly, in melanoma cell lines 634 and 453A0 and somewhat less pronounced in 93.08, all exhibiting *MAPK13* promoter methylation, proliferation was suppressed upon overexpression of MAPK13, particularly when the constitutively active form was used (Figure 4B, left panel). In contrast, proliferation of 9304C and 04.07 melanoma cells, in which *MAPK13* is not epigenetically silenced, was only marginally affected upon ectopic expression of MAPK13, even when the active form was used (Figure 4B, right panel). Extending these proliferation assays, long-term growth curves also illustrate that the reduction in population doublings after restoration of MAPK13 expression is more pronounced in melanoma cell lines in which MAPK13 is epigenetically silenced (Figure S3B, top versus bottom panels).

Consistent with this, bromodeoxyuridine (BrdU) incorporation assays showed that expression of wild-type MAPK13 or activated mutants reduced BrdU uptake more profoundly in the melanoma cell lines in which MAPK13 was epigenetically silenced (Figure 4C, top versus bottom panels). Together, these results suggest that restoration of either wild-type or kinase mutant MAPK13 expression in melanoma cells with *MAPK13* promoter methylation can reduce the proliferative capacity of these cells. Our results raise the intriguing possibility that during progression of melanoma, loss of MAPK13 expression due to promoter methylation confers a selective advantage, which would be consistent with its previously proposed tumor suppressor function[27]. Lastly, considering the cytostatic effect that MAPK13 elicits in melanoma cells and the involvement of MAPK14 (p38α) and MAPK12 (p38γ) in oncogene-induced senescence[30,31], we asked whether MAPK13 might be involved in this tumor suppressive mechanism. For this, we examined whether MAPK13 depletion allowed human fibroblasts (TIG-3) to bypass the cell cycle

arrest that typically accompanies the senescence response induced by $BRAF^{V600E}$. Similar experiments have been reported recently, uncovering a critical role for PTEN in this setting[18]. Although shRNAs no. 1 and no. 3 significantly reduced MAPK13 expression (Figure S4A), it failed to result in a bypass from $BRAF^{V600E}$-induced cell cycle arrest (Figure S4B, C). Taken together, these results suggest that MAPK13 may act as a tumor suppressor that is selected against during melanomagenesis, at least in part because of its role in regulating the proliferative potential of melanoma cells.

Discussion

Aberrant DNA methylation is a key epigenetic event associated with tumorigenesis, as it results in deregulated expression of genes with a critical function in fundamental cellular processes. This study provides the first genome-wide view of promoter methylation in primary cutaneous melanoma. Detection of methylation at 27,578 CpG loci spread across 14,495 genes in fresh-frozen primary melanoma and melanocytic naevus samples revealed the presence of many highly recurrent and novel methylation events that were validated using independent techniques. Our results show that melanoma is characterized by widespread and heterogeneous epigenetic deregulation with many genes showing tumor-selective aberrant methylation. The multitude of DNA methylation events in melanoma might be related to the recently observed genomic loss of 5-hydroxymethylcytosine and decreased activity of IDH2 and TET family enzymes in this tumor type[8]. Epigenomic studies previously performed on breast cancer and glioblastoma using similar BeadChip technology have revealed a large number of de novo-methylated promoter regions that differ substantially from those identified in melanoma, confirming tumor type specificity of promoter hypermethylation[32,33]. Most of the genes we identified as hypermethylated in primary melanoma are novel methylation targets. Eleven of the 106 genes identified as most frequently hypermethylated in melanoma in this study have previously been reported to be hypermethylated in melanoma, while 32 genes have been found to be hypermethylated in other cancer types. Among the genes frequently hypermethylated in melanoma were several established tumor suppressor genes, including *CDH11* and *SERPINB5* (Maspin). Interestingly, epigenetic silencing of these genes has been demonstrated to enhance metastatic behavior of melanoma cells[34,35]. The most frequently methylated gene in primary melanoma was *HOXA9*, showing methylation in over 80% of melanoma samples analyzed, but also in a subset of benign naevi. Methylation of *HOXA9* has previously been demonstrated in a melanoma cell line as well as in other cancer types[36,37]. Among gene promoters hypermethylated in melanoma, there was enrichment for other homeobox genes, which are attracting increasing attention for their contribution to oncogenesis[38]. In previous studies, dozens of genes have been reported to be

hypermethylated in melanoma[5,6]. In most of these studies, metastatic melanoma samples or cell lines were analyzed using candidate gene approaches. *RASSF1A*, *SOCS2*, *RAR-β2*,*TNFSF10C*, and *TNFSF10D* are among genes shown to display promoter hypermethylation in metastatic melanoma in multiple studies[39,40]. Whereas RAR-*β*2 is also represented in the 106 most frequently methylated genes that we identified in primary melanoma, several previously reported methylation targets were not detected in this study as frequently hypermethylated in primary melanoma. In the few published genome-wide methylation analyses of melanoma, immunoprecipitation-based MeDIP and demethylation gene reactivation methods were applied to melanoma cell lines[41,42]. One of the few studies aimed at primary cutaneous melanoma employed a BeadChip assay that analyzed methylation of 807 cancer-related genes on formalin-fixed paraffin-embedded tumor samples[43]. In this study, six genes were identified as hypermethylated and 16 genes as hypomethylated in melanoma, with one hypermethylated gene (*COL1A2*) and two hypomethylated genes (*EMR3*, *RUNX3*), showing overlap with our results. Discrepancies of our findings with those of other studies can be explained by differences in the applied methylation assay, statistical analysis as well as in the sample size of the studies. Additionally, some of the reported methylation events in metastatic melanoma cells and not detected in this study of primary melanoma might be acquired during metastatic progression or melanoma cell culture[44].

Among the most frequently hypermethylated genes in primary melanoma was *MAPK13*, a gene encoding the p38δ isoform. The *MAPK13* gene was hypermethylated in 26 of 39 primary melanomas (67%) and in 17 of 20 metastatic melanoma samples (85%). Promoter hypermethylation of *MAPK13* was previously demonstrated in a subset of malignant pleural mesothelioma cases[45]. Mouse embryonic fibroblasts lacking *MAPK13* (p38δ) have been found to proliferate and migrate faster and to have diminished cell contact inhibition than their wild-type counterparts, suggesting tumor suppressive properties of this gene[27]. We show here that *MAPK13* promoter hypermethylation is associated with silencing of its transcript and protein expression in melanoma cells. Previous gene expression profiling showed that treatment of melanoma cells with the demethylating agent 5- aza-2'-deoxycytidine resulted in increased *MAPK13* expression, supporting the observation that promoter hypermethylation of this gene is associated with transcriptional repression[41]. Importantly, restoration of MAPK13 expression in melanoma cells with epigenetically silenced *MAPK13* resulted in suppression of proliferation, the effect being more pronounced when a constitutively active form of MAPK13 was expressed. In contrast, for two melanoma cell lines that were not affected by *MAPK13* promoter methylation and that expressed the protein, ectopic expression of wild type or constitutively active MAPK13 only marginally affected proliferation. These observations suggest that MAPK13 has cytostatic functions in melanoma cells and that

epigenetic silencing of *MAPK13* expression confers a growth advantage to melanoma cells. MAPK13 has been reported to contribute to delayed cell cycle progression through its capacity to phosphorylate p53 on serine 33, providing a possible mechanism for the cytostatic properties we observed in melanoma cells[46]. A critical tumor suppressive mechanism in melanocytic neoplasia is oncogene-induced senescence where expression of mutant BRAF or RAS elicits a stable cell cycle arrest from which incipient melanoma cells can escape through acquisition of additional genetic and epigenetic events[47]. Signaling through the MAPK14 (p38α) and MAPK12 (p38γ) isoforms has been shown to be required for mutant *RAS*-induced senescence[30,39]. We therefore examined whether MAPK13 could be involved in the senescence response but observed that its depletion in human fibroblasts did not prevent the proliferative arrest induced by expression of mutant BRAF. Although our results point to a tumor suppressive role of MAPK13 in melanoma, in cutaneous squamous cell carcinoma MAPK13 has been proposed to have oncogenic properties[48]. Similar paradoxical observations regarding oncogenic properties have been made for p38α[28]. The apparently contradicting functions of MAPK13 and other p38 proteins in tumorigenesis as either a tumor suppressor gene or oncogene appear to be dependent on cell type, pattern of oncogenic mutations, and stage of tumor development. Recently, genetic events that affect p38 signaling have been identified in melanoma, including inactivating mutations in the *MAP3K5* gene that mediates sustained activation of p38 and JNK proteins in response to cytotoxic stresses in melanoma samples[4]. In addition, a point mutation in *MAPK13* was detected in melanoma in a recent exome sequencing study[25]. Our finding of frequent epigenetic silencing of *MAPK13* further implicates disruption of p38 signaling in the pathogenesis of melanoma.

Clinical application of aberrant DNA methylation as a molecular biomarker in the diagnosis of melanoma is attractive as early stage melanoma and benign melanocytic lesions such as dysplastic naevi can be difficult to discriminate for clinical pathologists based on histomorphological grounds. Methylation targets identified in this study as frequently and selectively methylated in melanoma may be used as new diagnostic biomarkers for melanoma. The diagnostic discriminatory value of the epigenetic melanoma biomarkers in clinical practice should be validated in a large set of benign melanocytic tumors, including dysplastic and Spitz naevi, which we are currently addressing. In addition, the epigenomic maps of primary melanoma may reveal crucial information for the identification of specific epigenetic patterns associated with metastatic propensity and an unfavorable prognosis. The high degree of promoter methylation observed in melanoma could also have implications for melanoma therapy, as it might be associated with sensitivity to demethylating agents. Demethylating agents such as decitabine have pleiotropic effects affecting expression of hundreds of genes simultaneously and have only limited beneficial effects in solid tumors. However, recently

it was shown that inhibition of *STAT3* acetylation in melanoma results in demethylation and reactivation of multiple tumor suppressor genes, which indicates the feasibility of targeted therapeutic reversal of melanoma suppressor gene hypermethylation through interference with a common epigenetic silencing mechanism[49].

This study illustrates the multitude of epigenetic events that occur in primary cutaneous melanoma. In this assessment of promoter methylation, many novel genes were found that show highly recurrent, selective hypermethylation in melanoma that might be applied as molecular diagnostic markers in the clinic. Restoration of expression of the *MAPK13* gene, which is epigenetically silenced in the majority of melanoma samples, was shown to inhibit the proliferative capacity of melanoma cells, compatible with a tumor suppressive function of this gene. Indeed, several other genes affected by promoter hypermethylation in melanoma are established tumor suppressors. We feel that this study merits further analysis of the oncogenic role and diagnostic applications of the methylated genes identified.

Acknowledgements

We thank W.H. Zoutman and J.J. Out-Luiting for help with methylation analysis experiments, P.A. Possik and J. Kaplon for help with melanocyte senescence experiments, S.H. van der Burg for kindly providing early passage melanoma cell lines, R. van Soest and W. van Workum (Service XS) for help with the methylation assay analysis, and D. Engelberg for kindly providing *MAPK13* expression constructs.

References

1. Berger, M.F. *et al.* Melanoma genome sequencing reveals frequent PREX2 mutations. *Nature* **485**(7399), 502-506 (2012).
2. Hodis, E. *et al.* A Landscape of Driver Mutations in Melanoma. *Cell* **150**(2), 251-263 (2012).
3. Nikolaev, S.I. *et al.* Exome sequencing identifies recurrent somatic MAP2K1 and MAP2K2 mutations in melanoma. *Nat. Genet.* **44**(2), 133-139 (2012).
4. Stark, M.S. *et al.* Frequent somatic mutations in MAP3K5 and MAP3K9 in metastatic melanoma identified by exome sequencing. *Nat. Genet.* **44**(2), 165-169 (2012).
5. Rothhammer, T. and Bosserhoff, A.K. Epigenetic events in malignant melanoma. *Pigment Cell Res.* **20**(2), 92-111 (2007).
6. Sigalotti, L. *et al.* Epigenetics of human cutaneous melanoma: setting the stage for new therapeutic strategies. *J. Transl. Med.* **8**, 56 (2010).
7. De Carvalho, D.D. *et al.* DNA Methylation Screening Identifies Driver Epigenetic Events of Cancer Cell Survival. *Cancer Cell* **21**(5), 655-667 (2012).
8. Lian, C. *et al.* Loss of 5-Hydroxymethylcytosine Is an Epigenetic Hallmark of Melanoma. *Cell* **150**(6), 1135-1146 (2012).
9. Winnepenninckx, V. *et al.* Gene Expression Profiling of Primary Cutaneous Melanoma and Clinical Outcome. *J. Natl. Cancer Inst.* **98**(7), 472-482 (2006).
10. van Eijk, R. *et al.* Rapid KRAS, EGFR, BRAF and PIK3CA mutation analysis of fine needle aspirates from non-small-cell lung cancer using allele-specific qPCR. *PLoS. One.* **6**(3), e17791 (2011).
11. van Wieringen, W.N., van de Wiel, M.A., and van der Vaart, A.W. A Test for Partial Differential Expression. *J. Am. Stat. Assoc.* **103**(483), 1039-1049 (2008).
12. Benjamini, Y. and Hochberg, Y. Controlling the False Discovery Rate: A Practical and Powerful Approach to Multiple Testing. *J. R. Statist. Soc. B* **57**(1), 289-300 (1995).
13. Garcia-Manero, G. *et al.* DNA Methylation of Multiple Promoter-associated CpG Islands in Adult Acute Lymphocytic Leukemia. *Clin. Cancer Res.* **8**(7), 2217-2224 (2002).
14. Toyota, M. *et al.* Methylation profiling in acute myeloid leukemia. *Blood* **97**(9), 2823-2829 (2001).
15. Vandesompele, J. *et al.* Accurate normalization of real-time quantitative RT-PCR data by geometric averaging of multiple internal control genes. *Genome Biol.* **3**(7), RESEARCH0034 (2002).
16. Morgenstern, J.P. and Land, H. Advanced mammalian gene transfer: high titre retroviral vectors with multiple drug selection markers and a complementary helper-free packaging cell line. *Nucleic Acids Res.* **18**(12), 3587-3596 (1990).
17. Michaloglou, C. *et al.* BRAFE600-associated senescence-like cell cycle arrest of human naevi. *Nature* **436**(7051), 720-724 (2005).
18. Vredeveld, L.C.W. *et al.* Abrogation of BRAFV600E-induced senescence by PI3K pathway activation contributes to melanomagenesis. *Genes Dev.* **26**(10), 1055-1069 (2012).
19. Edgar, R., Domrachev, M., and Lash, A.E. Gene Expression Omnibus: NCBI gene expression and hybridization array data repository. *Nucleic Acids Res.* **30**(1), 207-210 (2002).
20. Huang, d.W., Sherman, B.T., and Lempicki, R.A. Systematic and integrative analysis of large gene lists using DAVID bioinformatics resources. *Nat. Protoc.* **4**(1), 44-57 (2009).
21. Vire, E. *et al.* The Polycomb group protein EZH2 directly controls DNA methylation. *Nature* **439**(7078), 871-874 (2006).
22. Widschwendter, M. *et al.* Epigenetic stem cell signature in cancer. *Nat. Genet.* **39**(2), 157-158 (2007).
23. Bracken, A.P. *et al.* Genome-wide mapping of Polycomb target genes unravels their roles in cell fate transitions. *Genes Dev.* **20**(9), 1123-1136 (2006).
24. Tellez, C.S. *et al.* CpG island methylation profiling in human melanoma cell lines. *Melanoma Res.* **19**(3), 146-155 (2009).
25. Krauthammer, M. *et al.* Exome sequencing identifies recurrent somatic RAC1 mutations in melanoma. *Nat. Genet.* **44**(9), 1006-1014 (2012).
26. Higgins, M.E. *et al.* CancerGenes: a gene selection resource for cancer genome projects. *Nucleic Acids Res.* **35**(suppl 1), D721-D726 (2007).
27. Cerezo-Guisado, M.I. *et al.* Evidence of p38+¦ and p38+¦ involvement in cell transformation processes. *Carcinogenesis* **32**(7), 1093-1099 (2011).
28. Wagner, E.F. and Nebreda, A.R. Signal integration by JNK and p38 MAPK pathways in cancer development. *Nat Rev. Cancer* **9**(8), 537-549 (2009).

29. Askari, N. *et al.* Hyperactive variants of p38alpha induce, whereas hyperactive variants of p38gamma suppress, activating protein 1-mediated transcription. *J. Biol. Chem.* **282**(1), 91-99 (2007).
30. Kwong, J. *et al.* p38alpha and p38gamma mediate oncogenic ras-induced senescence through differential mechanisms. *J. Biol. Chem.* **284**(17), 11237-11246 (2009).
31. Sun, P. *et al.* PRAK is essential for ras-induced senescence and tumor suppression. *Cell* **128**(2), 295-308 (2007).
32. Fackler, M.J. *et al.* Genome-wide Methylation Analysis Identifies Genes Specific to Breast Cancer Hormone Receptor Status and Risk of Recurrence. *Cancer Res.* **71**(19), 6195-6207 (2011).
33. Noushmehr, H. *et al.* Identification of a CpG island methylator phenotype that defines a distinct subgroup of glioma. *Cancer Cell* **17**(5), 510-522 (2010).
34. Carmona, F.J. *et al.* Epigenetic disruption of cadherin-11 in human cancer metastasis. *J. Pathol.* **228**(2), 230-240 (2012).
35. Denk, A.E. *et al.* Loss of maspin expression contributes to a more invasive potential in malignant melanoma. *Pigment Cell Res.* **20**(2), 112-119 (2007).
36. Furuta, J. *et al.* Promoter methylation profiling of 30 genes in human malignant melanoma. *Cancer Sci.* **95**(12), 962-968 (2004).
37. Rauch, T.A. *et al.* High-resolution mapping of DNA hypermethylation and hypomethylation in lung cancer. *Proc. Natl. Acad. Sci. U. S. A.* **105**(1), 252-257 (2008).
38. Shah, N. and Sukumar, S. The Hox genes and their roles in oncogenesis. *Nat. Rev. Cancer* **10**(5), 361-371 (2010).
39. Liu, S. *et al.* Identification of novel epigenetically modified genes in human melanoma via promoter methylation gene profiling. *Pigment Cell Melanoma Res.* **21**(5), 545-558 (2008).
40. Spugnardi, M. *et al.* Epigenetic inactivation of RAS association domain family protein 1 (RASSF1A) in malignant cutaneous melanoma. *Cancer Res.* **63**(7), 1639-1643 (2003).
41. Koga, Y. *et al.* Genome-wide screen of promoter methylation identifies novel markers in melanoma. *Genome Res.* **19**(8), 1462-1470 (2009).
42. Muthusamy, V. *et al.* Epigenetic silencing of novel tumor suppressors in malignant melanoma. *Cancer Res.* **66**(23), 11187-11193 (2006).
43. Conway, K. *et al.* DNA-methylation profiling distinguishes malignant melanomas from benign naevi. *Pigment Cell Melanoma Res.* **24**(2), 352-360 (2011).
44. Smiraglia, D.J. *et al.* Excessive CpG island hypermethylation in cancer cell lines versus primary human malignancies. *Hum. Mol. Genet.* **10**(13), 1413-1419 (2001).
45. Goto, Y. *et al.* Epigenetic profiles distinguish malignant pleural mesothelioma from lung adenocarcinoma. *Cancer Res.* **69**(23), 9073-9082 (2009).
46. Hawkes, W.C. and Alkan, Z. Delayed Cell Cycle Progression in Selenoprotein W Depleted Cells Is Regulated By a Mitogen-Activated Protein Kinase Kinase 4 (MKK4)-p38/c-Jun NH2-Terminal Kinase (JNK)-p53 Pathway. *J. Biol. Chem.* **287**(33), 27371-27379 (2012).
47. Mooi, W.J. and Peeper, D.S. Oncogene-induced cell senescence--halting on the road to cancer. *N. Engl. J. Med.* **355**(10), 1037-1046 (2006).
48. Schindler, E.M. *et al.* p38delta Mitogen-activated protein kinase is essential for skin tumor development in mice. *Cancer Res.* **69**(11), 4648-4655 (2009).
49. Lee, H. *et al.* Acetylated STAT3 is crucial for methylation of tumor-suppressor gene promoters and inhibition by resveratrol results in demethylation. *Proc. Natl. Acad. Sci. U. S. A.* **109**(20), 7765-7769 (2012).

Supplementary Data

Supplementary Table S1 (**A**) **Fresh-frozen biopsies of naevus, primary cutaneous melanoma and melanoma metastases**. MA, sample used for genome-wide methylation analysis; VA, sample used for validation of identified methylation targets; DBN, dermal benign naevus; CBN, compound benign naevus; PT, primary tumor; CM, cutaneous metastasis. Ulceration was identified according to EORTC criteria (Spatz A, Cook MG, Elder DE, Piepkorn M, Ruiter DJ, Barnhill RL. Interobserver reproducibility of ulceration assessment in primary cutaneous melanomas. Eur J Cancer. 2003 Sep;39(13):1861-1865). Mitotic rate was determined using the "hot-spot" method which identifies the maximum number of dermal mitotic figures in a 1-mm^2 area of the invasive part of the melanoma according to American Joint Committee on Cancer (AJCC) recommendations for diagnosis and treatment of malignant melanoma (Gershenwald JE, Soong S, Balch CM. 2010 TNM staging system for cutaneous melanoma… and beyond. Ann Surg Oncol. 2010;17:1475-1477).

Naevus

Code	ID	Application	Type	Mutation	Site	Gender	Age
N1	K22691	MA/VA	DBN	BRAFV600E	Leg	F	29
N2	K23142	MA/VA	DBN/CBN	BRAFV600E	Trunk	F	43
N3	K23342	MA/VA	DBN	BRAFV600E	Upper leg	M	55
N4	K24383	MA/VA	DBN	BRAFV600E	Trunk	F	40
N5	K24848	MA/VA	DBN	BRAFV600E	Trunk	F	38
-	LUMC-N01	VA	DBN	-	-	F	31
-	LUMC-N03	VA	DBN	-	-	M	46
-	LUMC-N04	VA	DBN	-	-	F	39
-	LUMC-N05	VA	DBN	-	-	F	27
-	LUMC-N06	VA	DBN	-	-	M	21
-	LUMC-N07	VA	DBN	-	-	M	57
-	LUMC-N09	VA	DBN	-	-	F	52
-	LUMC-N10	VA	DBN	-	-	F	24
-	LUMC-N11	VA	DBN	-	-	F	30
-	LUMC-N13	VA	DBN	-	-	F	30

Primary melanoma

Code	ID	Application	Type	Mutation	Site	Breslow	Clark	Ulcer	Mitoses	Diagnosis	Gender	Age
PM1	K5940	MA/VA	PT	wt	Lower leg	1,67	IV	-	3	SSMM	F	53
PM2	K7206	MA/VA	PT	BRAFV600E	Lower leg	2,08	IV	+	6	SSMM	M	68
PM3	K7376	MA/VA	PT	wt	Foot	4,48	V	+	13	ALMM	M	65
PM4	K14294	MA/VA	PT	wt	Trunk	2,05	IV	-	2	SSMM	F	65
PM5	K17504	MA/VA	PT	wt	Foot	3,88	IV	-	5	ALMM	F	60
PM6	K17716	MA/VA	PT	wt	Ear	0,81	III	-	1	SSMM	M	58
PM7	K12832	MA/VA	PT	BRAFV600K	Back	0,91	IV	-	0	SSMM	F	42
PM8	K8269	MA/VA	PT	wt	Shoulder	0,94	IV	-	2	SSMM	F	34
PM9	K17155	MA/VA	PT	BRAFV600E	Back	1,06	IV	-	2	SSMM	M	36
PM10	K10454	MA/VA	PT	BRAFV600E	Buttock	0,73	III	-	0	SSMM	F	35
PM11	K5666	MA/VA	PT	NRASG12D	Nailbed Toe	1,70	IV	+	2	ALMM	F	59
PM12	K5912	MA/VA	PT	wt	Foot	3,36	IV	+	6	ALMM	F	73
PM13	K7393	MA/VA	PT	wt	Neck	15,60	V	-	2	Desmopl MM	M	85
PM14	K14277	MA/VA	PT	wt	Scalp	3,46	IV	-	4	SSMM	M	54
PM15	K15582	MA/VA	PT	NRASQ61K	Thigh	9,20	V	+	10	SSMM	F	48
PM16	K20015	MA/VA	PT	BRAFV600E	Lower leg	18,00	V	+	12	SSMM	M	82
PM17	K21160	MA/VA	PT	wt	Buttock	6,29	IV	+	8	SSMM	F	62
PM18	K4554	MA/VA	PT	wt	Back	1,28	IV	-	1	SSMM	F	65
PM19	K24091	MA/VA	PT	BRAFV600K	Scalp	17,2	V	+	9	NMM	M	79
PM20	K9900	MA/VA	PT	wt	Back	3,04	IV	+	4	SSMM	F	45
PM21	K6386	MA/VA	PT	wt	Lower leg	2,02	IV	+	4	SSMM	M	78
PM22	K5557	MA/VA	PT	wt	Axilla	12,2	V	-	7	SSMM	M	70
PM23	K16334	MA/VA	PT	wt	Vulva	10,1	IV	+	8	SSMM	F	56
PM24	K20506	MA/VA	PT	BRAFV600E	Foot	2,08	IV	-	7	SSMM	F	75

Melanoma metastasis

Code	ID	Application	Type	Mutation	Site	Gender	Age
MM1	K5317	VA	CM	BRAFV600E	Thigh	M	68
MM2	K9600	VA	CM	BRAFV600E	Neck	M	76
MM3	K14772	VA	CM	wt	Lower leg	F	75
MM4	K17323	VA	CM	NRASQ61R	Lower leg	F	48
MM5	K19394	VA	CM	wt	Shoulder	F	56
MM6	K23602	VA	CM	BRAFV600E	Trunk	M	69
MM7	K24883	VA	CM	BRAFV600E	Upper leg	F	87

Supplementary Table S1 (**B**) **Early-passage melanoma cell lines, isolated from metastatic lesions of patients treated at Leiden University Medical Center**. MA, sample used for genome-wide methylation analysis; VA, sample used for validation of identified methylation targets; LN, Lymph Node; SC, subcutaneous; Stage AJCC III, local / loco-regional metastasis; Stage AJCC IV, distant metastasis; M, methylated; U, unmethylated; m, mono-allelic methylation.

Cell line	Application	Passage	Mutation	Pigment	Site	Stage	Gender	Age	*MAPK13* promoter
05.06	VA	8	BRAFV600E	No	LN	IV	M	59	M
06.24	VA	7	NRASQ61R	No	LN	IV	F	60	M
518A2	VA	8	BRAFV600E	No	LN	III	M	19	m
453A0	VA	5	BRAFV600E	No	SC	IV	M	42	M
9304C	VA	10	BRAFV600E	Yes	SC	III	F	37	U
94.07	VA	7	BRAFV600E	No	Mesenterial	IV	M	39	M
94.13	VA	10	BRAFV600E	No	Omentum	IV	F	47	M
9903A	VA	13	BRAFV600E	No	LN	III	F	31	M
04.07	VA	8	BRAFV600E	No	SC	IV	F	59	U
607B	VA	36	NRASQ61K	No	SC	IV	F	51	M
93.08	VA	32	BRAFV600E	No	SC	IV	M	30	M
Mz7.4	VA	30	BRAFV600E	No	na	na	na	na	M
634	VA	27	NRASQ61R	No	SC	IV	F	52	M

Supplementary Table S2 (**A**) **Bisulphite primers**. No. of CpG's, position relative to TSS, size (bp) and Tm (°C) in regard to respective amplicon.

Gene	Primer sequence 5'> 3'	No. of CpG's	Position relative to TSS		Size (bp)	ATG relative to TSS	Tm (°C) unmethylated	Tm (°C) methylated
HOXA9	ATGGTTATTATTGGGGTTTTGGGTAA TAAACTCCAACCAAAAACGCATATAC	38	74 +	416 +	343	74 +	80,8	85,6
MAPK13	GAGGGAATTGGGAAGTATTGTTTT AACCTATCCAACCCTACGCTCC	18	273 -	90 -	184	99 +	81,8	86
CDH11	GTCGTTGATTTGTGAATGGGAT CACCTCACCTAAAACCCTTAAAAAT	8	35 +	153 +	119	443 +	79,6	82,6
PLEKHG6	AGGGTATCGTTACGTGAGTTGTTTT CCCGATACCCAACCTAAAACTAAAAT	20	103 +	316 +	214	149 +	81,6	85,2
PPP1R3C	GTTTTAGTTGGGCGTTGGTTG AACCACAACTCCAAACCTTACCC	14	84 -	77 +	161	133 +	81,4	85
CLDN11	GTATTTGGGTAGGTATTGTTTAGTTTAGG CAAATCACCACCCAATCATTAATAAA	10	112 +	291 +	180	191 +	80,4	83,2

Supplementary Table S2 (**B**) **qPCR primers**.

cDNA	Primer sequence 5'> 3	Accession No.	Exonic Location	Amplicon size (bp)
HOXA9	GAGAATGAGAGCGGCGGA CCGCTTTTTCCGAGTGGA	NM_152739	1, 2	90
MAPK13	GGCTGTATCATGGCAGAGATG CTTTCAGGATCTGGGTCAGC	NM_002754	8, 9	85
CDH11	CGCCTGCATCGTCATTCT CACGGACATCTTCTTCCTCAA	NM_001797	12, 13	101
BMP4	AGGAGCTTCCACCACGAAG GGGATGCTGCTGAGGTTAAA	NM_001202	3, 4	92
PLEKHG6	CTCTATCGGGACCAGGACAGG GGATAATGGTCGAGAACTCAGGAG	NM_018173	14, 15	112

Supplementary Table S2 (**C**) ***BRAF*** **and** ***NRAS*** **sequencing primers**.

Gene	Sequence	Exonic location	Interrogated codon
BRAF	AACTCTTCATAATGCTTGCTCTGATAGG GCCTCAATTCTTACCATCCACAAAATG	15	600
NRAS	GATTCTTACAGAAAACAAGTG ATGACTTGCTATTATTGATGG	2	61
NRAS	CTAGGGTTTTCATTTCCATTGATTAT TACCACTGGGCCTCACCTCTAT	1	12

Supplementary Table S3 (**A**) List of the 106 unique genes (P <0.05 and average β-value difference >0,20) identified as hypermethylated in primary melanoma. Validated genes are highlighted.

Gene name	Description	Δ average β-value	adjusted p-value	hypermethylated in melanoma	hypermethylated in cancer
HOXA9	Homeobox A9	0.386483234	0.012	x	x
C1orf106	Chromosome 1 open reading frame 106	0.322837474	0		
HIST1H3E	Histone cluster 1, H3e	0.316605725	0		x
MAPK13	Mitogen-activated protein kinase 13	0.311837229	0.034		x
LEP	Leptin (obesity homolog, mouse)	0.311563859	0		
CDH11	Cadherin 11, type 2, OB-cadherin (osteoblast)	0.298408797	0.016	x	x
C4orf8	Chromosome 4 open reading frame 8	0.297335994	0		
EFCAB1	EF-hand calcium binding domain 1	0.283580672	0.029		
CNTN1	Contactin 1	0.282425828	0		
GNMT	Glycine N-methyltransferase	0.281172377	0		x
ABCA3	ATP-binding cassette, sub-family A (ABC1), member 3	0.279902377	0.023		
PLEKHG6	Pleckstrin homology domain containing, family G (with RhoGef domain) member 6	0.271057913	0.026		
HIST1H3G	Histone cluster 1, H3g	0.269972293	0		
PDE4DIP	Phosphodiesterase 4D interacting protein (myomegalin)	0.269764956	0		
PPP1R3C	Protein phosphatase 1, regulatory (inhibitor) subunit 3C	0.269496395	0	x	
ME3	Malic enzyme 3, NADP(+)-dependent, mitochondrial	0.268329645	0		
MYL9	Myosin, light chain 9, regulatory	0.267168652	0.034		x
HOXD12	Homeobox D12	0.266988536	0	x	
NDST4	N-deacetylase/N-sulfotransferase (heparan glucosaminyl) 4	0.265946667	0		
HLA-G	HLA-G histocompatibility antigen, class I, G	0.263079106	0	x	x
SLC6A6	Solute carrier family 6 (neurotransmitter transporter, taurine), member 6	0.262815719	0		
CLDN11	Claudin 11 (oligodendrocyte transmembrane protein)	0.259287545	0.04		x
LCAT	Lecithin-cholesterol acyltransferase	0.258877843	0		
TRIM50C	Tripartite motif containing 74	0.258660963	0		
CLDN7	Claudin 7	0.257209464	0.038		x
OVOL1	Ovo-like 1(Drosophila)	0.255892223	0.048		
GPR135	G protein-coupled receptor 135	0.255310147	0.033		
DCDC2	Doublecortin domain containing 2	0.251983999	0.046		
CDK3	Cyclin-dependent kinase 3	0.250844565	0		
MEST	Mesoderm specific transcript homolog (mouse)	0.249726168	0		x
ALDH2	Aldehyde dehydrogenase 2 family (mitochondrial)	0.249604266	0		x
GBGT1	Globoside alpha-1,3-N-acetylgalactosaminyltransferase 1	0.248456228	0		
LOXL1	Lysyl oxidase-like 1	0.248370347	0		x
FAM3B	Family with sequence similarity 3, member B	0.247974455	0.036		
SERPINB5	Serpin peptidase inhibitor, clade B (ovalbumin), member 5	0.24599395	0		x
GPT	Glutamic-pyruvate transaminase (alanine aminotransferase)	0.244655194	0		
COL1A2	Collagen, type I, alpha 2	0.244446308	0.029	x	x
ALOX12	Arachidonate 12-lipoxygenase	0.243363656	0		x
COL14A1	Collagen, type XIV, alpha 1 (undulin)	0.240319162	0.014		x
HAAO	3-hydroxyanthranilate 3,4-dioxygenase	0.239623765	0		x
RARB	Retinoic acid receptor, beta	0.238093203	0	x	x
FLJ36070	Likely ortholog of MEF2-activating SAP transcriptional regulator	0.236784713	0.014		
RNF43	Ring finger protein 43	0.235797878	0		
OTP	Orthopedia homeobox	0.235315488	0.014		x
PRDM14	PR domain containing 14	0.235166177	0		
IL20RA	Interleukin 20 receptor, alpha	0.234413165	0		x
GPR109B	G protein-coupled receptor 109B	0.234166841	0		
LOC222171	Proline rich 15	0.233727994	0		
PPP1R13L	Protein phosphatase 1, regulatory (inhibitor) subunit 13 like	0.233637254	0.019		
DES	Desmin	0.232837864	0.013		
UNQ2446	Neuritin 1-like	0.232180459	0		
CCL27	Chemokine (C-C motif) ligand 27	0.231546716	0		
ZNF710	Zinc finger protein 710	0.231358867	0		
MSX1	Msh homeobox 1	0.230475548	0		x
CYP1B1	Cytochrome P450, family 1, subfamily B, polypeptide 1	0.230267325	0	x	x
CHFR	Checkpoint with forkhead and ring finger domains	0.229806888	0		x
CENTB5	Centaurin, beta 5	0.229121547	0		
PRTFDC1	Phosphoribosyl transferase domain containing 1	0.227675219	0		x
NNAT	Neuronatin	0.227436253	0		x
LRRC8C	Leucine rich repeat containing 8 family, member C	0.225715702	0		
FAM83A	Family with sequence similarity 83, member A	0.22562881	0		

Gene name	Description	Δ average β-value	adjusted p-value	hypermethylated in melanoma	hypermethylated in cancer
PAX3	Paired box 3	0.223214654	0	x	x
PLXNB1	Plexin B1	0.22538469	0.021		
ARHGAP8	Rho GTPase activating protein 8	0.225166562	0		
ABHD9	Abhydrolase domain containing 9	0.222971815	0	x	x
ANGPTL5	Angiopoietin-like 5	0.221433652	0		
KCTD12	Potassium channel tetramerisation domain containing 12	0.221238936	0		
P2RY6	Pyrimidinergic receptor P2Y, G-protein coupled, 6	0.221209139	0.038		
DISP1	Dispatched homolog 1 (Drosophila)	0.21881343	0.014		
VSX1	Visual system homeobox 1	0.218541035	0.032		
DDR1	Discoidin domain receptor family, member 1	0.217786303	0		
PDK4	Pyruvate dehydrogenase kinase, isozyme 4	0.216572648	0.023		
WISP2	WNT1 inducible signaling pathway protein 2	0.215433672	0		
GAL3ST3	Galactose-3-O-sulfotransferase 3	0.214561831	0.014		
C16orf30	Chromosome 16 open reading frame 30	0.213297461	0.017		x
ALDH3A1	Aldehyde dehydrogenase 3 family, memberA1	0.212722554	0		
APH1B	Anterior pharynx defective 1 homolog B (C. elegans)	0.212651362	0		
FBXO44	F-box protein 44	0.212464867	0		
ANKDD1A	Ankyrin repeat and death domain containing 1A	0.211560778	0		x
STAP2	Signal transducing adaptor family member 2	0.211557564	0		
CRB1	Crumbs homolog 1 (Drosophila)	0.211260864	0.023		
SEC31L2	SEC31 homolog B (S. cerevisiae)	0.210806802	0.04		
MTSS1	Metastasis suppressor 1	0.210716672	0		x
RTKN	Rhotekin	0.210450445	0.03		
SERHL	Serine hydrolase-like	0.210364197	0.026		
GPR25	G protein-coupled receptor 25	0.210280693	0		
FXYD3	FXYD domain containing ion transport regulator 3	0.208717214	0.015		
CCDC19	Coiled-coil domain containing 19	0.208457588	0.049		
FLJ39599	MPV17 mitochondrial membrane protein-like	0.207319001	0		
LAMB3	Laminin, beta 3	0.206753259	0	x	x
LACTB	Lactamase, beta	0.206389962	0		
SDCBP2	Syndecan binding protein (syntenin) 2	0.20625116	0		
HKDC1	Hexokinase domain containing 1	0.20583116	0.014		
NR4A1	Nuclear receptor subfamily 4, group A, member 1	0.204840796	0		
NDUFS2	NADH dehydrogenase (ubiquinone) Fe-S protein 2, 49kDa (NADH-coenzyme Q reductase)	0.204087485	0.024		
KCNQ1	Potassium voltage-gated channel, KQT-like subfamily, member 1	0.20399222	0.017		
FOXD2	Forkhead box D2	0.203879025	0		
APCDD1	Adenomatosis polyposis coli down-regulated 1	0.203854304	0		
ADORA2A	Adenosine A2a receptor	0.203064992	0		
LOC349236		0.202228801	0		
CRYBA2	Crystallin, beta A2	0.201666542	0.023		x
TACSTD1	Tumor-associated calcium signal transducer 1	0.201129306	0.04		
CLIC6	Chloride intracellular channel 6	0.201080863	0.03		
NFKBIB	Nuclear factor of kappa light polypeptide gene enhancer in B-cells inhibitor, beta	0.20101736	0		
CMTM2	CKLF-like MARVEL transmembrane domain containing 2	0.200457024	0.04		
SLC15A2	Solute carrier family 15 (H+/peptide transporter), member 2	0.200430401	0		
				n=11	n=32
				10.4 %	30.2 %

Supplementary Table S3 (**B**) List of the 44 unique genes (P <0.05 and average β-value difference > - 0,20) identified as hypomethylated in primary melanoma.

Gene name	Description	Δ average β-value	adjusted p-value	hypomethylated in melanoma	hypomethylated in cancer
HLA-DRA	Major histocompatibility complex, class II, DR alpha	-0,287684014	0		
SLC1A2	Solute carrier family 1 (glial high affinity glutamate transporter), member 2	-0,269827355	0		x
MGC35206	Testis expressed 33	-0,265220728	0		
PRSS2	Protease, serine, 2 (trypsin 2)	-0,262463936	0		
SIRPB1	Signal-regulatory protein beta 1	-0,253688211	0		
GIMAP7	GTPase, IMAP family member 7	-0,247822312	0,012		
GIMAP2	GTPase, IMAP family member 2	-0,240934883	0,014		
FCGR1A	Fc fragment of IgG, high affinity Ia, receptor (CD64)	-0,238817512	0		
KCNK17	Potassium channel, subfamily K, member 17	-0,238487672	0		
NALP12	NLR family, pyrin domain containing 12	-0,238234352	0		
TRIM40	Tripartite motif-containing 40	-0,23679714	0		
FLJ25773	Chromosome 14 open reading frame 177	-0,233879123	0		
ITGAL	Integrin, alpha L (antigen CD11A (p180), lymphocyte function-associated antigen 1; alpha polypeptide)	-0,233231346	0		
UNQ3033	V-set and transmembrane domain containing 1	-0,231175937	0		
TPM3	Tropomyosin 3	-0,230938917	0		
LIFR	Leukemia inhibitory factor receptor alpha	-0,228878156	0,049		x
C1orf150	Chromosome 1 open reading frame 150	-0,227742979	0,015		
ELSPBP1	Epididymal sperm binding protein 1	-0,227216147	0		
FCRL3	Fc receptor-like 3	-0,225753462	0		
LILRA2	Leukocyte immunoglobulin-like receptor, subfamily A (with TM domain), member 2	-0,224523114	0		
RUNX1	Runt-related transcription factor 1 (acute myeloid leukemia 1; aml1 oncogene)	-0,224087321	0,033		x
K6IRS3	Keratin 73	-0,223643593	0,013		
NALP9	NLR family, pyrin domain containing 9	-0,223223861	0		
MGAM	Maltase-glucoamylase (alpha-glucosidase)	-0,220814253	0		
FAIM3	Fas apoptotic inhibitory molecule 3	-0,218429252	0,016		
AQP5	Aquaporin 5	-0,217565045	0		x
GIMAP4	GTPase, IMAP family member 4	-0,214211774	0,015		
ASGR2	Asialoglycoprotein receptor 2	-0,212790738	0		
GIMAP1	GTPase, IMAP family member 1	-0,210846219	0		
MGC29671	Spinster homolog 3 (Drosophila)	-0,210725154	0		
SLA2	Src-like-adaptor 2	-0,210128702	0		
PGK2	Phosphoglycerate kinase 2	-0,209436678	0		
LILRA1	Leukocyte immunoglobulin-like receptor, subfamily A (with TM domain), member 1	-0,206384966	0		
PSMB6	Proteasome (prosome, macropain) subunit, beta type, 6	-0,206295895	0,04		
GPR154	Neuropeptide S receptor 1	-0,204509133	0		
RBP3	Retinol binding protein 3, interstitial	-0,204407391	0,025		
C15orf2	Chromosome 15 open reading frame 2	-0,203557247	0,039		
PTPN22	Protein tyrosine phosphatase, non-receptor type 22 (lymphoid)	-0,203401133	0,03		
OR1A1	Olfactory receptor, family 1, subfamily A, member 1	-0,202507508	0,02		
KRTAP10-8	Keratin associated protein 10-8	-0,202131896	0		
EMR3	Egf-like module containing, mucin-like, hormone receptor-like 3	-0,200710901	0		x
MRGPRX2	MAS-related GPR, member X2	-0,200622617	0		
RUNX3	Runt-related transcription factor 3	-0,200567687	0,034	x	x
MARCO	Macrophage receptor with collagenous structure	-0,200136166	0		
				n=1	n=6
				2.3 %	13.6 %

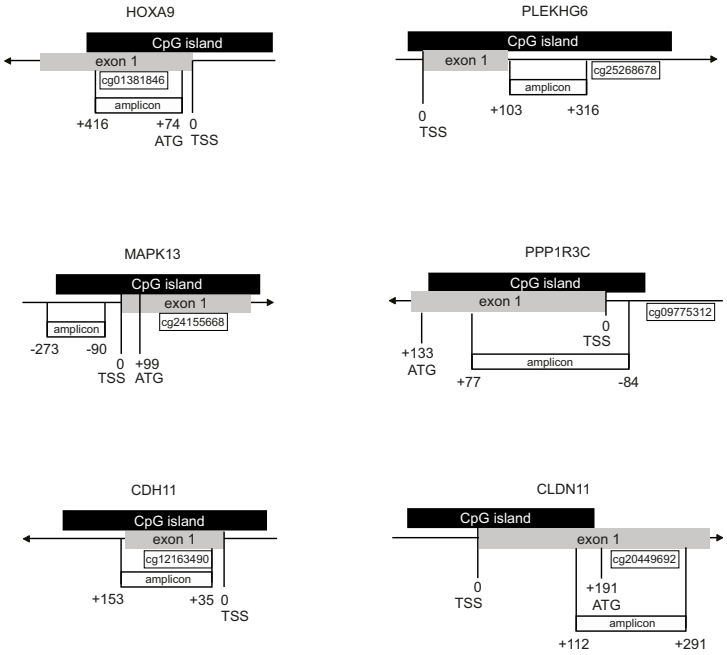

Supplementary Figure S1. **CpG islands within gene promoter regions are analyzed for validation of gene methylation status**. Schematic representation of the first exon, location of the CpG island, the region amplified for bisulphite melting curve and sequence analysis (amplicon) and the region corresponding to the CpG probe on the Infinium beadchip (cg) of *HOXA9*, *MAPK13*, *CDH11*, *PLEKHG6*, *PPP1R3C* and *CLDN11*.

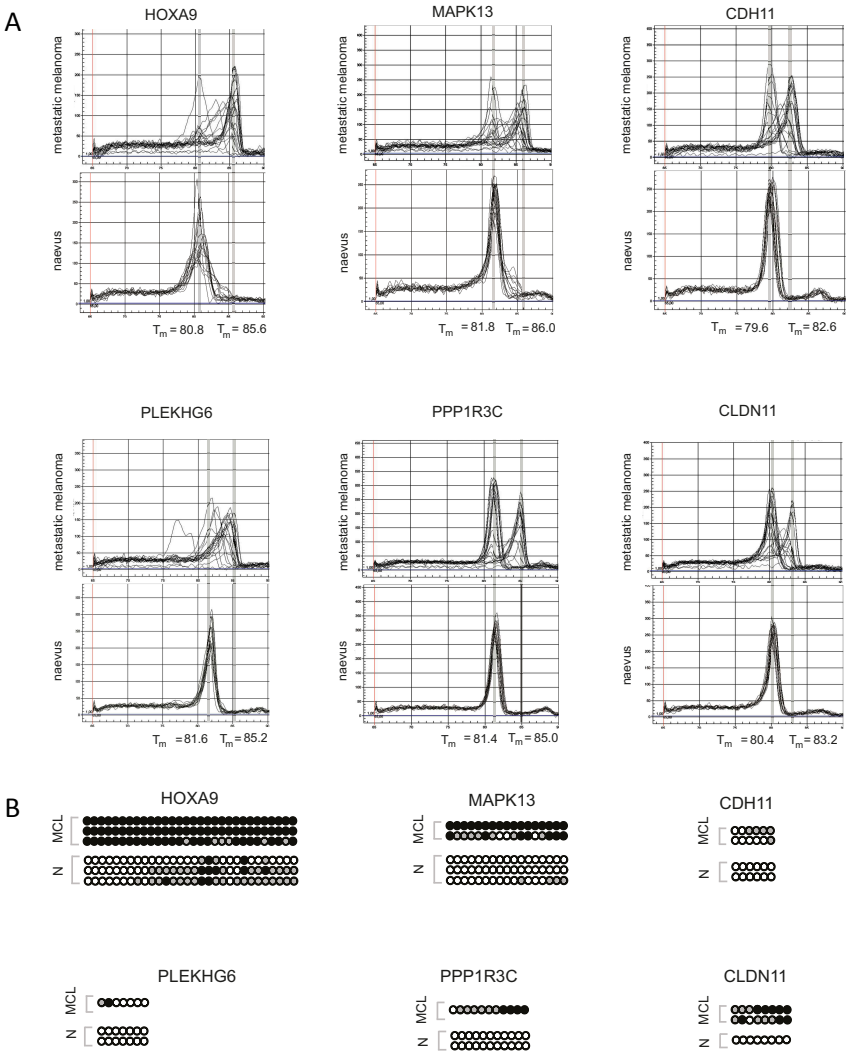

Supplementary Figure S2. **Promoter methylation status of *HOXA9*, *MAPK13*, *CDH11*, *PLEKHG6*, *PPP1R3C* and *CLDN11* in metastatic melanoma samples.** (**A**) Bisulphite melting curve profiles of seven cutaneous melanoma metastases and 13 early-passage metastatic melanoma cell lines were plotted overlapping in one graph (top) for each gene. The overlap of melting curves of the 15 naevi in one graph is included for comparison (bottom). The melanoma metastases show a peak in their melting curve patterns at the melting temperature (Tm) for methylated DNA, whereas naevi show a peak at the Tm for unmethylated DNA in the absence of a methylated DNA peak. Methylated DNA peaks in the melting curve pattern with a height of 0.5 or more relative to the unmethylated DNA peaks were considered indicative of methylation for the investigated CpG island amplicon. (**B**) Bisulphite sequencing analysis of CpG dinucleotides in the *HOXA9*, *MAPK13*, *CDH11*, *PLEKHG6*, *PPP1R3C* and *CLDN11* promoter regions in a selected number of metastatic melanoma cell lines (MCL) and naevi (N). An unmethylated cytosine of an interrogated CpG dinucleotide is depicted as a white circle, a methylated cytosine as a black circle, a partially methylated cytosine as a grey circle. An interrogated CpG island amplicon was considered methylated if the density of methylated CpG dinucleotides was 15% or more.

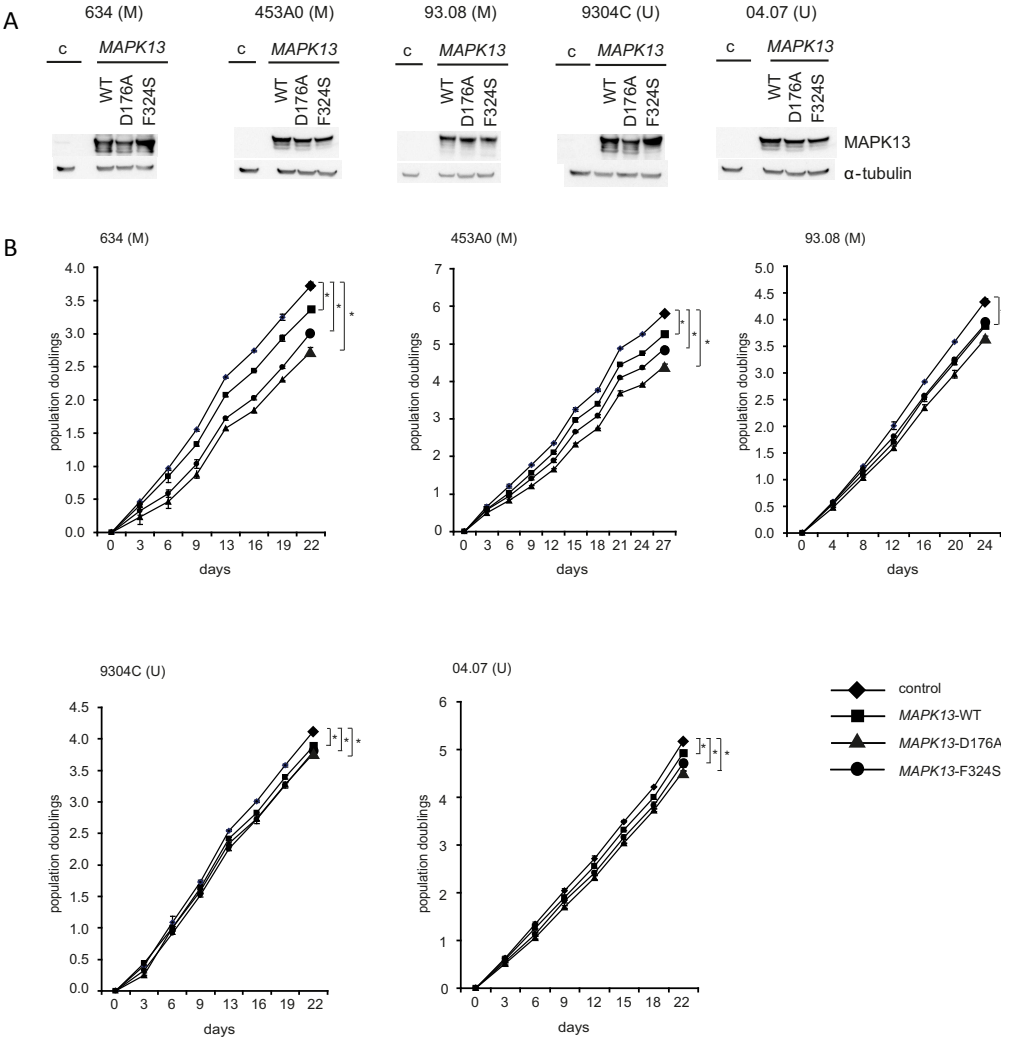

Supplementary Figure S3. **Restoration of MAPK13 expression in melanoma cells with *MAPK13* promoter methylation attenuates proliferation, long-term growth curves**. (**A**) Melanoma cell lines 634, 453A0, 93.08, 9304C and 04.07 were transduced using retroviral vectors (pBABE-puro-HA-MAPK13) expressing $MAPK13^{WT}$ or either of the active kinase mutants $MAPK13^{D176A}$ and $MAPK13^{F324S}$ and selected for succesful integration. Empty vectors were used as controls (c). Samples were analyzed for MAPK13 expression by Western blot 9 days post-infection, α-tubulin served as loading control. (Note that a short exposure was used to detect overexpressed MAPK13, explaining the seeming absence of the two corresponding endogenous protein in 9304C and 04.07 cells). The *MAPK13* promoter methylation status is indicated for each cell line; M, methylated (left); U, unmethylated (right). (**B**) Samples of the transduced melanoma cells were seeded at equal numbers and counted every three to four days starting at three days post-infection for at least three weeks. Error bars indicate standard deviation from triplicate cell counts at each time point; two-tailed t-test was applied for statistical analysis. *MAPK13* promoter methylation status is indicated; M, methylated (top row); U, unmethylated (bottom row). **P* <0.05.

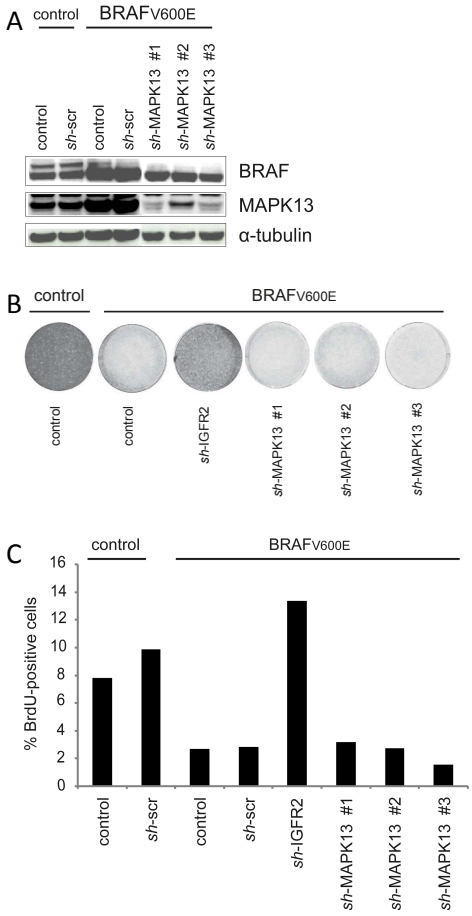

Supplementary Figure S4. **Depletion of *MAPK13* does not prevent cell cycle arrest induced by *BRAF*^{V600E} in human fibroblasts**. (**A**) TIG-3 human fibroblasts stably expressing one of the three independent *MAPK13* shRNAs (#1, #2 or #3) in addition to the ecotropic receptor, hTERT and a shRNA targeting *p16*^{INK4A}, were transduced with *BRAF*^{V600E}-encoding retrovirus and selected for integration of the construct. Empty vectors (control) and scrambled shRNA (sh-scr) were included as controls. Samples were analyzed for MAPK13 and BRAF expression by Western blot nine days post-infection, α-tubulin served as loading control. The depicted lanes originate from a single blot and were re-aligned for reading convenience of the figure. (**B**) Samples were seeded at equal densities and stained with crystal violet 13 days post-infection. Empty vectors were used as controls. An shRNA targeting *IGFR2* served as positive control for bypass of *BRAF*^{V600E}-induced proliferative arrest (Thomas Kuilman and D.S.P., unpublished results). Data are representative for three independent experiments. (**C**) Samples were seeded at equal densities and analyzed for BrdU incorporation 11 days post-infection. Empty vector (control) and scrambled shRNA (sh-scr) were included as controls.

Chapter 3

Near-genomewide RNAi screening for regulators of $BRAF^{V600E}$-induced senescence identifies *RASEF*, a gene epigenetically silenced in melanoma

Joanna Kaplon[1], Cornelia Hömig-Hölzel[1,4,‡], Linda Gao[2,‡], Katrin Meissl[1,5], Els M. E. Verdegaal[3], Sjoerd H. van der Burg[3], Remco van Doorn[2] and Daniel S. Peeper[1]

[1]Division of Molecular Oncology, The Netherlands Cancer Institute, Amsterdam, The Netherlands
[2]Department of Dermatology, Leiden University Medical Center, Leiden, The Netherlands
[3]Department of Clinical Oncology, Leiden University Medical Center, Leiden, The Netherlands
[4]Current address: Department of Clinical Chemistry and Clinical Pharmacology, University of Bonn, Siegmund-Freud-Str., 2553105, Bonn, Germany
[5]Current address: Institute of Animal Breeding and Genetics, University of Veterinary Medicine, Veterinärplatz 1, A-1210, Vienna, Austria
[‡]These authors contributed equally to this work.

Pigment Cell & Melanoma Research 2014; 27(4):640-52

Abstract

The activation of oncogenes in primary cells blocks proliferation by inducing oncogene-induced senescence (OIS), a highly potent in vivo tumor-suppressing program. A prime example is mutant BRAF, which drives OIS in melanocytic nevi. Progression to melanoma occurs only in the context of additional alteration(s) like the suppression of *PTEN*, which abrogates OIS. Here, we performed a near-genomewide short hairpin (sh)RNA screen for novel OIS regulators and identified by next generation sequencing and functional validation seven genes. While all but one were upregulated in OIS, depletion of each of them abrogated $BRAF^{V600E}$-induced arrest. With genome-wide DNA methylation analysis, we found one of these genes, *RASEF*, to be hypermethylated in primary cutaneous melanomas but not nevi. Bypass of OIS by depletion of *RASEF* was associated with suppression of several senescence biomarkers including senescence-associated (SA)-*β*-galactosidase activity, interleukins, and tumor suppressor $p15^{INK4B}$. Restoration of *RASEF* expression inhibited proliferation. These results illustrate the power of shRNA OIS bypass screens and identify a potential novel melanoma suppressor gene.

Introduction

Several tumor-suppressive mechanisms have evolved to prevent malignant transformation including self-destructive programs such as apoptosis[1] and autophagy[2]. Work in recent years has uncovered that cells at risk for oncogenic transformation can embark on another strategy: in response to obstinate stress signals, they activate signaling networks comprising several potent tumor suppressor proteins. In this way, a system is established enacting a dominant break that actively halts cell proliferation. This type of cell cycle arrest, termed 'oncogene-induced senescence (OIS)', can be maintained even in the context of persistent oncogenic cues[3]. In recent years, a large body of evidence has shown that OIS acts as a pathophysiologic mechanism suppressing cancer in model systems and humans alike. Indeed, senescence biomarkers have been reported for a plethora of precancerous lesions including melanocytic nevi, pulmonary adenomas, prostate intraepithelial neoplasia, and mammary lesions[4].

Cellular senescence denotes a state of virtually irreversible withdrawal of cells from the proliferative pool. While we have come to realize that its onset can be triggered by a plethora of stress-related signals, it was first recognized in cultured human diploid fibroblasts (HDFs) following explantation and in vitro culturing. With every cell division, telomeres get progressively shorter, causing cells to hit their 'Hayflick limit' at the end of their replicative life span[5]. Such replicative senescence has correlates in the context of other stress signals, most notably the activation of oncogenes or loss of tumor suppressor alleles. As the latter occurs independently of telomere malfunction, it is referred to as premature cellular senescence[3].

Next to long-term cell cycle arrest, which is the central characteristic of senescent cells, OIS is characterized by the activation of tumor suppressor pathways including-but not restricted to-those constituted by p16^{INK4A}-RB and ARF-p53[6-8]. Conversely, cell cycle progression factors such as cyclins A and B and PCNA are inhibited[3]. Oncogene-induced senescence is accompanied also by morphological changes, induction of senescence-associated *β*-galactosidase activity (SA-*β*-Gal)[9], and chromatin condensation into senescence-associated heterochromatin foci (SAHF)[10,11].

Another characteristic of cells undergoing OIS is the activation of an inflammation-associated secretory program called senescence-messaging secretome (SMS) as we and others have shown[12-14] or senescence-associated secretory phenotype (SASP), the latter of which is associated with a DNA damage response[15,16]. The physiologic relevance of the inflammatory phenotype is reflected by the production of a number of interleukins and chemokines in senescent cells in benign murine and human neoplasms[17]. But secreted senescence-associated (SA) factors also limit tissue damage[18] and correlate with premature aging[19]. Yet another function of senescence-associated secreted factors is to activate the innate immune system, setting up incipient cancer cells for their own demise[20,21]. Further supporting a cell non-autonomous role for senescence, it was recently shown that this program can be brought about also in a paracrine fashion[22].

Lately, we and others have discovered functional connections between the cellular metabolism and OIS. Aird et al. (2013)[23] have demonstrated that stable cell cycle arrest in OIS is established and maintained through suppression of nucleotide metabolism. Others have highlighted the importance of malic enzyme activity in OIS[24]. We identified mitochondrial gatekeeper pyruvate dehydrogenase (PDH) as an enzyme critically contributing to OIS[25]. In OIS, PDH is activated upon downregulation of its inhibitory kinase PDK1 and simultaneous upregulation of PDH activating phosphatase PDP2. Normalization of the levels of these enzymes inactivates PDH resulting in abrogation of OIS. Translating these findings to a clinical context, we demonstrated that PDK1 depletion eradicates established melanomas, highlighting this metabolic enzyme as a potentially attractive therapeutic metabolic cancer target.

The benign melanocytic nevus was the first human lesion for which evidence was shown in favor of the idea that OIS prevents malignant progression[26]. Three years prior to that, *BRAF^{V600E}* was identified as a common mutation in melanoma and other cancer types[27]. Remarkably, in spite of the presence of oncogenic mutations in the *BRAF* (or, in some cases, *NRAS*) gene[28], nevi are typically associated with an exceedingly low proliferative activity. However, while this proliferative arrest can be maintained for decades[29], several studies provide genetic evidence that a fraction of nevi still progresses to melanoma[30-32]. As a *BRAF^{V600E}* mutation alone is insufficient to drive melanomagenesis, nevi must acquire additional genetic and/or epigenetic alterations to evade growth

restraints and become malignant. Several genetic events frequently occurring in melanoma have been described, including the loss of *CDKN2A* and *ARF*, amplification of *CCND1* or *CDK4*[33,34], alterations in *MMP8*, *GRM3*, *ERBB4*, *GRIN2A*, *MITF* [35-39], and activation of the PI3K pathway[40]. We have demonstrated previously that the latter event, for example by reduction in the expression levels of *PTEN*, reflects a rate-limiting step in OIS abrogation on the path to oncogenic transformation[41]. Moreover, recent exome and whole genome sequencing studies reported frequent mutations in melanoma of several genes including *RAC1* and *PREX2*[42-44].

In addition to genetic alterations, tumor suppressor genes can be inactivated by epigenetic means. Promoter hypermethylation has emerged as an important epigenetic mechanism responsible for transcriptional repression of a multitude of genes in human cancer cells. In melanoma, several established tumor suppressor genes have been shown to be inactivated secondary to promoter hypermethylation, including *CDH1*, *RASSF1A*, and *SERPINB5*[45]. Although the role of some of the above-mentioned genes affected by mutation or promoter hypermethylation in melanoma has been demonstrated, the mechanistic relationship with OIS is unclear for most. Hence, the molecular mechanism and the identity of the factors underlying malignant transformation in relation to OIS and OIS bypass are largely unknown. Therefore, we set out to perform a near-genomewide (sh)RNA screen for novel OIS factors. Such genes would be predicted to function as tumor suppressor genes in tumor cells expressing an activated oncogene, with PTEN serving as a prime example[46,47]. We have recently performed a genome-wide analysis of promoter methylation in primary melanoma and benign nevus and identified a large number of genes, including several tumor suppressor genes, to be hypermethylated in melanoma[48]. Here, we have integrated the data from both RNAi screening and methylation analyses.

Methods

Cell culture, viral transduction, and senescence induction

The HDF cell line TIG3 expressing the ectopic receptor, hTERT, and sh-p16^{INK4A} as well as melanoma cell lines (04.04, 04.07, 05.06, 518A2, 06.24, 607B, 634, 93.08, 94.03C, 94.07, 94.13, A875, BLM, Mz7.4) were maintained in DMEM, supplemented with 9% fetal bovine serum (Sigma, St. Louis, MO) and 2mM glutamine (GIBCO, Carlsbad, CA, USA). Melanocytes were maintained as described previously[49]. Lentiviral and retroviral infections were performed using HEK293T cells and Phoenix cells, respectively, as producers of viral supernatants. For senescence experiments, HDF or melanocytes were infected with shRNA-encoding or protein-coding retro- or lentivirus, selected pharmacologically (puromycin or blasticidin) and subsequently infected with BRAF^{V600E}-encoding or control virus. After selection, cells were seeded for cell proliferation assay, BrdU incorporation assay, SA-*β*-galactosidase activity and analyzed.

Cell proliferation assay

Cells were seeded into a six-well plate (at different densities: $2x10^5$, $4x10^5$, or $6x10^5$ cells, respectively) and selected pharmacologically. Fixation and staining with crystal violet was performed 9–18 days after the $BRAF^{V600E}$-encoding or control virus infection, or 12–16 days after RASEF-encoding or control eGFP-encoding virus infection. Images of cell proliferation assays reflect representative results of at least three independent experiments.

BrdU incorporation assay

BrdU labeling was carried out for 3h followed by fixation. Incorporated BrdU was detected by immunostaining as described in Serrano et al., 1997[3] and FACS analysis. Results are represented as mean with SD of at least three independent experiments.

Analysis of SA-β-galactosidase activity

Senescence-associated β -galactosidase was stained using the 'Senescence Associated β -Galactosidase Staining Kit' from Cell Signaling (Danvers, MA, USA) at pH6 according to the manufacturer's protocol. Images reflect representative results of at least three independent experiments.

Trypan blue exclusion assay

Cells were brought into suspension using trypsin, centrifuged and resuspended in a small volume of culture medium. Trypan blue (Sigma) was added to the cell suspension (dilution factor = 2), and stained cells were counted as dead. The number of dead cells was quantitated, and the values were expressed as the fold change over control. Results are represented as mean with SD of at least three independent experiments.

Plasmids

The human TRC1 shRNA Library was purchased from Sigma-Aldrich. pMSCV-blast-$BRAF^{V600E}$ and pMSCV-blast, KH1-GFP-shPTEN#1, HIV-CSCG-blast-$BRAF^{V600E}$, and HIV-CSCG-blast were previously described[13,41]. For the re-expression of RASEF, the pLX304-RASEF-V5 as well as control pLX304-eGFP-V5 plasmids, both from CCSB-Broad Lentiviral Expression Library (Cambridge, MA, USA), were purchased from Thermo Scientific (Waltham, MA, USA).

shRNAs

The human TRC1 shRNA Library was purchased from Sigma-Aldrich (http://www.sigmaaldrich.com/life-science/functional-genomics-and-rnai/shrna/products/lentiplex.html). Lentiviral knockdown constructs were purchased from Sigma-Aldrich in pLKO.1 backbone:

shUBE2V1#1–TRCN0000033708 – 5'-CGCCTAATGATGTCTAAAGAA-3'

shUBE2V1#2–TRCN0000033706 – 5′-CCAAGAGCCATATCAGTGCTA-3′
shNMRAL1#1–TRCN0000036912 – 5′-GGGACATTCAAGGTTCGAGT-3′
shNMRAL1#2–TRCN00000036913 – 5′-CAAGATGACTCCTGAGGACTA-3′
shPCDHGA10#1–TRCN0000053343 – 5′-TTTCTATTTCATAGAAACCGG-3′
shPCDHGA10#2– TRCN0000053344 – 5′-ATTCCTCAGGAATTGAGTAGG-3′
shSLC1A4#1– TRCN0000038641 – 5′-AGAGGATCAGCAGGTTTAT-3′
shSLC1A#2– TRCN0000038642 – 5′-CCACCTGAATCAGAAGGCAA-3′
shWT1#1– TRCN0000001114 – 5′-AAAGTTTACATTAGCAGACAC-3′
shWT1#2– TRCN0000001117 – 5′-AAGTCACACTGGTATGGTTTC-3′
shGEMIN6#1– TRCN0000147641 – 5′-TTCATAGTTTCAACAGTCTGC-3′
shGEMIN6#2– TRCN0000146917 – 5′-TATACTCATTCTTCTCACTGG-3′
shRASEF#1– TRCN0000055624 – 5′-TAATGGGAACAGTCTCATGGG-3′
shRASEF#2– TRCN0000055625 – 5′-TTTCCGTGTCTTATGTTCTGC-3′
shRASEF#3– TRCN0000055626 – 5′-ATTCTCGTATGTTAAGAAAGC-3′

Quantitative real-time PCR

Total RNA was DNase-treated with RQ1 RNase-Free DNase (Promega, Madison, WI, USA). Reverse transcription was performed with SuperScript II First Strand Kit (Invitrogen, Carlsbad, CA, USA). Quantitative real-time PCR was performed with the SYBR Green PCR Master Mix (Applied Biosystems, Carlsbad, CA, USA) on an ABI PRISM 7700 Sequence detection System (Applied Biosystems). Primer sets used were as follows:
UBE2V1: 5′-GGAGAGGTTCAAGCGTCTTACC-3′ and 5′-TTCGAGTTCTTCCAACAGTCG-3′
NMRAL1: 5′-GCTTACGCCACCTTCATCG-3′ and 5′-CAGATCAGCGAGCAGCTTCC-3′
PCDHGA1′: 5′-CTGCAAGCCATGATCTTGG-3′ and 5′-AGACATTCTGGCGGTAGTCG-3′
SLC1A4: 5′-TCCGAAGGAGAAGACCTCATCC-3′ and 5′-CTTCCAACAAGGAACATGATGC-3′
WT1: 5′-TACAGCACGGTCACCTTCG-3′ and 5′-CACCGAGTACTGCTGCTCAC-3′
GEMIN6: 5′-CGAGTGACAGCCAGTGAGAAG-3′ and 5′-ATCTTCAAGGAAGTTCACAAGG-3′
RASEF: 5′-GCTGCTACAGAGGGACAAAAA-3′ and 5′-CAGAATAATGCCCCATACGTC-3′
Or 5′-ATCAGACTTCAAAGCACAGAAATGG-3′ and 5′-TTCCTCTTCCAACTCACTCAACTG-3′
IL6, IL8, C/EBP*β*, and RPL13 (standard) primer sequences were described previously[13]. All primer pairs except C/EBP*β* span exon-exon borders. *RPL13* was used as control. For analysis, the ΔCT method was applied. Data are represented as mean SD of three or more independent experiments.

Antibodies

Antibodies used for immunoblotting were BRAF (sc-5284; Santa Cruz, Dallas, TX, USA), Hsp90 (4874; Cell Signaling), MAP kinase p44/42 (9102; Cell Signaling); phospho-MAP kinase p44/42 (9106; Cell signaling), MEK1/2 (L38C12; 4694; Cell Signaling), phospho-MEK1/2 [Ser217/221] [(41G9); 9154; Cell Signaling], PCNA [(PC10); sc-56; Santa Cruz], $p21^{Waf1/Cip1}$ [(C19); sc-397; Santa Cruz], $p15^{INK4B}$ (sc-612; Santa Cruz), p53 [(DO-1); sc-126; Santa Cruz]; phospho-RB (Ser807/811) (9308; Cell Signaling), total RB (9309; Cell Signaling); RASEF (HPA021431; Sigma), V5-tag (R960-25; Invitrogen).

Patient samples

Fresh-frozen and paraffin-embedded biopsy specimens were obtained from 76 primary cutaneous melanomas and from 15 benign melanocytic nevi, all containing at least 70% melanocytic cells (for detailed clinical information, see Table S2). The *BRAF* and *NRAS* mutation status of a subset of five nevi and 24 primary melanomas was determined using allele-specific PCRs for $BRAF^{V600E}$, $BRAF^{V600K}$, $NRAS^{G12D}$, $NRAS^{Q61K}$, $NRAS^{Q61L}$, $NRAS^{Q61R}$, and $NRAS^{Q61H}$ mutations on a CFX384 Real-Time Detection System (Bio-Rad, Hercules, CA). DNA was extracted with the Genomic-tip kit (Qiagen, Hilden, Germany) or RecoverAll Nucleic Acid kit (Ambion, Carlsbad, CA).

Bisulfite melting curve analysis and BSA

Bisulfite conversion was performed with the EZ DNA methylation kit (Zymo Research, Orange, CA). *RASEF* bisulfite primers for BMCA and BSA were designed to amplify a 126-base pair region at +259 from the TSS, located within the CpG island that covers the promoter region and first exon of the *RASEF* gene (5'-GGGATGGAGGCGGATGGG-3' and 5'-GGTATTGTGTACGGAGTTGCGG-3'; Figure 3B). Sensitivity of the primer set for BMCA was validated using mixtures, 1:1, 1:3, 1:9, and 1:9.5, of completely methylated CpGenome universal methylated DNA (Chemicon, Hampshire, UK) and unmethylated semen DNA, respectively, showing that methylation could be accurately detected if 10% of the total analyzed DNA was methylated. Generated bisulfite melting curves of the *RASEF* CpG island amplicon were scored as previously described[48]. Sequences obtained from BSA were considered methylated if the density of methylated CpG dinucleotides within the interrogated amplicon was 15% or more, a threshold value that has been previously used as a scoring standard[50,51].

5-aza-2'-deoxycytidine treatment

Melanoma cell lines 634 and 06.24 were seeded at 15% confluency and treated with 2μM 5-aza-2'-deoxycytidine (Decitabine; Sigma) for 96h. Culture medium was replaced with medium containing freshly prepared 5-aza-2'-deoxycytidine every 24h. Cells were harvested for RNA extraction with the RNeasy Mini kit (Qiagen), and expression of *RASEF* was analyzed by qRT-PCR. Stable expression of the reference genes *TBP* and *CPSF6* was validated using geNorm analysis[52].

Statistical analysis

Statistical analyses were done with t-tests, unless stated otherwise. *P* values of less than 0.05 were considered significant. *$0.01 < P < 0.05$; **$0.001 < P < 0.01$; ***$P < 0.001$.

Results

Near-genomewide shRNA screen identifies genes required for BRAF^{V600E}-induced senescence

To identify factors required for BRAF^{V600E} to induce senescence, we performed a function-based knockdown screen for genes that can rescue this type of cell cycle arrest (Figure 1A). Human diploid fibroblasts (HDF) were transduced with a near-genomewide lentiviral shRNA library targeting approximately 15,000 human genes, organized in 10 pools with some five shRNAs per gene target. Transduction was performed at a multiplicity of infection (MOI) of 0.5 to ensure that in most cases only a single shRNA integrated per cell. The number of cells used for transduction was calculated to obtain a minimum coverage of 10. After pharmacological selection, cells were transduced with BRAF^{V600E}-encoding retrovirus. While cells containing empty vector control underwent cell cycle arrest as expected, cells that contained library shRNAs abrogating BRAF^{V600E}-induced senescence kept growing and formed colonies. These colonies were subsequently picked individually, expanded, and their genomic DNA was isolated. To identify hits, gDNAs isolated from individual colonies derived from independent shRNA pools were grouped and received a unique index. shRNAs were re-amplified and analyzed by deep sequencing. If a particular shRNA gave rise to more than one colony, it would be present in more than one group.

Candidates for validation were selected based on two criteria: (i) the presence of at least two shRNAs targeting the same gene to reduce the chance of off-target effects and (ii) the extent of senescence abrogation: only shRNAs identified in independent colonies were further analyzed (Table S1). On the basis of these criteria, shRNAs targeting 40 genes were re-evaluated, one by one, for their ability to abrogate BRAF^{V600E}-induced cell cycle arrest. Seven genes (*UBE2V1*, *NMRAL1*, *PCDHGA10*, *SLC1A4*, *WT1*, *GEMIN6*, *RASEF*) could be validated in multiple rounds each with two shRNAs in cell proliferation assays (Figure 1B) and BrdU incorporation assays (Figure 1C).

We next tested whether the identified shRNAs were on-target, that is, whether they deplete the gene of interest. Quantitative real-time (qRT) PCR analysis confirmed that in all cases, the expression of the target gene was decreased (Figure 1D–J). We previously demonstrated that OIS genes are commonly induced by the oncogenic stressor, for example interleukins[13]. Consistent with this notion, the expression of all genes but *SLC1A4* was induced in senescent cells. Taken together, this near-genomewide function-based shRNA screen identified seven genes crucial for BRAF^{V600E}-induced cell cycle arrest.

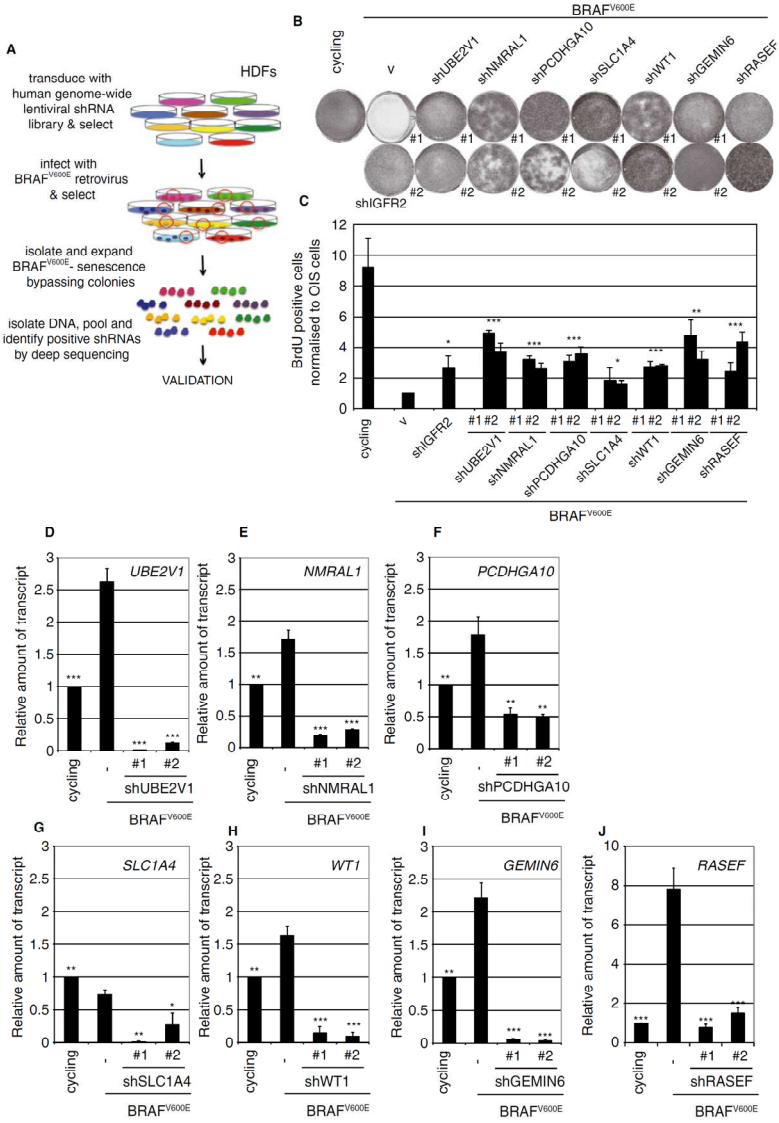

Figure 1. **Near-genomewide shRNA screen identifies genes required for BRAFV600E-induced senescence**. (**A**) Schematic summary of the screen setup. (**B**) Cell proliferation assay on human diploid fibroblasts transduced with vector control or shRNA targeting candidate genes identified in the screen. Cells were fixed and stained 11 days after exposure to BRAF^{V600E}. shRNA targeting IGFR2 was used as a positive control (Kuilman T., Peeper D.S., unpublished data). (**C**) BrdU incorporation of samples described in B, measured 9 days after exposure to BRAF^{V600E}. Levels are represented as mean of three independent validation rounds. Error bars represent SD. Significance was determined by one-way ANOVA comparing OIS cells with cells depleted of the indicated target gene. (**D–J**) Regulation of gene transcripts of the samples described in B as determined by quantitative real-time qRT-PCR. Measurements are standardized to the vector-expressing cells. Error bars represent SD from triplicate qRT-PCRs *P* values of less than 0.05 were considered significant. *0.01 < *P* < 0.05; **0.001 < *P* < 0.01; ***$P <$ 0.001.

RASEF is a new OIS gene

Of the seven genes identified in the screen, the expression of RAS and EF-hand domain containing (*RASEF*) transcript, also known as *RAB45*, was induced by $BRAF^{V600E}$ to the highest extent (Figure 1J). Additionally, the RASEF locus was previously shown to be associated with predisposition to hereditary melanoma[53] and epigenetically regulated in uveal melanoma[54]. In light of those observations, and because $BRAF^{V600E}$-induced senescence prevents nevi from progressing to melanomas[49], we studied the role of RASEF in OIS and OIS abrogation in more detail.

For this, with the use of an additional shRNA, we confirmed that *RASEF* depletion (Figure 2A) abrogates $BRAF^{V600E}$-induced cell cycle arrest as determined by cell proliferation (Figure 2B) and BrdU incorporation assays (Figure 2C). The abrogation of cell cycle arrest was seen already at day 10 after introduction of $BRAF^{V600E}$ (around the day when senescence is fully established) and was maintained up to at least 18 days (Figure 2B). Importantly, this could not be explained by loss of $BRAF^{V600E}$ expression or loss of activation of downstream MEK/ERK signaling (Figure 2D). The rescue of proliferation by RASEF knockdown was associated with restoration of expression of the DNA replication-associated protein PCNA (Figure 2D). Moreover, *RASEF* depletion resulted in a profound suppression of other common senescence-associated biomarkers (SA)-*β*-galactosidase activity (Figure 2E), expression of the SA $p15^{INK4B}$ tumor suppressor (Figure 2D), and the number of SAHF-positive cells (Figure 2F). Whereas RB as expected accumulated in its hypo-phosphorylated form in $BRAF^{V600E}$ senescent cells, *RASEF* depletion reversed its phosphorylation status (Figure S1), suggesting cross talk between RASEF and RB signaling. In contrast, p53 expression levels remained unaffected. Notably, RASEF depletion also led to a marked reduction in IL6 and IL8 transcript levels, typical of cells abrogating OIS (Figure 2G). We have previously identified C/EBP*β* to be a critical mediator in the interleukin pathway leading to OIS[13]. Indeed, while the *C/EBPβ* transcript was highly induced in OIS, this was significantly reduced upon RASEF silencing (Figure 2H). From these findings, we conclude that *RASEF* is a new and essential component of OIS.

RASEF is hypermethylated in melanoma

Recently, we reported a genome-wide analysis of promoter hypermethylation in primary cutaneous melanomas and benign nevi, interrogating the methylation status of 14,495 genes[48]. The identification in the present study of seven genes required for $BRAF^{V600E}$-induced senescence prompted us to examine whether any of these genes is epigenetically silenced in melanoma harboring a mutant *BRAF* gene. We reanalyzed the epigenomic profiling data taking into account the *BRAF* mutation status of the melanoma and nevus samples. From the samples subjected to genome-wide methylation analyses, all five nevi

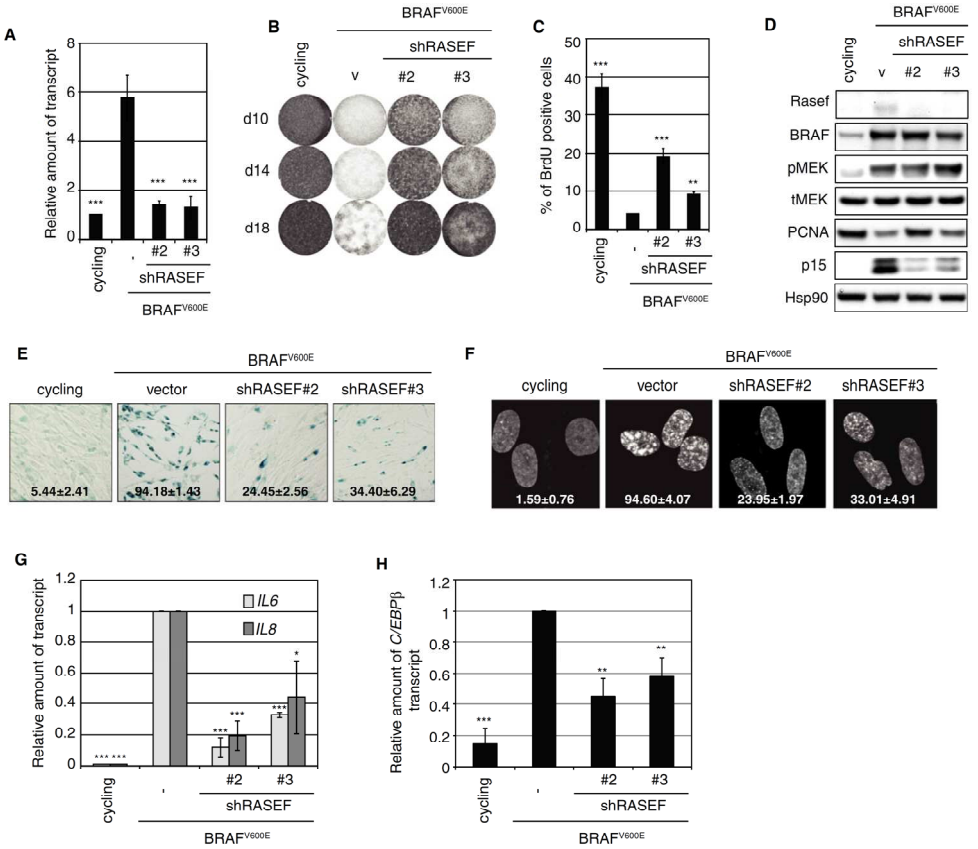

Figure 2. ***RASEF* is a new OIS gene**. (**A**) Regulation of *RASEF* transcript in human diploid fibroblasts expressing vector control or non-overlapping shRNAs targeting *RASEF* in the presence and absence of oncogenic BRAF^{V600E}. Level of expression is determined by quantitative real-time qRT-PCR. Measurements are based on three independent experiments and standardized to the vector-expressing senescent cells. Error bars represent SD. (**B**) Cell proliferation assay on samples from A. Cells were fixed and stained 13 days after exposure to BRAF^{V600E}. (**C**) BrdU incorporation of samples described in A, measured 9 days after infection with BRAF^{V600E}-encoding retrovirus. Levels are represented as mean of at least three independent experiments. Error bars represent SD. (**D**) Samples from A were analyzed by immunoblotting with antibodies as indicated. Hsp90 serves as loading control. (**E**) Representative images of senescence-associated (SA)-*β*-galactosidase staining for the cells described in A. Quantification of SA-*β*-galactosidase-positive cells was performed on three independent experiments, with SD. (**F**) Representative images of DAPI staining for the cells described in A. Quantification of SAHF-positive cells was performed on two independent experiments, with SD from triplicate. (G, H) Regulation of *IL6* and *IL8* (**G**) and *C/EBPβ* (**H**) transcripts of the samples described in A., as determined by qRT-PCR. Measurements are based on three independent experiments and standardized to the BRAF^{V600E}-expressing senescent cells. Error bars represent SD. *P* values of less than 0.05 were considered significant. *0.01 < *P* < 0.05; **0.001 < *P* < 0.01; ***$P <$ 0.001.

and five of 24 melanomas harbored a *BRAF^{V600E}* mutation, while two had a *BRAF^{V600K}* mutation. It appeared that, of the seven genes identified in the shRNA screen, only the *RASEF* gene was differentially methylated in nevi and melanomas. In fact, *RASEF* was among the 16 most frequently hypermethylated genes in *BRAF*-mutant melanomas,

whereas its methylation was absent from nevi. Comparative analysis pointed to hypermethylation in four of seven *BRAF*-mutant melanomas with an average *β*-value difference (a measure of differential methylation) of 0.32 (Figure 3A). We proceeded with the validation of *RASEF* promoter hypermethylation in a panel of 76 primary melanoma and 15 nevus biopsy specimens using bisulfite melting curve analysis (BMCA). In 16 of 76 melanoma samples (21%), the *RASEF* promoter was hypermethylated, whereas none of the 15 nevi showed methylation (Figure 3B). Bisulfite sequencing analysis (BSA) of five nevi, three primary melanomas, and two early-passage melanoma cell lines further confirmed dense *RASEF* hypermethylation in the primary tumors and melanoma cell lines, against a general absence of *RASEF* methylation in the nevi (Figure 3C). To further assess whether an association exists between *RASEF* promoter methylation and *BRAF* mutation in melanoma, we performed mutation analysis of *BRAF* and *NRAS* on a subset of 24 primary melanomas. In four of these, *RASEF* was methylated; this included one melanoma with a *BRAF* mutation, no melanoma with *NRAS* mutation, and three not harboring mutations in these melanoma oncogenes (Table S2). This result shows that *RASEF* methylation is not confined to melanomas that carry a *BRAF* mutation.

Next, we assessed the correlation between *RASEF* promoter methylation and transcript abundance in a panel of melanoma cell lines. In addition, we analyzed whether a relationship exists between *RASEF* silencing, MAP kinase pathway activation, and the RB pathway. *RASEF* transcript expression was very low to undetectable in the six melanoma cell lines with promoter hypermethylation, whereas significantly higher *RASEF* expression was present in several cell lines with absent *RASEF* promoter methylation (Figure 3D, Figure S2). RASEF expression levels neither correlated with MAP kinase pathway activation (as judged by lack of differences in ERK and MEK phosphorylation; Figure S3) nor with RB phosphorylation (Figure S4). Treatment with 5-aza-20-deoxycytidine of two different cell lines derived from melanoma metastases, both positive for *RASEF* promoter methylation, resulted in reactivation of *RASEF* gene expression with an induction of 7- and 3.5-fold in the cell lines 634 and 06.24, respectively (Figure 3E), suggesting that promoter methylation of *RASEF* is correlated with transcriptional silencing. Collectively, these results demonstrate that hypermethylation of the *RASEF* gene affects 21% of primary cutaneous melanomas.

RASEF acts as potential tumor suppressor

The essential role of *RASEF* in OIS, together with data on its differential methylation in nevi and melanomas, would be consistent with a tumor-suppressive role for *RASEF*. This hypothesis would predict that restoration of *RASEF* expression in cells in which the gene has been silenced by methylation acts cytostatically. Therefore, we reexpressed *RASEF* in

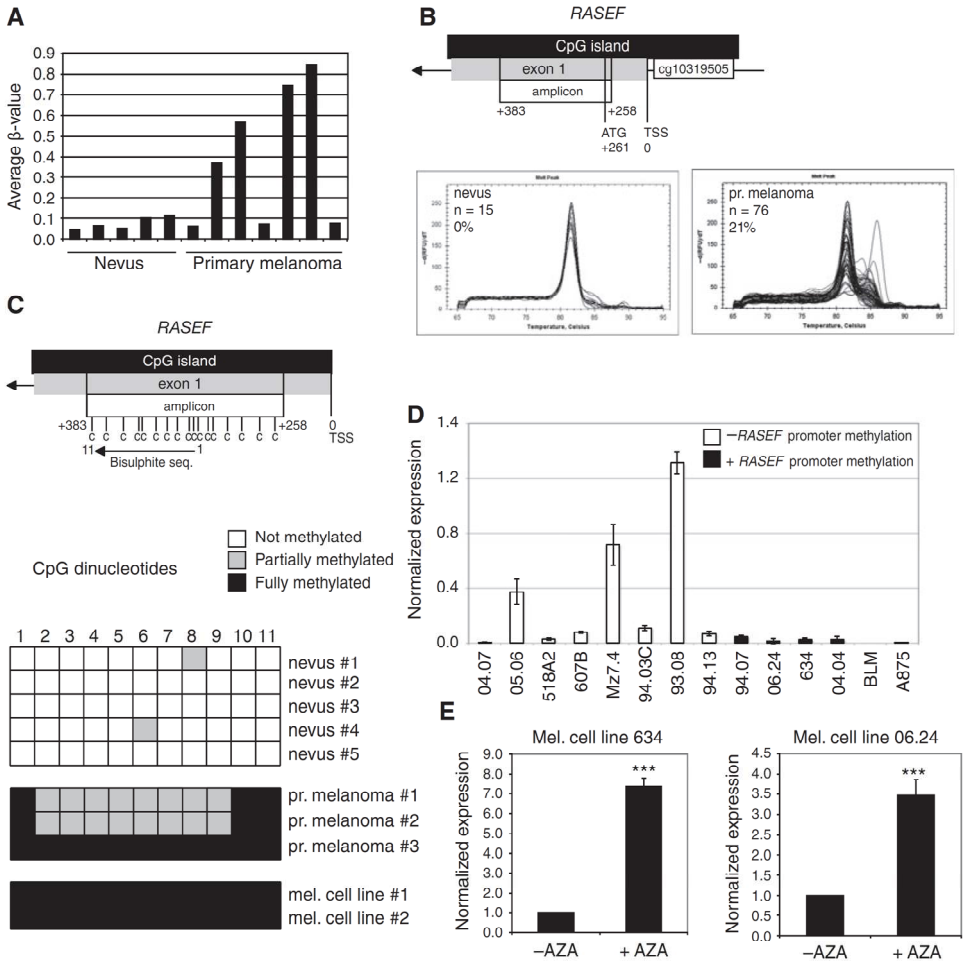

Figure 3. ***RASEF* is hypermethylated in melanoma**. (**A**) Hypermethylation of the *RASEF* promoter in *BRAF*-mutant primary melanoma samples as measured by Infinium's 27 K genome-wide beadchip assay. Normalized average *β*-values represent extent of methylation of probe cg10319505 for five *BRAF*-mutant nevi and seven *BRAF*-mutant primary melanoma samples. (**B**) *RASEF* promoter methylation status by bisulfite melting curve analysis of the indicated *RASEF* CpG island region performed in 15 benign nevi and 76 primary melanoma biopsy samples. (**C**) *RASEF* promoter methylation analysis by bisulfite sequencing of the indicated CpG dinucleotides in five benign nevi, three primary melanomas, and two early-passage melanoma cell lines. (**D**) *RASEF* mRNA expression levels in early-passage melanoma cell lines with known *RASEF* promoter methylation status as determined by quantitative real-time qRT-PCR. Error bars represent SD from triplicate qRT-PCRs. (**E**) Reactivation of *RASEF* mRNA expression upon 5-aza-2'-deoxycytidine treatment in early-passage melanoma cell lines 634 and 06.24 with pre-existent *RASEF* methylation. Measurements are representative for treatment experiments performed in duplicate, SD from triplicate qRT-PCRs. *P* values of less than 0.05 were considered significant. *0.01 < *P* < 0.05; **0.001 < *P* < 0.01; ****P* < 0.001.

two *BRAF*-mutant melanoma cell lines (04.04 and A875) with a hypermethylated *RASEF* promoter and very low *RASEF* mRNA expression (Figure 3D). We ectopically expressed V5-tagged *RASEF* (Figure 4A) and analyzed the effect on cell proliferation and survival. In both cell lines, this resulted in the induction of cell cycle arrest as measured by cell proliferation and BrdU incorporation assays (Figure 4B, C). This was associated with a decrease in the steady state levels of PCNA and an induction in the levels of the SA protein $p21^{Cip1}$ (Figure 4A). We could not detect $p15^{INK4B}$ protein in these cell lines, possibly owing to a deletion of the locus, which is commonly seen in melanoma. The *RASEF*-induced cell cycle arrest was not associated with cell death (Figure 4D,E). Melanoma cell lines in which *RASEF* was methylated were more prone to halt cell cycle progression upon its reintroduction than were the *RASEF*-proficient cells (Figure S5). These observations together are compatible with a model in which *RASEF* has a tumor suppressor function.

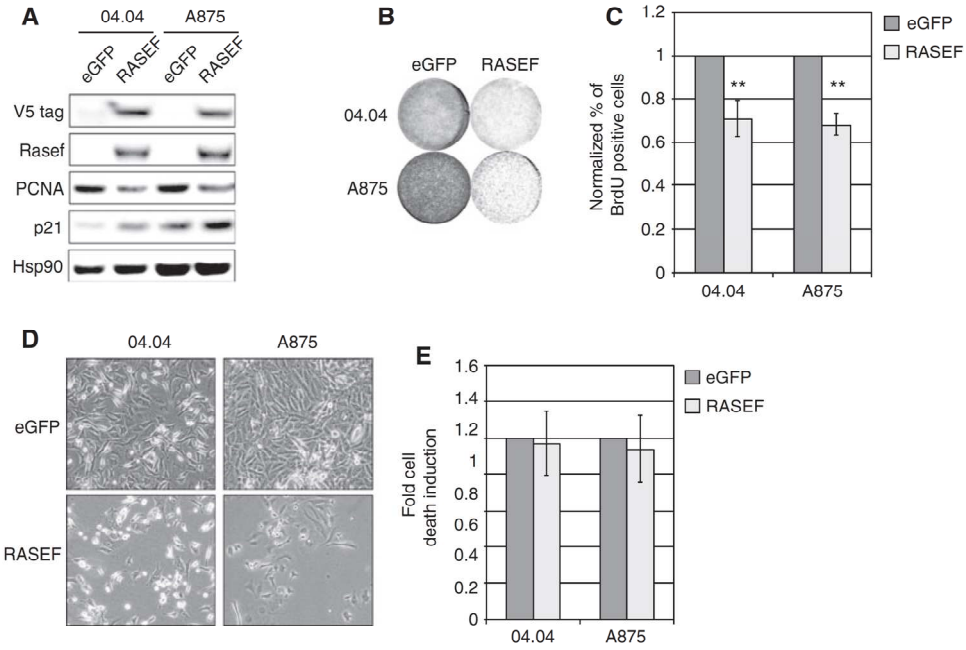

Figure 4. ***RASEF* acts as potential tumor suppressor**. (**A**) Immunoblotting analysis of two indicated melanoma cell lines expressing eGFP as control or RASEF. Hsp90 serves as loading control. (**B**) Cell proliferation assay on samples from A. Cells were fixed and stained 12 days after exposure to RASEF. (**C**) BrdU incorporation of samples described in A, measured 16 days after infection with RASEF-encoding lentivirus. Levels are represented as mean of at least three independent experiments. Error bars represent SD. (**D**) Representative phase contrast images for the cells described in A. (**E**) Cell death induction of cells described in A as measured by trypan blue exclusion assay. Results represent mean of at least three independent experiments. Error bars represent SD. *P* values of less than 0.05 were considered significant. *$0.01 < P < 0.05$; **$0.001 < P < 0.01$; ***$P < 0.001$.

RASEF contributes to BRAF^{V600E}-induced senescence in melanocytes

We identified and subsequently validated *RASEF* in a function-based screen for genes that are required for OIS in a model system, cultured HDFs (Figures 1 and 2). The results above indicate that this gene is frequently silenced in melanoma (Figure 3). Together, these data predict that *RASEF* plays an important role also in melanocytes, in the context of OIS. We therefore validated the key results obtained in fibroblasts in cultured human melanocytes. Indeed, *RASEF* depletion in BRAF^{V600E}-expressing melanocytes caused an almost five-fold induction of cell proliferation, as measured by BrdU incorporation assay (Figure 5A,B), similar to what we previously reported for *PTEN*[41]. This was associated with a drop in several senescence biomarkers, particularly *IL6* and *IL8*, as well as *C/EBPβ* transcripts (Figure 5C–E). We conclude from these results that *RASEF* is a candidate melanoma susceptibility gene that acts, at least in part, by contributing to OIS.

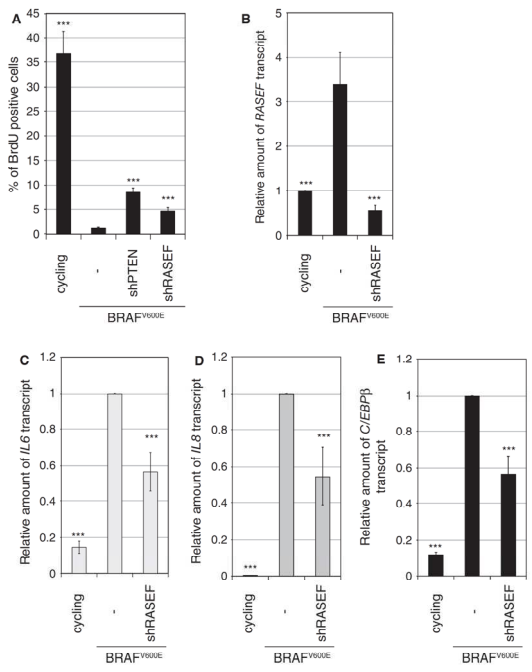

Figure 5. ***RASEF* contributes to BRAF^{V600E}-induced senescence in melanocytes**. (**A**) BrdU incorporation in cultured human melanocytes expressing vector control or shRNA targeting *RASEF* in the presence and absence of oncogenic BRAF^{V600E}. shRNA targeting *PTEN* was used as a positive control. Measurement was performed 15 days after infection with BRAF^{V600E}-encoding lentivirus. Levels are represented as mean of two independent experiments with SD from triplicate. (**B**) Regulation of *RASEF* transcript in samples described in A, as determined by quantitative real-time qRT-PCR. Measurements are based on two independent experiments and standardized to the vector-expressing senescent cells. Error bars represent SD from triplicate qRT-PCRs. (**C–E**) Regulation of *IL6* (C), *IL8* (D), and *C/EBPβ* (E) transcripts in samples described in A, as determined by qRT-PCR. Measurements are based on two independent experiments and standardized to the BRAF^{V600E}-expressing senescent cells. Error bars represent SD from triplicate qRT-PCRs. *P* values of less than 0.05 were considered significant. *0.01 < *P* < 0.05; **0.001 < *P* < 0.01; ***$P < 0.001$.

Discussion

Over the last decade, OIS has been established as a safeguard program protecting against cancer. However, we have only begun to dissect the underlying mechanism. There is ample evidence to argue that genes critically required for OIS are endowed with tumor suppressor functions, with p16^{INK4A}, p15^{INK4B}, p53, and PTEN serving as paradigms[6,41]. In this study, we performed a near-genomewide shRNA screen to uncover novel factors

essential for $BRAF^{V600E}$ to induce senescence. We identified seven genes, one of which we characterized in more detail, because we found it was frequently methylated in melanomas. *RASEF* depletion prevented the induction of senescence by $BRAF^{V600E}$ both in fibroblasts and melanocytes. This was accompanied by the suppression of several biomarkers of senescence including (SA)-β-galactosidase activity, expression of p15 tumor suppressor protein, and SAHF. Furthermore, *RASEF* depletion reversed the increase in components of the SMS/SASP, which represent key factors for the induction of SA cell cycle arrest[13].

Function-based screens for mediators of OIS have been performed previously, too, in several different experimental settings and with gain-of-function libraries as well as loss-of-function libraries[14,55-58]. The latter study was carried out in the context of $BRAFV^{600E}$-induced senescence; we found an overlap of two genes, *BUB1* and *NF2*. Moreover, we identified two genes with an established function in OIS, that is, *TSC22* and *IL6R* (albeit with single shRNAs in the primary screen[13,59]). These results show that the current screens are not saturating and that multiple approaches ought to be used to draw a complete map of critical OIS regulators.

None of the seven genes identified in our screen have been previously studied in the context of $BRAF^{V600E}$-induced senescence. Depletion of *RASEF* suppressed the expression of *IL6* and *IL8* transcripts via downregulating *C/EBPβ*, a key controller of the SMS/SASP contributing to OIS[13]. It will be interesting to determine the relationship between *C/EBPβ* and *RASEF*. We have previously identified additional regulators of senescence, including the putative tumor suppressor TSC22[59] and the metabolic enzymes PDK1 and PDP2[25]. Interestingly, all these genes are essential to drive the expression of *IL6* and *IL8* transcripts in the face of an oncogenic signal. These results not only support model in which RASEF controls OIS by regulating components of the senescence secretome, but also highlight the central role of specific interleukins in OIS.

Among the genes identified here, only *Wilms Tumor 1* (*WT1*) has been previously associated with tumorigenesis[60]. Moreover, none were found to be among the genes that were recently reported to be frequently mutated in melanoma[43,44,61]. We find that, of seven genes identified in the screen, only the *RASEF* gene shows promoter hypermethylation in a substantial fraction of primary cutaneous melanomas (21%). Benign melanocytic nevi did not show *RASEF* promoter methylation. Although the results from our initial genome-wide methylation analysis suggested selective *RASEF* hypermethylation in mutant *BRAF* melanomas, we observed in a subsequent assessment of a larger group of tumors that *RASEF* hypermethylation occurred equally in *BRAF*-mutant and *BRAF*-wild-type tumor samples. *RASEF* hypermethylation was associated with transcriptional downregulation and chemical demethylation resulted in transcriptional reactivation of this gene. *RASEF* promoter hypermethylation has previously been reported to occur in uveal

melanoma, a melanoma subtype with genetic and clinical features that are distinct from cutaneous melanoma[54]. In that study, methylation of *RASEF* was found in primary uveal melanomas and more prominently in uveal melanoma cell lines lacking *RASEF* expression. Only cell lines lacking *RASEF* methylation were found to express the gene. This pattern of correlation between promoter methylation status and gene expression is similar to our findings for *RASEF* in cutaneous melanoma. Interestingly, in another study of three Danish families with multiple cutaneous and uveal melanoma cases, a susceptibility locus was mapped to a 3 Mb chromosomal region on 9q21.32 harboring the *RASEF* gene[53]. Although the presence of germ-line mutations in the *RASEF* gene was not analyzed in this study, reduced expression of this gene was found in melanoma patients, further supporting *RASEF* as a candidate melanoma susceptibility gene, but this should be explored further. To begin delineating such a role for *RASEF*, we show that its restored expression in a limited number of melanoma cells in which this gene is methylated causes cell cycle arrest. Clearly, a more definitive characterization of *RASEF* as a tumor suppressor will require in vivo models. Notably, *RASEF* has been previously reported to have differential functions depending on the cancer type; it has been attributed with a tumor-suppressive function in myeloid leukemia[62], while it has an oncogenic function in lung cancer[63]. Our study is consistent with a model in which *RASEF* acts as a tumor suppressor in melanoma.

References

1. Lowe, S.W., Cepero, E., and Evan, G. Intrinsic tumour suppression. *Nature* **432**(7015), 307-315 (2004).
2. Mathew, R., Karantza-Wadsworth, V., and White, E. Role of autophagy in cancer. *Nat. Rev. Cancer* **7**(12), 961-967 (2007).
3. Serrano, M. *et al.* Oncogenic ras provokes premature cell senescence associated with accumulation of p53 and p16INK4a. *Cell* **88**(5), 593-602 (1997).
4. Collado, M. and Serrano, M. Senescence in tumours: evidence from mice and humans. *Nat. Rev. Cancer* **10**(1), 51-57 (2010).
5. Hayflick, L. THE LIMITED IN VITRO LIFETIME OF HUMAN DIPLOID CELL STRAINS. *Exp. Cell Res.* **37**, 614-636 (1965).
6. Campisi, J. Senescent cells, tumor suppression, and organismal aging: good citizens, bad neighbors. *Cell* **120**(4), 513-522 (2005).
7. Kuilman, T. *et al.* The essence of senescence. *Genes Dev.* **24**(22), 2463-2479 (2010).
8. Sherr, C.J. Divorcing ARF and p53: an unsettled case. *Nat. Rev. Cancer* **6**(9), 663-673 (2006).
9. Dimri, G.P. *et al.* A biomarker that identifies senescent human cells in culture and in aging skin in vivo. *Proc. Natl. Acad. Sci. U. S. A.* **92**(20), 9363-9367 (1995).
10. Narita, M. *et al.* Rb-mediated heterochromatin formation and silencing of E2F target genes during cellular senescence. *Cell* **113**(6), 703-716 (2003).
11. Zhang, R., Chen, W., and Adams, P.D. Molecular dissection of formation of senescence-associated heterochromatin foci. *Mol. Cell Biol.* **27**(6), 2343-2358 (2007).
12. Acosta, J.C. *et al*. Chemokine signaling via the CXCR2 receptor reinforces senescence. *Cell* **133**(6), 1006-1018 (2008).
13. Kuilman, T. *et al.* Oncogene-induced senescence relayed by an interleukin-dependent inflammatory network. *Cell* **133**(6), 1019-1031 (2008).
14. Wajapeyee, N. *et al.* Oncogenic BRAF induces senescence and apoptosis through pathways mediated by the secreted protein IGFBP7. *Cell* **132**(3), 363-374 (2008).
15. Rodier, F. *et al.* Persistent DNA damage signalling triggers senescence-associated inflammatory cytokine secretion. *Nat. Cell Biol.* **11**(8), 973-979 (2009).
16. Coppe, J.P. *et al.* Senescence-associated secretory phenotypes reveal cell-nonautonomous functions of oncogenic RAS and the p53 tumor suppressor. *PLoS Biol.* **6**(12), 2853-2868 (2008).
17. Kuilman, T. and Peeper, D.S. Senescence-messaging secretome: SMS-ing cellular stress. *Nat. Rev. Cancer* **9**(2), 81-94 (2009).
18. Krizhanovsky, V. *et al.* Senescence of activated stellate cells limits liver fibrosis. *Cell* **134**(4), 657-667 (2008).
19. Baker, D.J. *et al.* Clearance of p16Ink4a-positive senescent cells delays ageing-associated disorders. *Nature* **479**(7372), 232-236 (2011).
20. Kang, T.W. *et al.* Senescence surveillance of pre-malignant hepatocytes limits liver cancer development. *Nature* **479**(7374), 547-551 (2011).
21. Wang, X. *et al.* Inhibition of mammalian target of rapamycin induces phosphatidylinositol 3-kinase-dependent and Mnk-mediated eukaryotic translation initiation factor 4E phosphorylation. *Mol. Cell Biol.* **27**(21), 7405-7413 (2007).
22. Acosta, J.C. *et al*. A complex secretory program orchestrated by the inflammasome controls paracrine senescence. *Nat. Cell Biol.* **15**(8), 978-990 (2013).
23. Aird, K.M. *et al.* Suppression of nucleotide metabolism underlies the establishment and maintenance of oncogene-induced senescence. *Cell Rep.* **3**(4), 1252-1265 (2013).
24. Jiang, P. *et al.* Reciprocal regulation of p53 and malic enzymes modulates metabolism and senescence. *Nature* **493**(7434), 689-693 (2013).
25. Kaplon, J. *et al.* A key role for mitochondrial gatekeeper pyruvate dehydrogenase in oncogene-induced senescence. *Nature* **498**(7452), 109-112 (2013).
26. Gray-Schopfer, V.C. *et al.* Cellular senescence in naevi and immortalisation in melanoma: a role for p16? *Br. J. Cancer* **95**(4), 496-505 (2006).
27. Davies, H. *et al.* Mutations of the BRAF gene in human cancer. *Nature* **417**(6892), 949-954 (2002).
28. Pollock, P.M. *et al.* High frequency of BRAF mutations in nevi. *Nat. Genet.* **33**(1), 19-20 (2003).
29. Mooi, W.J. and Peeper, D.S. Oncogene-induced cell senescence--halting on the road to cancer. *N. Engl. J. Med.* **355**(10), 1037-1046 (2006).
30. Bogdan, I. *et al.* Melanoma ex naevo: a study of the associated naevus. *Melanoma Res.* **13**(2), 213-217 (2003).

31. Dadzie, O.E. *et al.* RAS and RAF mutations in banal melanocytic aggregates contiguous with primary cutaneous melanoma: clues to melanomagenesis. *Br. J. Dermatol.* **160**(2), 368-375 (2009).
32. Yazdi, A.S. *et al.* Mutations of the BRAF gene in benign and malignant melanocytic lesions. *J. Invest. Dermatol.* **121**(5), 1160-1162 (2003).
33. Curtin, J.A. *et al.* Distinct sets of genetic alterations in melanoma. *N. Engl. J. Med.* **353**(20), 2135-2147 (2005).
34. Kamb, A. *et al.* A cell cycle regulator potentially involved in genesis of many tumor types. *Science* **264**(5157), 436-440 (1994).
35. Garraway, L.A. *et al.* Integrative genomic analyses identify MITF as a lineage survival oncogene amplified in malignant melanoma. *Nature* **436**(7047), 117-122 (2005).
36. Palavalli, L.H. *et al.* Analysis of the matrix metalloproteinase family reveals that MMP8 is often mutated in melanoma. *Nat. Genet.* **41**(5), 518-520 (2009).
37. Prickett, T.D. *et al.* Analysis of the tyrosine kinome in melanoma reveals recurrent mutations in ERBB4. *Nat. Genet.* **41**(10), 1127-1132 (2009).
38. Wei, X. *et al.* Exome sequencing identifies GRIN2A as frequently mutated in melanoma. *Nat. Genet.* **43**(5), 442-446 (2011).
39. Yokoyama, S. *et al.* A novel recurrent mutation in MITF predisposes to familial and sporadic melanoma. *Nature* **480**(7375), 99-103 (2011).
40. Stahl, J.M. *et al.* Deregulated Akt3 activity promotes development of malignant melanoma. *Cancer Res.* **64**(19), 7002-7010 (2004).
41. Vredeveld, L.C. *et al.* Abrogation of BRAFV600E-induced senescence by PI3K pathway activation contributes to melanomagenesis. *Genes Dev.* **26**(10), 1055-1069 (2012).
42. Berger, M.F. *et al.* Integrative analysis of the melanoma transcriptome. *Genome Res.* **20**(4), 413-427 (2010).
43. Hodis, E. *et al.* A landscape of driver mutations in melanoma. *Cell* **150**(2), 251-263 (2012).
44. Krauthammer, M. *et al.* Exome sequencing identifies recurrent somatic RAC1 mutations in melanoma. *Nat. Genet.* **44**(9), 1006-1014 (2012).
45. Rothhammer, T. and Bosserhoff, A.K. Epigenetic events in malignant melanoma. *Pigment Cell Res.* **20**(2), 92-111 (2007).
46. Dankort, D. *et al.* Braf(V600E) cooperates with Pten loss to induce metastatic melanoma. *Nat. Genet.* **41**(5), 544-552 (2009).
47. Lin, W.M. *et al.* Modeling genomic diversity and tumor dependency in malignant melanoma. *Cancer Res.* **68**(3), 664-673 (2008).
48. Gao, L. *et al.* Genome-wide promoter methylation analysis identifies epigenetic silencing of MAPK13 in primary cutaneous melanoma. *Pigment Cell Melanoma Res.* **26**(4), 542-554 (2013).
49. Michaloglou, C. *et al.* BRAFE600-associated senescence-like cell cycle arrest of human naevi. *Nature* **436**(7051), 720-724 (2005).
50. Garcia-Manero, G. *et al.* DNA methylation of multiple promoter-associated CpG islands in adult acute lymphocytic leukemia. *Clin. Cancer Res.* **8**(7), 2217-2224 (2002).
51. Toyota, M. *et al.* Methylation profiling in acute myeloid leukemia. *Blood* **97**(9), 2823-2829 (2001).
52. Vandesompele, J. *et al.* Accurate normalization of real-time quantitative RT-PCR data by geometric averaging of multiple internal control genes. *Genome Biol.* **3**(7), RESEARCH0034 (2002).
53. Jonsson, G. *et al.* Mapping of a novel ocular and cutaneous malignant melanoma susceptibility locus to chromosome 9q21.32. *J. Natl. Cancer Inst.* **97**(18), 1377-1382 (2005).
54. Maat, W. *et al.* Epigenetic regulation identifies RASEF as a tumor-suppressor gene in uveal melanoma. *Invest. Ophthalmol. Vis. Sci.* **49**(4), 1291-1298 (2008).
55. Berns, K. *et al.* A large-scale RNAi screen in human cells identifies new components of the p53 pathway. *Nature* **428**(6981), 431-437 (2004).
56. Peeper, D.S. *et al.* A functional screen identifies hDRIL1 as an oncogene that rescues RAS-induced senescence. *Nat. Cell Biol.* **4**(2), 148-153 (2002).
57. Rowland, B.D., Bernards, R., and Peeper, D.S. The KLF4 tumour suppressor is a transcriptional repressor of p53 that acts as a context-dependent oncogene. *Nat. Cell Biol.* **7**(11), 1074-1082 (2005).
58. Vredeveld, L.C. *et al.* Functional identification of LRF as an oncogene that bypasses RASV12-induced senescence via upregulation of CYCLIN E. *Carcinogenesis* **31**(2), 201-207 (2010).
59. Homig-Holzel, C. *et al.* Antagonistic TSC22D1 variants control BRAF(E600)-induced senescence. *EMBO J.* **30**(9), 1753-1765 (2011).
60. Huff, V. Wilms' tumours: about tumour suppressor genes, an oncogene and a chameleon gene. *Nat. Rev. Cancer* **11**(2), 111-121 (2011).

61. Berger, M.F. *et al.* Melanoma genome sequencing reveals frequent PREX2 mutations. *Nature* **485**(7399), 502-506 (2012).
62. Nakamura, S. *et al.* Small GTPase RAB45-mediated p38 activation in apoptosis of chronic myeloid leukemia progenitor cells. *Carcinogenesis* **32**(12), 1758-1772 (2011).
63. Oshita, H. *et al.* RASEF is a novel diagnostic biomarker and a therapeutic target for lung cancer. *Mol. Cancer Res.* **11**(8), 937-951 (2013).

Supplementary Data

Table S1. Candidate genes identified in the near-genomewide shRNA screen required for BRAF^{V600E}-induced senescence.

GenBank accesion number	Gene symbol	Number of shRNAs identified	shRNAs from screen used for validation	shRNA number used in manuscript	Number colonies per shRNA
NM_000245	MET	5	TRCN0000040045	1	2
			TRCN0000040044	2	4
NM_024775	GEMIN6	4	TRCN0000147641	1	4
			TRCN0000146917	2	4
NM_021988	UBE2V1	3	TRCN0000033708	1	7
			TRCN0000033706	2	2
NM_020786	PDP2	3	TRCN0000036742	1	4
			TRCN0000036741	2	3
XM_166453	TTBK1	2	TRCN0000037537	1	6
			TRCN0000037538	2	2
XM_166256	MAP6	2	TRCN0000005180	1	2
			TRCN0000005181	2	2
NM_178543	ENPP7	2	TRCN0000002744	1	2
			TRCN0000002742	2	4
NM_173647	RNF149	2	TRCN0000034154	1	2
			TRCN0000034156	2	2
NM_173540	FUT11	2	TRCN0000035675	1	3
			TRCN0000035674	2	4
NM_153028	ZNF75A	2	TRCN0000020245	1	3
			TRCN0000020247	2	2
NM_152464	TMEM199	2	TRCN0000160087	1	3
			TRCN0000159467	2	2
NM_147174	HS6ST2	2	TRCN0000036300	1	2
			TRCN0000036299	2	4
NM_032037	TSSK6	2	TRCN0000037459	1	5
			TRCN0000037462	2	3
NM_031498	GNGT2	2	TRCN0000036854	1	5
			TRCN0000036858	2	3
NM_031460	KCNK17	2	TRCN0000043856	1	2
			TRCN0000043855	2	3
NM_024779	PIP4K2C	2	TRCN0000037722	1	4
			TRCN0000037720	2	4
NM_020677	NMRAL1	2	TRCN0000036912	1	7
			TRCN0000036913	2	5
NM_018913	PCDHGA10	2	TRCN0000053343	1	7
			TRCN0000053344	2	4
NM_018069	CEP192	2	TRCN0000135014	1	4
			TRCN0000135060	2	3
NM_012219	MRAS	2	TRCN0000036990	1	2
			TRCN0000036992	2	2
NM_006714	SMPDL3A	2	TRCN0000048885	1	4
			TRCN0000048887	2	2
NM_006458	TRIM3	2	TRCN0000033744	1	3
			TRCN0000033746	2	2
NM_005827	SLC35B1	2	TRCN0000044403	1	3
			TRCN0000044404	2	2
NM_004525	LRP2	2	TRCN0000053292	1	5
			TRCN0000053291	2	2
NM_004390	CTSH	2	TRCN0000003699	1	2
			TRCN0000003698	2	2
NM_003038	SLC1A4	2	TRCN0000038641	1	4
			TRCN0000038642	2	3
NM_001701	BAAT	2	TRCN0000035463	1	2
			TRCN0000035460	2	4
XM_376350	RAPGEF2	2	TRCN0000036985	1	3
			TRCN0000036987	2	2
NM_198483	RUFY4	2	TRCN0000129798	1	3
			TRCN0000130783	2	2
NM_015865	SLC14A1	2	TRCN0000043608	1	2
			TRCN0000043609	2	3
NM_024424	WT1	2	TRCN0000001114	1	3

			TRCN0000001117	2	3
NM_006042	HS3ST3A1	2	TRCN0000035837	1	4
			TRCN0000035836	2	2
NM_006212	PFKFB2	2	TRCN0000037962	1	3
			TRCN0000037961	2	2
NM_006244	PPP2R5B	2	TRCN0000039935	1	4
			TRCN0000039937	2	2
NM_152573	RASEF	2	TRCN0000055625	1	2
			TRCN0000055624	2	3
NM_000876	IGF2R	2	TRCN0000060254	1	5
			TRCN0000060253	2	3
NM_007215	POLG2	2	TRCN0000053055	1	2
			TRCN0000053054	2	3
NM_017549	EPDR1	2	TRCN0000055590	1	6
			TRCN0000055589	2	2
NM_004875	POLR1C	2	TRCN0000052904	1	2
			TRCN0000052906	2	3
NM_139075	TPCN2	2	TRCN0000043921	1	3
			TRCN0000043920	2	2

Table S2. *RASEF* methylation status and clinical data of the benign nevi, primary melanomas, and early-passage melanoma cell lines used in the study. U, unmethylated; M, methylated.

Normal naevus

Sample number	*RASEF* methylation status	Gender	Age (yrs)	Mutation status
N1	U	F	29	BRAFV600E
N2	U	F	43	BRAFV600E
N3	U	M	55	BRAFV600E
N4	U	F	40	BRAFV600E
N5	U	F	38	BRAFV600E
N6	U	F	31	-
N7	U	M	46	-
N8	U	F	39	-
N9	U	F	27	-
N10	U	M	21	-
N11	U	M	57	-
N12	U	F	52	-
N13	U	F	24	-
N14	U	F	30	-
N15	U	F	30	-

Primary melanoma

Sample number	*RASEF* methylation status	Gender	Age (yrs)	Mutation status	Breslow (mm)
PM 1	U	F	53	wt	1,67
PM 2	U	M	68	BRAFV600E	2,08
PM 3	U	M	65	wt	4,48
PM 4	U	F	65	wt	2,05
PM 5	M	F	60	wt	3,88
PM 6	U	M	58	wt	0,81
PM 7	U	F	42	BRAFV600K	0,91
PM 8	U	F	34	wt	0,94
PM 9	U	M	36	BRAFV600E	1,06
PM 10	U	F	35	BRAFV600E	0,73
PM 11	U	F	59	NRASG12D	1,70
PM 12	U	F	73	wt	3,36
PM 13	U	M	85	wt	15,60
PM 14	U	M	54	wt	3,46
PM 15	U	F	48	NRASQ61K	9,20
PM 16	M	M	82	BRAFV600E	18,00
PM 17	U	F	62	wt	6,29
PM 18	U	F	65	wt	1,28
PM 19	U	M	79	BRAFV600K	17,20
PM 20	U	F	45	wt	3,04
PM 21	U	M	78	wt	2,02
PM 22	M	M	70	wt	12,20
PM 23	M	F	56	wt	10,10
PM 24	U	F	75	BRAFV600E	2,08
PM 25	M	M	64	-	3,00

PM 26	U	M	46	-	2,00
PM 27	U	M	83	-	1,80
PM 28	U	F	73	-	1,40
PM 29	U	M	61	-	6,00
PM 30	U	F	51	-	3,40
PM 31	U	M	64	-	2,20
PM 32	M	F	51	-	5,90
PM 33	U	F	35	-	1,20
PM 34	U	M	62	-	3,50
PM 35	U	F	27	-	2,30
PM 36	M	M	72	-	5,20
PM 37	U	F	42	-	3,90
PM 38	U	F	68	-	1,50
PM 39	U	F	35	-	1,30
PM 40	U	F	29	-	2,60
PM 41	U	M	64	-	4,50
PM 42	U	F	53	-	3,40
PM 43	U	M	64	-	3,00
PM 44	U	M	37	-	2,20
PM 45	U	F	89	-	3,30
PM 46	M	F	57	-	2,00
PM 47	U	F	80	-	2,90
PM 48	U	M	48	-	3,60
PM 49	U	F	34	-	2,10
PM 50	M	F	81	-	3,00
PM 51	U	M	55	-	3,00
PM 52	U	M	70	-	2,20
PM 53	U	F	70	-	2,70
PM 54	U	M	54	-	4,00
PM 55	U	M	67	-	2,00
PM 56	U	M	62	-	4,80
PM 57	U	M	43	-	3,10
PM 58	U	F	74	-	3,30
PM 59	U	F	38	-	2,30
PM 60	U	M	65	-	3,60
PM 61	M	M	74	-	7,00
PM 62	M	M	77	-	6,00
PM 63	U	M	33	-	2,50
PM 64	U	F	26	-	2,50
PM 65	M	M	55	-	2,40
PM 66	U	F	84	-	5,00
PM 67	U	F	59	-	7,00
PM 68	U	F	82	-	2,50
PM 69	U	F	57	-	3,20
PM 70	M	M	88	-	4,20
PM 71	U	F	62	-	2,00
PM 72	U	F	50	-	2,80
PM 73	M	M	58	-	7,50
PM 74	U	F	60	-	2,10
PM 75	M	F	67	-	2,50
PM 76	M	M	85	-	3,20

Melanoma cell lines

Cell line	*RASEF* methylation status	Gender	Age (yrs)	Mutation status
05.06	U	M	59	BRAFV600E
06.24	M	F	60	NRASQ61R
518A2	U	M	19	BRAFV600E
94.03C	U	F	37	BRAFV600E
94.07	M	M	39	BRAFV600E
94.13	U	F	47	BRAFV600E
04.07	U	F	59	BRAFV600E
607B	U	F	51	NRASQ61K
93.08	U	M	30	BRAFV600E
Mz7.4	U	n/a	n/a	BRAFV600E
634	M	F	52	NRASQ61R
04.04	M	F	36	BRAFV600E

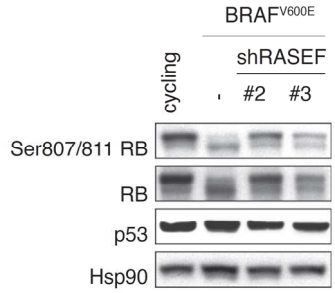

Figure S1. **Regulation of RB and p53 proteins in cycling, OIS and cells bypassing OIS upon depletion of *RASEF***. HDFs expressing vector control or nonoverlapping shRNAs targeting *RASEF* in the presence and absence of oncogenic BRAF^{V600E} were analyzed by immunoblotting with antibodies as indicated. Hsp90 serves as loading control.

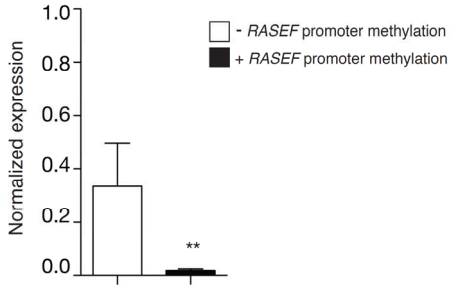

Figure S2. ***RASEF* expression in early-passage melanoma cell lines**. *RASEF* mRNA expression levels in early-passage melanoma cell lines with known *RASEF* promoter methylation status as determined by qRT-PCR. Bars represent mean of normalized *RASEF* expression in cell lines with hypermethylated *RASEF* promoter versus cells with absent *RASEF* methylation. Error bars represent S.E.M.

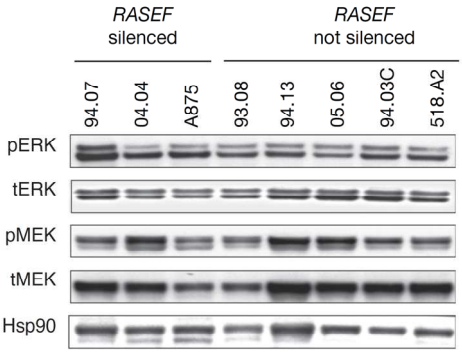

Figure S3. **Comparison of MAP kinase pathway activation in melanoma cell lines**. Melanoma cell lines with and without *RASEF* silencing were analyzed by immunoblotting with antibodies as indicated. Hsp90 serves as loading control.

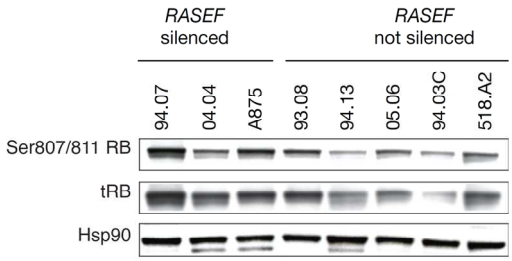

Figure S4. **Regulation of RB protein in melanoma cell lines**. Melanoma cell lines with and without *RASEF* silencing were analyzed by immunoblotting with antibodies as indicated. Hsp90 serves as loading control.

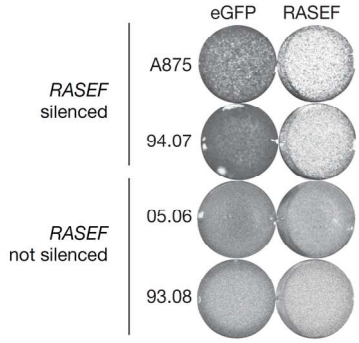

Figure S5. **Effect of ecotropic expression of RASEF on melanoma cell lines viability**. Cell proliferation assay on melanoma cell lines with and without *RASEF* silencing expressing eGFP as control or RASEF. Cells were fixed and stained 12 days after exposure to RASEF.

Chapter 4

Promoter CpG island hypermethylation in dysplastic naevus and melanoma: *CLDN11* as an epigenetic biomarker for malignancy

Linda Gao[1,*], Karin van den Hurk[2,*], Peter T.M. Moerkerk[2], Jelle J. Goeman[3,6], Samuel Beck[4], Nelleke A. Gruis[1], Joost J. van den Oord[5], Véronique J. Winnepenninckx[2,*], Manon van Engeland[2,*] and Remco van Doorn[1,*]

[1]Department of Dermatology, Leiden University Medical Center, Leiden, The Netherlands
[2]Department of Pathology, GROW-School for Oncology and Developmental Biology, Maastricht University Medical Center, Maastricht, The Netherlands
[3]Department of Medical Statistics and Bioinformatics, Leiden University Medical Center, Leiden, The Netherlands
[4]Leiden Cytology and Pathology Laboratory, Leiden, The Netherlands
[5]Laboratory of Translational Cell and Tissue Research, Department of Pathology, University Hospital, University of Leuven, Leuven, Belgium
[6]Current address: Department for Health Evidence, Radboud University Medical Center, Geert Grooteplein 21, 6525 EZ, Nijmegen, The Netherlands
*The first two and last three authors contributed equally to this work.

Journal of Investigative Dermatology 2014; 10.1038/jid.2014.270

Abstract

Dysplastic naevi are melanocytic lesions that represent an intermediate stage between common naevus and melanoma. Histopathological distinction of dysplastic naevus from melanoma can be challenging and there is a requirement for molecular diagnostic markers. In this study, we examined promoter CpG island methylation of a selected panel of genes, identified in a genome-wide methylation screen, across a spectrum of 405 melanocytic neoplasms. Promoter methylation analysis in common naevi, dysplastic naevi, primary melanomas, and metastatic melanomas demonstrated progressive epigenetic deregulation. Dysplastic naevi were affected by promoter methylation of genes that are frequently methylated in melanoma but not in common naevi. We assessed the diagnostic value of the methylation status of five genes in distinguishing primary melanoma from dysplastic naevus. In particular, *CLDN11* promoter methylation was specific for melanoma, as it occurred in 50% of primary melanomas but in only 3% of dysplastic naevi. A diagnostic algorithm that incorporates methylation of the *CLDN11*, *CDH11*, *PPP1R3C*, *MAPK13*, and *GNMT* genes was validated in an independent sample set and helped distinguish melanoma from dysplastic naevus (area under the curve 0.81). Melanoma-specific methylation of these genes supports the utility as epigenetic biomarkers and could point to their significance in melanoma development.

Introduction

Cutaneous melanoma is a malignant tumor that arises from melanocytes residing in the skin. The lifetime risk of developing melanoma is approximately 2% in the United States and Europe and both incidence and mortality rates continue to rise[1,2]. Early diagnosis is important to prevent the formation of lethal metastasis. However, the clinical diagnosis of melanoma is challenging in a proportion of cases. This applies to visual assessment of pigmented skin lesions and to histopathological examination of biopsied tissue, the standard for melanoma diagnosis. A substantial inter-observer discordance rate of 14% in the pathological diagnosis of melanoma has been reported[3,4]. In particular, the sensitivity for diagnosing early-stage melanomas is low and distinction with dysplastic melanocytic naevus can be problematic.

Dysplastic naevi are irregular in shape and pigmentation and occur in approximately 10% of the population[5]. Histologically, these lesions demonstrate random cytological atypia, architectural disorder, and stromal changes. The relevance of dysplastic naevus to melanoma progression is underscored by observations that dyplastic naevi are found in contiguity with melanoma in a significant subset of cases[6,7]. On the basis of morphological and biological characteristics, dysplastic naevi have been proposed to represent an intermediate lesion between common naevi and malignant melanoma in the multistep tumor progression model of melanocytic neoplasia[8].

In the melanoma progression model proposed by Clark, melanocytic cells acquire malignant traits in discrete steps, a process driven by accumulation of genetic and epigenetic alterations[9]. Although there is limited information about genetic and epigenetic alterations in dysplastic naevi, patterns of intragenic mutations, chromosomal aberrations, and DNA methylation alterations are assumed to differ from those in melanoma. Therefore, detection of these molecular differences could aid in the correct classification of those cases in which morphological diagnosis fails to discriminate.

Systematic characterization of molecular alterations in melanoma has provided a wealth of information on acquired DNA alterations in melanoma cells, which could be used in the molecular diagnosis of this malignant disease. Recently, we performed a genome-wide promoter methylation analysis of 14.495 genes in melanoma and common naevus samples and found widespread aberrant promoter methylation in melanoma[10]. Among the hundreds of gene promoters that exhibited methylation in melanomas but not in common naevi, we identified several tumor suppressor genes, causally implicating epigenetic mechanisms in melanoma development.

The objectives of this study were to gain insight into epigenetic deregulation in the different stages of melanocytic neoplasia and to assess the potential diagnostic value of genes differentially methylated between melanoma and dysplastic naevus. To this end, we examined the methylation status of genes that were previously identified in a genome-wide methylation screen in a cohort of 251 melanocytic neoplasms and subsequently validated a diagnostic algorithm incorporating different gene methylation features in a second independent series of 154 dysplastic naevus and primary melanoma samples. The combined analysis of promoter CpG island methylation of the five genes proposed in this study could be of help in the histopathological distinction of melanoma from dysplastic naevus.

Methods

Patient samples

To prioritize the 12 candidate genes, we analyzed an independent set of fresh-frozen or boonfix-fixed, paraffin-embedded (BFPE) tissues from patients diagnosed with common naevus (n=10), dysplastic naevus (n=20), and primary melanoma (n=15) at Leiden University Medical Center (LUMC), the Netherlands. For confirmation of methylation frequencies and testing of diagnostic discriminatory value of the final five genes, we examined FFPE tissues from patients diagnosed with common naevus (n=62), dysplastic naevus (n=72), primary melanoma (n=101), and metastatic melanoma (n=16) at the Maastricht University Medical Center (MUMC), the Netherlands, and University Hospitals of the University of Leuven (KUL), Belgium (series 1). For validation of the diagnostic algorithm, we examined fresh-frozen, BFPE, and FFPE tissues from patients diagnosed with

dysplastic naevus (n=74) and primary melanoma (n=82) at LUMC, MUMC, and KUL (series 2). The grade of atypia (mild and moderate-severe) of dysplastic naevi was determined by an experienced dermatopathologist (VJW), based on criteria formulated by Arumi-Uria et al., 2003[11]. Detailed clinicopathological information of all samples is listed in Supplementary Table S7. Tissues were processed as previously described[12]; biopsy samples contained at least 50% melanocytic cells, as analyzed on hematoxylin and eosin-stained sections. Patient consent for experiments was not required because French laws consider human tissue left over from surgery as discarded material.

DNA isolation and bisulfite conversion

Genomic DNA from fresh-frozen and BFPE tissues was extracted with the Genomic-tip kit (Qiagen, Venlo, The Netherlands) and the RecoverAll Nucleic Acid kit (Ambion, Carlsbad, CA), respectively; DNA from FFPE tissues was extracted by macrodissection with theQIAamp DNA Micro Kit (Qiagen) or with the Maxwell 16 FFPE Plus LEV DNA Purification kit (Promega, Leiden, The Netherlands). Bisulfite conversion was performed using either the EZ DNA methylation kit (Zymo Research, Orange, CA; BMCA) or the EpiTect Bisulfite Kit (Qiagen; MSP analysis).

Bisulfite melting curve analysis

Bisulfite primers were designed, and the sensitivity of primer sets was tested as previously described[10] (Supplementary Table S8). Methylation could be accurately detected if 10% of the analyzed DNA was methylated. Melting curves were generated for each biopsy sample; a sample was considered methylated if the amplicon had at least 10% methylated DNA, with the melting curve pattern of a 1:9 methylated to unmethylated DNA mixture serving as scoring standard.

Methylation-specific PCR

MSP analysis using MSP primers on bisulfite-treated DNA was performed as described[13,14] (Supplementary Table S8). To facilitate MSP analysis on DNA retrieved from FFPE tissue, DNA was first amplified with flanking PCR primers used as template for the PCR. All PCRs were performed with controls for unmethylated alleles (DNA from human umbilical vein endothelial cells, methylated alleles (normal lymphocyte DNA treated in vitro with Sssl methyltransferase (IVD)), and a control without DNA. To ensure reproducibility, MSP reactions have been performed in duplicate or triplicate starting from DNA amplification with flanking PCR primers. The reproducibility was 493% for all primer sets. Non-concordant MSP results were analyzed a third time, and two out of three concordance was used as the end result. Bands with approximately equal intensity for unmethylated and methylated DNA were scored as positive for methylation. Faint methylated bands

were considered negative for methylation. Unclear results were analyzed a second time. In most cases, methylation levels were clearly negative (no M-band detected) or positive (strong M-band detected).

Statistical analysis

Fisher's exact test was applied to measure the association between two sample groups within a 2x2 contingency table; a two-sided *P* value <0.05 was considered significant. Logistic regression analysis was used to test the diagnostic value of the five genes in the training data set. The logistic regression did not converge because of the strong diagnostic effect of *CLDN11*; therefore, we opted for a two-step model: data were filtered for samples without *CLDN11* methylation, followed by binary logistic regression analysis with a single covariate counting how many of *CDH11*, *PPP1R3C*, *MAPK13*, and *GNMT* were methylated. In the resulting diagnostic score, a patient sample was classified as melanoma if either *CLDN11* was methylated or if at least 1, 2, 3, or 4 of *CDH11*, *PPP1R3C*, *MAPK13*, and *GNMT* were methylated, depending on the chosen cutoff. A receiver operating characteristic curve was plotted for this diagnostic score. For this assessment, an independent test set was used in order to prevent any optimism bias due to overfit. Statistical analyses were performed using SPSS 20 (IBM, Armonk, NY) and R (R Core Team (2013) - http://R-project.org/).

Results

Selection of genes for promoter CpG island methylation analysis in common naevus, dysplastic naevus, primary melanoma, and metastatic melanoma

In a previously performed genome-wide methylation analysis using Infinium 27-k beadchips, we identified 106 genes that were significantly and frequently more methylated in primary cutaneous melanomas than in common naevi[10]. Here, we set out to analyze the methylation status of the 12 most differentially methylated genes in dysplastic naevi, next to an independent set of common naevi and primary melanomas (Figure 1A and B). Primers for bisulfite melting curve analysis (BMCA) were designed to encompass or to be in close proximity of the corresponding 50-mer probe sequence on the beadchip. *C4orf8* and *HIST1H3E* were excluded for further methylation analyses owing to suboptimal primer design; in their place, *PPP1R3C* and *CLDN11* were included, as we had observed that they exhibited notable differential methylation between primary melanoma and common naevus samples[10]. In the independent set of 10 common naevus, 20 dysplastic naevus, and 15 primary melanoma biopsy samples, BMCA showed that *C1orf106*, *MAPK13*, *CDH11*, *GNMT*, *PPP1R3C*, and *CLDN11* methylation was absent in common and dysplastic naevi, whereas frequent methylation (20–67%) was observed in primary melanomas (Figure 1C). The promoters of *HOXA9* and *CNTN1* were non-progressively

methylated in 10–80% of common naevi, dysplastic naevi, and primary melanomas. Interestingly, *PLEKHG6* showed progressively higher levels of methylation with tumor progression, that is, in 0% of common naevi, 35% of dysplastic naevi, and 60% of primary melanomas, suggesting that transition from a benign melanocytic lesion to a malignant tumor can be accompanied by a gradual increase in methylation of certain genes (Figure 1C). *LEP* showed mosaic methylation in melanoma and naevi, with only subtle differences between these sample groups, whereas the *ABCA3* promoter region appeared to be unmethylated in melanoma, as well as in naevi (Supplementary Figure S1). Genes showing frequent methylation in melanoma, but not, or scarcely, in common and dysplastic naevi, were prioritized for further analyses in a large series of samples.

Differential promoter methylation of *CLDN11*, *CDH11*, *PPP1R3C*, *MAPK13*, and *GNMT* in common naevus, dysplastic naevus, and melanoma

Promoter methylation of *CLDN11*, *CDH11*, *PPP1R3C*, *MAPK13*, and *GNMT* was assessed in a large series of 251 formalin-fixed, paraffin-embedded (FFPE) biopsy samples consisting of 62 common naevi, 72 dysplastic naevi, 101 primary melanomas, and 16 melanoma metastases, designated series 1. We applied nested methylation-specific PCR (MSP) because this method is better suited for analysis of FFPE samples than BMCA[14]. To compare the results of BMCA and MSP, we subjected 31 samples to methylation analysis using BMCA and MSP. This revealed a high concordance rate of 84–97% between both techniques, with higher sensitivity for detecting methylation of MSP (Supplementary Table S1). *C1orf106* was excluded at this stage owing to suboptimal MSP primer design, and methylation analysis by MSP was performed for *CLDN11*, *CDH11*, *PPP1R3C*, *MAPK13*, and *GNMT*. The characteristics of the five genes are detailed in Table 1. The promoter CpG island regions of these genes as studied by MSP and BMCA are depicted in Figure 2A. MSP was successfully performed in 87–98% of the samples in series 1 (Figure 2B, Supplementary Table S2).

Methylation frequencies of *CLDN11*, *CDH11*, *PPP1R3C*, *MAPK13*, and *GNMT* in common naevi, dysplastic naevi, and primary and metastatic melanomas are presented in Table 2. For further analyses and generation of a diagnostic algorithm, only methylation data of samples for which MSP was performed successfully for all five genes (55 common naevi, 57 dysplastic naevi, 79 primary melanomas, and 15 metastatic melanomas) are included in Table 2 and Figure 3. (Results for all analyzed samples of series 1 are given in Supplementary Table S3.) Remarkably, *CLDN11* displayed the absence of methylation in both common and dysplastic naevi, whereas it was methylated in 48% of primary melanomas and 73% of metastatic melanomas in series 1 (Table 2). *CDH11* and *PPP1R3C* showed the absence of methylation in common naevi; only 5 and 14% of dysplastic naevi harbored methylation for *CDH11* and *PPP1R3C*, respectively. Methylation frequencies in

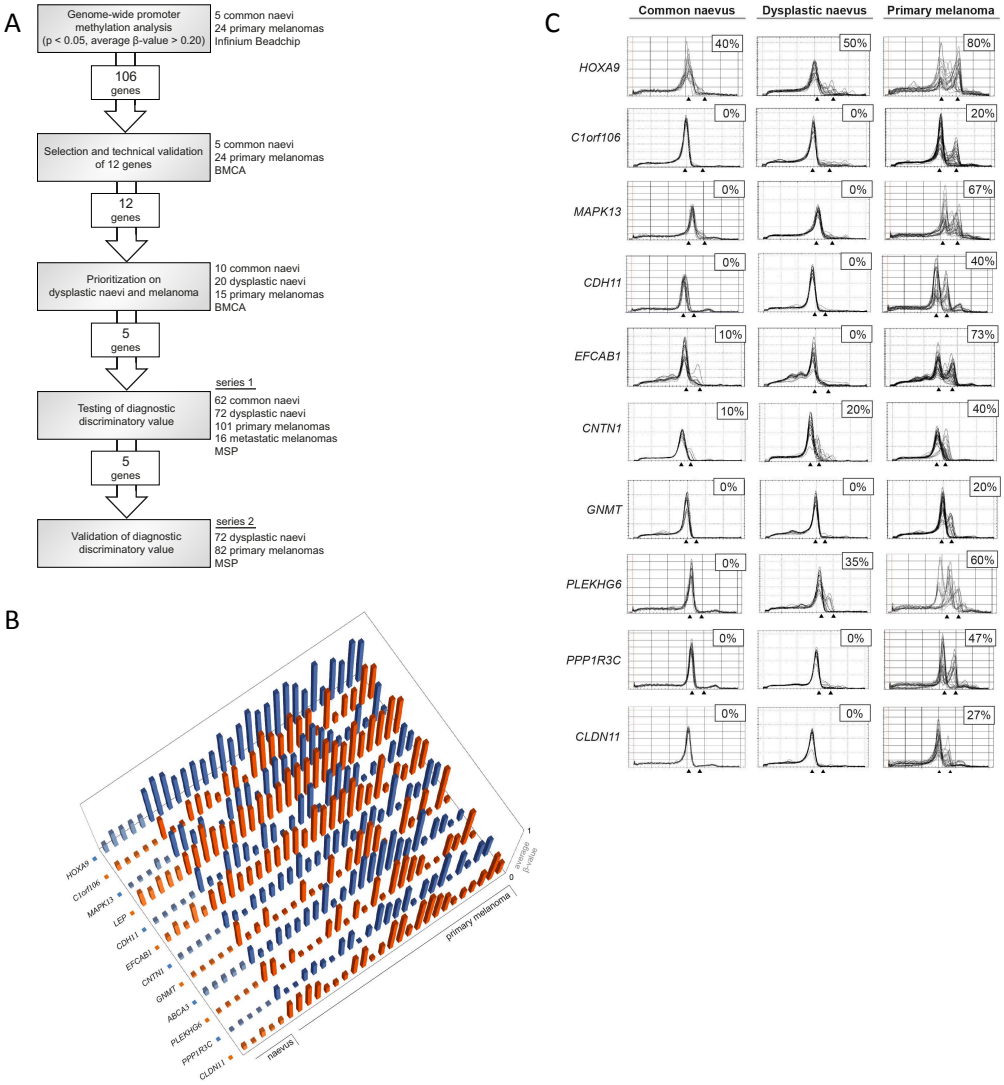

Figure 1. **Differential promoter methylation of *HOXA9*, *C1orf106*, *MAPK13*, *CDH11*, *EFCAB1*, *CNTN1*, *GNMT*, *PLEKHG6*, *PPP1R3C*, and *CLDN11* in common naevi, dysplastic naevi, and primary melanomas**. (**A**) Schematic depiction of the workflow used to select candidate genes for methylation analyses in large series of melanocytic biopsy samples. (**B**) The 12 most frequently methylated genes identified by comparative analysis of genome-wide methylation data from 24 primary melanomas and five common naevi. (**C**) Methylation frequency of 10 genes in an independent set of 10 common naevi, 20 dysplastic naevi, and 15 primary melanomas as assessed by bisulfite melting curve analysis (BMCA). Black triangles indicate the position of the melting curve peak for the respective positive (fully methylated) and negative (fully unmethylated) control.

Table 1. Characteristics of five genes that were selected for methylation analysis in common naevus, dysplastic naevus, primary melanoma, and metastatic melanoma biopsy samples.

Gene	Function	Location	Tumor suppressor	Methylation-associated silencing	Described in literature as methylated in:	
					Cancer	Melanoma
MAPK13	p38 MAP kinase involved in relaying intracellular signals for a variety of cellular processes.	chr6: 36098261 - 36112301	putative[1]	yes[1]	x	x
CDH11	Type II classical cadherin that is an integral membrane protein mediating calcium-dependent cell-cell adhesion.	chr16: 64980683 - 65155919	established[2,3,4]	yes[1]	x	x
GNMT	Enzyme that catalyzes the conversion of S-adenosyl-L-methionine to S-adenosyl-L-homocysteine and sarcosine.	chr6: 42928500 - 42931618	putative[5]	yes[7]	x	x
PPP1R3C	Regulatory subunit of protein phosphatase-1 (PP1) that catalyzes reversible protein phosphorylation important for a variety of cellular activities.	chr10: 93388197 - 93392858	putative[6]	yes[6]		x
CLDN11	Claudin family member that is an integral membrane protein and component of tight junction strands.	chr3: 170136653 - 170152479	putative[1]	yes[8]	x	x

primary and metastatic melanomas were 41 and 47% for *CDH11*, and 52 and 60% for *PPP1R3C*, respectively. *GNMT* harbored promoter methylation in 4% of common and 11% of dysplastic naevi, but yet again higher methylation frequencies were found in primary (46%) and metastatic (47%) melanomas. For *MAPK13*, methylation was observed in 18% of common and 26% of dysplastic naevi, with higher methylation frequencies in primary (62%) and metastatic (67%) melanomas. The methylation patterns of the five genes, showing progressive increase in methylation frequency in different stages of melanocytic neoplasia, are depicted in Figure 3A. We noted significantly higher promoter methylation frequencies in particular following the transition to melanoma. Methylation of each of the five genes was detected only 12 times (4%) in 55 common naevi and 32 times (11%) in 57 dysplastic naevi, significantly lower when compared to 196 times (50%) in 79 primary melanomas (P <0.001) and 44 times (59%) in 15 metastatic melanomas (Figure 3B). Complete absence of methylation for all five genes was found in 44 of 55 (80%) common naevi, 39 of 57 (68%) dysplastic naevi, 18 of 79 (23%) primary melanomas, and 2 of 15 (13%) metastatic melanomas (Figure 3C). There was no significant correlation between the grade of atypia of dysplastic naevi and promoter methylation frequency.

Promoter hypermethylation is known to increase with age, and the mean age of the melanoma patients was higher (63 years) than of the dysplastic naevus patients (46 years). The differences in methylation frequencies of *CLDN11*, *CDH11*, *PPP1R3C*, *MAPK13*, and *GNMT* between melanomas and dysplastic naevi were comparable in the subset of patients younger than 50 years and those older than 50 years (Supplementary Table S4A). From this it can be concluded that the observed methylation differences between melanoma and dysplastic naevus cannot be attributed to age. For gender, similar results

were obtained (Supplementary Table S5a). *CLDN11*, *CDH11*, *PPP1R3C*, *MAPK13*, and *GNMT* promoter methylation has been demonstrated to be associated with transcriptional silencing in tumor cell lines (Table 1). Additional pathway analysis specified that the products of these five genes and their predicted interactors are part of gene signaling networks involved in cell–cell adhesion, cell junction assembly, and adherens junction organization (Supplementary Figure S2).

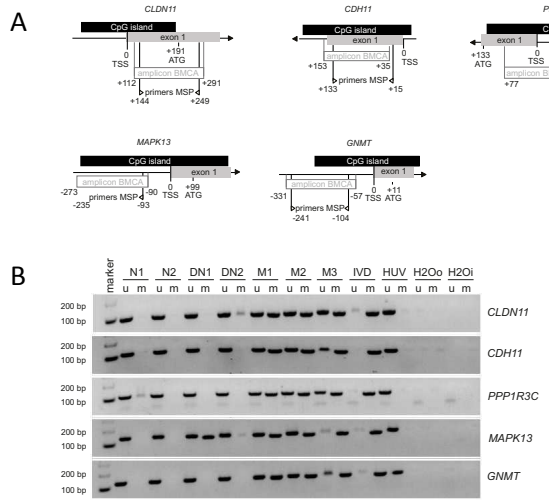

Figure 2. **Methylation analysis of *CLDN11*, *CDH11*, *PPP1R3C*, *MAPK13*, and *GNMT* in large series of common naevi, dysplastic naevi, primary and metastatic melanomas**. (**A**) CpG island promoter region of the five genes, with the location of the primers used for methylation-specific PCR (MSP) and bisulfite melting curve analysis (BMCA) in this study. (**B**) Electrophoretic analysis of MSP amplification products of *CLDN11*, *CDH11*, *PPP1R3C*, *MAPK13*, and *GNMT*. N, common naevus; DN, dysplastic naevus; M, melanoma; u, unmethylated; m, methylated; IVD, positive control for methylated alleles (lymphocyte DNA treated with Sss1 methyltransferase); HUV, negative control for unmethylated alleles (DNA from human umbilical vein endothelial cells); H2Oo, no template control for first amplification with flanking primers; H2Oi, no template control for second amplification with primers specific for methylated and unmethylated DNA.

Table 2. Methylation frequency of five candidate genes in biopsy samples of series 1 (55 common naevi, 57 dysplastic naevi, 79 primary melanomas and 15 metastatic melanomas), together with the specificity and sensitivity of each gene for the distinction of primary melanoma samples from dysplastic naevus samples of series 1. DN, dysplastic naevus; PM, primary melanoma.

	Common naevus		**Dysplastic naevus**		**Primary melanoma**		**Metastatic melanoma**		**DN n = 57 PM n = 79**	
	Methylation frequency									
		No. of samples		No. of samples		No. of samples		No. of samples	**Specificity**	**Sensitivity**
CLDN11	**0%**	0/55	**0%**	0/57	**48%**	38/79	**73%**	11/15	**100%**	**48%**
CDH11	**0%**	0/55	**5%**	3/57	**41%**	32/79	**47%**	7/15	**95%**	**41%**
PPP1R3C	**0%**	0/55	**14%**	8/57	**52%**	41/79	**60%**	9/15	**86%**	**52%**
MAPK13	**18%**	10/55	**26%**	15/57	**62%**	49/79	**67%**	10/15	**74%**	**62%**
GNMT	**4%**	2/55	**11%**	6/57	**46%**	36/79	**47%**	7/15	**89%**	**46%**

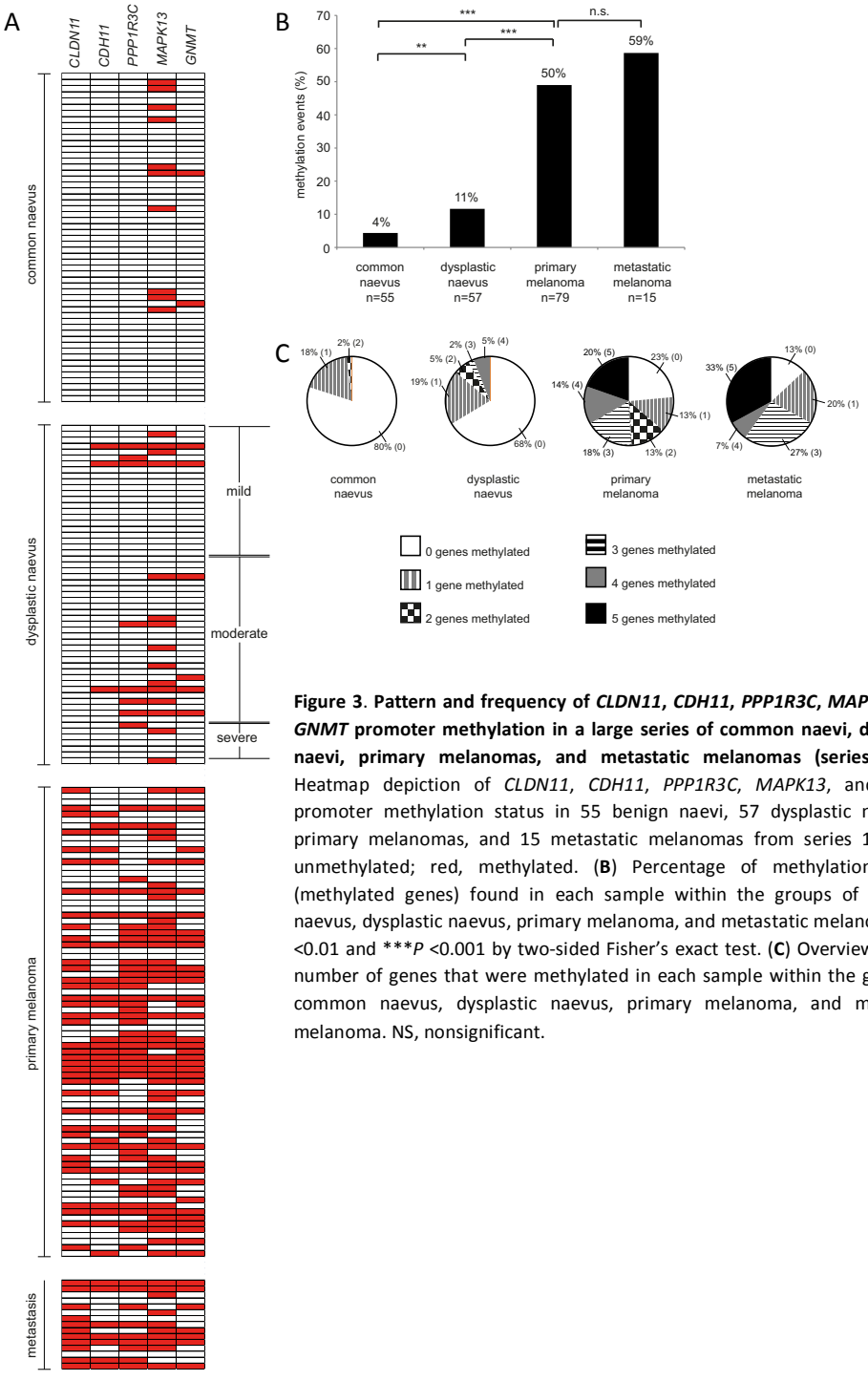

Figure 3. **Pattern and frequency of *CLDN11*, *CDH11*, *PPP1R3C*, *MAPK13*, and *GNMT* promoter methylation in a large series of common naevi, dysplastic naevi, primary melanomas, and metastatic melanomas (series 1)**. (**A**) Heatmap depiction of *CLDN11*, *CDH11*, *PPP1R3C*, *MAPK13*, and *GNMT* promoter methylation status in 55 benign naevi, 57 dysplastic naevi, 79 primary melanomas, and 15 metastatic melanomas from series 1. White, unmethylated; red, methylated. (**B**) Percentage of methylation events (methylated genes) found in each sample within the groups of common naevus, dysplastic naevus, primary melanoma, and metastatic melanoma. ***P* <0.01 and ****P* <0.001 by two-sided Fisher's exact test. (**C**) Overview of total number of genes that were methylated in each sample within the groups of common naevus, dysplastic naevus, primary melanoma, and metastatic melanoma. NS, nonsignificant.

A diagnostic algorithm combining epigenetic markers to distinguish melanoma and dysplastic naevus

The diagnostic specificities and sensitivities of *CLDN11*, *CDH11*, *PPP1R3C*, *MAPK13*, and *GNMT* for the distinction of primary melanomas from dysplastic naevi of series 1 are given in Table 2. After having determined these characteristics of the five methylation markers individually, we continued by examining which combinations of markers could aid in the differential diagnosis of primary melanoma and dysplastic naevus. Diagnostic algorithms were created using the set of 57 dysplastic naevi and 79 primary melanomas from series 1, and the accuracy of these models was subsequently tested in a second sample set consisting of 72 dysplastic naevus and 82 primary melanoma biopsy samples, designated series 2. In series 1, the three most differentially methylated genes were *CLDN11*, *CDH11*, and *PPP1R3C*. A first, simple three-gene diagnostic model was created that considers methylation of either of these three genes as indicative of melanoma. This model yielded a specificity of 89% and sensitivity of 67% in series 2 used as test set (Figure 4A).

As *CLDN11* methylation occurred exclusively in melanoma in series 1 used as training set, this epigenetic event had the highest discriminatory value with a specificity of 100% and sensitivity of 48% (Table 2). On the basis of a logistic regression model, a diagnostic algorithm was constructed consisting of two discrete steps. First, *CLDN11* methylation was evaluated, and, if present, a lesion was classified as melanoma. Second, methylation of *CDH11*, *PPP1R3C*, *MAPK13*, and *GNMT* was taken in consideration for samples with no *CLDN11* methylation (Figure 4A). Adding methylation information of the other four genes generated additional diagnostic value by increasing the sensitivity of the model to detect melanoma. This model has a receiver operating characteristic curve with an area under the curve of 0.806 (Figure 4B). The condition that a lesion is classified as melanoma if *CLDN11* or at least two other genes are methylated yields a specificity of 89% and sensitivity of 66% in series 2 (Figure 4A). Promoter methylation frequencies and patterns of the five interrogated genes in series 2, visualized in Figure 4C and D and reported in Supplementary Table S6a, were generally similar to that of series 1. In series 2, *CLDN11* methylation was detected in 6% of dysplastic naevus samples and 52% of primary melanoma samples. Validation of methylation frequencies for the five genes in sample series 2 demonstrated that, in addition to *CLDN11*, also methylation of *CDH11*, *PPP1R3C*, and *GNMT* has high specificity for melanoma.

A

	Series 1 (training set)		Series 2 (test set)	
	Specificity	Sensitivity	Specificity	Sensitivity
3-gene model that considers methylation of:				
CLDN11 or *CDH11* or *PPP1R3C*	**86%**	**66%**	**89%**	**67%**
2-step model that considers methylation of:				
CLDN11 only	**100%**	**48%**	**94%**	**52%**
CLDN11 or 4 other genes	**95%**	**49%**	**94%**	**56%**
CLDN11 or ≥ 3 other genes	**93%**	**57%**	**90%**	**60%**
CLDN11 or ≥ 2 other genes	**88%**	**65%**	**89%**	**66%**
CLDN11 or ≥ 1 other genes	**68%**	**77%**	**67%**	**79%**

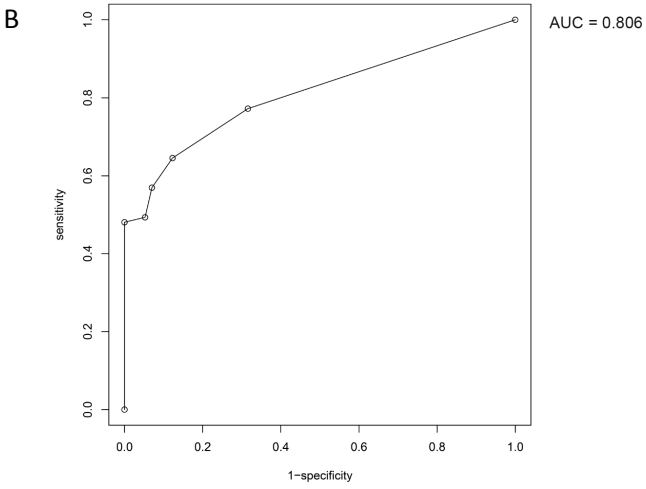

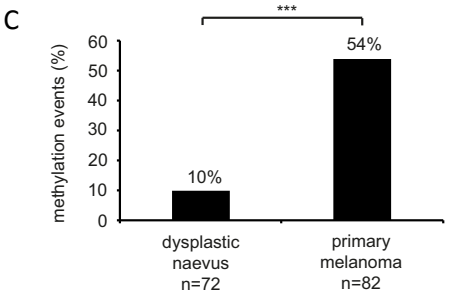

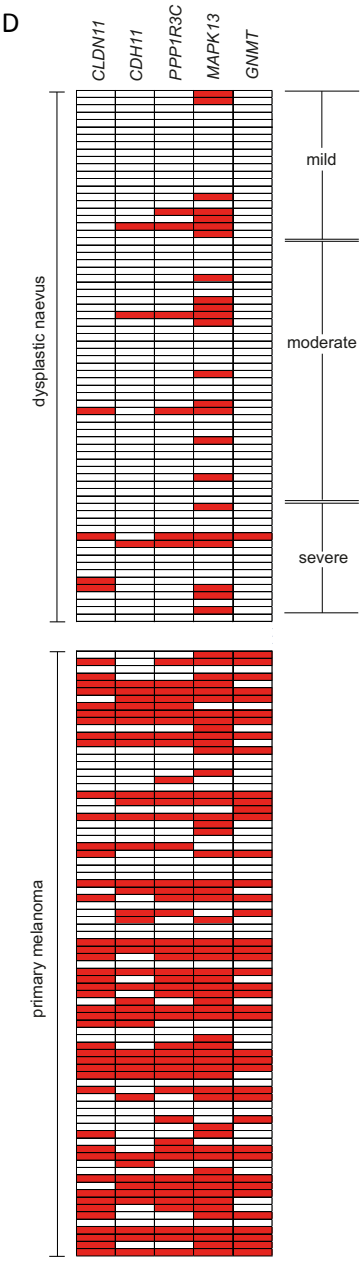

Figure 4. **Testing and validation of diagnostic models that incorporate *CLDN11*, *CDH11*, *PPP1R3C*, *MAPK13*, and *GNMT* promoter methylation**. (**A**) Diagnostic value was tested in 57 dysplastic naevi and 79 primary melanomas from series 1 (training set), yielding diagnostic scores in the form of a three-gene model and a two-step model, followed by validation of these models in 72 dysplastic naevi and 82 primary melanomas from series 2 (test set). (**B**) Receiver operating characteristic curve of the two-step diagnostic model. (**C**) Percentage of methylation events within the dysplastic naevi and primary melanomas of series 2. ***P <0.001 by two-sided Fisher's exact test. (**D**) Promoter methylation status of the five genes in 72 dysplastic naevi and 82 primary melanomas from series 2. White, unmethylated; red, methylated.

Discussion

Dysplastic naevi are melanocytic neoplasms with cytonuclear and architectural atypia and stromal alterations and are generally considered to constitute an intermediate stage between common naevi and melanoma. These lesions have an increased risk of developing into melanoma, and it can be difficult to clinically distinguish dysplastic naevus from early-stage melanoma[5]. In this study, we examined promoter CpG island methylation of 12 genes, previously identified in a genome-wide methylation screen, in metastatic and primary melanoma, dysplastic naevus, and common naevus biopsy specimens. We observed progressive promoter CpG island hypermethylation of these genes, with the methylation frequencies increasing from common naevus to metastatic melanoma. Dysplastic naevi, although less commonly than melanoma, demonstrate promoter hypermethylation of genes with tumor-suppressive functions, including *CDH11*. This shows that dysplastic naevi may already resemble their malignant counterparts at the epigenetic level and suggests that epigenetic instability can occur early, in premalignant stages of melanocytic neoplasia. In addition, it reinforces the notion of dysplastic naevus as an intermediate step in melanoma progression.

Promoter CpG island methylation analysis in a first, smaller series of samples using BMCA suggested that promoters of the *CLDN11*, *CDH11*, *PPP1R3C*, *MAPK13*, and *GNMT* genes could be selectively methylated in melanoma. This would render these methylation events suitable epigenetic biomarkers to improve the diagnosis of melanoma and to allow distinction with dysplastic naevus. Using MSP in a large series of 251 melanocytic neoplasm samples, we were able to show the discriminatory value of detecting promoter methylation of these five genes. Methylation detection by the MSP technique is especially suited in this setting, as it yields reproducible results and can directly be applied to FFPE-based samples in the clinic. On the basis of a logistic regression model analysis, we developed a diagnostic score that incorporates different gene methylation features, consisting of assessment of *CLDN11* methylation first, followed by determination of the methylation frequency of *CDH11*, *PPP1R3C*, *MAPK13*, and *GNMT* in DNA isolated from a biopsy sample. Testing of the diagnostic accuracy of this score in another independent series consisting of 82 primary melanoma and 72 dysplastic naevus samples revealed a receiver operating characteristic area under the curve of 0.806 in this independent test set. A simpler three-gene model that incorporates only *CLDN11*, *CDH11*, and *PPP1R3C* as marker of melanoma has a specificity of 89% and sensitivity of 67% in the validation sample set. In our analysis, we have pursued methylation events that are present in melanoma and do not occur in dysplastic naevus. This has resulted in a panel of epigenetic markers with very high specificity for melanoma, but with moderate sensitivity. In particular for screening purposes, a sensitive test would be preferred over a more specific test. By varying the parameters of the logistic regression model or addition of

genes that are more frequently methylated in melanoma, such as *HOXA9*, an increase in sensitivity can be achieved, but at the expense of specificity. The binary results of methylation detection may confer an advantage over comparative genomic hybridization, fluorescent in situ hybridization, or combined immune-histochemical detection of melanoma markers, where interpretation of results can have higher interobserver variability[15-17]. Comparative genomic hybridization and fluorescent in situ hybridization, genomic methodologies used primarily in the research setting, may yield higher diagnostic accuracy than methylation detection of a few genes.

Remarkably, methylation of the *CLDN11* gene was completely specific for melanoma, that is, methylation affected 48% of primary melanoma and 73% of metastatic samples, whereas it was absent in common and dysplastic naevi in the first large sample series. In the second sample series, used to validate the diagnostic algorithm, *CLDN11* was found to be methylated in 6% of dysplastic naevus samples. Detection of *CLDN11* methylation might in particular be used clinically to distinguish malignant from benign melanocytic lesions. Its methylation was shown previously to be associated with transcriptional silencing[18]. *CLDN11* encodes a member of the claudin family, components of tight junctions that maintain a physical barrier and polarity of cells. *CLDN11* hypermethylation was previously reported in bladder and gastric cancer, where epigenetic silencing increased cell motility and invasiveness[18,19]. Interestingly, in mouse skin tumorigenesis, changes were found in the distribution pattern of claudin tight-junction proteins, where epidermal expression of claudin proteins including *CLDN11* decreased during tumor progression[20]. We hypothesize that in melanoma development loss of *CLDN11* expression through promoter hypermethylation facilitates invasive behavior by disrupting intercellular cohesion provided by tight-junction structures. In addition, methylation of *CDH11*, *PPP1R3C*, and *GNMT* occurred in more than half of melanomas but rarely in dysplastic naevi. The results for *CDH11* are in line with previous studies showing that methylation of this cadherin gene that inhibits tumor growth and metastasis preferentially occurs in lymph node metastases of melanoma patients[21]. Tumor-suppressive properties have also been reported for *PPP1R3C* and *GNMT*.

Thus far, promoter methylation studies in melanoma often used a limited number of clinical specimens and lacked examination of non-malignant samples, thereby making it impossible to distinguish cancer-specific from tissue-specific methylation events[22]. Only few studies analyzed promoter methylation in dysplastic naevi, and most of them examined single candidate genes in small sample sets[23-25]. To our knowledge, this is a previously unreported study that makes use of a large series of clinical specimens to show that promoter methylation of several genes, including tumor suppressor genes, is present to a small extent in dysplastic naevi. Using the methylation pattern of five genes, we propose a diagnostic algorithm to distinguish melanoma from benign melanocytic lesions.

The presence of *CLDN11*, *CDH11*, *PPP1R3C*, and *GNMT* methylation in a suspicious melanocytic lesion might be regarded as an indicator of malignancy. Taken together, the findings presented in this study provide insight in the epigenetic changes that occur in melanoma development and can aid in the molecular diagnosis of melanocytic lesions.

Acknowledgments

RvD is supported by a Melanoma Research Alliance young investigator award. This work was supported by Profileringsfonds Maastricht University Medical Center (PF=278). We thank Kathleen Daenen and Kim van Straeten for excellent technical assistance.

References

1. Bauer, J. and Garbe, C. Acquired Melanocytic Naevi as Risk Factor for Melanoma Development. A Comprehensive Review of Epidemiological Data. *Pigment Cell Res.* **16**(3), 297-306 (2003).
2. Ferlay, J. *et al.* Estimates of worldwide burden of cancer in 2008: GLOBOCAN 2008. *Int. J. Cancer* **127**(12), 2893-2917 (2010).
3. Brochez, L. *et al.* Inter-observer variation in the histopathological diagnosis of clinically suspicious pigmented skin lesions. *J. Pathol.* **196**(4), 459-466 (2002).
4. Shoo, B.A., Sagebiel, R.W., and Kashani-Sabet, M. Discordance in the histopathologic diagnosis of melanoma at a melanoma referral center. *J. Am. Acad. Dermatol.* **62**(5), 751-756 (2010).
5. Naeyaert, J.M. and Brochez, L. Dysplastic Naevi. *N. Engl. J. Med.* **349**(23), 2233-2240 (2003).
6. Sagebiel, R.W. Melanocytic naevi in histologic association with primary cutaneous melanoma of superficial spreading and nodular types: effect of tumor thickness. *J. Invest. Dermatol.* **100**(3), 322S-325S (1993).
7. Weatherhead, S.C., Haniffa, M., and Lawrence, C.M. Melanomas arising from naevi and de novo melanomas--does origin matter? *Br. J. Dermatol.* **156**(1), 72-76 (2007).
8. Elder, D.E. Dysplastic naevi: an update. *Histopathology.* **56**(1), 112-120 (2010).
9. Clark, W.H., Jr. *et al.* A study of tumor progression: the precursor lesions of superficial spreading and nodular melanoma. *Hum. Pathol.* **15**(12), 1147-1165 (1984).
10. Gao, L. *et al.* Genome-wide promoter methylation analysis identifies epigenetic silencing of MAPK13 in primary cutaneous melanoma. *Pigment Cell Melanoma Res.* **26**(4), 542-554 (2013).
11. Arumi-Uria, M., McNutt, N.S., and Finnerty, B. Grading of atypia in naevi: correlation with melanoma risk. *Mod. Pathol.* **16**(8), 764-771 (2003).
12. Winnepenninckx, V. *et al.* Gene expression profiling of primary cutaneous melanoma and clinical outcome. *J. Natl. Cancer Inst.* **98**(7), 472-482 (2006).
13. Herman, J.G. *et al.* Methylation-specific PCR: a novel PCR assay for methylation status of CpG islands. *Proc. Natl. Acad. Sci. U. S. A.* **93**(18), 9821-9826 (1996).
14. Derks, S. *et al.* Methylation-specific PCR unraveled. *Cell Oncol.* **26**(5-6), 291-299 (2004).
15. Gerami, P. *et al.* Fluorescence in situ hybridization for distinguishing nevoid melanomas from mitotically active naevi. *Am. J. Surg. Pathol.* **33**(12), 1783-1788 (2009).
16. Kashani-Sabet, M. *et al.* A multi-marker assay to distinguish malignant melanomas from benign naevi. *Proc. Natl. Acad. Sci. U. S. A.* **106**(15), 6268-6272 (2009).
17. Zhang, G. and Li, G. Novel multiple markers to distinguish melanoma from dysplastic naevi. *PLoS One.* **7**(9), e45037 (2012).
18. Agarwal, R. *et al.* Silencing of claudin-11 is associated with increased invasiveness of gastric cancer cells. *PLoS One.* **4**(11), e8002 (2009).
19. Awsare, N.S. *et al.* Claudin-11 decreases the invasiveness of bladder cancer cells. *Oncol. Rep.* **25**(6), 1503-1509 (2011).
20. Arabzadeh, A., Troy, T.C., and Turksen, K. Changes in the distribution pattern of Claudin tight junction proteins during the progression of mouse skin tumorigenesis. *BMC Cancer.* **7**, 196 (2007).
21. Carmona, F.J. *et al.* Epigenetic disruption of cadherin-11 in human cancer metastasis. *J. Pathol.* **228**(2), 230-240 (2012).
22. van den Hurk, K. *et al.* Genetics and epigenetics of cutaneous malignant melanoma: a concert out of tune. *Biochim. Biophys. Acta* **1826**(1), 89-102 (2012).
23. Sharma, S.P. New prediction model for melanoma. *Lancet Oncol.* **7**(9), 711 (2006).
24. Conway, K. *et al.* DNA-methylation profiling distinguishes malignant melanomas from benign naevi. *Pigment Cell Melanoma Res.* **24**(2), 352-360 (2011).
25. Helmbold, P. *et al.* RASSF10 promoter hypermethylation is frequent in malignant melanoma of the skin but uncommon in naevus cell naevi. *J. Invest. Dermatol.* **132**(3 Pt 1), 687-694 (2012).

Supplementary Data

Supplementary Table S1. Percentage of samples that had concordant results when methylation analysis was performed using BMCA and MSP on the same set of common naevi (n=11), dysplastic naevi (n=10) and melanomas (n=10).

	CLDN11		***CDH11***		***PPP1R3C***		***MAPK13***		***GNMT***	
		No. of samples		No. of samples		No. of samples		No. of samples		No. of samples
Common naevus	**100%**	11/11	**100%**	11/11	**100%**	11/11	**64%**	7/11	**100%**	11/11
Dysplastic naevus	**90%**	9/10	**90%**	9/10	**80%**	8/10	**90%**	9/10	**90%**	9/10
Primary melanoma	**80%**	8/10	**100%**	10/10	**90%**	9/10	**100%**	10/10	**70%**	7/10
Total	**90%**	28/31	**97%**	30/31	**90%**	28/31	**84%**	26/31	**87%**	27/31

Supplementary Table S2. Percentage of bisulphite-converted genomic DNA samples that was successfully amplified using MSP. In series 1, DNA was obtained from FFPE biopsy specimens of common naevus, dysplastic naevus, primary melanoma and metastatic melanoma (n=251). In series 2, DNA was obtained from FFPE, BFPE (boonfix-fixed, paraffin-embedded) and fresh frozen biopsy specimens of dysplastic naevus and primary melanoma (n=156).

	Series 1		**Series 2**	
		No. of samples		No. of samples
CLDN11	**98%**	247/251	**99%**	154/156
CDH11	**92%**	230/251	**99%**	154/156
PPP1R3C	**97%**	244/251	**99%**	155/156
MAPK13	**87%**	218/251	**99%**	155/156
GNMT	**96%**	240/251	**99%**	155/156

Supplementary Table S3. Methylation-specific PCR (MSP) was performed on series 1 consisting of 62 common naevus, 72 dysplastic naevus, 101 primary melanoma and 16 metastatic melanoma samples to determine methylation frequency of five candidate genes. In this table, all MSP results are presented whereas in Table 2, only samples for which MSP data was complete for all five genes were included.

	CLDN11		***CDH11***		***PPP1R3C***		***MAPK13***		***GNMT***	
		No. of samples		No. of samples		No. of samples		No. of samples		No. of samples
Common naevus	**0%**	0/61	**0%**	0/57	**0%**	0/62	**17%**	10/58	**3%**	2/60
Dysplastic naevus	**0%**	0/72	**5%**	3/66	**11%**	8/71	**25%**	15/59	**8%**	6/71
Primary melanoma	**47%**	46/98	**38%**	35/92	**45%**	43/95	**64%**	54/85	**44%**	41/93
Metastatic melanoma	**69%**	11/16	**47%**	7/15	**56%**	9/16	**67%**	11/16	**50%**	8/16

Supplementary Table S4a. Methylation frequency of five candidate genes in dysplastic naevus and primary melanoma biopsy samples from series 1 based on age of the patients. Dysplastic naevus and primary melanoma samples for which age was known (n=130) were grouped into patients younger than 50 years (n=57) and those that were 50 years or older (n=73).

	< 50 years (n=57)					≥ 50 years (n=73)				
	dysplastic naevus n=40		primary melanoma n=17		*P* value	dysplastic naevus n=17		primary melanoma n=56		*P* value
		no. of samples		no. of samples			no. of samples		no. of samples	
CLDN11	**0%**	0	**41%**	7	0.000	**0%**	0	**46%**	26	0.000
CDH11	**5%**	2	**47%**	8	0.000	**6%**	1	**34%**	19	0.029
PPP1R3C	**13%**	5	**53%**	9	0.002	**18%**	3	**48%**	27	0.028
MAPK13	**28%**	11	**71%**	12	0.003	**24%**	4	**57%**	32	0.025
GNMT	**10%**	4	**35%**	6	0.051	**12%**	2	**46%**	26	0.011

Supplementary Table S4b. **Methylation frequency of five candidate genes in dysplastic naevus and primary melanoma biopsy samples from series 2 based on age of the patients**. Dysplastic naevus and primary melanoma samples (n=154) were grouped into patients younger than 50 years (n=53) and those that were 50 years or older (n=101).

	< 50 years (n=53)					≥ 50 years (n=101)				
	dysplastic naevus n=35		primary melanoma n=18		*P* value	dysplastic naevus n=37		primary melanoma n=64		*P* value
		no. of samples		no. of samples			no. of samples		no. of samples	
CLDN11	**3%**	1	**56%**	10	0.000	**8%**	3	**52%**	33	0.000
CDH11	**0%**	0	**50%**	9	0.000	**8%**	3	**45%**	29	0.000
PPP1R3C	**3%**	1	**50%**	9	0.000	**14%**	5	**56%**	36	0.000
MAPK13	**26%**	9	**61%**	11	0.017	**38%**	14	**70%**	45	0.002
GNMT	**0%**	0	**44%**	8	0.000	**3%**	1	**52%**	33	0.000

Supplementary Table S5a. Methylation frequency of five candidate genes in the dysplastic naevus and primary melanoma biopsy samples from series 1 based on gender of the patients. The dysplastic naevus and primary melanoma samples for which gender was known (n=130) were grouped into male (n=53) and female (n=77) patients.

	Male (n=53)					Female (n=77)				
	dysplastic naevus n=25		primary melanoma n=28		*P* value	dysplastic naevus n=32		primary melanoma n=45		*P* value
		no. of samples		no. of samples			no. of samples		no. of samples	
CLDN11	**0%**	0	**54%**	15	0.000	**0%**	0	**40%**	18	0.000
CDH11	**0%**	0	**39%**	11	0.000	**9%**	3	**36%**	16	0.014
PPP1R3C	**8%**	2	**61%**	17	0.000	**19%**	6	**42%**	19	0.047
MAPK13	**16%**	4	**64%**	18	0.000	**34%**	11	**58%**	26	0.064
GNMT	**0%**	0	**61%**	17	0.000	**19%**	6	**33%**	15	0.199

Supplementary Table S5b. Methylation frequency of five candidate genes in the dysplastic naevus and primary melanoma biopsy samples from series 2 based on gender of the patients. The dysplastic naevus and primary melanoma samples for which gender was known (n=153) were grouped into male (n=76) and female (n=77) patients.

	Male (n=76)					**Female (n=77)**				
	dysplastic naevus n=31		**primary melanoma n=45**		***P* value**	**dysplastic naevus n=40**		**primary melanoma n=37**		***P* value**
		no. of samples		no. of samples			no. of samples		no. of samples	
CLDN11	**10%**	3	**53%**	24	0.000	**3%**	1	**51%**	19	0.000
CDH11	**10%**	3	**53%**	24	0.000	**0%**	0	**38%**	14	0.000
PPP1R3C	**16%**	5	**60%**	27	0.000	**3%**	1	**49%**	18	0.000
MAPK13	**55%**	17	**73%**	33	0.140	**15%**	6	**62%**	23	0.000
GNMT	**3%**	1	**56%**	25	0.000	**0%**	0	**43%**	16	0.000

Supplementary Table S6a. Methylation frequency of five candidate genes in biopsy samples of series 2 (72 dysplastic naevi and 82 primary melanomas), together with the specificity and sensitivity of each gene for the distinction of primary melanoma samples from dysplastic naevus samples.

Series 2 (test set)						
	Dysplastic naevus		**Primary melanoma**		**Dysplastic naevus n = 72 Primary melanoma n = 82**	
	Methylation frequency				**Specificity**	**Sensitivity**
	No. of samples		No. of samples			
CLDN11	**6%**	4/72	**52%**	43/82	**94%**	**52%**
CDH11	**4%**	3/72	**46%**	38/82	**96%**	**46%**
PPP1R3C	**8%**	6/72	**55%**	45/82	**92%**	**55%**
MAPK13	**32%**	23/72	**68%**	56/82	**68%**	**68%**
GNMT	**1%**	1/72	**50%**	41/82	**99%**	**50%**

Supplementary Table S6b. Methylation frequency of five candidate genes in biopsy samples of series 1 and 2 (129 dysplastic naevi and 161 primary melanomas), together with the specificity and sensitivity of each gene for the distinction of primary melanoma samples from dysplastic naevus samples.

Series 1 + 2 (training set + test set)						
	Dysplastic naevus		**Primary melanoma**		**Dysplastic naevus n = 129 Primary melanoma n = 161**	
	Methylation frequency				**Specificity**	**Sensitivity**
	No. of samples		No. of samples			
CLDN11	**3%**	4/129	**50%**	81/161	**97%**	**50%**
CDH11	**5%**	6/129	**43%**	70/161	**95%**	**43%**
PPP1R3C	**11%**	14/129	**53%**	86/161	**89%**	**53%**
MAPK13	**29%**	38/129	**65%**	105/161	**71%**	**65%**
GNMT	**5%**	7/129	**48%**	77/161	**95%**	**48%**

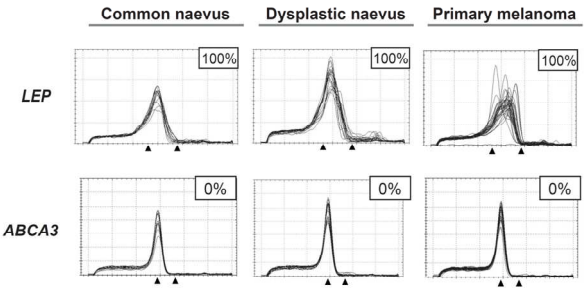

Supplementary Figure S1. *LEP* and *ABCA3* promoter methylation status in 20 dysplastic naevi, next to an independent set of 10 common naevi and 15 primary melanomas as analyzed by bisulphite melting curve analysis (BMCA). Black triangles indicate position of the melting curve peak for the respective positive (fully methylated) and negative (fully unmethylated) control.

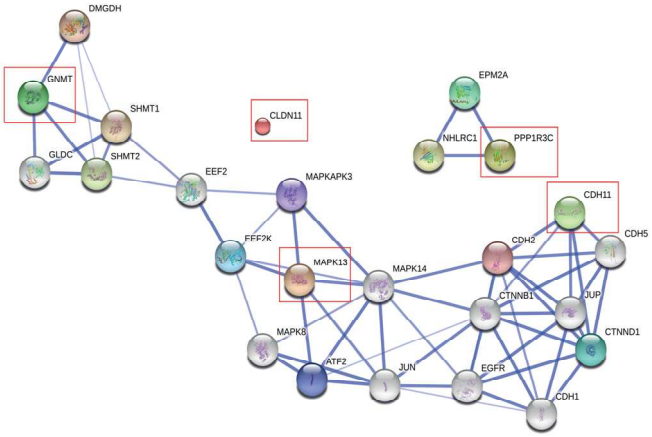

GO Biological Processes*

GO ID	Term	Number of Genes	*P* value FDR
GO:0034332	adherens junction organization	6	6.99E-7
GO:0016337	cell-cell adhesion	6	4.65E-3
GO:0045216	cell-cell junction organization	5	4.65E-3
GO:0034329	cell junction assembly	5	4.65E-3
GO:0034330	cell junction organization	5	4.65E-3
GO:0000165	MAPK cascade	5	6.96E-3
GO:0032880	regulation of protein localization	5	4.28E-2
GO:0035666	TRIF-dependent toll-like receptor signaling pathway	4	4.65E-3
GO:0034138	toll-like receptor 3 signaling pathway	4	4.65E-3
GO:0002756	MyD-88independent toll-like receptor signaling pathway	4	4.65E-3
GO:0034130	toll-like receptor 1 signaling pathway	4	4.65E-3
GO:0034134	toll-like receptor 2 signaling pathway	4	4.65E-3
GO:0002755	MyD-88dependent toll-like receptor signaling pathway	4	4.65E-3
GO:0034142	toll-like receptor 4 signaling pathway	4	4.65E-3
GO:0008063	Toll signaling pathway	4	4.65E-3
GO:0043406.	positive regulation of MAP kinase activity	4	4.28E-2

*Only Biological Processes with 4 or more involved genes and p-value < 0.05 are listed

GO Molecular Functions*

GO ID	Term	Number of Genes	*P* value FDR
GO:0019903	protein phosphatase binding	5	2.33E-4
GO:0019902	phosphatase binding	5	1.19E-3
GO:0042153	RPTP-like protein binding	4	1.24E-7
GO:0019842	vitamin binding	4	2.55E-2
GO:0008168	methyltransferase activity	4	4.37E-2
GO:0004708	MAP kinase kinase activity	3	1.73E-3
GO:0004712	protein serine/threonine/tyrosine kinase activity	3	1.19E-2
GO:0004793	threonine aldolase activity	2	1.73E-3
GO:0008732	L-allo-threonine aldolase activity	2	1.73E-3
GO:0016832	aldehyde-lyase activity	2	8.88E-3

*Only Molecular Functions with p-value < 0.05 are listed

Supplementary Figure S2. Interaction network analysis of *CLDN11*, *CDH11*, *PPP1R3C*, *MAPK13* and *GNMT*. Predicted physical or functional associations are depicted by blue lines. Stronger associations are represented by thicker lines.

Chapter 5

Genome-wide analysis of gene and protein expression of dysplastic naevus cells

Linda Gao[1,*], Frans A. van Nieuwpoort[1,*], Jacoba J. Out-Luiting[1], Paul J. Hensbergen[2], Femke A. de Snoo[3], Wilma Bergman[1], Remco van Doorn[1] and Nelleke A. Gruis[1]

[1]Department of Dermatology, Leiden University Medical Center, Leiden, The Netherlands
[2]Department of Parasitology, Leiden University Medical Center, Leiden, The Netherlands
[3]Center for Human and Clinical Genetics, Leiden University Medical Center, Leiden, The Netherlands
*These authors contributed equally to this work.

Journal of Skin Cancer 2012; 2012: 981308

Abstract

Cutaneous melanoma, a type of skin tumor originating from melanocytes, often develops from premalignant naevoid lesions via a gradual transformation process driven by an accumulation of (epi)genetic lesions. These dysplastic naevi display altered morphology and often proliferation of melanocytes. Additionally, melanocytes in dysplastic naevi show structural mitochondrial and melanosomal alterations and have elevated reactive oxygen species (ROS) levels. For this study we performed genome-wide expression and proteomic analysis of melanocytes from dysplastic naevus (DNMC) and adjacent normal skin (MC) from 18 patients. Whole genome expression profiles of the DNMC and MC of each individual patient subjected to GO-based comparative statistical analysis yielded significantly differentially expressed GO classes including "organellar ribosome," "mitochondrial ribosome," "hydrogen ion transporter activity," and "prefoldin complex." Validation of 5 genes from these top GO classes revealed a heterogeneous differential expression pattern. Proteomic analysis demonstrated differentially expressed proteins in DNMC that are involved in cellular metabolism, detoxification, and cytoskeletal organization processes, such as GTP-binding Rho-like protein CDC42, glutathione-S-transferase omega-1 and prolyl 4-hydroxylase. Collectively these results point to deregulation of cellular processes, such as metabolism and protein synthesis, consistent with the observed elevated oxidative stress levels in DNMC potentially resulting in oxidative DNA damage in these cells.

Introduction

Cutaneous melanoma is a malignant tumor that originates from melanocytes, the pigment producing cells of the skin. Melanoma development is a multistep process driven by the acquisition of genetic and epigenetic abnormalities. Although a subset of melanomas develop in normal skin de novo, in many instances premalignant naevoid pigmented lesions can be discerned in melanoma formation. Approximately a third of melanomas develop from a precursor naevus that is most commonly dysplastic[1]. Consistently, individuals with dysplastic naevi are at increased risk of developing melanoma[2].

Dysplastic naevi can progress into radial and subsequently vertical growth phase melanomas[3,4]. The complex multistage development process of melanoma is characterized by various morphological, cellular, and biochemical alterations. Histopathologically dysplastic naevi show characteristic morphological alterations, including proliferation and variable atypia of epidermal melanocytes, formation of irregular cell nests in the epidermis and basement membrane zone, and the interconnection of these nests and layers (bridging). Melanocytes in dysplastic naevi (DNMC) furthermore exhibit morphological alterations in melanosomes and mitochondria, similar to those observed in melanoma cells[5]. We have previously shown that DNMC in

comparison with normal melanocytes show higher pheomelanin, iron, and calcium levels resulting in elevated reactive oxygen species (ROS) levels[6,7]. The diminished levels of antioxidant enzymes in DNMC further highten ROS levels and reinforce chronic oxidative stress in these cells[8,9].

In the present study we compared the gene expression and protein expression patterns of melanocytes from dysplastic naevus and from normal skin of 18 individuals. From a surgically removed dysplastic naevi and adjacent normal skin, melanocytes were isolated and briefly cultured for gene expression analysis using whole genome expression arrays and proteome analysis by peptide mass fingerprinting. Gene ontology-based gene expression analysis and protein expression analysis revealed differentially expressed pathways involved in cellular metabolism, detoxification, and cell shape organization. These findings appear to signify deregulated processes that all together may contribute to an increase in the levels of reactive oxygen species and oxidative stress, as is often observed in DNMC. The resultant oxidative DNA damage is an endogenous mutagenic force that might contribute to melanoma development.

Methods

Cell culture

After approval by the Medical Review Board of Leiden University Medical Center and patient consent, 18 clinically atypical naevi were excised from 18 different patients. All 18 samples were confirmed after pathologist review as dysplastic naevus. The elliptical incision consisted of the dysplastic naevus in the central part and normal skin at the tips. To ensure separate isolation of melanocytes from the dysplastic naevus and from adjacent normal skin, the central part and tip of each surgical specimen were first divided before further processing. For isolation of the melanocytes from the dysplastic naevus and normal skin from the epidermal compartment, we used an established protocol described previously[6,7]. Briefly, after removal of subcutaneous fat, epidermis and dermis were separated by overnight incubation with dispase grade II (Boehringer Mannheim Inc, Indianapolis, IN). The epidermis was trypsinized to obtain a single cell suspension using 0.25% trypsin. The cells from this single cell suspension were plated in Ham's F10 melanocyte medium supplemented with penicillin (100 U/mL), streptomycin (100 U/mL), L-glutamine (Invitrogen, Breda, The Netherlands), 1% Ultroser G (BioSepra, Fremont, CA), Endothelin-1 (5 ng/mL), basic-FGF (5 ng/mL), cholera toxin (30 µg/mL), IBMX (33 µM), and TPA (8 nM, Sigma-Aldrich, Zwijndrecht, The Netherlands). This melanocyte medium contains ingredients that are toxic to keratinocytes present in the epidermal cell suspension. Under these conditions pure melanocyte cultures are obtained at 10 days after start of culture. Purity of these melanocyte cultures was confirmed by microscopic examination of cell morphology by clockwise assessment of the culture plate surface; after

10 days all cells invariably had the dendritic, star-shaped or spindle-like morphology of melanocytes and no cells with epithelioid morphology were present in the culture dish. Additional stainings of representative melanocyte cell cultures with melanocytic cell markers HMB45 and Melan-A confirmed the purity of these melanocyte cultures. Melanocytes isolated from dysplastic naevus (DNMC) and from normal skin (MC) were cultured for a maximum of six passages to ensure logarithmic growth and keep the time in culture as short as possible. To minimize the variation introduced by cell culture on gene and protein expression, all MC and DNMC patient samples underwent identical treatment in culture and were harvested at the same passage number with the same harvesting methods.

Sample preparation for microarrays and peptide mass fingerprinting

RNA was isolated from melanocytes with the RNeasy Mini Kit (Qiagen, Venlo, Netherlands). Antisense amplified RNA (aRNA) was generated with theMessageAMP II aRNA Kit (Ambion, Austin, TX) for hybridization to the Human Genome U133 Plus 2.0 Array (Affymetrix, Santa Clara, CA) following manufacturer's protocol. RNA concentrations were determined by nanodrop measurements and RNA quality control was performed prior to hybridization by Lab-on-a-chip on Agilent's Bioanalyzer. RNA quality was further confirmed by post-hybridization quality control measurements performed as part of the Affymetrix microarray analysis, including normalization scaling factor across the microarrays and cRNA transcript integrity as assessed by 3' to 5' probe set signal intensity ratios, as routinely performed at the Leiden Genome Technology Center. Protein was isolated from melanocyte cell pellets using TRIzol reagent (Invitrogen); protein concentrations were determined by the Pierce BCA Protein Assay Kit. Protein samples (10 μg) were labeled with 1000 pmol fluorescence amine-reactive cyanine dyes for two-dimensional difference gel electrophoresis (2D DIGE) following manufacturer's protocol (Amersham-Pharmacia Biotech).

Statistical analysis of gene expression data

Probe set signal intensities derived from microarray scans were subjected to the robust multi-array average (RMA) algorithm as previously described[10]. This algorithm results in background-corrected, quantile normalized and log(base2)-transformed final probe intensities that serve as measures of gene expression; this log scale measure of expression will be further referred to as "(gene) expression value." To identify genes that were differentially expressed in DNMC when compared to MC, a statistical analysis method (random variance model (RVM)-based t-test) suited for detection of gene expression differences in microarray experiments comprising relatively smaller sample sizes was used[11], while controlling the number and proportion of false discoveries with a multivariate permutation test as described previously[12]. Additional hierarchical clustering

based on Euclidean distance was performed; clustering reproducibility was assessed using calculated R (reproducibility) and D (discrepancy) indices[13].

Functional class scoring based on gene ontology annotations

All gene ontology annotations were obtained through http://www.geneontology.org/. Gene ontology (GO) classes with fewer than five and more than 100 genes represented in the array data were not considered in order to exclude very small and very large classes. The DNMC sample of one individual patient was compared to the paired MC sample, in order to assess whether differential expression of GO classes existed across all microarrays between the paired melanocyte sample set. Functional class scoring, based on semi-supervised gene expression data analysis, was performed according to the statistical method as previously described[14]. This method does not require prior gene selection and *P* values are assigned based on interrogated genes in a GO class.

2D DIGE and mass spectrometry analysis

2D DIGE was performed as previously described[15]. Dye swap experiments were performed to check for labeling differences between Cy3 and Cy5. Gels were scanned in low-fluorescent glass plates with a Typhoon 9400 scanner (GE Health care UK Ltd., Buckinghamshire, UK). TIFF images of the gels were analyzed with Delta2D v3.4 software (Dodecon, Greifswald, Germany). Spots were quantified and normalized based on total spot volume of one gel. The matched spot volumes were subsequently normalized across the whole set of gels and normalized spot volumes were compared between images in the set. Statistical significant differences between normalized spot volumes were determined using the Welch-modified Student's t-test and step-down Westfall and Young method as correction for the false discovery rate. Protein spots of interest were excised from the gel for analysis on a MALDI-TOF/TOF instrument (Ultraflex, Bruker, Germany). All mass fingerprint and MS/MS data were searched against the human protein database with the Mascot program (Matrix Science, Boston, MA).

Quantitative real-time PCR

cDNA was generated from DNase-treated RNA (1µg) with the iScript cDNA synthesis kit (BioRad, Hercules, CA). qRT-PCR was performed with iQ SYBR Green Supermix on a MyiQ Real-Time PCR Detection System (BioRad). *RPS11* served as reference gene in experiments. qRT-PCR expression data is presented as mean of two measurements.

Results

Microarray analysis of melanocytes from dysplastic naevus and normal skin

Previously it was demonstrated that melanocytes isolated from dysplastic naevus (DNMC) show differences in morphology, pigmentation, and growth abilities when compared to

melanocytes isolated from normal skin (MC) in culture[7]. For this study paired DNMC and MC were obtained from dysplastic naevi and normal skin of 18 patients. Similarly we observed that the cultures of dysplastic naevus cells differed in morphology from that of normal melanocytes; Figure 1A displays a representative picture from melanocyte cultures derived from either normal skin (left, MC) or from dysplastic naevus (right, DNMC), showing that the MC have more equally-shaped dendrites as compared to the DNMC that consistently show a distinct stretched and thinner dendrite morphology. Microarray gene expression profiling was performed on these 18 paired melanocytic cell sets to gain insight into differences between these melanocyte sample groups on molecular level. Analysis of Affymetrix U133 plus 2.0 microarray data revealed that melanocytes from dysplastic naevi and from normal skin expressed 45% of the interrogated genes at a measurable level. Figure 1B depicts a scatter plot where the expression ratio's of a representative sample set of DNMC and MC of one patient is plotted, indicating that gene expression differences between the DNMC and MC of the same patient were generally modest. Except for two samples, hierarchical clustering of the microarray data showed that the DNMC samples resembled their autologous normal counterparts more closely than they resemble the DNMC of another individual (Figure 1C). Of note, samples 0310B and 0223B clustered separately from the remaining samples; this distinction was not reflected in a different morphology of these cell samples, since cell morphology across the 18 DNMC samples was homogeneous without notable differences between the samples. In addition, all dysplastic naevi included in this study were histopathologically very similar and also in this respect samples 0310 and 0223 did not significantly differ from other patient samples.

We considered the possibility that in our melanocyte sample sets, smaller but parallel effects among groups or sets of genes may exist that act together within pathways. In this way we would not so much identify individual marker genes differentially expressed by DNMC, but rather obtain an impression of dysregulated biological processes in DNMC. We aimed to uncover genes that were highly relevant when placed in a larger network of genes that interact with it, even though showing small differential expression individually. We proceeded to analyze for each pair of DNMC and MC from a single patient, which functional groups of genes were differentially expressed. The top GO classes identified by functional class scoring as differentially expressed in DNMCs when compared to MCs, are listed in Table 1A. Among the top represented GO classes were "organellar ribosome," "mitochondrial ribosome," "hydrogen ion transporter activity," "prefoldin complex," and "cAMP-dependent protein kinase regulator activity." Table 1B presents the details of the top five GO classes that are differentially expressed between 18 sets of DNMCs and MCs. The genes in each GO class all had a *P* value <0.05. Additional comparative statistical analysis of the gene expression data between the entire

group of 18 DNMCs and 18 normal MCs did not yield significantly differentially expressed genes (data not shown).

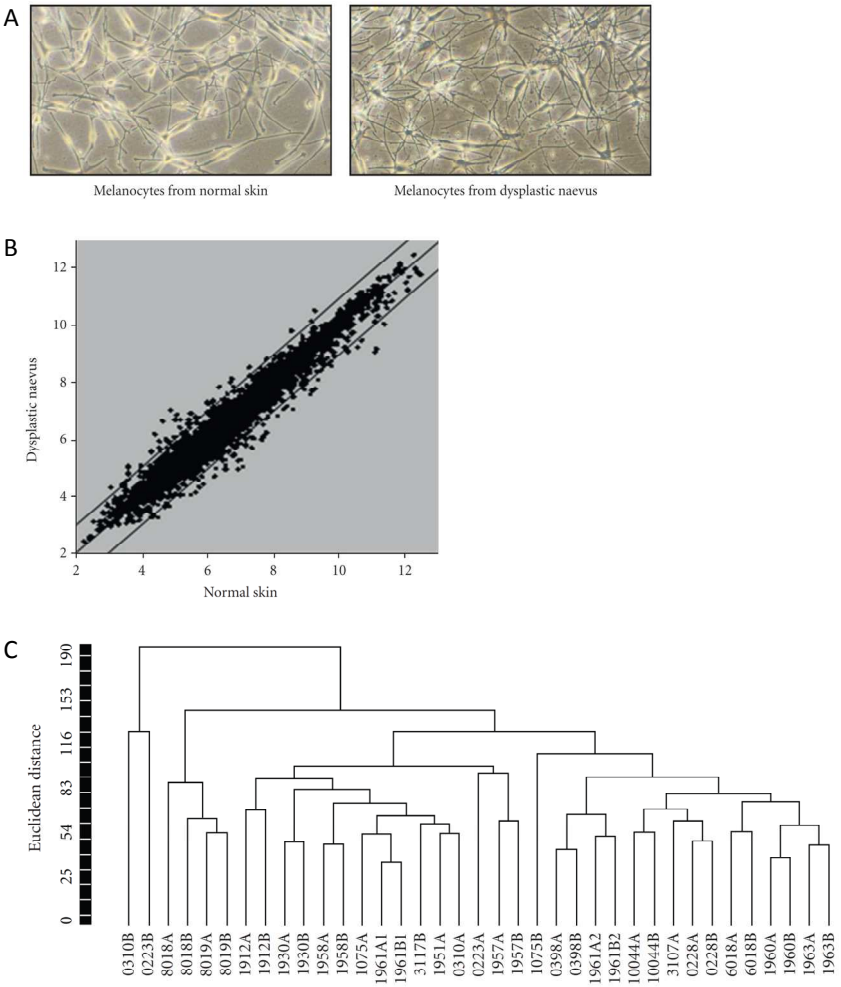

Figure 1. (**A**) Photos (4x magnification) taken from cultures of melanocytes derived from normal skin (left, MC) and dysplastic naevus (right, DNMC), representative of the MC and DNMC cultures of all 18 patients from which each of the melanocyte cultures were derived. (**B**) Scatter plot with average-log expression ratio's within one DNMC sample plotted against the average-log ratio's within the paired MC sample from one representative patient sample set. Each dot represents an interrogated probeset. The diagonal lines in the graph are outlier lines that indicate a 2-fold difference in the geometric mean of the expression ratio's between the DNMC and MC sample. (**C**) Clustering dendrogram of the expression values of all melanocyte samples. The vertical axis indicates the Euclidean distance with complete linkage as a measure for the extent of similarity between the samples. The horizontal axis contains all samples; A-labeled sample numbers, melanocytes derived from normal skin; B-labeled sample numbers, melanocytes derived from dysplastic naevus. The calculated R-index (0.997) and D-index (0.02) showed that the clusters were highly reproducible.

Table 1A. Differentially expressed GO classes resulting from comparative GO-based analysis of paired DNMC and MC sample sets of 18 patients

	GO category[1]	GO Term[2]	GO description	Number of genes	LS Permutation *P* value[3]	KS Permutation *P* value[4]
1	313	CC	organellar ribosome	30	1.00E-05	0.0120303
2	5761	CC	mitochondrial ribosome	30	1.00E-05	0.0120303
3	15078	MF	hydrogen ion transporter activity	94	9.22E-05	9.01E-05
4	16272	CC	prefoldin complex	13	0.0003082	0.001475
5	8603	MF	cAMP-dependent protein kinase regulator activity	9	0.0006046	0.0080679
6	4164	MF	diphthine synthase activity	5	0.0006262	9.03E-05
7	8629	BP	induction of apoptosis by intracellular signals	17	0.0006292	0.0060299
8	79	BP	regulation of cyclin-dependent protein kinase activity	30	0.0009682	0.0006918
9	8022	MF	protein C-terminus binding	28	0.0010178	0.0332401
10	30274	MF	LIM domain binding	5	0.0027241	0.0278159
11	17182	BP	peptidyl-diphthamide metabolism	8	0.0031029	0.001998
12	17183	BP	peptidyl-diphthamide biosynthesis from peptidyl-histidine	8	0.0031029	0.001998
13	18202	BP	peptidyl-histidine modification	8	0.0031029	0.001998
14	8428	MF	ribonuclease inhibitor activity	5	0.0031816	0.0130247
15	45815	BP	positive regulation of gene expression, epigenetic	7	0.0032192	0.0187543
16	43028	MF	caspase regulator activity	5	0.0035432	0.3403788
17	31202	MF	RNA splicing factor activity, transesterification mechanism	23	0.0042451	0.0013586
18	8757	MF	S-adenosylmethionine-dependent methyltransferase activity	76	0.0044728	0.0618698
19	7021	BP	tubulin folding	5	0.0046218	0.0028239
20	8013	MF	beta-catenin binding	7	0.0048826	0.0031594
21	118	CC	histone deacetylase complex	38	0.0080248	0.0020909
22	9897	CC	external side of plasma membrane	9	0.0085632	0.0021181
23	45736	BP	negative regulation of cyclin-dependent protein kinase activity	5	0.0182021	0.0028634
24	3747	MF	translation release factor activity	8	0.045947	0.0046691
25	8079	MF	translation termination factor activity	8	0.045947	0.0046691
26	42393	MF	histone binding	18	0.172388	0.0043185

1. The 26 GO categories found to be significant at the nominal 0.005 level of the LS permutation test or KS permutation test (sorted by *P* values of the LS permutation test). For each GO category, the table lists the unique identifier, the number of genes in the project gene list that belong to the GO category, and the LS and KS *P* values. The presented GO categories are ordered by the *P* value of the LS test (smallest first).

2. GO-Term: CC = cellular component, BP = biological process and MF = molecular function.

3. Fisher (LS) statistic is defined as the mean negative natural logarithm of the *P* values of the appropriate single gene univariate test.

4. Kolmogorov-Smirnov (KS) statistic is used for testing if the *P* values are of a uniform distribution.

Table 1B. Genes from the top four identified differentially expressed GO classes

	GO Term[1]	GO description	Probeset	Description[2]	Gene symbol	Parametric *P* values
1	CC	organellar ribosome	219220_x_at	mitochondrial ribosomal protein S22	MRPS22	0.0001097
2	CC	organellar ribosome	223480_s_at	mitochondrial ribosomal protein L47	MRPL47	0.000131
3	CC	organellar ribosome	218558_s_at	mitochondrial ribosomal protein L39	MRPL39	0.006304
4	CC	organellar ribosome	224869_s_at	mitochondrial ribosomal protein S25	MRPS25	0.0151834
5	CC	organellar ribosome	222775_s_at	mitochondrial ribosomal protein L35	MRPL35	0.0171902
6	CC	mitochondrial ribosome	219220_x_at	mitochondrial ribosomal protein S16	MRPS16	0.0005530
7	CC	mitochondrial ribosome	223480_s_at	mitochondrial ribosomal protein L44	MRPL44	0.000131
8	CC	mitochondrial ribosome	219819_s_at	mitochondrial ribosomal protein S28	MRPS28	0.0029398
9	CC	mitochondrial ribosome	217919_s_at	mitochondrial ribosomal protein L42	MRPL42	0.0303516
10	CC	mitochondrial ribosome	222993_at	mitochondrial ribosomal protein S37	MRPL37	0.003539
11	MF	hydrogen ion transporter activity	213846_at	cytochrome c oxidase subunit VIIc	COX7C	0.0020774
19	MF	hydrogen ion transporter activity	218484_at	NADH dehydrogenase (ubiquinone) 1	NDUFA4L2	0.00585351
12	MF	hydrogen ion transporter activity	238765_at	ATPase, H+ transporting, lysosomal 13kDa, V1 subunit G1	ATP6V1G1	0.0059421
13	MF	hydrogen ion transporter activity	209065_at	ubiquinol-cytochrome c reductase binding protein	UQCRB	0.0171665
14	MF	hydrogen ion transporter activity	231487_at	cytochrome c oxidase subunit 8C	COX8C	0.021483
15	MF	hydrogen ion transporter activity	1552286_at	ATPase, H+ transporting, lysosomal 31kDa, V1 subunit E2	ATP6V1E2	0.0279023
16	MF	hydrogen ion transporter activity	202698_x_at	cytochrome c oxidase subunit IV isoform 1	COX4I1	0.0380242
17	MF	hydrogen ion transporter activity	228142_at	ubiquinol-cytochrome c reductase complex (7.2 kD)	UCRC	0.0389511
18	MF	hydrogen ion transporter activity	220834_at	membrane-spanning 4-domains, subfamily A, member 12	MS4A12	0.0460068
20	CC	prefoldin complex	207132_x_at	prefoldin subunit 5	PFDN5	0.0086113
21	CC	prefoldin complex	218336_at	prefoldin subunit 2	PFDN2	0.0225808
22	CC	prefoldin complex	222019_at	prefoldin subunit 6	PFDN6	0.0326926
23	CC	prefoldin complex	201472_at	von Hippel-Lindau binding protein 1	VBP1	0.0345687
25	CC	prefoldin complex	205963_s_at	DnaJ homolog, subfamily A, member 3	DNAJA3	0.04568034
26	MF	oxidoreductase activity	207843_x_at	cytochrome b5 type A	CYB5A	0.01245134
27	MF	oxidoreductase activity	1560609_at	crystallin zeta (quinone reductase)-like 1	CRYZL1	0.0496658

1. Parametric GO-Term: CC = cellular component; MF= molecular function; BP= biological process.

2. Genes found to be differentially expressed with a parametric *P* value of less than 0.05 in the top 5 of GO categories.
They are ordered by the parametric *P* value associated with the GO category for each class.

Validation of genes from differentially expressed GO Classes

Not all genes belonging to a certain GO class will necessarily exhibit differential expression between the DNMC and MC samples. To subsequently validate and assess whether individual genes from the identified GO classes are differentially expressed in DNMC as compared to MC, we selected 14 genes that were among the top four GO classes and analyzed expression levels by qRT-PCR in the sample groups. Table 2 provides an overview of the 14 selected genes for validation and the corresponding qRT-PCR primer sequences. Figure 2 shows the qRT-PCR results for five of these validated genes (*MRPL42*, *PSMD10*, *HSPD1*, *MRPL47*, and *MRSP22*) with expression depicted as the ratio of gene expression in the DNMC to the corresponding expression in MC (vertical axis) plotted per sample for all 18 samples (horizontal axis). Differential gene expression seemed to vary per patient, as gene expression was either increased or decreased in DNMC as compared to MC for all interrogated paired melanocyte sample sets; this pattern was observed for all five genes. Some specific patient samples showed a higher increase in expression than other sample sets that also showed increased expression (sample 8018; expression *PSMD10* and *MRPL47*), but a consistent differential expression pattern similar for all five genes was not observed for individual samples. This heterogeneous differential expression pattern in DNMC when compared to MC across the 18 samples seems to be in line with the observations from the microarray expression analysis.

Table 2. The 14 selected genes for validation of gene expression and qRT-PCR primer sequences

	Gene	GO description	forward primer (5'-3')	reverse primer (5'-3')
1	MRPS22	Organellar ribosome	GAACTGAAGCCACCAACCTATAAG	GCTGCCTCAACTGCCTGTC
2	MRPL42	Organellar ribosome	TCCAGTCCAAAATGGAGCTT	CCACAGAAGGGTGGTAGCAT
3	MRPL47	Organellar ribosome	ACCTGGTGCTTGGAGAAGAGAC	CACATAAGGCAAGGCAAAGAATCG
4	MRPL21	Organellar ribosome	GAGCCGAGATAGCTTCCTGA	CTCCTTCCCATTGGTTCTCA
5	MRPL7	Organellar ribosome	ACGCTTTGATTGCTCGATCT	TTGCCTCTTTGAAGCGTTTT
6	MRPL10	Organellar ribosome	GCAGAACAAGGAGCATGTGA	TTTCAGCCACCATGTCTTCA
7	MRPL17	Organellar ribosome	CACTCGTGAAACTGCTCAGG	CGTCGGAATGGTACACACTG
8	NDUFS1	hydrogen ion transporter activity	TGCCCTAACCTCTAAGCCCTATG	ACTTCCAACCGCATCCATTACATC
9	NOX1	hydrogen ion transporter activity	GCCTCCATTCTCTCCAGCCTATC	CACATACTCCACTGTCGTGTTTCG
10	ACADM	Mitochondrial	AGCCTTTACTGGATTCATTGTGG	ATTCCTCTAGTATCTGAACATCGC
11	HSPD1	prefoldin complex	TACTGGCTCCTCATCTCACTCG	TGCTCAATAATCACTGTTCTTCCC
12	PSMF1	prefoldin complex	AACACCTGGGTGACTTCCAC	CCCACTGCTCATGGATAGGT
13	PSMB9	prefoldin complex	CGGGCGGGAGCACCAACC	GCAGACACTCGGGAATCAGAACC
14	PSMD10	prefoldin complex	AGGTGCTCAAGTGAATGCTGTC	TGTAGCCTCATAATGGTCCTTAGC

Proteome analysis of melanocytes from dysplastic naevus and normal skin

The 18 matched melanocyte sample sets, derived from either dysplastic naevus or normal skin, were additionally subjected to mass spectrometry analysis to assess whether protein expression differences existed between the melanocyte sample groups. Figure 3 shows a representative example of proteins expressed in MC (visualized as green signal-Cy3) and the corresponding protein expression in DNMC (visualized as red signal-Cy5). Dye swap

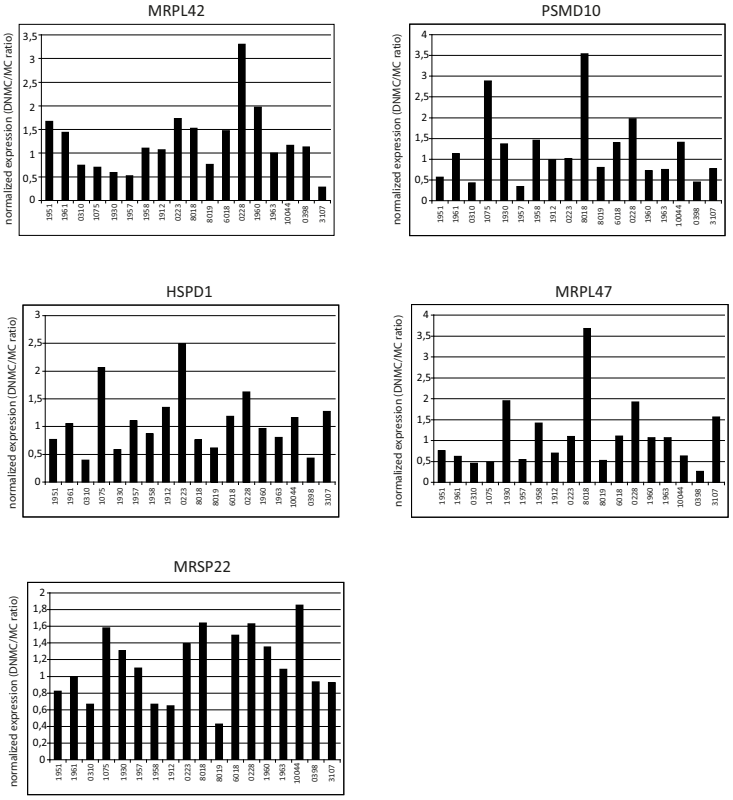

Figure 2. **qRT-PCR results across the 18 paired melanocyte sample groups for each of the five validated genes of GO-based statistical analysis**. Expression was calculated by taking the ratio between DNMC and the corresponding MC per patient sample set. *RPS11* served as reference gene in qRT-PCR experiments performed in duplicate. Values <1: gene expression is lower in DNMCs when compared to normal skin-derived melanocytes.

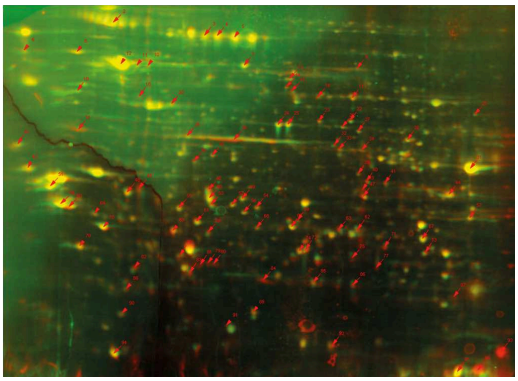

Figure 3. **Representative 2D DIGE image of protein analysis**. Red signal: overexpressed protein in DNMCs. Green signal: overexpressed protein in melanocytes from normal skin. Yellow signal: equal expression in both melanocyte types sample groups. Arrows indicate spots excised for MALDI-TOF/TOF analysis.

experiments to control for dye labeling efficiency performed on various samples indicated that no large differences in efficiency were present between both dyes (data not shown). Each of the 2D DIGE gels contained on average 2205 spots, 90% of these spots were reproducible in at least 15 gel sets. Protein spots (n = 99) that were differentially expressed between normal and atypical melanocytes in at least 15 gel sets determined by statistical analysis were excised and subsequent MALDI TOF/TOF analysis was performed. Database mining resulted in the annotation of 70 proteins (see Table 1 available as Supplementary Material online at doi:10.1155/2012/981308). Additional statistical analysis yielded 16 most differentially expressed proteins ($P < 0.03$, fold-change in expression difference ≥2 between DNMC and MC) (Table 3).

Among these 16 proteins, there was decreased expression of vimentin and increased GTP-binding Rho-like protein CDC42 expression in the DNMC; these proteins are involved in regulation of cell shape and morphology. In addition, glutathione-S-transferase omega and tyrosine 3- monooxygenase, proteins involved in cellular detoxification processes, were found to be expressed at lower level in DNMC than in MC. Proteins that were involved in protein metabolism (prolyl 4-hydroxylase, eukaryotic translation initiation factor 3) we found to be higher expressed in DNMC.

To assess whether overlap existed between the protein expression data and RNA expression data, we asked if for the 16 most differentially expressed proteins a similar expression pattern existed on the mRNA level. For each paired sample set of DNMC and MC, the corresponding gene expression fold-change was calculated. The fold-change in expression values was <1.5 for all probe sets and a consistent pattern in either increase or decrease in gene expression for a particular gene across all samples could not be observed (data not shown).

Discussion

In this study we compared the genome-wide gene expression and protein expression patterns of melanocytes derived from dysplastic naevus (DNMC) and melanocytes derived from adjacent normal skin (MC) from 18 patients. We aimed to find alterations in gene and protein expression that could inform us about biological processes underlying the earliest stage of melanoma development. Our results indicated that gene expression differences as measured using microarrays between melanocytes derived from normal skin and dysplastic naevus are rather small. Unbiased gene ontology analysis of the expression data of dysplastic naevus and normal melanocytes from a single patient enabled us to reveal differentially expressed GO classes; these included “organellar ribosome,” “mitochondrial ribosome,” “hydrogen ion transporter activity,” “prefoldin complex,” and “cAMP-dependent protein kinase regulator activity.” These GO classes reflect deregulated metabolic activity and growth of the DNMC as compared to MC, a

Table 3. Top 16 differentially expressed proteins between melanocytes from dysplastic naevus and from normal skin.

Swiss-prot id	Protein name	Mol. Mass Calculated (Da)[1]	p_I obs.[2]	p_I calc.[3]	% Pept. Coverage[4]	Ratio (DNMC/MC)[5]	*P* value	General function
Q9Y2R9	Ribosomal protein S7	22113	10.09	10	43	0.1310	0.010946	Translational elongation
P32969	Ribosomal protein L9	21964	9.96	9.96	29	0.22334	0.016167	Translational elongation
P78417	Glutathione S-transferase omega 1-1	27833	6.23	6.24	21	0.23627	0.013815	Exhibits glutathione-dependent thiol transferase and dehydroascorbate reductase activities
P62753	Ribosomal protein S6	28842	10.9	10.85	23	0.31890	0.012139	Controlling cell growth and proliferation through the selective translation of particular classes of mRNA
O75947	ATP synthase, H+ transporting, mitochondrial F0 complex, subunit d	18537	5.21	5.21	41	0.32135	0.027965	Mitochondrial membrane ATP synthase that produces ATP from ADP
P04792	Heat shock protein 27	22427	7.83	5.98	57	0.36622	0.023047	Involved in stress resistance and actin organization
P02794	Ferritin heavy chain	21252	5.3	5.08	46	0.40067	0.006873	Stores iron in a soluble, nontoxic, readily available form. Important for iron homeostasis
Q59EQ2	Tyrosine 3-monooxy-genase/tryptophan 5-monooxygenase activation protein	28179	4.76	4.73	26	0.41836	0.012436	Oxidoreductase
P08670	Vimentin	53710	5.06	5.06	43	0.4478	0.023374	Vimentins are class-III intermediate filaments
P07355	Annexin A2	36631	8.32	7.56	53	0.47142	0.00642	May be involved in heat-stress response
P47985	Cytochrome b-c1 complex subunit Rieske	29934	8.55	6.3	5	0.47725	0.008578	Component of the ubiquinol-cytochrome c reductase complex
Q5U0F4	Eukaryotic translation initiation factor 3	36878	5.38	5.38	32	32.155	0.018194	Protein synthesis
O94844	GTP-binding Rho-like protein cdc42	20123	5.25	4.83	55	288.699	0.017896	The protein may play a role in small GTPase-mediated signal transduction and the organization of the actin filament system
P07237	Prolyl 4-hydroxylase	57480	4.76	4.69	46	279.651	0.009987	This multifunctional protein catalyzes the formation, breakage, and rearrangement of disulfide bonds
Q6IBR6	Platelet-activating factor acetylhydrolase	25569	5.57	5.57		246.963	0.008975	Lipid metabolic process
Q9UBS4	DnaJ (Hsp40) homolog, subfamily B	40774	5.81	5.81	30	233.737	0.011076	Binds directly to both unfolded proteins that are substrates for ERAD and nascent unfolded peptide chains

1 Calculated molecular mass of the protein in Dalton (Da). **2** Isoelectric point (pI) observed in this study.
3 p I calculated according to the Mascot database. **4** Percentage peptide coverage.
5 Protein ratio melanocytes from dysplastic naevus (DNMC)/melanocytes from normal skin (MC).

factor that could contribute to the accumulation of cellular ROS levels.

We also aimed to determine differences in protein expression between the DNMC and melanocytes derived from normal skin. Comparison of the protein profiles between the two melanocyte sample groups resulted in 16 significantly differentially expressed proteins. Lower expression of cytoskeletal proteins such as vimentin and annexin in DNMC was observed, which is possibly associated with morphological alterations of DNMC observed in culture when compared to melanocytes derived from normal skin[7]. Proteins that were higher expressed in DNMC included eukaryotic translation initiation factor 3, GTP-binding Rholike protein CDC42, prolyl 4-hydroxylase, platelet-activating factor acetylhydrolase, and DnaJ homolog subfamily B. These proteins are involved in protein synthesis, protein folding, and metabolism as well as lipid metabolism and cell shape organization[16,17].

We did not observe an overlap of the 16 differentially expressed proteins with the microarray gene expression data, as a clear pattern in mRNA expression across all 18 sample sets was not found. This could be related to the overall small gene expression differences found in the microarray data. Dissimilarity between mRNA and protein abundance has been found in many combined genomic and proteomic studies. Nonetheless, among the differentially expressed proteins there were several involved in translation and growth, a functional class of proteins also identified in gene expression analysis.

For this study, melanocytes were isolated from patient biopsy samples and expanded in culture to obtain sufficient material for gene expression and proteome profiling. Cell culture, although short, will have impacted on mRNA and protein levels in these cells. However, the relative number of melanocytes present in the epidermis would be too small and variable across naevus and normal skin samples to allow for similar comparative analysis of whole tissue samples. Microdissection of the dysplastic naevus and normal skin biopsy samples prior to RNA and protein isolation would ensure isolated melanocyte populations, but it would not yield sufficient material for the type of microarray and proteomic analysis performed in the described study. The technology to isolate single melanocytic cells and perform whole transcriptome and proteome analyses is not yet available to us, if at all feasible currently. Evidently, a subset of pre-existing biological differences in the transcriptomes and proteomes between the DNMC and MC may not be detected with the approach employed in this study, as the impact of culturing may overwhelm more subtle distinctions in expression. Any gene and protein expression differences however that may be induced by culturing will be comparable between MC and DNMC since identical culture procedures have been followed for all DNMC and MC cultures, in addition to harvesting cultures at the same passage numbers with the same harvesting methods. Moreover, we have compared DNMC and MC from the same patient

from a single lesion and body site to maximize comparability. In spite of the impact of short-term culture on both types of cells, comparisons between these cells may be expected to yield meaningful results therefore.

For many gene and protein expression profiling studies established tumor cell lines and benign primary cells have often been comparatively analyzed. For this study early-passage cultures were used and comparisons were performed with benign cells of the same patient isolated from the vicinity of the lesional dysplastic cells. This approach, combined with the fact that expression patterns of dysplastic instead of malignant cells were compared to those of benign cells, probably also provides an explanation for the relatively limited range of expression differences we observed.

For the melanocyte cultures, we made additional observations of representative MC and DNMC cultures in order to find out whether differences existed between the two melanocyte groups. Directly after plating of the epidermal single cell suspensions, the melanocytes from dysplastic naevus did not display differences in the rate of cell death or plate adherence as compared to the melanocytes from normal skin. In addition, DNMC and MC did not display significant differences in proliferation rate when seeded at equal densities at passage four in 6W plates and counted every day for seven days. However, the DNMC cultures underwent senescence after prolonged periods in culture where normal MC cultures continued to proliferate. In addition modest but consistent differences in cellular morphology between DNMC and MC were observed, in particular pertaining to the shape of the dendrites. Together these findings are in agreement with previous electron microscopic studies revealing bloated mitochondria in DNMC and not in the MC as well as elevated ROS level measurements in DNMC when compared to MC[6,7].

Until now, very little comparative gene expression and protein expression studies have focused on dysplastic naevi. Usually, melanocytes from either dysplastic naevi or normal skin are included in large expression studies aimed at later stages of melanoma development, involving melanoma samples[18-20]. In a comprehensive gene expression study that included biopsies from normal skin and dysplastic naevus, in addition to radial and vertical growth phase melanomas and melanoma metastases, it was observed that dysplastic naevi do not differ to a large extent from normal naevi based on gene expression profiles[21]. Even though the dysplastic naevi showed higher expression of proliferation-related genes compared to normal naevi and displayed similar molecular features to vertical growth phase melanomas, they displayed significant heterogeneity in gene expression profiles. Our results now indicate that differences between melanocytes from dysplastic naevus compared to melanocytes from normal skin are also modest.

Protein expression studies are to a similar extent often aimed at identifying changes occurring in late melanoma development stages; recently, it was found that 6.1% of dysplastic naevi nuclei versus 1.2% of normal, benign naevi nuclei stained positive for

mini chromosome maintenance (MCM) protein 2, a polypeptide belonging to the MCM family of proteins that are involved in DNA replication and are assumed to be prognostically useful as cell proliferation marker similar to Ki-67[22]. In comparison, 49.1% nuclei of primary cutaneous melanomas stained positive. In addition, an earlier study found positive cyclin D1-nuclei staining in 0.34%, 5%, and 7.75% and positive cyclin D3-nuclei staining in 1.8%, 6.4%, and 17.8% in normal naevi, dysplastic naevi and melanoma biopsy sections, respectively[23]. These observations together indicate that expression differences of proteins that mark proliferating cells may also be limited in DNMC compared to MC whereas the most significant differences in protein expression remains when comparing dysplastic naevi with the primary melanoma stage.

A recent study however, found that the HLA class I heavy chain *β*2m and HLA class II*β* chain were expressed in 8.6% of the investigated normal, benign naevi and in 72% of atypical melanocytic lesions, where the level of expression correlated with degree of cytologic atypia and morphological disorder[24]. Further validation of a selected number of targets from our list of differentially expressed proteins could further confirm whether specific proteins also show significant difference in expression in DNMC compared to melanocytes from normal skin.

Since some dysplastic naevi bear more molecular similarity to their normal counterparts, whereas other dysplastic naevi more closely resemble more advanced primary melanoma in gene expression patterns[21], it may be not surprising that overall expression patterns of DNMC are heterogeneous. Differences that do occur between DNMC and melanocytes from normal skin tissue may be specific and exclusive for only a subset of dysplastic naevus and potentially associated with the grade of atypia. The occurrence of such expression differences may also partially depend on history of formation of the original benign naevus; melanocytes from a dysplastic naevus that readily progresses to melanoma may have been more “primed” for transformation even before the initial naevus formation stage compared to melanocytes that may display characteristics of dysplasia, but are more restricted in their potential to progress to malignancy. It will be a challenge to design experimental approaches that can more accurately delineate gene expression alterations typical of dysplastic naevi, given the heterogeneity of their cellular composition and gene expression patterns. Novel single cell sequencing methodologies or sequencing of microdissected lesions may partially address some of these challenges.

Melanocytic cells are especially prone to oxidative DNA damage due to cellular metabolism processes such as melanin biosynthesis specific to these cells and exposure to UVA radiation. Deregulated expression of proteins involved in crucial oxidative stress management pathways in melanocytes of a dysplastic naevus can be detrimental and may contribute to their further progression towards malignancy. Recently exome analysis of

melanoma has demonstrated that approximately 9% of driver mutations are G > T transversions reflecting the relevance of oxidative DNA damage as a mutagenic force in melanoma development[25]. Via a proteomic approach, we found several proteins differentially expressed in melanocytes from dysplastic naevus when compared to melanocytes from normal skin. Notably, proteins involved in the mitochondrial respiratory electron transport chain and overall oxidative phosphorylation process showed a decrease in expression in DNMC. A decrease in expression of proteins involved in oxidation reduction, cytoskeletal organization, and protein folding was also observed. Some of the proteins that showed significant higher level of expression in the DNMC were involved in protein metabolism, lipid oxidation, positive regulation of inflammatory responses, and protein refolding. The pattern of differential protein expression that our comparative analysis has yielded, may indicate that DNMC are indeed exposed to elevated levels of oxidative stress due to their own deregulated cellular metabolic processes, particularly mitochondrial oxidative phosphorylation, additionally suffering from faulty protein folding, and cytoskeletal organization. Which (epi)genetic alterations are causing oxidative stress to occur in melanocytes within a dysplastic naevus and whether these sets of alterations can serve to identify the dysplastic naevus cells are important issues that remain to be elucidated.

Conclusion

Genome-wide expression profiling of melanocytes derived from dysplastic naevus (DNMC) and melanocytes from normal skin (MC) resulted in significantly differentially expressed “organellar ribosome,” “mitochondrial ribosome,” “hydrogen ion transporter activity,” and “prefoldin complex”Gene Ontology classes, with overall gene expression differences between both melanocyte groups being relatively small. *MRPL42*, *PSMD10*, *HSPD1*, *MRPL47*, and *MRSP22* were among the top GO classes; validation of these genes showed a heterogeneous differential expression pattern across the DNMC and MC samples. Proteomic analysis revealed differentially expressed proteins in DNMC compared to MC with a role in cellular metabolism, detoxification, and cytoskeletal organization processes. Together these results indicate possible deregulated processes such as metabolism and protein synthesis in the melanocytes from dysplastic naevus; this is in line with the observed elevated oxidative stress levels that can potentially result in oxidative DNA damage in these cells. Further studies are needed to validate the identified differentially expressed proteins. Furthermore, investigations into which set of (epi)genetic alterations underlie the deregulated cellular processes that lead to increased oxidiatve stress, and whether these aberrations can specifically identify dysplastic naevus cells are warranted.

Acknowledgments

The authors thank Pieter van der Velden and Remco Dijkman for fruitful discussions throughout the study. Professor W.J. Mooi (Department of Pathology, Free University Medical Center, Amsterdam, The Netherlands) is acknowledged for histopathological analysis of the excised nevi. F.A.v. Nieuwpoort is supported by the Netherlands Organization for Scientific Research (Grant no. 015.001.060) and by the Dutch Cancer Society (Grant no. RUL2003-2805). N.A. Gruis is a recipient of an Aspasia fellowship of The Netherlands Organisation for Scientific Research.

References

1. Seykora, J. and Elder, D. Dysplastic nevi and other risk markers for melanoma. *Semin. Oncol.* **23**(6), 682-687 (1996).
2. Schneider, J.S., Moore, D.H., and Sagebiel, R.W. Risk factors for melanoma incidence in prospective follow-up. The importance of atypical (dysplastic) nevi. *Arch. Dermatol.* **130**(8), 1002-1007 (1994).
3. Greene, M.H. *et al.* Acquired precursors of cutaneous malignant melanoma. The familial dysplastic nevus syndrome. *N. Engl. J. Med.* **312**(2), 91-97 (1985).
4. Clark, W.H., Jr. *et al.* A study of tumor progression: the precursor lesions of superficial spreading and nodular melanoma. *Hum. Pathol.* **15**(12), 1147-1165 (1984).
5. Rhodes, A.R. *et al.* Melanosomal alterations in dysplastic melanocytic nevi. A quantitative, ultrastructural investigation. *Cancer* **61**(2), 358-369 (1988).
6. Pavel, S. *et al.* Disturbed melanin synthesis and chronic oxidative stress in dysplastic naevi. *Eur. J. Cancer* **40**(9), 1423-1430 (2004).
7. Smit, N.P. *et al.* Increased melanogenesis is a risk factor for oxidative DNA damage--study on cultured melanocytes and atypical nevus cells. *Photochem. Photobiol.* **84**(3), 550-555 (2008).
8. Hussein, M.R. and Wood, G.S. hMLH1 and hMSH2 gene mutations are present in radial growth-phase cutaneous malignant melanoma cell lines and can be induced further by ultraviolet-B irradiation. *Exp. Dermatol.* **12**(6), 872-875 (2003).
9. Hussein, M.R. Genetic pathways to melanoma tumorigenesis. *J. Clin. Pathol.* **57**(8), 797-801 (2004).
10. Irizarry, R.A. *et al.* Exploration, normalization, and summaries of high density oligonucleotide array probe level data. **4**(2), 249-264 (2003).
11. Wright, G.W. and Simon, R.M. A random variance model for detection of differential gene expression in small microarray experiments. *Bioinformatics.* **19**(18), 2448-2455 (2003).
12. Korn, E.L. *et al.* Controlling the number of false discoveries: application to high-dimensional genomic data. *Journal of Statistical Planning and Inference* **124**(2), 379-398 (2004).
13. McShane, L.M. *et al.* Methods for assessing reproducibility of clustering patterns observed in analyses of microarray data. *Bioinformatics.* **18**(11), 1462-1469 (2002).
14. Pavlidis, P. *et al.* Using the gene ontology for microarray data mining: a comparison of methods and application to age effects in human prefrontal cortex. *Neurochem. Res.* **29**(6), 1213-1222 (2004).
15. Boxman, I.L.A. *et al.* Proteomic analysis of skin irritation reveals the induction of HSP27 by sodium lauryl sulphate in human skin. **146**(5), 777-785 (2002).
16. Kenmochi, N. *et al.* The human mitochondrial ribosomal protein genes: mapping of 54 genes to the chromosomes and implications for human disorders. *Genomics* **77**(1-2), 65-70 (2001).
17. O'Brien, T.W. Evolution of a protein-rich mitochondrial ribosome: implications for human genetic disease. *Gene* **286**(1), 73-79 (2002).
18. Smith, A.P., Hoek, K., and Becker, D. Whole-genome expression profiling of the melanoma progression pathway reveals marked molecular differences between nevi/melanoma in situ and advanced-stage melanomas. *Cancer Biol. Ther.* **4**(9), 1018-1029 (2005).
19. Mischiati, C. *et al.* cDNA-array profiling of melanomas and paired melanocyte cultures. *J. Cell Physiol* **207**(3), 697-705 (2006).
20. Hoek, K. *et al.* Expression profiling reveals novel pathways in the transformation of melanocytes to melanomas. *Cancer Res.* **64**(15), 5270-5282 (2004).
21. Scatolini, M. *et al.* Altered molecular pathways in melanocytic lesions. *Int. J. Cancer* **126**(8), 1869-1881 (2010).
22. Boyd, A.S., Shakhtour, B., and Shyr, Y. Minichromosome maintenance protein expression in benign nevi, dysplastic nevi, melanoma, and cutaneous melanoma metastases. *J. Am. Acad. Dermatol.* **58**(5), 750-754 (2008).
23. Alekseenko, A. *et al.* Cyclin D1 and D3 expression in melanocytic skin lesions. *Arch. Dermatol. Res.* **302**(7), 545-550 (2010).
24. Campoli, M. *et al.* HLA antigen expression in melanocytic lesions: Is acquisition of HLA antigen expression a biomarker of atypical (dysplastic) melanocytes? *J. Am. Acad. Dermatol.* **66**(6), 911-916 (2012).
25. Hodis, E. *et al.* A landscape of driver mutations in melanoma. *Cell* **150**(2), 251-263 (2012).

Supplementary Data

Supplementary Table 1. **Differentially expressed proteins in DNMC and MC**. Melanocytes derived from dysplastic naevus (DNMC) and normal adjacent skin (MC) of 18 different patients were subjected to mass spectrometry analysis. Mass fingerprint and MS/MS data were searched against the human protein database and resulted in annotation of 70 proteins.

1) Calculated molecular mass of the protein (Da)
2) Isoelectric point (pI) observed in this study
3) pI calculated according to the Mascot database
4) Percentage peptide coverage

Swiss-prot id	Mol. Mass calculated (Da)[1]	pI obs.[2]	pI calc.[3]	% Pept. Coverage[4]
Metabolism				
Q9NR45	40738	6,49	6,29	25
P37837	37556	6,35	6,36	38
Q15181	33095	5,54	5,54	46
A8K4W3	23704	4,45	4,45	30
P78417	27833	6,23	6,24	21
P07339	26457	5,31	5,56	32
Q6IBR6	25569	5,57	5,57	-
P04792	22427	7,83	5,98	57
P63104	25994	5,15	4,73	50
P60174	26807	6,51	6,51	74
P52565	23250	5,02	5,03	55
P30048	26107	7,04	7,68	18
Q15907	24591	5,46	5,65	44
P30085	26180	8,41	8,75	31
P02794	21252	5,30	5,08	46
P22392	17309	5,83	6,11	66
P00441	16020	8,76	6,74	12
Cytoskeletal				
Q9UQ80	41996	7,14	6,13	38
P04632	28453	5,05	5,05	43
O00562	31997	6,11	5,64	
Q13748	46440	4,85	4,98	34
P08670	53604	5,09	5,06	30
P08670	53710	5,06	5,06	43
P60709	41923	6,03	5,29	26
P52907	32955	5,58	5,45	16
P07355	36631	8,32	7,56	53
O15144	34426	6,84	6,84	22
P47756	30952	5,69	5,36	49
Q13637	24056	6,34	6,10	27
P13693	19697	4,84	4,84	56
P08729	51312	5,50	5,50	25
P23528	18588	8,26	8,26	50

Protein processing				
Q99733	42823	4,60	4,60	
P07237	57480	4,76	4,69	46
Q9UBS4	40774	5,81	5,81	30
Q5U0F4	36878	5,38	5,38	32
Q13765	23370	4,52	4,52	37
P07858	29571	5,34	5,23	35
P28070	25950	5,70	5,47	41
P25786	29822	6,15	6,15	30
Q99436	27978	7,07	7,58	7
P62937	18098	7,82	7,82	70
P25787	25865	7,12	6,91	34
Q06323	28876	5,78	5,78	49
P25787	25865	7,12	6,91	34
P11021	29032	6,77	5,07	32
P62937	18209	7,44	7,82	59
Vesicles				
P07900	83445	5,00	4,94	40
P06748	31090	4,71	4,64	27
PDIA3	57146	5,98	5,77	32
O14773	39790	5,74	5,74	
Q8N6T3	44982	5,46	5,46	24
P40121	38760	5,82	5,88	39
P47985	29934	8,55	6,30	5
P32969	21964	9,96	9,96	29
P62753	28842	10,90	10,85	23
O75947	18537	5,21	5,21	41
Q9Y2R9	22113	10,09	10,00	43
Q13907	26645	5,93	5,93	35
Q9BVK6	25277	6,40	6,20	39
Nuclear				
Q14103	30824	8,53	7,61	16
Q56A79	35003	6,29	6,29	22
O43432	29504	7,78	5,27	30
P84103	19546	11,64	11,64	26
P31942	31505	6,76	6,37	17
Unknown				
Q59GS1	25151	5,33	n.a.	72
O94844	20123	5,25	4,83	55
P63241	17049	5,08	5,07	59
Q59EQ2	28179	4,76	4,73	26

Chapter 6

Promoter CpG island hypermethylation of *MCHR1* and *SYNPO2* in primary cutaneous melanoma with metastatic behavior

Linda Gao[1], Joost J. van den Oord[2], Samuel Beck[3] and Remco van Doorn[1]

[1]Department of Dermatology, Leiden University Medical Center, Leiden, The Netherlands
[2]Department of Pathology, Katholieke Universiteit Leuven, Leuven, Belgium
[3]Leiden Cytology and Pathology Laboratory, Leiden, The Netherlands

Manuscript in preparation

Abstract

Cutaneous melanoma is characterized by its propensity to metastasize. Once metastasized, the overall survival of patients is generally poor. The molecular alterations that confer melanoma cells the capacity to disseminate and colonize distant body sites remain to be defined. DNA methylation constitutes an important mechanism that contributes to the aberrant expression of genes involved in metastasis. Previously we have obtained genome-wide DNA methylation data from 24 primary cutaneous melanoma biopsy samples using beadchip technology interrogating 14,495 genes. We retrieved follow-up data and re-analysed these data comparing DNA methylation patterns of 13 melanoma patients who had subsequently developed metastatic disease with those of 11 patients who had not experienced recurrence after surgical removal. This re-analysis revealed six genes that were more frequently methylated in primary melanoma with metastatic behavior. Validation in an independent sample set confirmed that promoter hypermethylation of *MCHR1* and *SYNPO2* occurred more frequently in melanoma with metastatic behavior, supporting their application as prognostic biomarkers. Kaplan-Meier survival analysis of TCGA genome-wide methylation data of metastasized melanoma revealed that *MCHR1*- and *SYNPO2*-methylated metastasized melanomas had poorer survival rates compared to the non-methylated metastasized melanomas. Additional genome-wide methylation profiling of melanoma metastasis biopsy specimens revealed a loss of *MAGEA3* and *MAGEA6*, members of the melanoma-antigen family A, in the melanoma metastases when compared to primary melanomas. Our findings warrant further investigation into the prognostic potential of *MCHR1* and *SYNPO2*, and suggest a loss of *MAGEA* family members in the progression from primary to metastasized melanoma.

Introduction

Cutaneous melanoma is a type of skin cancer that originates from melanocytes residing in the skin. Melanoma has a propensity to metastasize and once this occurs, the prognosis of patients is generally poor in spite of the introduction of targeted approaches to therapy. The central clinical factor predicting metastatic disease is tumor thickness. In addition, presence of tumor ulceration, mitotic activity, age, gender and tumor location have prognostic significance. In selected patients sentinel lymph node biopsy is performed for prognostic lymph node staging. The majority of patients are diagnosed early and present with a thin primary tumor which is curable by surgical excision. However, even in the group of patients with thin melanoma, a minority harbors lethal metastasis [1]. Patients at increased risk of metastatic disease could benefit from more extensive surgery and adjuvant treatment.

Metastasis results from a complex cascade of events where melanoma cells acquire multiple molecular alterations that confer metastatic capacity. Gene expression signatures have been defined that are associated with metastatic capacity and survival of primary melanoma [2,3]. Also metastatic melanomas were found to separate into subtypes with different prognosis based on their gene expression signatures [4,5]. Systemic characterization of melanoma has revealed a diversity of recurrent genetic alterations, some of which were shown to drive the tumorigenic process [6]. Still, the underlying molecular changes in melanoma that confer the capacity to migrate and colonize distant body sites remain to be defined.

Epigenetic alterations have been recognized as important contributors to the malignant phenotype of melanoma cells. Recent findings suggest that promoter CpG island hypermethylation constitutes a major mechanism responsible for the inappropriate expression of genes involved in metastasis. Findings in breast cancer revealed DNA methylation signatures that were associated with metastatic risk and surivival outcome [7]. Genes epigenetically silenced in melanoma and implicated in metastatic progression identified by us and others include *SerpinB1* (*Maspin*), *CDH11* and *RASSF1A* [8-12]. As an epigenetic biomarker for metastasis, promoter hypermethylation has the advantage that it is generally stable and can reliably be detected in clinical samples.

In a recent genome-wide analysis of promoter methylation in primary melanomas and melanocytic naevi interrogating 14,495 genes, we demonstrated widespread changes in DNA methylation patterns. For this study, we obtained clinical survival data for the interrogated samples and re-analyzed the results of the genome-wide analysis to identify DNA metylation alterations associated with metastatic behavior. In addition, we performed genome-wide methylation analysis on melanoma metastatic lesions to examine promoter methylation events occurring late in melanoma progression.

Methods

Melanoma biopsy specimens and patient information

Fresh-frozen (FF) or fixed-in-boonfix and paraffin-embedded (BFPE) biopsy samples from 72 patients diagnosed with primary melanoma and 28 patients with melanoma metastases (cutaneous, lymph node or visceral) were used (Supplementary Table S1a, S1b and S2). For the primary melanoma tumors, follow-up ranged from 60 months to 204 months (median 132 months, mean 129 months). Excised tumor biopsies were reviewed by an expert dermatopathologist as previously described [9]. DNA was extracted using either the Genomic-tip kit (Qiagen, Hilden, Germany) or RecoverAll Nucleic Acid kit (Ambion, Carlsbad, CA), followed by bisulphite conversion with the EZ DNA methylation kit (Zymo Research, Orange, CA).

Bisulphite melting curve analysis (BMCA)

Bisulphite primer sequences were designed, sensitivity of primer sets was tested, and scoring of BMCA melting curves was performed as previously described[9].

Analysis of Illumina Infinium HumanMethylation27K Beadchip promoter methylation data and BMCA data

β-values resulting from the genome-wide Illumina Infinium HumanMethylation27K Beadchip, ranging from 0 to 1, were quantile normalized to correct for unequal distributions within and between samples due to technical variation. Average *β*-values were calculated for each sample group (metastatic primary melanomas (M+), non-metastatic primary melanomas (M-) and melanoma metastases). Absolute average *β*-value differences were calculated to represent the extent of differential methylation between different sample groups. Fisher's Exact Test was applied to measure the association of promoter methylation frequency obtained by BMCA between two sample groups in IBM SPSS Statistics 20 (IBM Corp, Armonk, NY, USA); a two-sided *P* value <0.05 was considered significant.

Kaplan-Meier survival analysis of The Cancer Genome Atlas (TCGA) Illumina Infinium HumanMethylation450K data

Illumina Infinium HumanMethylation450K Level 3 DNA methylation data and clinical follow-up information of 229 metastasized melanoma specimens (stage IV) were obtained via the TCGA dataportal (https://tcga-data.nci.nih.gov/). The HumanMethylation 450K Beadchip contains nine cg-probes for *MCHR1* and 32 cg-probes for *SYNPO2* that map to the promoter region, gene body and 3'UTR. Since we were interested in promoter methylation status, we selected a single representative probe (*MCHR1* probe: cg14701072, *SYNPO2* probe: cg24326232) that was located in the gene promoter region, at the same time located in proximity of the interrogated cg-probe on the HumanMethylation27K Beadchip, and that did not overlap with the other *MCHR1* or *SYNPO2* probes on the HumanMethylation 450K beadchip. Melanoma specimens with a cg-probe *β*-value >0.5 were considered methylated. Kaplan-Meier survival analysis was performed and survival curves were plotted in IBM SPSS Statistics 20, a logrank test *P* value <0.05 was considered significant.

5-aza-2'-deoxycytidine treatment and quantitative real-time PCR

Melanoma cell lines 06.24 and 94.13 were treated with 5-aza-2'-deoxycytidine as previously described [9]. qRT-PCR was performed with iQ SYBR Green Supermix on a CFX384 Touch™ system (Bio-Rad). qRT-PCR primers were designed to span exon-exon barriers; expression of the reference genes *TBP* and *CPSF6* was validated using geNorm analysis[13].

Results

Re-analysis of genome-wide data to identify promoter methylation events associated with metastatic behavior

Our objective was to identify differential methylation events occurring in primary melanoma with metastatic behavior (M+) when compared to primary melanoma without metastatic behavior (M-). To this end, the clinical follow-up status of 24 patients with primary melanoma whose tumors had been previously subjected to genome-wide Illumina Infinium HumanMethylation27K profiling was obtained[9]. Thirteen of 24 patients diagnosed with primary melanoma had developed visceral or lymph node metastases during their disease course after a period of at least 60 months following diagnosis. In 11 of 24 primary melanoma patients, no metastasis had occurred during a follow-up period of at least 60 months. The metastatic (M+) primary melanomas had an average Breslow thickness of 8.0 mm, with an average patient age of 67 years and 69% (9/13) showing ulceration. The non-metastatic (M-) primary melanomas had an average Breslow thickness of 1.8 mm, average patient age of 53 years, with 18% (2/11) demonstrating ulceration (Supplementary Table S1a).

The difference in the extent of promoter methylation, expressed as the absolute difference in average *β*-value, was used to rank individual genes according to most differentially methylated in the primary melanomas with metastatic behavior (M+) compared to those without metastatic behavior (M-). The small group sizes limited meaningful statistical analysis of the genome-wide methylation data. A threshold value of 0.20 was applied; genes with an average *β*-value difference higher than 0.20 were considered more frequently hypermethylated. From this re-analysis six genes emerged as more frequently hypermethylated in the primary melanomas with metastatic behavior (M+): *MCHR1*, *SYNPO2*, *C1orf106*, *HIST1H3G*, *ZNF35* and *GNMT* (Figure 1a). We did not find genes with an average *β*-value difference less than -0.20 that were indicative of more frequent methylation in the primary melanomas without metastatic behavior (M-).

Validation of frequent *MCHR1* and *SYNPO2* promoter hypermethylation in primary melanoma with metastatic behavior

Bisulphite melting curve analysis (BMCA) of the seven genes on 21 of the 24 primary melanomas subjected to genome-wide methylation profiling, confirmed a significant difference in promoter methylation between M+ and M- primary melanoma tumors (*P <0.05 by two-sided Fisher's exact test) of *MCHR1*, *SYNPO2*, *C1orf106*, *ZNF35* and *GNMT* (Table 1a). *HIST1H3G* did not show significant differential methylation between both groups (Table 1a). To get an impression of *MCHR1* methylation in the different stages of melanoma development, Illumina Infinium HumanMethylation27K data of five common

naevus and seven melanoma metastasis biopsy specimens was examined in addition. This showed that *MCHR1* promoter methylation in the common naevi is at comparable level to the melanoma tissues (Figure 1b). Examination of *SYNPO2* methylation in a similar way showed near absence of *SYNPO2* methylation in the common naevi compared to the melanomas (Figure 1c); overall *SYNPO2* methylation levels were notably lower than *MCHR1* methylation in the common naevus and melanoma samples.

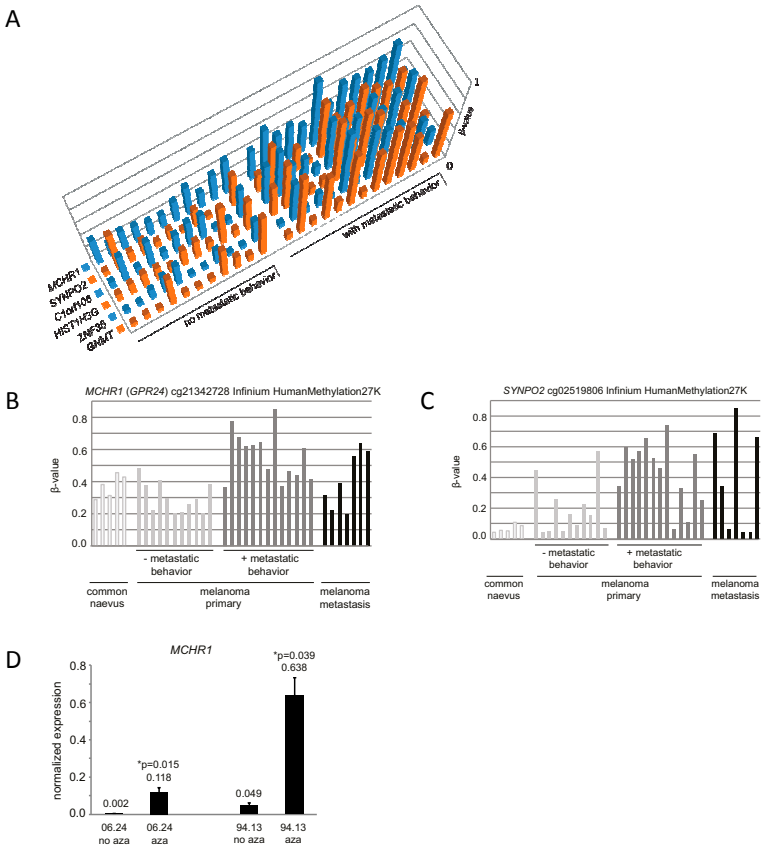

Figure 1. (**A**) Re-analysis was performed of available genome-wide methylation data that was generated by subjecting 24 primary melanoma tumors to Illumina Infinium HumanMethylation27K profiling. Clinical follow-up status was retrieved of the 24 patients from which the primary melanomas were derived; 13 of 24 patients had primary melanoma tumors that developed metastasis (with metastatic behavior), 11 of 24 patients had primary melanoma with no occurence of metastasis during a follow-up period of at least 60 months (no metastatic behavior). (**B**) *MCHR1* (probe: cg21342728) promoter methylation as obtained by genome-wide methylation profiling of common naevi, primary melanomas with and without metastatic behavior and metastatic melanoma. (**C**) *SYNPO2* (probe: cg02519806) promoter methylation as obtained by genome-wide methylation profiling of common naevi, primary melanomas with and without metastatic behavior and metastatic melanoma. (**D**) Melanoma cell lines 06.24 and 94.13 were treated with 2µM 5-aza-2'-deoxycytidine for 96hrs and harvested for RNA isolation on day 5. qRT-PCRs were performed in triplicate, results are representative for treatment experiments performed in duplicate. * *P* <0.05 by two-sided t-test.

Table 1a. Methylation status of six candidate genes in the Illumina Infinium HumanMethylation27K set of primary melanomas with metastatic behavior (n=12) and primary melanomas without metastatic behavior (n=9).

	Primary melanoma - metastatic behavior		Primary melanoma + metastatic behavior		Fisher's exact *P* value
		No. of samples		No. of samples	
MCHR1	**44%**	4/9	**100%**	12/12	0.006
SYNPO2	**33%**	3/9	**83%**	10/12	0.032
C1orf106	**0%**	0/9	**75%**	9/12	0.007
HIST1H3G	**44%**	4/9	**75%**	9/12	0.203
ZNF35	**0%**	0/9	**58%**	7/12	0.007
GNMT	**0%**	0/9	**67%**	8/12	0.005

Table 1b. Methylation status of six candidate genes in an independent set of primary melanomas with metastatic behavior (n=20) and primary melanomas without metastatic behavior (n=25).

	Primary melanoma - metastatic behavior		Primary melanoma + metastatic behavior		Fisher's exact *P* value
		No. of samples		No. of samples	
MCHR1	**52%**	13/25	**90%**	18/20	0.006
SYNPO2	**40%**	10/25	**65%**	13/20	0.096
C1orf106	**26%**	6/23	**37%**	7/19	0.453
HIST1H3G	**52%**	12/23	**70%**	14/20	0.233
ZNF35	**32%**	7/22	**30%**	6/20	0.899
GNMT	**25%**	5/20	**32%**	6/19	0.648

BMCA of *MCHR1*, *SYNPO2*, *C1orf106*, *HIST1H3G*, *ZNF35* and *GNMT* was performed on an independent set of 20 metastatic primary melanomas (M+) and 25 non-metastatic primary melanomas (M-). This showed that *MCHR1* promoter methylation occurred significantly more frequently in the metastatic primary melanomas (*P <0.05 by two-sided Fisher's exact test; Table 1b). Differential methylation of *SYNPO2* was not significant (P=0.096) but still substantial compared to the remaining genes (Table 1b). It should be noted that our analysis is restricted by the small size of the sample groups and we cannot exclude significant association with metastatic behavior for these hypermethylated genes. In our independent sample set, the metastatic primary melanomas (M+) had an average Breslow thickness of 4.0 mm with an average patient age of 62 years, while the non-metastatic primary melanomas (M-) had an average Breslow depth of 3.8 mm and an average patient age of 64 years (Supplementary Table S1b). The observation that *MCHR1* promoter hypermethylation occurred significantly more frequently in the primary melanomas with metastatic behavior (M+), while the clinical prognostic factors Breslow thickness and age were similar for the M+ and M- primary melanoma groups, suggests that promoter methylation of this gene represents an independent factor predicting metastatic dissemination.

To examine whether *MCHR1* methylation was correlated with expression, BMCA analysis was first performed on 12 melanoma cell lines to determine *MCHR1* methylation

status (data not shown). Two melanoma cell lines that were positive for *MCHR1* promoter methylation, 06.24 and 94.13, were selected for 5'-azadeoxycytidine treatment. qRT-PCR analyses showed that demethylation of 06.24 and 94.13 resulted in a modest but significant re-activation of *MCHR1* expression (Figure 1d).

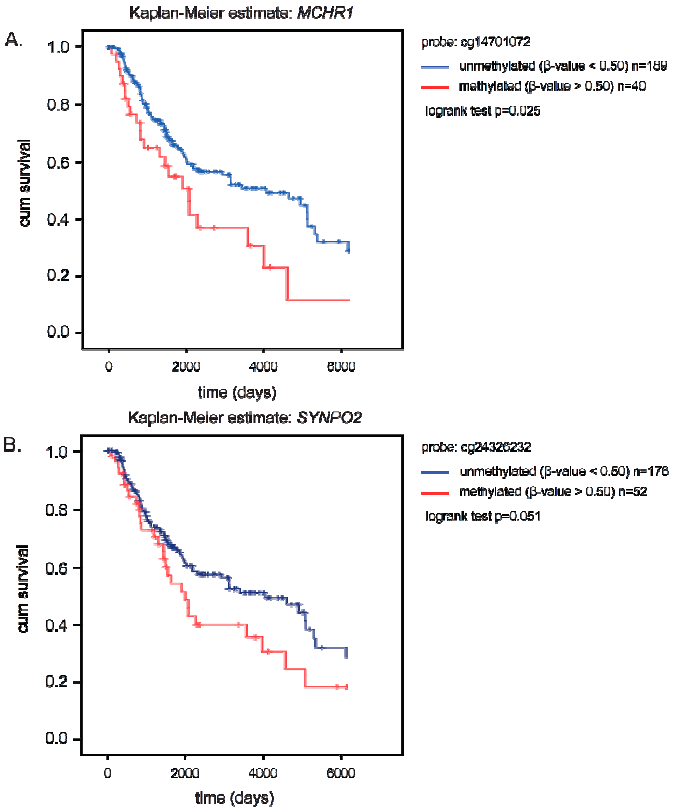

Figure 2. (**A**) Kaplan-Meier survival analysis was performed with TCGA genome-wide methylation data of 229 metastasized melanoma samples for *MCHR1*. (**B**) Kaplan-Meier survival analysis was performed with TCGA genome-wide methylation data of 228 metastasized melanoma samples for *SYNPO2*.

Evaluation of prognostic significance in metastasized melanoma (stage IV) of *MCHR1* and *SYNPO2* promoter methylation

In addition to predicting metastatic outcome of primary melanoma, we asked whether patients diagnosed with melanoma metastasis (stage IV) would differ in survival rate based on a difference in *MCHR1* or *SYNPO2* methylation status. Publicly available TCGA Illumina Infinium HumanMethylation450K Beadchip methylation data was subjected to Kaplan-Meier survival analysis in a TCGA cohort of 229 melanoma metastases samples with known clinical outcome (http://cancergenome.nih.gov/). For analysis, a single representative probe was selected for *MCHR1* (cg14701072) and *SYNPO2* (cg24326232). As cut-off, a normalized *β*-value of 0.50 was chosen; samples with *β*-value higher than

0.50 were considered methylated, samples with *β*-value lower than 0.50 were considered unmethylated. Kaplan-Meier survival analysis of *MCHR1* showed that metastasized melanomas with cg-probe *β*-value < 0.50 had a significantly higher survival rate than metastasized melanomas with cg-probe *β*-value > 0.50 (*P<0.05 by logrank test) (Figure 2a). Similarly, *SYNPO2*-unmethylated metastasized melanomas showed an overall better survival rate than *SYNPO2*-methylated metastasized melanomas, however this difference failed to reach statistical significance (P=0.051 by logrank test) (Figure 2b).

Loss of *MAGEA3* and *MAGEA6* promoter methylation in melanoma metastases

Next to genome-wide methylation profiling of the 24 primary melanomas using the Illumina Infinium HumanMethylation27K Beadchip as mentioned earlier in this chapter, we also generated genome-wide methylation data for seven melanoma metastasis tissues in order to evaluate whether further epigenetic alterations would occur in later stages of development following metastatic colonization. We were interested in comparing the methylation data of the primary melanomas and melanoma metastases for differential methylation events. Similar to the comparative analysis as mentioned earlier, the absolute difference in average *β*-value was used to rank genes according to most differentially methylated. From this analysis, five genes with an average *β*-value lower than -0.20 emerged: *KCNJ15*, *A2M*, *MAGEB6*, *MAGEA6* and *MAGEA3*. The methylation status of *MAGEA3*, *MAGEA6* and *MAGEB6* was assessed in an independent set of 15 primary melanomas and 21 melanoma metastases using BMCA (patient information can be found in Supplementary Table S1b and S2). *KCNJ14* and *A2M* were excluded from further analysis since the CpG density (0.76%) in both promoter regions was too low to perform reliable BMCA. *MAGEA3* and *MAGEA6* are both located on chromosome Xq28 in separate locations; *MAGEA3* and *MAGEA6* promoter methylation was interrogated using the same primer set since both genes share 99% similarity in DNA sequence for the +1450bp to -1000bp TSS region. BMCA on the independent sample set revealed a significant decrease of *MAGEA3* and *MAGEA6* promoter methylation in the melanoma metastasis tissues (Table 2).

Table 2. Methylation status of *MAGEA3*, *MAGEA6* and *MAGEB6* in an independent cohort of primary melanoma (n=15) and metastatic melanoma (n=21) samples.

	Primary melanoma		**Melanoma metastasis**		**Fisher's exact *P* value**
		No. of samples		No. of samples	
MAGEA3/MAGEA6	**100%**	15/15	**67%**	14/21	0.027
MAGEB6	**93%**	14/15	**76%**	16/21	0.367

Discussion

In order to identify CpG promoter island methylation events that are associated with metastatic behaviour of melanoma, we have performed re-analysis of genome-wide Illumina Infinium HumanMethylation27K Beadchip data followed by bisulphite melting curve analysis (BMCA) in independent sample sets of metastatic (M+) and non-metastatic (M-) primary melanomas. We observed increased *MCHR1* and *SYNPO2* promoter methylation in the metastatic primary melanomas compared to the non-metastatic primary lesions; for *MCHR1* the increased methylation frequency was statistically significant but not for *SYNPO2*. Methylation analyses in larger sample sets may show a significant association with metastic behaviour for *SYNPO2* and the remaining genes that we observed as hypermethylated in metastatic primary melanoma, *C1orf106*, *HIST1H3G* and *GNMT*. Although metastasis-associated hypermethylation of these genes was not replicated in the second sample set, prognostic value of these methylation events is still possible given the relatively small size of the independent sample set. The observation of *MCHR1* hypermethylation in our set of metastatic primary melanomas suggests that the event of *MCHR1* promoter methylation may be an independent factor predicting metastatic dissemination. Detection of *MCHR1* promoter methylation status might therefore be useful clinically in predicting the risk of metastasis in patients diagnosed with primary melanoma. Confirmation studies in large cohorts of metastatic and non-metastatic primary melanomas will be needed, with an assessment of the extent of association between *MCHR1* methylation with established clinical prognostic factors such as Breslow thickness, ulceration, mitotic index and age. Compared to the investigated naevi, a slight decrease in *MCHR1* methylation in the non-metastatic primary melanomas was observed, suggesting a hypomethylated state of *MCHR1* in primary melanomas with a good prognosis and a hypermethylated state of this gene in primary melanomas with poor prognosis. Our observation of the presence of *MCHR1* methylation in benign melanocytic tissue indicates that the differences in *MCHR1* methylation as detected in this study are based on differences in methylation density of the CpG promoter region, rather than based on a complete presence or absence of methylation. Further investigation will be needed to establish the effect of promoter CpG island methylation density on *MCHR1* expression.

In addition to finding methylation events associated with metastatic behaviour of melanoma, it would be informative to establish an association of individual methylation events with survival outcome of primary melanomas. In the TCGA Infinium HumanMethylation450K data set of 229 metastasized (stage IV) melanoma samples, a cg-probe *β*-value higher than 0.50 for *MCHR1* was significantly associated with a poorer survival rate. It is striking that, in addition to a significant association with metastatic behaviour observed in a set of primary melanomas, *MCHR1* methylation is also correlated

to survival outcome of metastasized melanomas. These findings indicate that epigenetic events that determine metastatic capacity and tumor malignancy occur in the course of primary tumor development. *MCHR1* (melanin-concentrating hormone receptor 1) has been identified as an auto-antigen that is targeted by auto-antibodies in vitiligo, an auto-immune disease that results from the loss of melanocytes in the skin [14]. Downregulation of *MCHR1* may give melanoma cells the advantage to evade the body's immune response. In our study we have found *SYNPO2* to be a good candidate gene as well. *SYNPO2* (synaptopodin 2 or myopodin) was found as a tumor suppressor in prostate cancer that suppresses motility and invasion of prostate cancer cells, with frequent deletion in aggressive prostate cancer [15,16]. Notably *SYNPO2* methylation was found to associate with poorer disease-specific survival in bladder and colon cancer [17,18]. Additional methylation analyses in larger sample sets are needed to confirm whether methylation of this gene is significantly associated with metastatic behavior in melanoma.

The *MAGE* (melanoma-antigen family A) genes *MAGEA3* and *MAGEA6* encode antigens that are presented by members of the major histocompatibility complex, class I family, recognized by cytolytic T-lymphocytes and expressed by melanoma tumors while rarely being expressed in normal human tissue [19-22]. *MAGEA3* gene expression was found to be regulated by methylation in melanoma, with correlating high expression levels and *MAGEA3* hypomethylation in melanoma cells [23]. In line with this, we observed in our independent set of melanoma metastases *MAGEA3* and *MAGEA6* hypomethylation compared to the primary melanoma lesions. The finding that hypomethylation of these cancer/testis antigens occurs late in the metastatic progression of melanoma is novel and may have relevance for the design of immunotherapeutic approaches directed towards MAGE proteins in melanoma.

In conclusion, the findings described in this chapter provide a starting point for further investigation into the potential of *MCHR1* and *SYNPO2* methylation status as epigenetic biomarkers in cutaneous melanoma.

References

1. Green, A.C. *et al.*, Population-based 20-year survival among people diagnosed with thin melanomas in Queensland, Australia, *J. Clin. Oncol.* **30**(13), 1462-1467 (2012).
2. Conway, C. *et al.*, Gene expression profiling of paraffin-embedded primary melanoma using the DASL assay identifies increased osteopontin expression as predictive of reduced relapse-free survival, *Clin. Cancer Res.* **15**(22), 6939-6946 (2009).
3. Winnepenninckx, V. *et al.*, Gene expression profiling of primary cutaneous melanoma and clinical outcome, *J. Natl. Cancer Inst.* **98**(7), 472-482 (2006).
4. Bogunovic, D. *et al.*, Immune profile and mitotic index of metastatic melanoma lesions enhance clinical staging in predicting patient survival, *Proc. Natl. Acad. Sci. U. S. A.* **106**(48), 20429-20434 (2009).
5. Jonsson, G. *et al.*, Gene expression profiling-based identification of molecular subtypes in stage IV melanomas with different clinical outcome, *Clin. Cancer Res.* **16**(13), 3356-3367 (2010).
6. Hodis, E. *et al.*, A landscape of driver mutations in melanoma, *Cell* **150**(2), 251-263 (2012).
7. Fackler, M.J. *et al.*, Genome-wide methylation analysis identifies genes specific to breast cancer hormone receptor status and risk of recurrence, *Cancer Res.* **71**(19), 6195-6207 (2011).
8. Carmona, F.J. *et al.*, Epigenetic disruption of cadherin-11 in human cancer metastasis, *J. Pathol.* **228**(2), 230-240 (2012).
9. Gao, L. *et al.*, Genome-wide promoter methylation analysis identifies epigenetic silencing of MAPK13 in primary cutaneous melanoma, *Pigment Cell Melanoma Res.* **26**(4), 542-554 (2013).
10. Maat, W. *et al.*, Epigenetic inactivation of RASSF1a in uveal melanoma, *Invest Ophthalmol. Vis. Sci.* **48**(2), 486-490 (2007).
11. Tanemura, A. *et al.*, CpG island methylator phenotype predicts progression of malignant melanoma, *Clin. Cancer Res.* **15**(5), 1801-1807 (2009).
12. Wada, K. *et al.*, Aberrant expression of the maspin gene associated with epigenetic modification in melanoma cells, *J. Invest. Dermatol.* **122**(3), 805-811 (2004).
13. Vandesompele, J. *et al.*, Accurate normalization of real-time quantitative RT-PCR data by geometric averaging of multiple internal control genes, *Genome Biol.* **3**(7), RESEARCH0034 (2002).
14. Kemp, E.H. *et al.*, The melanin-concentrating hormone receptor 1, a novel target of autoantibody responses in vitiligo, *J. Clin. Invest* **109**(7), 923-930 (2002).
15. Lin, F. *et al.*, Myopodin, a synaptopodin homologue, is frequently deleted in invasive prostate cancers, *Am. J. Pathol.* **159**(5), 1603-1612 (2001).
16. Yu, Y.P. and Luo, J.H., Myopodin-mediated suppression of prostate cancer cell migration involves interaction with zyxin, *Cancer Res.* **66**(15), 7414-7419 (2006).
17. Alvarez-Mugica, M. *et al.*, Myopodin methylation is associated with clinical outcome in patients with T1G3 bladder cancer, *J. Urol.* **184**(4), 1507-1513 (2010).
18. Esteban, S. *et al.*, Diagnostic and prognostic utility of methylation and protein expression patterns of myopodin in colon cancer, *Tumour. Biol.* **33**(2), 337-346 (2012).
19. Brasseur, F. *et al.*, Expression of MAGE genes in primary and metastatic cutaneous melanoma, *Int. J. Cancer* **63**(3), 375-380 (1995).
20. Herman, J. *et al.*, A peptide encoded by the human MAGE3 gene and presented by HLA-B44 induces cytolytic T lymphocytes that recognize tumor cells expressing MAGE3, *Immunogenetics* **43**(6), 377-383 (1996).
21. Schultz, E.S. *et al.*, A MAGE-A3 peptide presented by HLA-DP4 is recognized on tumor cells by CD4+ cytolytic T lymphocytes, *Cancer Res.* **60**(22), 6272-6275 (2000).
22. van der Bruggen, P. *et al.*, A peptide encoded by human gene MAGE-3 and presented by HLA-A2 induces cytolytic T lymphocytes that recognize tumor cells expressing MAGE-3, *Eur. J. Immunol.* **24**(12), 3038-3043 (1994).
23. Sigalotti, L. *et al.*, Intratumor heterogeneity of cancer/testis antigens expression in human cutaneous melanoma is methylation-regulated and functionally reverted by 5-aza-2'-deoxycytidine, *Cancer Res.* **64**(24), 9167-9171 (2004).

Supplementary Data

Supplementary Table S1. (**A**) Patients (primary tumor) used for re-analyses of Illumina Infinium HumanMethylation27K promoter methylation data.

	Metastatic	Metastasis type	Site	Breslow	Ulcer	Mitoses	Clark	Diagnosis	Gender	Age	Mutation
1	-	n/a	Lower leg	1.67	-	3	IV	SSMM	F	53	wildtype
2	-	n/a	Lower leg	2.08	+	6	IV	SSMM	M	68	BRAFV600E
3	-	n/a	Foot	4.48	+	13	V	ALMM	M	65	wildtype
4	-	n/a	Trunk	2.05	-	2	IV	SSMM	F	65	wildtype
5	-	n/a	Foot	3.88	-	5	IV	ALMM	F	60	wildtype
6	-	n/a	Ear	0.81	-	1	III	SSMM	M	58	wildtype
7	-	n/a	Back	0.91	-	0	IV	SSMM	F	42	BRAFV600K
8	-	n/a	Shoulder	0.94	-	2	IV	SSMM	F	34	wildtype
9	-	n/a	Back	1.06	-	2	IV	SSMM	M	36	BRAFV600E
10	-	n/a	Buttock	0.73	-	0	III	SSMM	F	35	BRAFV600E
11	-	n/a	Back	1.28	-	1	IV	SSMM	F	65	wildtype
12	+	brain, lymph node, skin	Nailbed Toe	1.70	+	2	IV	ALMM	F	59	NRASG12D
13	+	lymph node, skin	Foot	3.36	+	6	IV	ALMM	F	73	wildtype
14	+	skin, lung, bone	Neck	15.6	-	2	V	Desmopl MM	M	85	wildtype
15	+	local recurrence	Scalp	3.46	-	4	IV	SSMM	M	54	wildtype
16	+	lymph node	Thigh	9.20	+	10	V	SSMM	F	48	NRASQ61K
17	+	lymph node	Lower leg	18.0	+	12	V	SSMM	M	82	BRAFV600E
18	+	liver, bone	Buttock	6.29	+	8	IV	SSMM	F	62	wildtype
19	+	Unknown	Scalp	17.2	+	9	V	NMM	M	79	BRAFV600K
20	+	Unknown	Back	3.04	+	4	IV	SSMM	F	45	wildtype
21	+	Unknown	Lower leg	2.02	+	4	IV	SSMM	M	78	wildtype
22	+	Unknown	Axilla	12.2	-	7	V	SSMM	M	70	wildtype
23	+	Unknown	Vulva	10.1	+	8	IV	SSMM	F	56	wildtype
24	+	Unknown	Foot	2.08	-	7	IV	SSMM	F	75	BRAFV600E

Supplementary Table S1. (**B**) Patients (primary tumor) used for independent validation by BMCA.

	Metastatic	Metastasis type	Site	Breslow	Gender	Age	Validation of*
1	-	n/a	back	6.0	M	74	1, 2
2	-	n/a	lower leg	2.2	M	77	1, 2
3	-	n/a	upper arm	5.9	F	65	1, 2
4	-	n/a	neck	1.2	F	49	1, 2
5	-	n/a	back	3.5	M	76	1, 2
6	-	n/a	back	2.3	F	40	1, 2
7	-	n/a	back	5.2	M	85	1, 2
8	-	n/a	upper leg	3.9	F	55	1, 2
9	-	n/a	shoulder	1.3	F	47	1, 2
10	-	n/a	back	2.2	M	37	1
11	-	n/a	upper arm	2.0	F	57	1
12	-	n/a	back	3.0	F	81	1
13	-	n/a	trunk	2.2	M	70	1
14	-	n/a	lower arm	4.0	M	54	1
15	-	n/a	shoulder	4.8	M	62	1
16	-	n/a	neck	3.3	F	74	1
17	-	n/a	upper arm	3.6	M	65	1
18	-	n/a	head	6.0	M	77	1
19	-	n/a	back	2.5	F	26	1
20	-	n/a	lower leg	2.5	F	82	1
21	-	n/a	head	4.2	M	88	1
22	-	n/a	thigh	2.8	F	50	1

23	-	n/a	back	2.1	F	60	1
24	-	n/a	lower leg	2.5	F	67	1
25	-	n/a	trunk	3.2	M	85	1
26	+	Visceral	shoulder	3.0	M	76	1, 2
27	+	nnll_toilet_k	lower leg	1.4	F	86	1, 2
28	+	spinal cord	lower leg	1.5	F	80	1, 2
29	+	Cutaneous	back	4.5	M	64	1
30	+	Visceral	back	3.0	M	64	1
31	+	Cutaneous	lower leg	3.3	F	89	1
32	+	Cutaneous	upper leg	2.9	F	80	1
33	+	Visceral	back	2.1	F	34	1
34	+	Visceral	back	3.0	M	55	1
35	+	Visceral	upper leg	2.7	F	70	1
36	+	Visceral	head/neck	2.0	M	67	1
37	+	Parotis	upper leg	3.1	M	43	1
38	+	Brain	abdomen right	2.3	F	38	1
39	+	Visceral	back	7.0	M	74	1
40	+	Brain	neck left	2.5	M	33	1
41	+	Brain	thorax left	2.4	M	55	1
42	+	Cutaneous	back	7.0	F	59	1
43	+	Visceral	labia left	3.2	F	57	1
44	+	Cutaneous	back	2.0	F	62	1
45	+	Cutaneous	lower arm	7.5	M	58	1
46	unknown	n/a	trunk	2.0	M	46	2
47	unknown	n/a	knee	1.8	M	83	2
48	unknown	n/a	lower leg	3.4	F	51	2

*Sample was used for validation of the candidate gene set:
1 = *MCHR1*, *SYNPO2*, *C1orf106*, *HIST1H3G*, *ZNF35*, *GNMT*
2 = *MAGEA3*, *MAGEA6*, *MAGEB6*

Supplementary Table S2. (**A**) Melanoma metastasis biopsy specimens (n=7) used for genome-wide Illumina Infinium HumanMethylation27K Beadchip profiling.

Characteristics	No. of Specimens	%
Metastasis type		
cutaneous	7	100

Supplementary Table S2. (**B**) Melanoma metastasis biopsy specimens (n=21) used for independent validation by BMCA of *MAGEA3*, *MAGEA6* and *MAGEB6*.

Characteristics	No. of Specimens	%
Metastasis type		
cutaneous	6	29
lymph node	8	38
visceral	1	5
unknown	6	29

Chapter 7

Summary and Discussion

The development of melanoma is driven by an accumulation of molecular aberrations in melanocytes. These aberrations can be genetic and epigenetic events as research has shown over the years. Epigenetic events such as DNA methylation alterations and histone modifications are involved in chromatin organization and regulation of gene expression. Promoter CpG island hypermethylation of tumor suppressor genes has also been found in melanoma. Until now, DNA methylation studies have focused on selected genes and were mostly limited to metastatic melanoma cell lines (described in **Chapter 1**). Our aim was to obtain a genome-wide view of promoter methylation in primary melanoma biopsy tissue in order to identify melanoma suppressor genes, and to identify diagnostic and prognostic biomarkers.

Promoter hypermethylation in primary melanoma

In this thesis, we report the first genome-wide profiling of DNA methylation alterations in primary cutaneous melanoma and common naevus biopsy specimens. Genome-wide DNA methylation profiling identified 106 genes as significantly and frequently hypermethylated in primary melanoma when compared to common naevus. Among the genes most frequently hypermethylated in melanoma were *HOXA9*, *MAPK13*, *CDH11*, *PLEKHG6*, *PPP1R3C* and *CLDN11*. Aside from *HOXA9*, for which methylation was found in a sizeable proportion of common naevi, promoter methylation of the other genes was almost absent in naevi but occurred frequently in melanomas (**Chapter 2**). Of the 106 most frequently methylated genes, 11 genes have been reported as methylated in melanoma and 32 genes as methylated in other cancer types. The *PPP1R3C*, *CDH11* and *HOXA9* gene promoters have previously been reported to be hypermethylated in melanoma cell lines and metastatic samples[1-4]. Methylation of the *MAPK13*, *PLEKHG6* and *CLDN11* gene promoters, occurring in up to 67% of primary melanoma cases as detected by bisulphite melting curve analysis, has not been reported in melanoma yet. From the 106 identified genes, one gene (*RNF43*) was listed in the Cancer Gene Census as a putative tumor suppressor gene[5]. The Cancer Gene Census has 54 genes (8%) that overlap with the tumor suppressor gene database (TSGene) that consists of 716 human genes up to date. From the 106 genes *SERPINB5* (Maspin), *CHFR* and *RARβ* were listed in TSGene as known tumor suppressors based on multiple independent studies in literature. *CDH11*, *GNMT*, *NR4A1* and *MTSS1* were listed as putative tumor suppressors[6].

Genome-wide methylation profiling has revealed the presence of widespread and frequent DNA methylation alterations in primary melanoma. Based on further methylation analyses in sets of common naevi, dysplastic naevi, primary and metastatic melanomas, we have begun to obtain a view of the onset of methylation events that may be important in the development of melanoma (Figure 1). We have observed the presence of *HOXA9*, *MAPK13* and *CNTN1* promoter methylation in a subset of common and dysplastic naevi,

and in 40% - 80% of primary melanomas. Interestingly, genes such as *CDH11*, *PPP1R3C* and *PLEKHG6* were progressively hypermethylated in dysplastic naevi, primary and metastatic melanomas, with almost absent methylation in common naevi (**Chapter 3**). This suggests a potential role of these genes in suppressing the onset of dysplastic features in melanocytic lesions.

The promoter hypermethylation frequency of a selected panel of genes appeared to increase gradually from the common naevus to the dysplastic naevus stage. In primary melanoma samples however, the number of methylated genes demonstrated a sharp increase, indicating that malignant transformation is associated with epigenetic deregulation. Using this approach, we have identified *CLDN11* as a potential biomarker to distinguish dysplastic naevi from primary melanoma (**Chapter 3**). *CLDN11* encodes a member of the claudin family, components of tight junctions that maintain a physical barrier and the polarity of cells. Loss of *CLDN11* expression through promoter hypermethylation during melanoma development may facilitate invasive behavior by disrupting intercellular cohesion provided by tight junction structures[7].

Genome-wide methylation profiling was performed using Illumina's Infinium HumanMethylation27K platform that interrogates 27,578 CpG sites located within the promoter regions of a total of 14,495 genes. Recently, beadchips have become available that allow examination of methylomes with an even higher resolution; the 450K beadchip interrogates more than 480.000 cytosines distributed over the whole genome inside and outside of gene promoter regions. Whole-genome bisulphite sequencing, based on next-generation sequencing of bisulphite-treated DNA, has made it possible to analyze the approximately 30 million CG-dinucleotides in the human genome. These more recent techniques can aid in the identification of additional differentially methylated CpG sites that hold potential diagnostic or prognostic value, since they enable interrogating an extensive number of CpG sites at once. The additional value of methylation analyses using these high-resolution platforms, however, may be limited. One reason is that promoter CpG island methylation remains the most relevant when it comes to direct implications in gene transcription regulation. Approximately 50% of all 30.000 human gene promoters contain a CpG island, methylation of which is often associated with transcriptional repression. The 14,495 gene promoters interrogated by Illumina's 27k beadchip covers almost all of these CpG island-containing gene promoters.

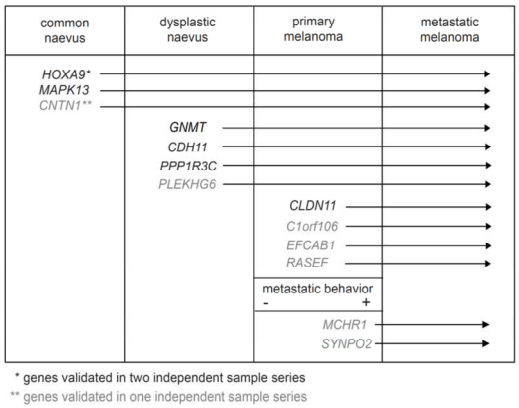

Figure 1. A melanoma progression model with the hypothesized timing of the most frequently occurring epigenetic events in the different stages of melanocytic neoplasia.

MAPK13 and *RASEF*, candidate melanoma suppressor genes

Promoter CpG island methylation is believed to contribute to the development and progression of cancer by transcriptional repression of tumor suppressor genes, providing a selective advantage to tumor cells. Established tumor suppressor genes that are often inactivated in cancer such as *CDKN2A* and *PTEN* have been found to be affected by aberrant promoter methylation in melanoma. We hypothesized that among the 106 most frequently methylated genes could be potential novel genes with a tumor suppressive role in melanoma. *MAPK13*, encoding p38δ, belonged to the five most frequently hypermethylated genes in primary melanoma that were identified. Due to its suggested tumor suppressive function and the potential involvement of p38 MAPK proteins in oncogene-induced senescence, we have performed additional experiments focused on MAPK13. To evaluate tumor suppressive properties, MAPK13 expression was restored in several melanoma cell lines affected by promoter hypermethylation of this gene; we observed that this resulted in a significant decrease of proliferative capacity of these cells (**Chapter 2**). Together with the finding of *MAPK13* promoter methylation in a proportion of common naevi, our data suggests that *MAPK13* silencing by methylation might be an early event that has a role in melanoma development. Similar to our findings but in a different cancer type, MAPK13 has been suggested to be involved in the suppression of oesophageal squamous cell carcinoma (OESCC) through observations of decreased cell proliferation and migration, and altered anchorage-independent growth when MAPK13 was introduced in OESCC cells that did not have endogenous MAPK13 expression, with an even greater effect when the active phosphorylated form of MAPK13 was used[8]. Mouse embryonic fibroblasts lacking MAPK13 were previously found to have diminished cell contact inhibition and to proliferate and migrate faster than their wildtype counterparts[9]. Another study observed that phosphorylation of p53 by members of the p38 and JNK family of MAP-kinases, including p38δ, upon depletion of SEPW1 mediated a transient G1 cell cycle arrest in epithelial cells[10]. For keratinocytes it was found that PKCδ suppressed

proliferation via activation of MAPK13, leading to an increase in p53 levels and increased expression of $p21^{Cip1,11}$. Together these findings point to potential tumor suppressive properties of MAPK13 that involves stabilization and activation of p53.

In the process of malignant transformation towards cancer, oncogene-induced senescence (OIS) has been identified as a mechanism to protect against the onset of cancer in response to aberrant oncogenic activity. We were not able to observe a bypass of $BRAF^{V600E}$-induced senescence upon MAPK13 depletion. This can be due to redundancy in function of the four p38 MAPK isoforms in melanoma cells and therefore depletion of MAPK13 was not sufficient to bypass senescence. Recently it was shown that RAS-activated p38 induced the pro-senescent function of Tip60 via phosphorylation of both Tip60 and PRAK, providing evidence for a signaling pathway involving p38 that mediated oncogene-induced senescence. Upon activation by oncogenic RAS only two isoforms, p38α (MAPK14) and p38δ (MAPK13), were observed to mediate phosphorylation of Tip60 at Thr158/106 in senescent cells, while all four p38 isoforms (p38α, MAPK14; p38β, MAPK11; p38γ, MAPK12; p38δ, MAPK13) phosphorylated Tip60 in vitro. These results indicate potentially overlapping functions for the p38α and p38δ isoforms in mediating senescence[12]. Another study however found that p38δ was able to mediate RAS-induced senescence, with enhancement of p38δ expression during senescence via induction of the RAF1-MEK-ERK pathway by oncogenic RAS[13]. Since these studies found p38δ involved in senescence induced by oncogenic RAS, it may be mainly involved in the response induced by this oncogene and not by mutant BRAF. Differences exist between the four p38 isoforms in terms of different cofactors that regulate phosphorylation, and different accessibility to phosphorylation targets. Insight into how the phosphorylation activity of each p38 isoform is regulated and how it affects signaling downstream, may aid in further understanding the role of the p38 kinases in mutant BRAF-induced senescence.

In Chapter 2, bisulphite melting curve analysis (BMCA) was used to assess the promoter methylation status of fresh-frozen biopsy specimens. Here, no significant *MAPK13* promoter methylation was observed in the investigated common naevi. In Chapter 4 *MAPK13* methylation was observed in 18% of investigated formalin-fixed paraffin-embedded (FFPE) biopsy samples using methylation-specific PCR (MSP). The MSP as applied in Chapter 4 is able to detect one methylated allele in a background of at least 1000 unmethylated alleles[14]. Therefore MSP has been more sensitive than BMCA in detecting methylation even in a tiny fraction of cells. At least 5% of methylated DNA was required in order for BMCA to detect methylation. *MAPK13* methylation assessment using BMCA and MSP on a set of naevi and melanomas showed 84% concordance (described in Chapter 4). Cases that did not have concordant results between the BMCA and MSP techniques were all specimens that were considered as 'unmethylated' using BMCA, and as 'methylated' when MSP was used. From our observations of methylation detection

with BMCA and MSP, we assume that small subpopulations of melanoma cells exist that are positive for methylation of *MAPK13* that are not detectable by BMCA.

In order to identify novel genes required for induction of senescence following expression of mutant BRAF, a functional shRNA screen was performed targeting approximately 15.000 genes. Primary analysis yielded 40 genes and from secondary validation seven genes essential for BRAF-induced senescence emerged, including the *RASEF* gene. Upon reanalysis of genome-wide methylation profiles *RASEF* was among the genes most frequently methylated in *BRAF*-mutant melanoma. Subsequent analysis in a larger series of melanoma samples demonstrated that *RASEF* was methylated in 21% of primary melanomas. Upon validation, *RASEF* methylation appeared not to be restricted to tumors with *BRAF* mutation. (**Chapter 3**). Depletion of *RASEF* mediated a bypass of $BRAF^{V600E}$-induced senescence and the suppression of senescence biomarkers including senescence-associated (SA)-*β*-galactosidase activity, interleukins and tumor suppressor $p15^{INK4B}$. In addition, a growth-restrictive effect was observed in melanoma cells where epigenetically silenced *RASEF* expression was restored. These findings suggest the identification of a potential new tumor suppressor gene in melanoma (**Chapter 3**). *RASEF* promoter hypermethylation and a correlation between *RASEF* methylation and expression have been previously described in uveal melanoma, a melanoma subtype that differs in genetic and clinical characteristics from cutaneous melanoma[15]. The chromosomal region on 9q21.32 where *RASEF* is located has been proposed previously as a susceptibility locus in members of three Danish families with cases of cutaneous and uveal melanoma[16]. Together with our findings, these results indicate that *RASEF* inactivation may be important for both cutaneous and uveal melanoma development, suggesting a common ground that may underlie tumorigenesis of both melanoma subtypes. We propose that *RASEF* is a melanoma suppressor gene, inactivation of which prevents the onset of a senescence response that normally occurs upon expression of mutant BRAF.

For *MAPK13* and *RASEF*, we have made a start in Chapter 2 and Chapter 3 of this thesis to characterize their potential tumor suppressive function in melanoma. An assessment of *MAPK13* and *RASEF* function using in vivo assays will be needed for a more definitive demonstration that *MAPK13* and *RASEF* are tumor suppressors[17]. *MAPK13* mutation was found in 2 of 319 (0.6%) melanoma tissues in the Catalogue of somatic mutations in cancer (COSMIC), and *RASEF* mutation was found in 3 of 314 (1.0%) of melanoma tissues. This may be an indication that inactivation of *MAPK13* and *RASEF* function is mainly brought about by promoter methylation. Also other genes, such as the *HIC1* tumor suppressor gene are known to be primarily inactivated by promoter hypermethylation rather than mutation[18].

Promoter methylation and gene expression in dysplastic naevus

The dysplastic naevus is considered an intermediate stage of melanocytic lesion between a common naevus and a primary melanoma. Clinically the distinction between dysplastic naevus and early-stage melanoma remains challenging for a proportion of cases. We set out to examine the promoter methylation status of a selection of genes that were identified using genome-wide methylation profiling, in a total of 405 melanocytic neoplasms (**Chapter 4**). Promoter methylation analysis in common naevi, dysplastic naevi, primary melanomas and metastatic melanomas demonstrated progressive epigenetic deregulation. We also observed that dysplastic naevi were affected by promoter methylation of genes that were frequently methylated in melanoma but not in common naevi. *CLDN11* promoter methylation was the most selective for melanoma as it occurred in 50% of primary melanomas and only 3% of dysplastic naevi. Promoter methylation of *CLDN11* has been previously reported in bladder and gastric cancer and was shown to be associated with transcriptional silencing[19,20] Next we assessed the diagnostic value of the methylation status of five genes in distinguishing primary melanoma from dysplastic naevus. A diagnostic model that incorporated methylation of *CLDN11*, *CDH11*, *PPP1R3C*, *MAPK13* and *GNMT* was validated in an independent sample series and helped distinguish melanoma from dysplastic naevus (AUC 0.81). We did not find a single gene methylation event that could completely distinguish melanoma from naevus samples in all cases. However the combined detection of *CLDN11*, *CDH11* and *PPP1R3C* promoter methylation yielded a specificity of 89% and sensitivity of 67%.

In addition to DNA methylation, we have also examined differences in gene expression of the melanocytes derived from dysplastic naevus and melanocytes from adjacent normal skin. To gain insight into the molecular pathways that may underlie the elevated oxidative stress levels in dysplastic naevus melanocytes, we compared the gene and protein expression patterns of cultured melanocytes derived from dysplastic naevus and melanocytes from adjacent normal skin. Our findings indicate that gene expression patterns from cultured melanocytes derived from dysplastic naevi are largely similar to those of melanocytes derived from normal skin. The main differences were observed with genes involved in cellular metabolism, detoxification and cytoskeletal organization. Melanocytes derived from dysplastic naevi also differed in morphology and proliferation rate from the melanocytes derived from adjacent normal skin (**Chapter 5**). However overall, the differences between the two melanocyte types were small. The initially existent expression differences may have been subtle due to artefacts introduced by short culturing of the melanocytes; it is possible that we were subsequently not able to detect significant differential mRNA levels between the melanocytes derived from dysplastic naevi and melanocytes derived from adjacent normal skin. Previous mRNA and protein expression studies that analyzed normal naevi, dysplastic naevi, primary and metastatic

melanomas observed that expression differences between normal melanocytes and melanocytes from dysplastic naevi are relatively small[21-24]. Our findings in Chapter 5 are in line with these observations. Dysplastic naevi were also previously found to display significant heterogeneity in their gene expression profiles, where some dysplastic naevi resembled their normal counterparts while other dysplastic naevi more closely resembled primary melanomas when comparing gene expression patterns. The existence of this heterogeneity can make it more difficult to correctly identify differential gene expression patterns in our microarray analysis and requires approaches that can more accurately determine differential expression in a more defined, small number of dysplastic naevus cells.

Taken together the observations made in Chapter 4 and 5 show that dysplastic naevi, also those with severe atypia, resemble common naevi more than primary melanoma on the epigenetic and gene expression level. We found no overlap upon comparison of the differentially methylated genes between common naevi and dysplastic naevi as observed in Chapter 4, with the differentially expressed genes and proteins found in Chapter 5. In Chapter 4, the identified genes were obtained by initially comparing common naevi with primary melanomas. The most frequently methylated genes from that comparison were subsequently analyzed in common naevi and dysplastic naevi. These genes were *HOXA9*, *C1orf106*, *MAPK13*, *CDH11*, *EFCAB1*, *CNTN1*, *GNMT*, *PLEKHG6*, *PPP1R3C* and *CLDN11* (Table 1). Out of these ten genes *HOXA9*, *MAPK13*, *CNTN1*, *PLEKHG6* and *PPP1R3C* were also observed to be hypermethylated in dysplastic naevi (Table 1). The possibility remains that if the initial promoter methylation profiling was performed using common naevi and dysplastic naevi as the initial comparison, genes different than those listed in Table 1 would have been identified. In addition the comparison in Chapter 5 was performed between melanocytes from dysplastic naevi and melanocytes derived from normal skin. Altogether this can explain why no overlap was found between the identified gene candidates in Chapter 4 and 5.

Prognostic biomarkers for primary melanoma with metastatic capacity

The acquisition of metastatic capacity is a crucial step in melanoma progression as metastatic melanoma is often fatal whereas a localized tumor can be cured by excision. It remains a challenge to correctly predict those patients that are at high risk for metastatic disease and to determine the prognosis for patients diagnosed with melanoma, in spite of the availability of several clinical prognostic factors such as tumor thickness. Current understanding about the role of epigenetic alterations that underlie the capacity of melanoma cells to invade deeper skin regions and disseminate from the primary tumor is limited. In order to identify genes that were differentially methylated between primary melanoma with and without metastatic capacity, a re-analysis of genome-wide methyla-

Table 1. **Hypermethylated genes in dysplastic naevi and primary melanomas**. Genes observed as hypermethylated in either dysplastic naevus compared to common naevus (left column) or primary melanoma compared to common naevus (right column). Genes were considered hypermethylated in dysplastic naevi when more than 5% of the number of analyzed dysplastic naevi showed methylation compared to the number of common naevi (see also Figure 1, Chapter 4).

common naevus vs. dysplastic naevus (Chapter 4)	**common naevus vs. melanoma (Chapter 2)**
HOXA9	*HOXA9*
X	*C1orf106*
MAPK13	*MAPK13*
X	*CDH11*
X	*EFCAB1*
CNTN1	*CNTN1*
X	*GNMT*
PLEKHG6	*PLEKHG6*
PPP1R3C	*PPP1R3C*
X	*CLDN11*

-tion data followed by validation in an independent set of primary melanomas was performed (**Chapter 6**). This showed that *MCHR1* was significantly hypermethylated in primary melanomas with metastatic capacity. *SYNPO2* was the second gene that showed substantial, but not significant, hypermethylation. Kaplan-Meier survival analysis was performed using methylation data from the TCGA database containing HumanMethylation450K Beadchip methylation data of 48 primary melanoma and 229 metastasized melanoma biopsy specimens. Due to the limited amount of patient information on metastatic capacity of the primary melanomas, the number of primary melanomas with known metastatic capacity was too small to analyze the value of potential prognostic factors. Instead, Kaplan-Meier survival analysis was carried out on the 229 metastasized melanomas from the TCGA database. This showed that a cg-probe *β*-value higher than 0.50 for *MCHR1* was significantly associated with a poorer survival rate (**Chapter 6**). It is interesting that in addition to a significant association with metastatic behavior observed in a set of primary melanomas, *MCHR1* methylation is also correlated to survival outcome of metastasized melanomas. Further comparative analysis of genome-wide methylation data between melanoma metastasis and primary melanoma biopsy specimens also showed significant hypomethylation of *MAGEA3* and *MAGEA6* in the melanoma metastasis samples.

Not surprisingly, the methylation differences that we observed in the comparative analysis of primary melanomas with and without metastatic behavior were relatively small. It is likely that methylation differences, if present will be smaller than when distinct stages of melanoma progression are compared (for example naevus to melanoma). The observation of *MCHR1* methylation in benign melanocytic tissue indicates that the differences in *MCHR1* methylation as detected in this study are based on

differences in methylation density of the CpG promoter region, rather than a complete presence or absence of methylation. Since the comparative analysis was performed on a small group of primary melanomas with known metastatic capacity, it is possible that upon comparison between larger sample series, more genes will be identified with significant differential methylation.

Our findings in Chapter 6 suggest that the methylation status of *MCHR1* and perhaps also *SYNPO2* may be useful in predicting the metastatic behavior of a primary melanoma. However we have only started with a first methylation analysis. Because of the small sample sets, some methylation events may be random occurrences within the specific tumor samples used. Additional validation involving large sample sets of primary melanoma biopsies with known clinical information on metastatic capacity is necessary to determine the prognostic value of *MCHR1* and *SYNPO2*. Especially the question whether these genes have prognostic value independent of existing clinical parameters used to predict prognosis such as Breslow's thickness, ulceration, mitotic index, gender and age will be important.

We have identified *MCHR1* as a novel gene that is differentially methylated between primary melanoma with and without metastatic behavior. *MCHR1* promoter methylation has not yet been previously described in cancer. *MCHR1* was found to be an auto-antigen, normally expressed by human melanocytes and is thought to serve as a target for auto-immune responses in certain cases[25]. Additional analyses will be needed to establish the effect of promoter CpG island methylation density on *MCHR1* expression. In line with our findings for *SYNPO2*, a commonly deleted region in prostate cancer was mapped to the encoding sequence of *SYNPO2* (also known as Myopodin) on chromosome 4q25. Complete or partial deletion correlated with prostate cancer invasiveness and was found in 80% of the investigated invasive prostate cancer cases. *SYNPO2* hypermethylation has also been observed in colon cancer cells and colorectal tissue where it was found to correlate with overall survival in two independent validation series[26,27]. From the candidates in our diagnostic marker panel in Chapter 4, genes such as *CLDN11* and *CDH11* can also be considered for testing their value as prognostic biomarkers since these genes are frequently methylated in melanoma, in which they are more frequently methylated in metastatic melanoma than in primary melanoma lesions, and they have been implicated in the processes of invasion and metastasis.

Future perspectives

Cancer cell genomes generally exhibit a global loss of methylation (hypomethylation) together with an aberrant increase in methylation (hypermethylation) at CpG islands, GC-rich regions present in approximately half of all human gene promoters. Using promoter CpG island methylation profiling we have generated a comprehensive view of promoter

hypermethylation in primary melanoma and have found that aberrant methylation is widespread in melanoma when compared to common naevi. Questions still remain on what causes the widespread promoter hypermethylation in melanoma. This relates to the question on how in normal cells, CpG islands remain protected from DNA methylation. A challenge remains to further elucidate what causes epigenetic deregulation in cutaneous melanoma. Recently, ten-eleven translocation (TET) family of enzymes that oxidize 5-methylcytosine to 5'-hydroxymethylcytosine were discovered and led to the insight that DNA hydroxymethylation is important in the process of dynamic cytosine modification, where 5'-methylcytosines can undergo active demethylation and are reversed back to cytosine[28,29]. This implicates a more complex regulation of gene expression than initially thought in both normal and cancer cells.

The genetic lesions underlying cutaneous melanoma are becoming increasingly well understood. However an overview of the epigenetic alterations that underlie melanoma and the combined interaction between genetics and epigenetics to induce gene expression changes in the development of cutaneous melanoma is still lacking. Full insight into these molecular events and their interactions will certainly emerge in the near future. It seems that integrating data generated by new genomic and epigenomic profiling techniques is necessary to achieve this. The delineation of not only the pattern of DNA methylation, but also the pattern of histone modifications and chromatin remodeling will provide insight into the contribution of each of these epigenetic mechanisms to melanoma initiation and progression. An understanding of these underlying molecular events will aid in the search for new diagnostic and prognostic biomarkers and improve treatment of this disease.

References

1. Bonazzi, V.F. *et al.* Cross-platform array screening identifies COL1A2, THBS1, TNFRSF10D and UCHL1 as genes frequently silenced by methylation in melanoma. *PLoS. One.* **6**(10), e26121 (2011).
2. Carmona, F.J. *et al.* Epigenetic disruption of cadherin-11 in human cancer metastasis. *J. Pathol.* **228**(2), 230-240 (2012).
3. Furuta, J. *et al.* Promoter methylation profiling of 30 genes in human malignant melanoma. *Cancer Sci.* **95**(12), 962-968 (2004).
4. Rauch, T.A. *et al.* High-resolution mapping of DNA hypermethylation and hypomethylation in lung cancer. *Proc. Natl. Acad. Sci. U. S. A.* **105**(1), 252-257 (2008).
5. Futreal, P.A. *et al.* A census of human cancer genes. *Nat. Rev. Cancer* **4**(3), 177-183 (2004).
6. Zhao, M., Sun, J., and Zhao, Z. TSGene: a web resource for tumor suppressor genes. *Nucleic Acids Res.* **41**(Database issue), D970-D976 (2013).
7. Martin, T.A. and Jiang, W.G. Loss of tight junction barrier function and its role in cancer metastasis. *Biochim. Biophys. Acta* **1788**(4), 872-891 (2009).
8. O'Callaghan, C. *et al.* Loss of p38delta mitogen-activated protein kinase expression promotes oesophageal squamous cell carcinoma proliferation, migration and anchorage-independent growth. *Int. J. Oncol.* **43**(2), 405-415 (2013).
9. Cerezo-Guisado, M.I. *et al.* Evidence of p38-gamma and p38-delta involvement in cell transformation processes. **32**(7), 1093-1099 (2011).
10. Hawkes, W.C. and Alkan, Z. Delayed Cell Cycle Progression in Selenoprotein W Depleted Cells Is Regulated By a Mitogen-Activated Protein Kinase Kinase 4 (MKK4)-p38/c-Jun NH2-Terminal Kinase (JNK)-p53 Pathway. *J. Biol. Chem.* **287**(33), 27371-27379 (2012).
11. Saha, K. *et al.* p38delta regulates p53 to control p21Cip1 expression in human epidermal keratinocytes. *J. Biol. Chem.* **289**(16), 11443-11453 (2014).
12. Zheng, H. *et al.* A posttranslational modification cascade involving p38, Tip60, and PRAK mediates oncogene-induced senescence. *Mol. Cell* **50**(5), 699-710 (2013).
13. Kwong, J. *et al.* Induction of p38delta expression plays an essential role in oncogenic ras-induced senescence. *Mol. Cell Biol.* **33**(19), 3780-3794 (2013).
14. Derks, S. *et al.* Methylation-specific PCR unraveled. *Cell Oncol.* **26**(5-6), 291-299 (2004).
15. Maat, W. *et al.* Epigenetic regulation identifies RASEF as a tumor-suppressor gene in uveal melanoma. *Invest Ophthalmol. Vis. Sci.* **49**(4), 1291-1298 (2008).
16. Jonsson, G. *et al.* Mapping of a novel ocular and cutaneous malignant melanoma susceptibility locus to chromosome 9q21.32. *J. Natl. Cancer Inst.* **97**(18), 1377-1382 (2005).
17. Vredeveld, L.C. *et al.* Abrogation of BRAFV600E-induced senescence by PI3K pathway activation contributes to melanomagenesis. *Genes Dev.* **26**(10), 1055-1069 (2012).
18. Chen, W.Y. *et al.* Heterozygous disruption of Hic1 predisposes mice to a gender-dependent spectrum of malignant tumors. *Nat. Genet.* **33**(2), 197-202 (2003).
19. Agarwal, R. *et al.* Silencing of claudin-11 is associated with increased invasiveness of gastric cancer cells. *PLoS One.* **4**(11), e8002 (2009).
20. Awsare, N.S. *et al.* Claudin-11 decreases the invasiveness of bladder cancer cells. *Oncol. Rep.* **25**(6), 1503-1509 (2011).
21. Alekseenko, A. *et al.* Cyclin D1 and D3 expression in melanocytic skin lesions. *Arch. Dermatol. Res.* **302**(7), 545-550 (2010).
22. Boyd, A.S., Shakhtour, B., and Shyr, Y. Minichromosome maintenance protein expression in benign nevi, dysplastic nevi, melanoma, and cutaneous melanoma metastases. *J. Am. Acad. Dermatol.* **58**(5), 750-754 (2008).
23. Campoli, M. *et al.* HLA antigen expression in melanocytic lesions: Is acquisition of HLA antigen expression a biomarker of atypical (dysplastic) melanocytes? *J. Am. Acad. Dermatol.* **66**(6), 911-916 (2012).
24. Scatolini, M. *et al.* Altered molecular pathways in melanocytic lesions. *Int. J. Cancer* **126**(8), 1869-1881 (2010).
25. Kemp, E.H. *et al.* The melanin-concentrating hormone receptor 1, a novel target of autoantibody responses in vitiligo. *J. Clin. Invest* **109**(7), 923-930 (2002).
26. Esteban, S. *et al.* Diagnostic and prognostic utility of methylation and protein expression patterns of myopodin in colon cancer. *Tumour. Biol.* **33**(2), 337-346 (2012).
27. Lin, F. *et al.* Myopodin, a synaptopodin homologue, is frequently deleted in invasive prostate cancers. *Am. J. Pathol.* **159**(5), 1603-1612 (2001).

28. Kohli, R.M. and Zhang, Y. TET enzymes, TDG and the dynamics of DNA demethylation. *Nature* **502**(7472), 472-479 (2013).
29. Tahiliani, M. *et al.* Conversion of 5-methylcytosine to 5-hydroxymethylcytosine in mammalian DNA by MLL partner TET1. *Science* **324**(5929), 930-935 (2009).

Appendices

Nederlandse samenvatting
Curriculum vitae

Nederlandse samenvatting

De studies in dit proefschrift zijn gericht op het in kaart brengen van promoter CpG eiland methylatie patronen in cutaan melanoom, ter identificatie van epigenetische veranderingen die van belang zijn bij de ontwikkeling van melanoom, en die kunnen dienen als diagnostische en prognostische biomarkers.

Cutaan melanoom is een agressieve vorm van huidkanker die uitgaat van de pigmentcellen (melanocyten) van de huid. Waar melanoom beperkt tot de huid genezen kan worden door chirurgische excisie, is melanoom met metastasen op afstand vaak fataal. Het ontstaan en de progressie van melanoom wordt veroorzaakt door veranderingen in het erfelijk materiaal (het DNA) van de melanocyten. Een gen is een regio in het DNA die de code bevat voor het maken van een eiwit. Eerst vindt transcriptie van een gen naar messenger RNA (mRNA) plaats, vervolgens wordt de code van dit mRNA afgelezen voor productie van het eiwit; op deze manier wordt een gen tot expressie gebracht door de cel. Het optreden van een verandering in het DNA kan tot gevolg hebben dat een gen foutief tot expressie komt. Het foutief tot expressie komen van genen leidt tot een verstoring in het normaal functioneren van de cel. Foutieve expressie van een toenemend aantal genen heeft geleidelijke ontsporing van normale cellen naar kankercellen tot gevolg. Niet alleen genetische veranderingen, maar ook epigenetische veranderingen leiden tot foutieve expressie van genen die de transformatie van normale cellen naar kankercellen induceren.

In elke cel is het DNA op een speciale manier verpakt in de celkern. Elk DNA molecuul is gewikkeld rondom speciale eiwitten (histon eiwitten) en verpakt in clusters in de celkern; bij elkaar wordt de organiserende DNA-eiwit structuur aangeduid als chromatine. Hoe dicht het chromatine verpakt is heeft effect op welke genen wanneer afgeschreven worden. Bij epigenetische veranderingen gaat het om een verandering in de chromatine structuur, en niet een feitelijke verandering in het DNA zelf, die veranderingen in de expressie van een gen teweeg brengt. Een bekend epigenetisch mechanisme is methylatie. Bij methylatie van het DNA in een menselijke cel wordt een methylgroep vastgemaakt aan een cytosine nucleotide die zich naast een guanine nucleotide in het DNA bevindt. Een cytosine en guanine nucleotide naast elkaar in het DNA wordt ook aangeduid als een CpG dinucleotide. In het menselijk DNA zijn er afzonderlijke regio's met een groot aantal CpG dinucleotiden, de zogenaamde CpG eilanden. Meer dan de helft van alle menselijke genen bevat CpG eilanden aan het begin van het gen, in het gebied waar ook de promoter van het gen zit. De promoter is een regio in het DNA die de transcriptie van DNA naar RNA reguleert. Methylatie van CpG eilanden in de genpromoter leidt tot een verandering van het chromatine naar een gesloten conformatie. Tevens induceert de methylatie van CpG eilanden binding van eiwitcomplexen die transcriptie van het DNA verhinderen. In normale menselijke cellen hebben CpG eilanden in de promoter regio

veelal geen methylgroep, ze zijn zeer beperkt gemethyleerd. In kankercellen echter, vindt abnormale methylatie (hypermethylatie) plaats op deze CpG eilanden. In kankercellen gaat deze promoter CpG eiland hypermethylatie vaak gepaard met verminderde of afwezige transcriptie van genen getroffen door deze epigenetische verandering. Op deze manier kan hypermethylatie leiden tot inactivatie van tumor suppressor genen. Een tumor suppressor gen codeert voor eiwitten die de groei van een cel onderdrukken. Deze tumor suppressors spelen vaak een cruciale rol in de controle van celdeling, want in tegenstelling tot normale cellen, zijn verscheidene tumor suppressor eiwitten afwezig of defect in kankercellen. Zo is ook promoter hypermethylatie van genen die bekende tumor suppressor eiwitten coderen, zoals *CDKN2A*, *CDH1* en *PTEN*, gevonden in melanoom. Onderzoek naar methylatie veranderingen in cutaan melanoom heeft zich tot nog toe beperkt tot analyse van een klein aantal genen, waarbij het onderzochte materiaal beperkt bleef tot melanoom cellijnen of weefsel van metastatisch melanomen. In de studies opgenomen in dit proefschrift is gebruik gemaakt van bioptweefsel van normale naevi, dysplastische naevi, primaire melanomen en metastatische melanomen.

In **hoofdstuk 2** beschrijven we het in kaart brengen van promoter CpG eiland methylatie patronen in primaire cutaan melanomen en normale naevi met behulp van Beadchip array. Deze array analyseert 27.578 CpG dinucleotiden verspreid over 14.495 van de naar schatting 30.000 humane genen, d.w.z. bijna alle genen met een CpG eiland in de promoter. Wij vonden 106 genen met een significante toename in promoter mehylatie ten opzichte van normale naevi, onder deze genen bevonden zich *HOXA9*, *MAPK13*, *CDH11*, *PLEKHG6*, *PPP1R3C* and *CLDN11*. Het *MAPK13* gen was in 67% van de primair melanomen gemethyleerd. *MAPK13* codeert voor de isoform van een eiwit dat lid is van de p38 MAP kinase familie, p38δ. *MAPK13* promoter methylatie was geassocieerd met verminderde p38δ expressie. Daarnaast zagen we, wanneer we in melanoomcellen met *MAPK13* hypermethylatie die geen expressie van het gen meer hadden, de expressie van dit gen terugbrachten, dat deze melanoomcellen een afname in proliferatie vertoonden. Deze bevindingen zijn de eerste indicatie van een mogelijke tumor suppressieve rol voor *MAPK13* in melanoom. Daarnaast suggereren deze bevindingen, samen met de aanwezigheid van *MAPK13* promoter methylatie in een deel van de normale naevi, dat uitschakeling van *MAPK13* door methylatie een vroege gebeurtenis is in de ontwikkeling van melanoom.

Een belangrijk tumor suppressief mechanisme bij het ontstaan van melanoom is oncogen-geïnduceerde senescentie. Senescentie is het fenomeen waarbij een cel na een aantal celdelingen in een permanente groeistop raakt. Dit treedt op wanneer een normale cel wordt blootgesteld aan bepaalde vormen van stress. Een vorm van stress die senescentie kan induceren is activatie van een oncogen, zoals *BRAF*. In **hoofdstuk 3** wordt de zoektocht naar nieuwe genen die nodig zijn voor oncogen-geïnduceerde senescentie

beschreven. shRNA screening gericht op 15.000 genen gevolgd door validatie resulteerde in zeven genen, waaronder *RASEF*. Uit reanalyse van genoom-wijde methylatie data was *RASEF* één van de genen die onderhevig was aan frequente hypermethylatie in *BRAF*-mutante melanomen. In een onafhankelijke groep primaire melanomen en normale naevi was de methylatie frequentie van *RASEF* 21%, hier bleek *RASEF* methylatie niet beperkt tot lesies met *BRAF* mutatie. Opvallend was dat depletie van *RASEF* resulteerde in het uitblijven van een $BRAF^{V600E}$-geïnduceerde senescentie respons, en suppressie van senescentie biomarkers zoals (SA)-β-galactosidase activiteit, IL-6 en tumor suppressor $p15^{INK4B}$. Daarnaast leidde het terugbrengen van *RASEF* expressie in melanoomcellen waar expressie van dit gen door promoter methylatie was uitgeschakeld, tot een vertraging in celgroei. Samen suggereren deze bevindingen dat *RASEF* een potentieel nieuw tumor suppressor gen is in melanoom, dat werkt door het voorkomen van verder ontsporen van beginnende melanoomcellen door activatie van oncogen-geïnduceerde senescentie en het afremmen van celgroei.

Dysplastische naevi zijn een type moedervlek die er anders uit zien dan een normale moedervlek. Een dysplastische naevus kan groter zijn dan een normale moedervlek en verschillen in een aantal met het oog waarneembare kenmerken zoals kleur, symmetrie, oppervlakte en rand van de moedervlek. Onderscheid tussen een dysplastische naevus en een vroeg-stadium primair melanoom kan moeilijk zijn op grond van waargenomen veranderingen in de weefselarchitectuur en aspect van de melanocyten. Er bestaat behoefte aan moleculair-pathologische methoden om met zekerheid de diagnose melanoom te kunnen stellen. Voor de zoektocht naar potentiële diagnostische biomarkers zijn we uitgegaan van de 12 meest frequent in melanoom gehypermethyleerde genen. Dit betrof de genen *HOXA9*, *C1orf106*, *MAPK13*, *CDH11*, *EFCAB1*, *CNTN1*, *GNMT*, *PLEKHG6*, *PPP1R3C* en *CLDN11*. Het methylatiepatroon van deze 12 genen is in biopten van dysplastische naevi onderzocht en vergeleken met het methylatiepatroon van normale naevi, primaire melanomen en metastatische melanomen. In **hoofdstuk 4** worden de resultaten van dit onderzoek beschreven. Promoter methylatie analyse liet een progressief toenemende methylatie frequentie zien van genen zoals *CDH11*, *PPP1R3C* en *PLEKHG6*, met minimale methylatie in normale naevus, een geleidelijke toename van methylatie in dysplastisch naevus, en een scherpe toename in methylatie frequentie in primair en metastatisch melanoom. Dysplastische naevi vertoonden tevens aanwezigheid van methylatie van genen die frequent gemethyleerd waren in melanoom maar niet in normale naevi, zoals het *C1orf106* en *GNMT* gen. *HOXA9*, *MAPK13* en *CNTN1* promoter methylatie was aanwezig in een subset normale en dysplastische naevi en in 40% - 80% van de onderzochte primaire melanomen. *CLDN11* was bijzonder specifiek voor melanoom met promoter methylatie in 50% van de primaire melanomen en 3% in dysplastische naevi. De diagnostische waarde van de

methylatie status van een panel bestaande uit vijf genen *CLDN11*, *CDH11*, *PPP1R3C*, *MAPK13* en *GNMT* werd getest op onafhankelijke series van melanomen en dysplastische naevi. Hieruit bleek dat de methylatie status van *CLDN11* in combinatie met dat van *CDH11*, *PPP1R3C*, *MAPK13* en *GNMT* kon helpen met een onderscheid maken tussen primair melanoom en dysplastische naevus. Een gecombineerde detectie van *CLDN11*, *CDH11* en *PPP1R3C* promoter methylatie resulteerde in een specificiteit van 89% en sensitiviteit van 67%. De melanoom-specifieke methylatie van deze genen wijst op mogelijk toekomstige toepasbaarheid als diagnostische biomarker.

Volgend op DNA methylatie patronen in dysplastische naevi, is **hoofdstuk 5** gericht op identificatie van verschillen in gen- en eiwitexpressie van melanocyten afkomstig van dysplastische naevus, en melanocyten afkomstig van aangrenzende normale huid. Melanocyten zijn onderhevig aan oxidatieve stress, waarbij in de cel meer reactieve zuurstofverbindingen aanwezig zijn dan normaal. In melanocyten afkomstig van dysplastische naevi is een verhoogde toestand van oxidatieve stress gevonden. Om inzicht te verkrijgen in moleculaire signaleringspaden die ten grondslag liggen aan de verhoogde oxidatieve stress levels in dysplastisch naevus melanocyten, zijn het gen- en eiwitexpressie patroon van melanocyten afkomstig van dysplastische naevus en van normale huid met elkaar vergeleken. Teneinde dit te onderzoeken zijn melanocyten uit dysplastische naevi en melanocyten uit aangrenzende normale huid geïsoleerd en opgekweekt. Uit de opgekweekte melanocyten is RNA en eiwit verkregen voor respectievelijk genexpressie analyse middels Affymetrix array en massaspectrometrie analyse. Tijdens de studie kon in de melanocyt celkweken een verschil in morfologie en delingssnelheid worden waargenomen tussen melanocyten afkomstig uit dysplastische naevus en melanocyten afkomstig van normale huid. Hoewel de genexpressie profielen van beide melanocyt typen overeenkomstig waren, waren er ook verschillen in signaleringspaden betrokken bij de volgende cellulaire processen: metabolisme, detoxificatie en organisatie van het cytoskelet. Over het algemeen vertoonden melanocyten afkomstig van dysplastische naevi vergelijkbare gen- en eiwitexpressie patronen in vergelijking tot melanocyten afkomstig van aangrenzende normale huid.

Een deel van de melanomen zaait uit (metastaseert) en het is moeilijk om te voorspellen welk melanoom dat zal doen. De voornaamste klinische factor die wordt gebruikt om een voorspelling over mogelijk metastaseren van een melanoom te doen, is de dikte van de tumor. Het vinden van prognostische biomarkers waarmee een goede voorspelling over metastasering kan worden gedaan is noodzakelijk voor een optimale behandeling van de patiënt. Ter identificatie van methylatie patronen met potentiële prognostische waarde en die mogelijk ter grondslag liggen aan het verkrijgen van invasieve en metastatische capaciteit, is in **hoofdstuk 6** gezocht naar aanwezigheid van differentiële methylatie tussen primaire melanomen die wel of niet zijn gemetastaseerd.

Een analyse van genoom-wijde methylatie data werd uitgevoerd, met daaropvolgend validatie in een set biopten bestaande uit primaire melanomen met en zonder metastatisch gedrag. Hieruit kwamen *MCHR1* en *SYNPO2* naar voren als meer frequent gemethyleerd in melanomen met metastatisch gedrag. Vervolgonderzoek liet zien dat metastatische lesies met *MCHR1* methylatie een significant slechtere overleving hadden dan metastatische melanomen zonder *MCHR1* methylatie. Interessant aan deze bevinding is dat *MCHR1* methylatie naast een significante associatie met metastatisch gedrag van de primaire lesie, ook correleert met de overlevingskans van patiënten met reeds gemetastaseerd melanoom. Dit kan erop duiden dat methylatie van *MCHR1* een algemene indicator is voor agressief gedrag van melanoom.

Het onderzoek naar promoter methylatie in melanoom heeft laten zien dat tijdens de ontwikkeling van melanoom er abnormale methylatie plaatsvindt van vele tientallen genen. Waar normale naevi geringe promoter methylatie laten zien, vindt een duidelijke toename in de frequentie van promoter methylatie plaats in melanomen. Geïdentificeerde genen met frequente hypermethyatie in melanoom kunnen potentiële tumor suppressieve functies hebben. Wat de oorzaak is van de uitgebreide toename in promoter methylatie tijdens de ontwikkeling van melanoom is nog onduidelijk. De invloed van genetische mechanismen en de wisselwerking tussen epigenetische en genetische mechanismen in de totstandkoming van de veelvuldig aberrant gemethyleerde genen in melanoom ten opzichte van een melanocytaire benigne laesie hebben meer onderzoek nodig. Het ontrafelen hiervan zou mogelijk nieuwe aanknopingspunten voor de behandeling van cutaan melanoom kunnen bieden. Verder hebben we tijdens ons onderzoek gevonden dat de methylatiestatus van *CLDN11* in combinatie met vier anderen genen, *PPP1R3C*, *CDH11*, *MAPK13* en *GNMT* kan bijdragen aan het onderscheid tussen dysplastische naevus en een vroeg-stadium melanoom. Hoewel melanoom niet in alle gevallen door analyse van de methylatie van een enkel gen met zekerheid kan worden gediagnosticeerd, kan de detectie van een combinatie van differentieel gemethyleerde genen toegepast worden als diagnostische biomarkers in de toekomst.

Curriculum Vitae

Linda Gao werd geboren op 24 oktober 1984 te Beijing, China. Op haar vijfde verhuisde zij naar Nederland. Zij groeide op in Diemen en doorliep de middelbare school aan het Vossius Gymnasium te Amsterdam. Na behalen van het eindexamen gymnasium in 2003, begon zij in datzelfde jaar met de bacheloropleiding Bio-medische Wetenschappen aan de Universiteit van Amsterdam. Ter afsluiting van deze opleiding liep zij stage bij de afdeling Humane Genetica van het Academisch Medisch Centrum (AMC) in de groep van prof.dr. Rogier Versteeg onder leiding van Dr. Dirk Geerts. In 2006 behaalde zij haar bachelordiploma cum laude en vervolgde in datzelfde jaar het opleidingstraject Bio-medische Wetenschappen met de gelijknamige masteropleiding. Tijdens haar master vervolgde zij haar stage in de groep van prof.dr. Rogier Versteeg onder leiding van Dr. Dirk Geerts en onderzocht daar de rol van transcriptiefactor HAND1 in de regulatie van homeoboxgen MEIS1 in neuroblastoom. Ter afsluiting van haar masteropleiding liep zij stage bij de afdeling Moleculaire Oncologie van het Nederlands Kanker Instituut (NKI-AvL) en deed daar onderzoek in de groep van prof.dr. Daniel Peeper naar nieuwe targets betrokken bij IL6-gemedieerde oncogen-geïnduceerde senescentie onder leiding van Dr. Thomas Kuilman. In 2008 studeerde zij cum laude af aan de masteropleiding met een specialisatie in Oncologie. In het najaar van 2008 begon zij aan haar promotieonderzoek op de afdeling Dermatologie van het Leids Universitair Medisch Centrum (LUMC) in de groep van prof.dr. Rein Willemze naar promoter CpG eiland methylatie in de ontwikkeling van melanoom beschreven in dit proefschrift onder leiding van Dr. Remco van Doorn.